

UNCLASSIFIED

AD NUMBER

AD853719

LIMITATION CHANGES

TO:

Approved for public release; distribution is unlimited.

FROM:

Distribution: Further dissemination only as directed by Army Materiel Command, Alexandria, VA, APR 1969, or higher DoD authority.

AUTHORITY

USAMC ltr dtd 14 Jan 1972

THIS PAGE IS UNCLASSIFIED


gy 7 8-23

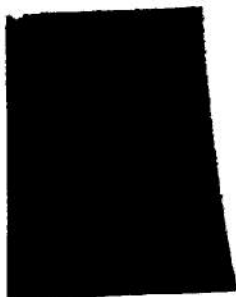
LOAN COPY ONLY - DO NOT DESTROY
PROPERTY OF
REDSTONE SCIENTIFIC INFORMATION CENTER
JUL 23 1969

ENGINEERING DESIGN HANDBOOK

APPROVED FOR PUBLIC RELEASE,
DISTRIBUTION UNLIMITED
DDC TAB 72-19

LIQUID-FILLED PROJECTILE DESIGN

REDSTONE SCIENTIFIC INFORMATION CENTER

5 0510 00078462 6



[Faint, illegible text]
DO NOT CIRCULATE

HEADQUARTERS
UNITED STATES ARMY MATERIEL COMMAND
WASHINGTON, D.C. 20315

AMC PAMPHLET
No. 706-165

18 April 1969

ENGINEERING DESIGN HANDBOOK
LIQUID-FILLED PROJECTILE DESIGN

<i>Paragraph</i>		<i>Page</i>
	Preface	ix
	List of Illustrations	vi
	List of Tables	viii

CHAPTER 1

BRIEF BACKGROUND OF THE PROBLEM OF THE DYNAMICS OF A LIQUID-FILLED PROJECTILE	1-1
---	-----

CHAPTER 2

DYNAMICS OF A RIGID PROJECTILE

2-0	List of Symbols	2-1
2-1	Introduction	2-2
2-2	Equation of Yawing Motion	2-2
2-3	Nonspinning Projectile	2-6
2-4	152mm WP Projectile, XM410	2-7
2-5	Some Considerations of Gyroscopic Stability With Liquid Filler	2-9
2-6	The Gyroscope	2-12
2-7	The Projectile and the Gyroscope	2-14
	References	2-15/2-16

CHAPTER 3

DYNAMICS OF A LIQUID-FILLED PROJECTILE

3-0	List of Symbols	3-1
3-1	Introduction	3-2
3-2	Equations of Perturbed Fluid Motion	3-4
3-2.1	Inviscid Approximation	3-5
3-2.2	Equations of Perturbed Fluid Motion in Cylindrical Coordinates	3-5
3-2.3	Boundary Conditions Imposed by the Yawing Motion of the Projectile	3-6
3-2.4	Boundary Conditions on a Free Surface	3-9
3-3	Reaction of the Liquid Upon the Projectile	3-9
3-3.1	Moments Due to the Liquid	3-10
3-3.2	Equations of Yawing Motion	3-11
3-4	Nonspinning Liquid	3-11
3-4.1	Completely Filled Cavity	3-11
3-4.2	Partially Filled Cavity	3-12
3-4.3	Computation of Effective Moments of Inertia	3-12
3-5	Spinning Liquid	3-13
3-5.1	Introduction	3-13
3-5.2	The Boundary Value Problem	3-14
3-6	Greenhill's Solution for Spheroidal Cavity	3-15
3-6.1	The Moment on a Projectile With Spheroidal Cavity	3-16

TABLE OF CONTENTS (Cont)

<i>Paragraph</i>		<i>Page</i>
3—6.1.1	Center of Rotation Coincides With Center of Cavity	3—16
3—6.1.2	Change of Center of Rotation	3—17
3—6.2	The Motion of the Projectile	3—18
3—6.3	Effective Moments of Inertia of a Spheroidal Mass of Liquid	3—20
3—7	Stewartson's Solution for a Cylindrical Cavity	3—20
3—7.1	Introduction	3—20
3—7.2	Method of Solution of the Boundary Value Problem	3—22
3—8	The Eigenvalue Problem	3—23
	References	3—2 5/3—2 6

CHAPTER 4

MILNE'S STABILITY GRAPH, STEWARTSON'S
AND CENTRAL COLUMN TABLES

4—0	List of Symbols	4—1
4—1	Milne's Stability Graph	4—1
4—1.1	Introduction	4—1
4—1.2	Instability Criteria	4—1
4—1.3	Milne's Stability Graph	4—2
4—1.4	Rate of Divergence	4—3
4—2	Stewartson's Tables	4—5
4—2.1	Introduction	4—5
4—2.2	The Tables and Their Application	4—7
4—3	An Example: 155 mm WP Projectile, XM410	4—8
4—4	Central Column Tables	4—11
	References	4—11

CHAPTER 5

EXPERIMENTS

5—0	List of Symbols	5—1
5—1	Introduction	5—1
5—2	Verification of Stewartson's Instability Criteria	5—1
5—2.1	Free-flight Firings	5—2
5—2.2	Experiments With Gyroscope	5—2
5—3	Instabilities in Noncylindrical Cavities	5—6
5—4	Instability During Spin-up or Transient Phase	5—10
5—5	Axial Spin Decay	5—13
	References	5—16

CHAPTER 6

EFFECT OF VISCOSITY

6—0	List of Symbols	6—1
6—1	Introduction	6—1

TABLE OF CONTENTS (Cont)

<i>Paragraph</i>		<i>Page</i>
6-2	Historical Background and Outline of the Problem	6-1
6-3	Theory of Viscous Corrections	6-2
6-3.1	The Rate of Divergence	6-2
6-3.2	Computation of Viscous Eigenfrequencies	6-5
6-4	Experimental Verification	6-8
	References	6-12

CHAPTER 7

NONCYLINDRICAL CAVITIES

7-0	List of Symbols	7-1
7-1	Introduction	7-1
7-2	Cavities of Rotational Symmetry	7-2
7-2.1	Theoretical Approach	7-2
7-2.2	Computation of Eigenfrequencies	7-4
7-2.3	Noncylindrical Free Surface	7-5
7-2.4	Range of Validity	7-5
7-2.5	Effect of Rounded Corners	7-5
7-2.6	Rounded Corners in Conjunction With Other Modifications	7-6
7-3	Noncylindrical Cavities of Rotational Symmetry	7-6
7-3.1	Residues	7-6
7-3.2	Experiments	7-7
7-3.2.1	Modified Cylindrical Cavities	7-9
7-3.2.2	Rounded Corners	7-9
7-4	Asymmetrical Cavities	7-12
7-4.1	Other Cavities and Ritz Method of Approximation	7-12
7-4.2	The Eigenvalue Problem	7-12
7-4.3	Ritz Method of Approximation	7-13
7-4.4	Example: Circular Cylinder	7-14
	References	7-15/7-16

CHAPTER 8

PARTIALLY SPINNING LIQUID

8-0	List of Symbols	8-1
8-1	Introduction	8-1
8-2	Attainment of Longitudinal Motion	8-2
8-3	Attainment of Rotational Motion	8-5
8-3.1	Theory of Spin-up	8-5
8-3.1.1	Equations of Motion	8-6
8-3.1.2	Computation of the Secondary Flow	8-8
8-3.1.2.1	Completely Filled Cavity	8-8
8-3.1.2.2	Partially Filled Cavity	8-9
8-3.1.3	Transition to a Turbulent Boundary Layer	8-9
8-3.1.4	Discussion of the Equation of Spin-up	8-9

TABLE OF CONTENTS (Cont)

<i>Paragraph</i>		<i>Page</i>
8—3.1.5	General Solution of the Reduced Equation of Spin-up	8—11
8—3.2	Velocity Distribution During Spin-up	8—11
8—3.2.1	Method of Computation	8—11
8—3.2.1.1	Initial Conditions	8—11
8—3.2.1.2	Laminar Case	8—12
8—3.2.1.3	Partially Filled Cavity	8—12
8—3.2.1.4	Total Angular Momentum	8—12
8—3.2.2	Computation of Angular Momentum	8—13
8—3.2.2.1	Laminar Boundary Layer	8—13
8—3.2.2.2	Turbulent Boundary Layer	8—16
8—3.2.2.3	Other Initial Conditions	8—16
8—4	Experimental Results on Spin-up	8—16
8—5	Instability During Spin-up	8—19
8—5.1	Theoretical Approach	8—20
8—5.1.1	Mathematical Difficulties of an Exact Computation	8—20
8—5.1.2	A Simplified Model	8—21
8—5.1.3	Eigenfrequencies for Rectangular Distributions	8—21
8—5.1.4	Stability Criteria	8—22
8—5.2	Experimental Data	8—24
	References	8—28
	Appendix A Derivation of Eq. 8—66.	
	Par. 8—5.1.3	A—A—1

CHAPTER 9

DESIGN OF A LIQUID-FILLED PROJECTILE

9—0	List of Symbols	9—1
9—1	Introduction	9—3
	Section I Steady State	
9—2	Preliminary Calculations: Gyroscopic Stability and Nutational Frequency	9—3
9—3	Cylindrical Cavity	9—5
9—3.1	Viscous Corrections	9—5
9—3.2	Reynolds Number	9—6
9—3.3	Design of Cylindrical Cavities	9—7
9—3.4	Examples	9—8
9—3.4.1	105 mm Chemical Projectile	9—8
9—3.4.2	75 mm Chemical Projectile	9—10
9—3.4.3	XM4 10 Projectile	9—11
9—3.5	Cylindrical Cavity With Central Burster	9—12
9—3.6	100% Filled Cavity With Central Burster	9—12
9—3.7	Partitioning of the Cavity	9—14
9—3.7.1	Full Transverse Baffles	9—14
9—3.7.2	Partial Transverse Baffles	9—15

TABLE OF CONTENTS (Cont)

<i>Paragraph</i>		<i>Page</i>
9-3.7.3	Cylindrical Partition.....	9-17
9 - 4	Noncylindrical Cavities.....	9-19
9-4.1	Evaluation of the Integral Eq. 9-16	9-20
9-4.2	Test of the Theory.....	9-22
9-4.3	The XM410 Projectile.....	9-24
9-4.4	Rounded Corners.....	9-25
9-4.5	Slow Spin.....	9-27

Section II Transient State

9-5	Introduction	9-28
9-5.1	Laminar Boundary Layer	9-29
9-5.2	Turbulent Boundary Layer.....	9-30
9-5.3	Amplification of Yaw	9-31
9-5.4	Experimental Evidence.....	9-32
9-5.5	Transient Instability of the XM410 Projectile.....	9-34
9-5.6	Amplification of Yaw in Noncylindrical Cavities.....	9-34
9-6	Brief Outline of Design Steps.....	9-36
	References.....	9-37 / 9-38

Appendix B	Treatment of Cavities With Partial Bursters	A-B-1
------------	--	-------

CHAPTER 10

AMPLITUDE DEPENDENT BEHAVIOR

10-0	List of Symbols.....	10-1
10-1	Introduction.....	10-1
10-2	Growth of Amplitude at Resonance	10-2
10-3	The Effect of Spin	10-8
10-4	Sudden Appearance of Instability	10-9
10-5	Some Theoretical Considerations	10-10
10-5.1	Transition to Cellular Boundary Layer	10-11
10-5.2	Damping Factors.....	10-12
	References	10-14

Appendix C	Bibliography and Survey of Papers on the Motion of Bodies Having Cavities Filled With Liquid	A-C-1
------------	--	-------

LIST OF ILLUSTRATIONS

<i>Figure No.</i>	<i>Title</i>	<i>Page</i>
2—1	Schematic of Coordinates.....	2—3
2—2	A Sketch of 152 mm, WP. XM410 Projectile	2—7
2—3	Ratio of an "Effective" Transverse Moment of Inertia of the Liquid to its Rigid Value	2—10
3—1	Schematic of Coordinates	3—7
4—1	Milne's Stability Graph	4—4
4—2	Resonance Band in the Cylindrical Cavity of the XM410 Projectile	4—9
5—1	Comparison of Stewartson's Theory with Free-flight Tests	5—3
5—2	BRL Gyroscope	5—4
5—3	Comparison of Stewartson's Theory Modified by Viscous Corrections with the Experiments	5—7
5—4	Types of Noncylindrical Cavities Tested	5—8
5—5	Results of Tests of Cavities in Figure 5—4(A)	5—9
5—6	Results of Tests of Cavities in Figure 5—4(B)	5—11
5—7	Instability During Spin-up of the Liquid	5—12
5—8	Examples of the Axial Spin Decay in Vacuum. $Re \approx 10^5$	5—14
5—9	Examples of the Axial Spin Decay in Vacuum. $Re \approx 10^3$	5—15
6—1	Scaled Representation of the Resonance Band for Various Values of Scaled Viscous Parameter	6—4
6—2	Rate of Undamping $-\Omega\tau_1$ vs Inviscid Eigenfrequency τ_{0i} ($\Omega = 5000$ rpm. Experiments by Karpov)	6—10
6—3	Real Part of the Frequency Shift vs Reynolds Number. Experimental Points by Karpov and Ward	6—11
6—4	Imaginary Part of Frequency Shift vs Reynolds Number. Experimental Points by Karpov and Ward	6—11
7—1	Fill Ratio vs Cone Angle θ at Fixed Frequency $\tau_0 = 0.055$, $c/a = 2.687$	7—8
7—2	The Effect of Modification of the Cylindrical Cavity on the Inviscid Residue	7—10
7—3	The Effect of Rounded Corners of the Cylindrical Cavity at Fixed Resonant Frequency	7—11
8—1(A)	Longitudinal Baffles	8—3
8—1(B)	Transverse Baffles	8—3
8—2	Velocity Distribution During Spin-up for Laminar Boundary Layer	8—14
8—3	Velocity Distribution During Spin-up for Turbulent Boundary Layer	8—14
8—4	Attainment of the Angular Momentum (Laminar Boundary Layer)	8—15

LIST OF ILLUSTRATIONS (Cont)

<i>Figure No.</i>	<i>Title</i>	<i>Page</i>
8-5	Attainment of the Angular Momentum (Turbulent Boundary Layer)	8-15
8-6	Attainment of the Angular Momentum (Turbulent Boundary Layer, 100% Fill) Comparison with Experiments	8-17
8-7	Attainment of the Angular Momentum (Laminar Boundary Layer, 70% Fill) Comparison with Experiments	8-18
8-8	Attainment of the Angular Momentum (Turbulent Boundary Layer, 70% Fill) Comparison with Experiments	8-18
8-9	Graph of an Element ($n = 1$) from Stewartson's Tables	8-23
8-10	Nutational Yaw Damping Rate of Test Projectile	8-25
8-11	Nutational Yaw Amplitude vs Time for 70% Filled Cavity of Test Projectile	8-26
8-12	Increase of Angular Momentum and Passage Through Resonance Band I or II	8-27
9-1	A Schematic of the Axial Velocity Distributions for Various Positions of the Transverse Baffle	9-16
9-2	Spin-up History of the 152 mm XM410 Projectile..	9-35
B-1	Cavities With Partial Bursters.	A-B-2
10-1(A)	Record of Amplitude History, Empty	10-3
10-1(B)	Record of Amplitude History, $\nu = 1$ cSt	10-3
10-1(C)	Record of Amplitude History $\nu = 3$ cSt	10-4
10-1(D)	Record of Amplitude History, $\nu = 5$ cSt	10-4
10-1(E)	Record of Amplitude History, $\nu = 13$ cSt	10-5
10-1(F)	Record of Amplitude History, $\nu = 49$ cSt	10-5
10-1(G)	Record of Amplitude History, $\nu = 100$ cSt	10-6
10-1(H)	Record of Amplitude History, $\nu = 350$ cSt	10-6
10-2(A)	Record of Amplitude History, Large Amplification	10-7
10-2(B)	Record of Amplitude History, Lower Amplification..	10-7
10-3	Growth of Amplitude at Resonance for Various Spin Rates	10-9
10-4	Viscous Damping Factors at Various Yaw Levels	10-13

LIST OF TABLES

<i>Table No.</i>	<i>Title</i>	<i>Page</i>
2—1	Aerodynamic Data for XM4 10 Projectile	2—8
3—1	Eigenfrequencies and Residues of the Basic Mode ($n = 1, j = 0$) for Cylinder and Spheroidal Cavity.....	3—24
4—1	Stewartson's Tables of Fluid Frequencies and Residues for Various Cylindrical Cavities of Height $2c$ and Diameter $2a$, and Various Fill-Ratios b^2/a^2 where $2b$ is the Diameter of the Air Column.....	4—12
4—2	Tables for Cylindrical Cavities with Central Column. Fluid Frequencies and Residues for Various Cylindrical Cavities of Height $2c$ and Diameter $2a$, with Cylindrical Central Column of Diameter $2r$. The Remaining Cavity is Always 100% Filled.	4—27
5—1	Oils and Reynolds Numbers	5—5
5—2	Maximum Rate of Divergence τ_{\max} of the Nuta- tional Amplitude, Corresponding Fill-Ratio, and Associated Fluid Frequency (Inviscid) τ_0	5—6
5—3	Percentage of the Angular Momentum at the Muzzle.....	5—13
7—1	Circular Cylinder: Comparison of Ritz Method and Exact Solution	7—15/ 7—16
9—1	Values of $t_1, t_2 - t_3$, and $t_2 \pm t_3$ for Various τ_0 's	9—6
9—2	Effectiveness of Partial Baffles	9—17
9—3	Fluid Frequency Analysis vs Baffle Position	9—17
10—1	Reynolds Numbers of Transition From the Laminar Boundary Layer	10—2
10—2	Maximum Steady State Amplitude at Resonance	10—8

PREFACE

The Engineering Design Handbook of the Army Materiel Command is a coordinated series of handbooks containing basic information and fundamental data useful in the design and development of Army materiel and systems. The Handbooks are authoritative reference books of practical information and quantitative facts helpful in the design and development of materiel that will meet the needs of the Armed Forces.

The present handbook is one of a series on ballistics. It deals with the dynamics of liquid-filled projectiles which are known to behave in an unpredictable manner in flight. Until rather recently the causes of such misbehavior were not well understood. Whenever such problems arose in practice they were usually treated on an ad hoc basis, i.e., by engineering trial and error methods. Such methods, as a rule, are time-consuming and expensive. Recently, however, considerable progress has been made in this field. For certain limited geometries of cavity shapes, such as the cylinder or near cylinder, it is now possible to give the designer a set of simple rules for the rational design of liquid-filled projectiles that will be dynamically stable in flight.

This handbook summarizes the state of our present knowledge which is directly useful to the designer. Many of the more abstruse theoretical developments, principally in Russian literature, are omitted. However, references to these are to be found in the Appendix C. Since the dynamics of the liquid-filled projectile is less familiar to the designers than the dynamics of the rigid projectile, this handbook gives more of the theoretical background of solved problems than is usually found in other volumes of the Engineering Handbook Series. The emphasis, however, is on the understanding the physics of the problem rather than mathematics. Thus Chapter 2 contains a brief review of the dynamics of a rigid projectile; Chapters 3 to 8, inclusive, deal with the dynamics of the liquid and its reaction on the containing cavity. Chapter 9 is the design chapter where the rules for the design of the liquid-filled projectile are explicitly stated. It would be unfortunate, however, if the designers were to use this chapter without the understanding of the theoretical background as given in the preceding chapters.

The text was prepared by Drs. B. G. Karpov and E. H. Wedemeyer, both former members of the U. S. Army Ballistic Research Laboratories at Aberdeen Proving Ground, Md.

The Handbooks are readily available to all elements of AMC including personnel and contractors having a need and/or requirement. The Army Materiel Command policy is to release these Engineering Design Handbooks to other DOD activities and their contractors, and other Government agencies in accordance with current Army Regulation 70-31, dated 9 September 1966. Procedures for acquiring these Handbooks follow:

PREFACE (CONT)

a. Activities within AMC and other DOD agencies should direct their request on an official form to:

Publications Distribution Branch
Letterkenny Army Depot
ATTN: AMXLE-ATD
Chambersburg, Pennsylvania 17201

b. Contractors who have Department of Defense contracts should submit their request, through their contracting officer with proper justification, to the address indicated in par. a.

c. Government agencies other than DOD having need for the Handbooks may submit their request directly to the Letterkenny Army Depot, as indicated in par. a above, or to:

Commanding General
U. S. Army Materiel Command
ATTN: AMCAD-PP
Washington, D. C. 20315

or

Director
Defense Documentation Center
ATTN: TCA
Cameron Station
Alexandria, Virginia 22314

d. Industry not having a Government contract (this includes Universities) must forward their request to:

Commanding General
U. S. Army Materiel Command
ATTN: AMCRD-TV
Washington, D. C. 20315

e. All foreign requests must be submitted through the Washington, D. C. Embassy to:

Office of the Assistant Chief of Staff
for Intelligence
ATTN: Foreign Liaison Office
Department of the Army
Washington, D. C. 20310

All requests, other than those originating within the DOD, must be accompanied by a valid justification.

Comments and suggestions on this handbook are welcome and should be addressed to Army Research Office-Durham, Box CM, Duke Station, Durham, N. C. 27706.

CHAPTER 1

BRIEF BACKGROUND OF THE PROBLEM OF THE DYNAMICS OF A LIQUID-FILLED PROJECTILE

The problem of the unpredictable behavior of liquid-filled projectiles in flight has been known to designers for a long time. Most frequently the difficulties are encountered with spin-stabilized white phosphorus (WP) projectiles. At normal temperature the WP filler is solid and the projectile, if properly designed, flies well. However, if these projectiles are exposed to an excessive heat — e.g., the result of lying in the sun — the WP melts (110°F) and becomes liquid. As a result, the projectile's flight behavior might be dramatically altered.

Until rather recently the cause or causes of such strange behavior were not well understood by the designers. Some designers conjectured that the failure of the liquid to initially acquire full spin, thereby not contributing its angular momentum to the gyroscopic stability of such a projectile, might be responsible for its dynamic instability. Perhaps this misconception is reflected in the most frequently used engineering solution to instability — the partitioning of the cavity by longitudinal baffles which force the liquid to acquire full spin at the muzzle.

In the United States, until recently, very little systematic research was done in this field. The reason may have been because the problem appeared to be of great complexity. Moreover, the relatively infrequent appearance of such instabilities in practice might not have justified a significant effort in this field, particularly since the encountered problems usually yielded to some sort of ad hoc engineering solution by trial and error methods. Such solutions, however, usually required a compromise with the performance of the projectile.

Nevertheless, sporadic efforts at a better understanding of this problem have been made. For example, during World War II a

fairly extensive experimental program was conducted by firing one-inch diameter liquid-filled models. Since the observations of flight were visual, the models were fired at low muzzle velocity. One of the difficulties of such visual experiments, unless the misbehavior is rather dramatic, is that of deciding whether or not the wind had a controlling influence on the flight of relatively light models. The results of these experiments, in elucidating the causes of the dynamic instability of liquid-filled projectile, were largely inconclusive.

Another investigation used, as an analog of the yawing motion of the projectile, a liquid-filled gyroscope. The gyroscope was designed to be moved, while spinning, through an arc of 45° thus simulating an ascending branch of the trajectory. Unfortunately, because of the experimental difficulties and for other reasons, nothing of value was accomplished.

In England, under the auspices of the Liquid-Filled Shell Panel of the Ministry of Supply, the studies of the liquid-filled projectile problem were more fruitful. In particular, E. A. Milne examined all available field trial records, from 1926 to 1940, of projectiles with liquid fillers. Examination of these data revealed no discernible universal characteristic which could account for the observed behavior. Earlier (1880), Greenhill developed the theory of the stability of a liquid-filled top containing a spheroidal cavity completely filled with the liquid which is spinning as a rigid body. This theory showed that, if disturbed, the liquid acquires a great many natural oscillations characterized by discrete frequencies or eigenfrequencies. These oscillations, in turn, produce pressure pulses on the casing. The unique feature of the spheroidal cavity, which is not true for cavities of

other geometries, is that only one characteristic frequency causes a hydrodynamic couple on the containing casing. The spinning top might become unstable if this eigenfrequency coincided with one of the natural frequencies of the top. Such coincidence of frequencies of two coupled oscillators is known as resonance. Thus resonance between the characteristic frequency of the liquid and the top is responsible for instability of the top. However, the trial projectiles in Milne's collection did not have spheroidal cavities and most, if not all, were only partially filled. Hence, the available mathematical model was inadequate. Nevertheless, in a search for some fruitful correlations among the available data, i.e., what characteristics of the projectile made some stable and others unstable, the mathematical model did suggest certain readily computable physical parameters of the projectile which might play an important role. When these were computed and the trial projectiles were arranged according to these parameters, a fairly well defined correlation curve could be drawn between stable and unstable projectiles as found in actual firing trials. This is well known Milne's stability graph. It is empirical in nature and should be used with considerable caution. More will be said about it later.

In 1953 K. Stewartson published the results of his investigation on the stability of liquid-filled projectile containing a cylindrical cavity which is either fully or partially filled. He found that in the cylindrical cavity a doubly infinite number of modes of free oscillations occur in contrast to the only one mode for the spheroidal cavity. The different modes of oscillation can be characterized by pairs of numbers (n, j) where n and j relate to the number of radial and axial half-waves, respectively, of oscillations of fluid particles. Associated with each mode (n, j) is a natural or eigenfrequency ω_{nj} or nondimensional frequency

$$\tau_{nj} = \frac{\omega_{nj}}{\Omega} \text{ where } \Omega \text{ is the axial spin of the}$$

projectile. These oscillations produce pressure pulses on the casing which might result in hydrodynamical moments. Such os-

cillations of the fluid particles in a spinning fluid are not to be confused with the sloshing of the surface waves in a nonspinning fluid, but are in the nature of traveling waves in the cavity.

It was shown again that resonance between the natural frequencies of the fluid and the projectile is the cause of the dynamic instability of the projectile containing such liquid-filled cavity. The extremely useful feature of this theory for the designer is that the nondimensional eigenfrequencies in a given cavity depend only on the geometry of the cavity, i.e., its fineness-ratio c/a where $2c$ and $2a$ are the height of the cavity and its diameter, respectively; and the amount of fluid in it. In principle, therefore, the eigenfrequencies are under the control of the designer. He can avoid resonance by a judicious design of the cavity.

Nevertheless, at first sight, the problem still appeared to be formidable. If there are an infinite number of hydrodynamic moments which must be added to the equation defining the yawing motion of the projectile, the solution of the equation may become prohibitively difficult. Fortunately, however, one needs to consider only resonating frequencies; the hydrodynamic moments associated with all other frequencies are negligible. But even among the resonating frequencies the theory shows that moments associated with higher modes, i.e., higher n, j values, very rapidly decrease in importance. Suppression of these higher modes also is markedly assisted by viscosity. Thus very few of the resonating frequencies are likely to be of practical importance. As a matter of fact, the experiments with a very sensitive gyroscope, to be described later, show that for practical design purposes the only resonant frequency which needs to be considered is the one associated with the smallest odd multiple of the radial and axial pressure half-wave lengths, i.e., lowest n, j , mode, which can be accommodated in a given cavity. This frequency, which can be called fundamental, gives rise to the largest hydrodynamic moment.

At present the eigenfrequencies can be computed only for the cylindrical cavities or, by slight modification of the cylindrical theory for cavities which depart only slightly from the cylindrical. But at least the fundamental cause of the dynamic instability of liquid-filled projectiles has been firmly established.

Stewartson's theory has been abundantly confirmed by the experiments designed to test its predictions. To enhance the agreement between the theory and the

experiments, it was necessary to incorporate small viscous correction to the frequencies of the inviscid theory. *Also* it was found feasible to extend the theory to noncylindrical cavities satisfying certain conditions. The experiments showed that the applicability of noncylindrical theory is considerably broader than its theoretical limitations would suggest. Thus Stewartson's theory with its modifications and extensions provides the basic tool which the designer of the liquid-filled projectile should use whenever it is possible to do so.

CHAPTER 2

DYNAMICS OF A RIGID PROJECTILE

2-0 LIST OF SYMBOLS

2a	= diameter of cavity, ft	I_x	= $I_{x0} \pm i_{x0}$, axial moment of inertia of loaded projectile, slug-ft ²
c/a	= fineness ratio	I_{y0}	= transverse moment of inertia of empty casing, slug-ft ²
C_D	= drag coefficient	i_{y0}	= transverse moment of inertia of frozen liquid, slug-ft ²
$C_{L\alpha}$	= lift coefficient, per rad	i_y	= "effective" transverse moment of inertia of liquid, slug-ft ² ? Note: all transverse moments are referred to the same center of mass.
$C_{M\alpha}$	= static moment coefficient, per rad	I_y	= transverse moment of inertia of loaded projectile, slug-ft ²
$C_{M\dot{\alpha}} + C_{M\ddot{\alpha}}$	= yaw damping moment coefficient, per rad/sec	i	= $\sqrt{-1}$
$C_{M_{P\alpha}}$	= magnus moment coefficient, per rad/sec, per rad	K_0	= gravitational moment of gyroscope, slug-ft ² /sec ²
$C_{N\alpha}$	= normal force coefficient, per rad	k_x^2	= axial radius of gyration, cal
C_{lp}	= axial torque coefficient, per rad/sec	k_y^2	= transverse radius of gyration, cal
2c	= height of cavity, ft	k	= a constant of integration
D	= as defined by Eq. 2-12	ℓ_n	= natural logarithm
d	= maximum diameter of projectile, ft	log	= common logarithm
e	= base of natural logarithm	M	= static moment factor as defined by Eq. 2-3; mass, slug
f	= a constant associated with bearing friction of gyroscope	M_f	= mass of liquid, slug
G	= as defined by Eq. 2-3	m	= mass of loaded projectile, slug
g	= acceleration due to gravity, ft/sec ²	n	= twist of rifling, cal/turn
H	= damping moment factor as defined by Eq. 2-3	P	= as defined by Eq. 2-3
h	= distance between center of mass and pivot point of gymbal, ft	p	= axial spin rate, rad/sec
I'	= angular momentum of fluid at muzzle, slug-ft ² rad/sec	p, q, r	= angular velocity components along x, y, z axes, respectively, rad/sec
I	= $\sqrt{I_{y0} I_{z0}}$ moment of inertia about either axis of gyroscope where $I_{y0} \approx I_{z0}$, slug-ft ²	P_0	= spin rate of projectile casing imparted by rifling, rad/sec
I_{x0}	= axial moment of inertia of empty casing, slug-ft ²	P_f	= final or equilibrium rate, rad/sec
i_{x0}	= axial moment of inertia of frozen liquid, slug-ft ²	S'	= $(\pi d^2)/4$ frontal area of projectile, ft ²

s	= arc length along trajectory, cal
s_g	= $P^2/4M$ gyroscopic stability factor
$(s_g)_L$	= gyroscopic stability factor of projectile with liquid filler
$(s_g)_R$	= gyroscopic stability factor of rigid projectile
T	= magnus moment factor as defined by Eq. 2-3
u, v, w	= velocity components along x, y, z -axes, respectively, ft/sec
V	= speed of projectile relative to air, ft/sec
\bar{V}	= velocity vector of center of mass of projectile, ft/sec
x	= difference in distance between center of gravity of filler and center of gravity of loaded projectile
X, Y, Z	= inertial, earth bound coordinate system
x, y, z	= body fixed coordinate system of the projectile, located at its center of mass with x -axis along axis of projectile

GREEK LETTERS

β	= ratio of liquid transverse moment of inertia to its rigid value
θ	= angle of deflection, rad
λ_{liq}	= yaw damping rate due to liquid filler, per cal or per ft
	= nutational yaw damping rate, per cal or per ft
	= precessional yaw damping rate, per cal or per ft
ξ	= v_{tiw}/V , a complex variable
ρ_a	= air density, slug/ft ³
σ	= $\sqrt{1 - 1/s_g}$
τ_n	= nondimensional nutational frequency of projectile

τ_p	= nondimensional precessional frequency of projectile
ϕ'_1	= nutational yaw rate of projectile, rad/cal
ϕ'_2	= precessional yaw rate of projectile, rad/cal
Ω	= axial spin rate of projectile, rad/sec
$\bar{\omega}$	= total angular velocity vector of projectile, rad/sec

MATH SYMBOLS

\sim	= approximately
\sim	= of the order
\propto	= proportional

2-4 INTRODUCTION

We shall review briefly the yawing motion of a rigid projectile. For a fuller appreciation of the dynamics of liquid-filled projectile, the knowledge and understanding of the dynamics of rigid projectile are essential. There are a number of excellent references in which this subject is fully treated^{1,2*}. One of the more concise and yet complete discussions is to be found in Ref. 1. Here we shall avoid giving a brief outline of the derivation of the differential equation of yawing motion because brevity may lead to misunderstanding. The full treatment, however, would take too much space. We shall begin, therefore, with the differential equation of the yawing motion of a rigid projectile, taken directly from Ref. 1 (Ch. VI, Eq. 6.12).

2-2 EQUATION OF YAWING MOTION

Let \bar{V} be the velocity vector of the center of mass of the projectile relative to the earth-bound or inertial system X, Y, Z . Let another body-fixed coordinate system (x, y, z) have its origin located at the center of

*Superscript numbers refer to references at the end of each chapter.

mass of the projectile with the x-axis coinciding with the axis of symmetry of the projectile and positive pointing toward the nose, with positive y-axis pointing to the right when looking in the positive x direction, and with the z-axis defined by the right-hand rule. The coordinates are illustrated in Fig. 2-1; the inertial system is omitted for simplicity.

The components of \bar{V} along the projectile fixed axes are u, v , and w , respectively. The components of the total angular velocity vector $\bar{\omega}$ along the same axes are p, q ,

and r . In Ref. 1 it is shown that greater convenience and simplicity results in writing the differential equation of the yawing motion in a nonrolling coordinate system, i.e., with the angular velocity of the coordinates defined by $(0, q, r)$. In this system we define

$$\xi = \frac{v - t}{V} \frac{iw}{V}$$

where

$i = \sqrt{-1}$. The complex variable ξ locates the plane containing the velocity vector and the projectile's axis. Its magnitude represents the magnitude of the sine of the

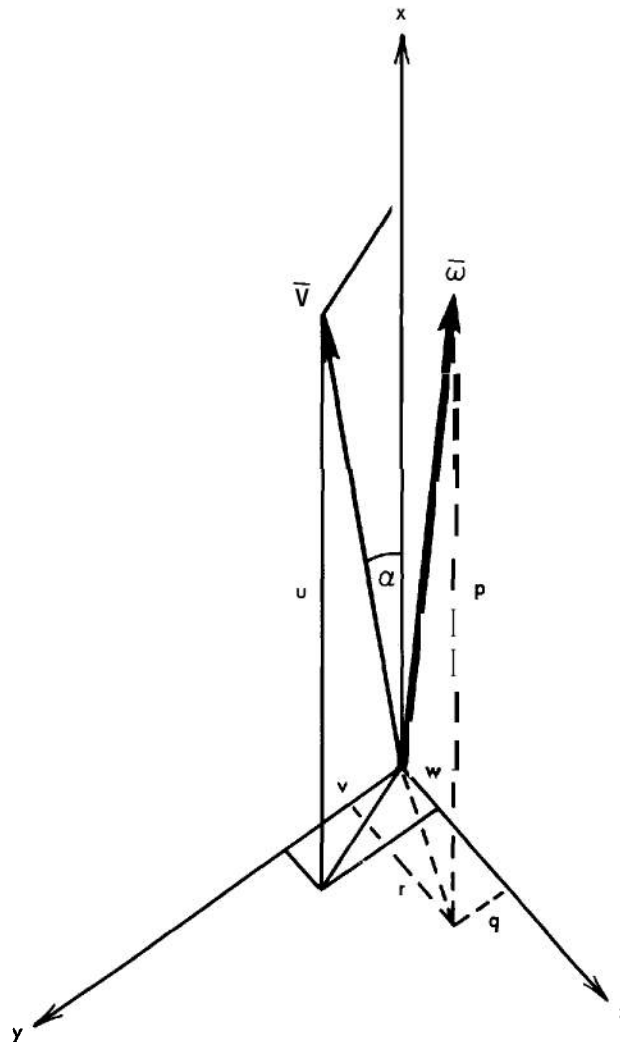


FIGURE 2-1. SCHEMATIC OF COORDINATES

yaw. For the small yaws, for which the yaw equation is valid (linearized system), the sine of the yaw is equivalent to the yaw angle. The differential equation of the yawing motion in the complex variable ξ is shown to be

$$\xi'' + (H - iP)\xi' - (M + iPT)\xi = G \quad (2-1)$$

where the derivatives are with respect to the arc length along the trajectory, in calibers, defined by:

$$s = \frac{1}{d} \int_{t_0}^t V dt \quad (2-2)$$

The use of the arc length as an independent variable, rather than the more natural "time", is done in order to remove velocity factors from the coefficients of the equation. Although the nondimensional aerodynamic functions H, M , and T themselves are functions of nondimensional parameters such as Mach number and Reynolds number, they change rather slowly and for a short segment of trajectory can be regarded as constants. These functions are defined by the following relations:

$$\left. \begin{aligned} H &= \frac{\rho_a S' d}{2m} \left[C_{L_\alpha} - C_D - k_y^{-2} (C_{M_q} + C_{M_{\dot{\alpha}}}) \right] \\ M &= \frac{\rho_a S' d}{2m} k_y^{-2} C_{M_{\alpha}} \\ T &= \frac{\rho_a S' d}{2m} \left[C_{L_{\alpha}} + k_x^{-2} C_{M_{p_\alpha}} \right] \\ P &= \frac{I_x}{I_y} \left(\frac{pd}{V} \right) = \frac{I_x}{I_y} \left(\frac{2\pi}{n} \right) \\ G &= PgdV^{-2} \\ k_x^{-2} &= \frac{md^2}{I_x} \\ k_y^{-2} &= \frac{md^2}{I_y} \end{aligned} \right\} (2-3)$$

where

ρ_a	= air density, slug/ft ³
S'	= $\frac{\pi d^2}{4}$ frontal area of projectile, ft ²
d	= maximum diameter of projectile, ft
m	= mass of projectile, slug
p	= axial spin rate, rad/sec
n	= twist of rifling, calibers per turn
V	= speed of projectile relative to air, ft/sec
I_x, I_y	= axial and transverse moments of inertia, respectively, slug-ft ²
k_x^{-2}, k_y^{-2}	= axial and transverse radius of gyration, respectively, cal
g	= acceleration due to gravity, ft/sec ²
C_D	= drag coefficient
C_{L_α}	= lift coefficient, per rad
$C_{M_{\alpha}}$	= static moment coefficient, per rad
$C_{M_q} + C_{M_{\dot{\alpha}}}$	= yaw damping moment coefficient, per rad/sec
$C_{M_{p_\alpha}}$	= magnus moment coefficient, per rad/sec, per rad

The dimensionless quantity $\frac{\rho_a S' d}{2m}$ is sometimes called the "density factor" because it is roughly the ratio of the air density to the average density of the projectile. Its usual value is of the order of 10^{-4} .

Since we are principally interested in the effect of a liquid filler on the yawing motion of the rigid casing, we shall neglect the small inhomogeneous term G in Eq. 2-1. This term is caused by the curvature of the trajectory due to gravity and gives rise to yaw of repose. So setting the right hand side of Eq. 2-1 equal to zero, the remaining homogeneous equation is of the second order in a complex variable ξ , with constant coefficients. Its solution, therefore is

the sum of two exponentials. To obtain the characteristic equation we substitute for ξ in Eq. 2-1, say, e^{ms} , and obtain a quadratic characteristic equation in m . Its roots are complex and can be written as

$$m_j = \lambda_j + i \phi_j' \\ = \frac{1}{2} \left[-H + iP \pm \sqrt{4M + H^2 - P^2 + 2iP(2T - H)} \right] \quad (2-4)$$

where ϕ_j' is the derivative with respect to s .

Thus the solution of Eq. 2-1 is

$$\xi = k_1 e^{i\phi_1} + k_2 e^{i\phi_2} \quad (2-5)$$

where

$$k_j = k_{j0} e^{\lambda_j s} \quad j = 1, 2$$

$$\phi_j = \phi_{j0} + \phi_j' s$$

The four constants of integration are the two initial amplitudes k_{j0} and the two initial orientation angles ϕ_{j0} of the amplitude vectors.

Eq. 2-5 describes the projectile's response to initial conditions. The amplitudes k_j of the disturbances can either grow or decrease exponentially while the orientation angle ϕ_j of each amplitude vector changes at a constant rate ϕ_j' . The resulting motion is known as damped epicyclic motion.

In the complex roots of the characteristic equation, Eq. 2-4, we can readily separate the real and the imaginary parts. We neglect H^2 under the square root sign as being of second order, expand the square root by the binomial expansion, and collect the real and the imaginary terms. Then the imaginary parts are the yaw rates

$$\phi_{1,2}' = \frac{1}{2} \left[P \pm \sqrt{P^2 - 4M} \right] \quad (2-6)$$

Since ϕ_j' must be real, the expression under the square root must always be positive, i.e.,

$$(P^2 - 4M) > 0$$

Or, written in another form

$$P^2/4M > 1$$

This is the gyroscopic stability condition. The gyroscopic stability factor is

$$s_g \equiv \frac{P^2}{4M} > 1 \quad (2-7)$$

Sometimes it is convenient to designate

$$\sqrt{1 - \frac{1}{s_g}} = \sigma$$

The rates can then be written as

$$\phi_{1,2}' = \frac{1}{2} P (1 \pm \sigma), \text{ rad/cal} \quad (2-8)$$

The higher rate ϕ_1' is usually called the "nutational" rate; the other, ϕ_2' , the "precessional" rate. Later we shall find it convenient to deal with these rates as fractions of the total spin rate $\frac{pd}{V}$. Using the definition of

$$P = \frac{I_x}{I_y} \left(\frac{pd}{V} \right), \text{ we have}$$

$$\tau_n = \frac{\phi_1'}{\frac{pd}{V}} = \frac{I_x}{2I_y} (1 \pm \sigma); \tau_p = \frac{\phi_2'}{\frac{pd}{V}} = \frac{I_x}{2I_y} (1 - \sigma) \quad (2-9)$$

and we shall speak of these as the "nutational" (τ_n) and the "precessional" (τ_p) frequencies of the projectile.

The real parts of the characteristic roots are the yaw damping rates

$$\lambda_{1,2} = -\left(\frac{1}{2}\right) \left[H \mp \frac{P(2T - H)}{\phi_1' - \phi_2'} \right] \quad (2-10)$$

Since, from Eq. 2-8,

$$\phi'_1 - \phi'_2 = P\sigma$$

Eq. 2-10 can conveniently be written in the form

$$\lambda_{1,2} = -(\frac{1}{2}) \left[H \left(1 \pm \frac{1}{\sigma} \right) \mp \frac{2T}{\sigma} \right] \quad (2-11)$$

Eq. 2-1 was derived with the assumption that the axial spin is constant. If a slow variation of the axial spin is taken into account, it can be shown that another small term should be added to the yaw damping rates. For a rigid projectile, this term is usually small and can be omitted. For a liquid-filled projectile, however, if the liquid is very dense, this term might play an important role as will be shown shortly. The term to be added is

$$+ \frac{(1 \pm \sigma)}{\sigma^2} D$$

where

$$D = \frac{\rho_a S^2 d}{2m} \left[C_D + k_x^2 C_{lp} \right] \quad (2-12)$$

C_{lp} is the axial torque coefficient which arises from viscous interaction between the air and the casing through the boundary layer. Thus the complete expression for the yaw damping rates, with slowly varying axial spin included, becomes

$$\lambda_{1,2} = -(\frac{1}{2}) \left[H \left(1 \pm \frac{1}{\sigma} \right) \mp \frac{2T}{\sigma} + \left(\frac{1 \pm \sigma}{\sigma^2} \right) D \right] \quad (2-13)$$

The yaw damping rates vary throughout the flight because H , T , D , and σ depend on the air density and are functions of Mach and Reynolds numbers. To require that the damping rates always be negative might be too restrictive. An occasional divergence of the yaw in flight, as when passing through the transonic range of velocities, may not be detrimental either to range or accuracy. What is essential, for a well designed projectile, is that the initial disturbances at the muzzle die out as rapidly as possible. For the initial part of the trajectory it is essential, therefore, to satisfy the dynamic stability condition that λ_j be negative.

23 NONSPINNING PROJECTILE

The motion of the liquid in a cavity of a nonspinning yawing projectile is usually described by the term "sloshing". In recent years the problem of sloshing of liquid in various types of containers has received a great deal of attention principally in connection with liquid-fueled rockets. For our purpose, however, the sloshing problem presents little interest. As will be shown in Chapter 3, see also Refs. 3 and 4, the motion of the liquid in nonspinning projectile causes no dynamical problems of the type encountered with liquid-filled spinning projectiles. If the nonspinning projectile is dynamically stable when the liquid is frozen (rigid projectile), it will continue to be dynamically stable with a liquid filler. The only effect a nonviscous liquid will have is to alter slightly the inertial properties of the system. The viscosity, in general, will aid the yaw damping rates.

The motion of a rigid nonspinning projectile is quite simple. We set $P = 0$ in Eq. 2-1. The resulting equation is:

$$\xi'' + H \xi' - M \xi = 0 \quad (2-14)$$

Its solution is the sum of two exponentials:

$$\xi = k_1 e^{i\phi_1} + k_2 e^{i\phi_2}$$

where

$$\begin{aligned} k_j &= k_{j0} e^{\lambda_j s} & j &= 1, 2 \\ \phi_j &= \phi_{j0} + \phi'_j s \\ 1 \quad 2 &= -\frac{1}{2}H \\ \phi'_1 &= -\phi'_2 = \sqrt{-M} \end{aligned} \quad (2-15)$$

The static moment factor M for a statically stable projectile is negative. Thus the two yaw damping rates are equal and so are the magnitudes of the turning rates. However, the two vectors $k_1 e^{i\phi_1}$ and $k_2 e^{i\phi_2}$ turn in the opposite directions. Hence the resulting motion is not epicyclic but an ellipse with a semi-major axis $k_1 + k_2$, and a semi-minor axis $|k_1 - k_2|$. We shall not pursue this subject further. For greater detail and additional information the reader should consult Ref. 1.

2-4 152 MM WP PROJECTILE, XM410

We shall consider an application of some of the formulas developed previously to the XM410 Projectile when the WP filler is solid and the system, therefore, is rigid. This projectile has experienced great difficulties with liquid WP and, hence, should provide a useful vehicle for illustration of design considerations for liquid-filled projectiles which we consider in some detail in Chapter 9.

In order to study the dynamics of this projectile we require certain information concerning its physical and aerodynamic properties. The physical characteristics — such as mass, location of the center of mass or center of gravity, and moments of inertia — are relatively easy to obtain either by computations or, preferably, by actual measurements. To obtain the aerodynamic information over the pertinent range of velocities is usually more difficult. Some estimates can be made from known prototypes, or some values can be estimated by experienced persons. Recently a good summary of the available aerodynamic information on a large variety of projectile shapes has been compiled in an Engineering Design Handbook⁵. As a last resort, models of the projectile can always be fired in the ballistic ranges.

In various attempts to solve the problem of its dynamic instability with liquid WP, the XM410 Projectile has undergone many design changes. The sketch in Fig. 2-2 is believed to represent an original design which has been shortened in overall length to increase its gyroscopic stability factor.

The physical characteristics of this projectile are given below. These may differ from other available sets, but for our purpose this is immaterial.

m , total mass of WP-loaded projectile	1.313 slug
CG, measured from nose	1.85 cal
Overall length	2.83 cal

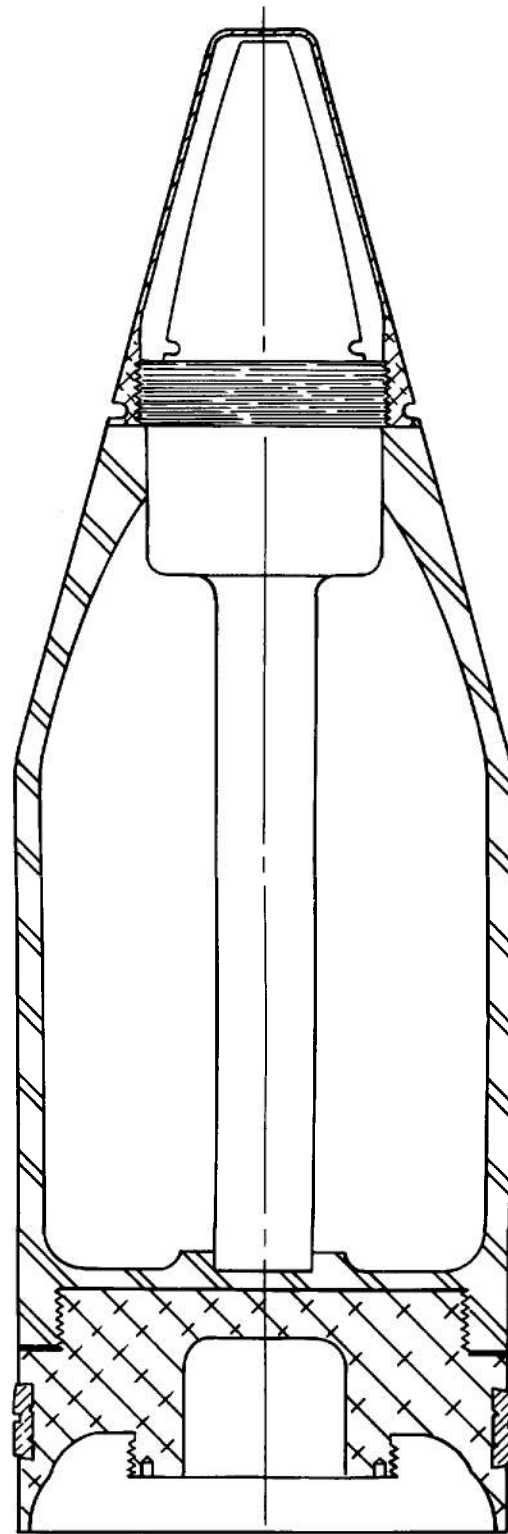


FIGURE 2-2. A SKETCH OF 152 MM WP XM410 PROJECTILE

d, maximum diameter	0.5 ft
I_x	0.0446 slug-ft ²
I_y	0.1548 slug-ft ²
n, twist of rifling	40 cal per turn

We compute

$$k^2 = 7.36 \text{ cal; } k_y^2 = 2.12 \text{ cal;}$$

$$S' = \frac{\pi d^2}{4} = 0.196 \text{ ft}^2$$

With air density $\rho_a = 0.233 \times 10^{-2} \text{ slug/ft}^3$,
the "density factor"
 $\frac{\rho_a S' d}{2m} = -0.87 \times 10^{-4}$.

The aerodynamic characteristics have been measured by ballistics range firings. Illustrative computations for the dynamic stability of this projectile are done for Mach 1.5 (see Table 2-1). The projectile also has adequate dynamic stability at Mach numbers 2.0 and 1.0 for which the aerodynamic data also are given in Table 2-1.

TABLE 2-1. AERODYNAMIC DATA FOR XM410 PROJECTILE

Mach No.	2.0	1.5	1.0
C_D	0.43	0.50	0.56
$C_{N\alpha}$	3.1	2.9	2.6
CP, cal from nose	1.5	1.4	1.3
$C_{Mq} + C_{M\dot{\alpha}}$	-4.0	-5.0	-2.0
C_M	0.1	0.3	-0.1
C_{lp} (assumed)	...	-0.01	...

If the center of gravity (CG) and the center of pressure (CP) are measured from the nose, then the static moment coefficient is given by

$$C_{M\alpha} = C_{N\alpha} (CG - CP)$$

Also

$$C_{L\alpha} \cong C_{N\alpha} - C_D$$

where $C_{N\alpha}$ is the normal force coefficient, per rad.

By use of the aerodynamic information from Table 2-1, the static moment at Mach 1.5 is

$$C_{M\alpha} = 2.9 (1.85 - 1.4) = 1.30$$

We compute:

$$M = \frac{4 \rho_a S' d}{2m} k_y^2 C_{M\alpha} = 9.59 \times 10^{-4}$$

$$P = \frac{I_x}{I_y} \left(\frac{2\pi}{n} \right) = 4.53 \times 10^{-2}$$

Therefore, the gyroscopic stability factor is

$$s_g = \frac{P^2}{4M} = 2.14$$

and

$$\sigma = 0.730$$

$$\tau_n = 0.25 \quad \text{nutation frequency}$$

$$\tau_p = 0.04 \quad \text{precessional frequency}$$

Next we compute the aerodynamic functions H, T, and D.

$$H = \frac{\rho_a S' d}{2m} \left[C_{L\alpha} - C_D - k_y^2 (C_{Mq} + C_{M\dot{\alpha}}) \right]$$

$$H = 0.87 \times \left[2.4 - 0.5 + 2.12 (5.0) \right] \\ = 10.88 \times 10^{-4}$$

$$T = \frac{\rho_a S' d}{2m} \left[C_{L\alpha} + k_x^2 C_{Mp\alpha} \right]$$

$$T = 0.87 \times 10^{-4} \left[2.4 + 7.36 (0.3) \right] = 4.01 \times 10^{-4}$$

$$D = \frac{\rho_a S' d}{2m} \left[C_D + k_x^2 C_{lp} \right]$$

$$D = 0.87 \times 10^{-4} \left[0.5 - 7.36 (0.01) \right] = 0.37 \times 10^{-4}$$

The D term is small and could have been omitted. Finally, using Eq. 2-13 we find, at Mach 1.5, the nutational λ_1 and the precessional λ_2 yaw damping rates

$$\lambda_1 = -7.99 \times 10^{-4} \text{ per cal or } -1.60 \times 10^{-3} \text{ per ft}$$

$$\lambda_2 = -3.57 \times 10^{-4} \text{ per cal or } -0.71 \times 10^{-3} \text{ per ft}$$

The projectile, therefore, is dynamically stable at Mach 1.5, i.e., it satisfies the dynamic stability condition that the two yaw damping rates be negative.

2-5 SOME CONSIDERATIONS OF GYROSCOPIC STABILITY WITH LIQUID FILLER

Detailed discussion of the stability of a rigid projectile is found in Ref. 6. Here, since we have all the pertinent information for the XM410 Projectile, we shall examine only what happens to its gyroscopic stability if the WP becomes liquid.

By Eq. 2-7, the gyroscopic stability factor is proportional to P^2 . From the definition of P, Eq. 2-3, s_g is proportional to the square of the axial angular momentum of the projectile, i.e.

$$s_g \propto P^2 \propto (I_x p)^2$$

where p is the axial spin. The axial moment of inertia I_x can be considered as composed of two parts — that of the casing I_{x0} and that of the filler regarded as rigid i_{x0} . Thus, at the muzzle, the s_g for a rigid projectile is proportional to:

$$s_g \propto (I_{x0} p_0 + i_{x0} p_0)^2$$

where p_0 is the spin of the casing as imparted by the rifling. With the liquid filler, however, the above equation should be modified to read

$$s_g \propto (I_{x0} p_0 + I')^2$$

where I' is the angular momentum of the liquid at the muzzle. Experiments show,

see Ch. 5, that unless the liquid is very viscous, the value of I' , at the muzzle, is usually only about 10% of its full rigid value. Hence, its contribution to the total angular momentum is small and can be neglected. Therefore, with the liquid filler, the gyroscopic stability factor at the muzzle is proportional only to $(I_{x0} p_0)^2$. This at once reduces s_g , relative to the rigid filler case, by a factor

$$\left(\frac{I_{x0}}{I_{x0} + i_{x0}} \right)^2$$

For many projectiles $i_{x0} \ll I_{x0}$ and such reduction in the value of s_g may not be significant. However, for thin-walled projectiles, as the XM410, such a reduction must be carefully examined. To express it differently: if the projectile is gyroscopically stable with a rigid filler, there is no assurance that it will be gyroscopically stable with a liquid filler.

If air effects are neglected, once the projectile is out of the gun, its total angular momentum remains the same. As the liquid gradually acquires full spin, it does so only at the expense of the original angular momentum of the casing $I_{x0} p_0$. Thus with a liquid filler, the axial spin of the casing decreases more rapidly with time or distance than with a rigid filler. This rate of decrease of the spin depends on a number of factors which will be discussed later. However, the final level of an equilibrium spin, when the casing and the liquid have the same spin, is governed by the conservation of angular momentum law

$$(I_{x0} + i_{x0}) p_f = I_{x0} p_0$$

where p_f is the final or equilibrium axial spin rate. This, therefore, is one inertial effect of a liquid filler on the gyroscopic stability.

What about the transverse moment of inertia I_y ? It, too, can be separated into two parts: I_{y0} without the filler (referred, however, to the *CG* of the system) and $i_{y0} + M_f x^2$ of the filler, where i_{y0} is the transverse moment of inertia of the filler about the filler's *CG* and $M_f x^2$ is the transfer term from the *CG* of the filler to that of the whole system. Here M_f is the mass of the filler and x is the difference in positions of the two *CG*'s.

In Chapter 3 — see also Refs. 3 and 7 — it is shown that if the filler is liquid, its “effective” transverse moment of inertia is less than when it is rigid, i.e., i_{y0} has to be reduced or multiplied by a factor, say β , which is less than unity. For a completely filled cylindrical cavity, β depends only on the fineness-ratio of the cavity, i.e., the ratio of its height $2c$ to its diameter $2a$. The curve of β vs c/a is shown in Fig. 2-3. Experiments* indicate that this function can be used with adequate accuracy for a fairly wide range of geometrical cavity shapes.

$$i_y = \beta i_{y0}$$

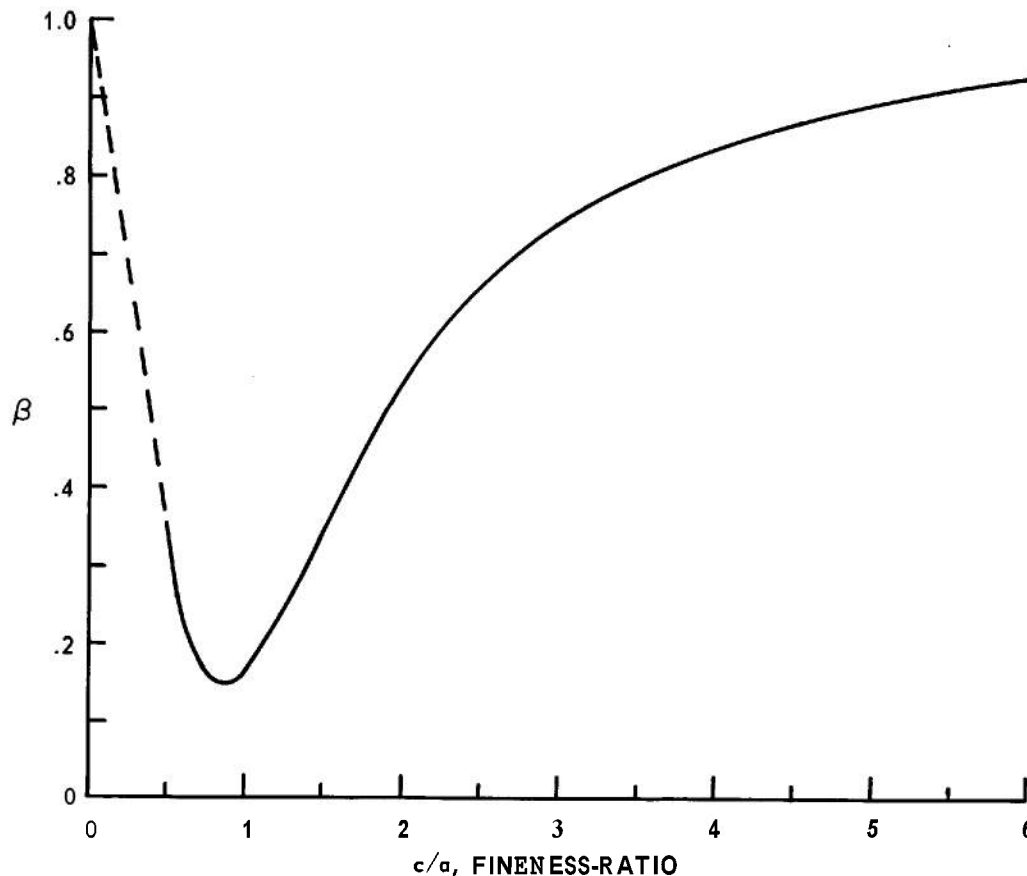


FIGURE 2-3. RATIO OF AN “EFFECTIVE” TRANSVERSE MOMENT OF INERTIA OF THE LIQUID TO ITS RIGID VALUE

Thus the transverse moment of inertia of the liquid filler becomes

$$i_y = \beta i_{y0} + M_f x^2$$

and the total moment of inertia I_y of a rigid projectile with a liquid filler must be replaced by $I_{y0} + i_y$. In the gyroscopic stabil-

ity factor the transverse moment of inertia appears in two places: in P^2 and in M in the radius of gyration. The replacement should be made in both places.

To summarize: if $(s_g)_R$ is the gyroscopic stability factor of a rigid projectile, then the gyroscopic stability factor at the muzzle of the same projectile when its filler is liquid is

$$(s_g)_L = (s_g)_R \left(\frac{I_{x0}}{I_x} \right)^2 \left(\frac{I_y}{I_{y0} + i_y} \right) \quad (2-16)$$

(s_g) should be >1.3 , which represents an arbitrarily imposed safe lower limit for the stability factor.

One more complication may arise in practice when the liquid filler is either exceptionally dense, such as mercury, or its angular momentum is a substantial fraction of the angular momentum of the casing. For a rigid projectile the minimum gyroscopic stability occurs at the muzzle. From this point the gyroscopic stability increases rapidly reaching maximum at the summit of the trajectory and then decreasing. It can be readily shown that initially

$$(\ell_n s_g)' = 2D$$

where prime indicates a derivative with respect to distance. D , as previously defined, is always positive for a rigid, spin-stabilized projectile, i.e., s_g begins to increase at the muzzle. However, if the liquid is very dense, or its angular momentum is large, the initial axial spin decay — due to transfer of an angular momentum from the casing to the liquid — may be very rapid, or the final equilibrium spin may be too low. If one were to represent, in the former

case, even roughly, such rapid spin decay by an “effective” axial torque coefficient C_{lp} , such an “effective” C_{lp} might be considerably larger than its normal aerodynamic value. C_{lp} is negative by definition

and when it is multiplied, in the expression for D , by a fairly large factor, the axial radius of gyration k_x^2 ; the product may overbalance the drag coefficient C_D thus making D negative. This means that, initially, at the muzzle, the gyroscopic stability factor will decrease and reach a minimum value some distance from the muzzle before beginning to increase in the usual manner. If the gyroscopic stability factor is marginal at the muzzle, its further decrease may lead to trouble. Whenever this possibility is suspected, it is safer to guard against it by replacing, in the definition of the gyroscopic stability factor, the initial axial spin p_0 imparted by the rifling, with its final value p_f as determined from the conservation of angular momentum. The designer, therefore, should impose on the gyroscopic stability factor an additional factor of safety, i.e., multiply Eq. 2-16 by

$\left(\frac{I_{x0}}{I_x} \right)^2$. Thus the final design requirement for the gyroscopically stable projectile with a very dense liquid filler would be

$$(s_g)_L = (s_g)_R \left(\frac{I_{x0}}{I_x} \right)^2 \left(\frac{I_y}{I_{y0} + i_y} \right) \left(\frac{I_{x0}}{I_x} \right)^2 \quad (2-17)$$

We shall apply some of these ideas to the XM410 Projectile. Pertinent physical information follows:

$$\begin{aligned} I_x &= 0.0446 \text{ slug-ft}^2 \\ I_{x0} &= 0.0076 \text{ slug-ft}^2 \\ I_{x0} &= 0.0370 \text{ slug-ft}^2 \\ \therefore \left(\frac{I_{x0}}{I_x} \right)^2 &= 0.69 \\ I_y &= 0.1548 \text{ slug-ft}^2 \\ i_{y0} &= 0.0140 \text{ slug-ft}^2 \end{aligned}$$

$$\begin{aligned}
M_f &= 0.310 \text{ slug} \\
a &= 0.22 \text{ ft (cavity radius)} \\
\text{CG, filler from base,} &= 0.515 \text{ ft} \\
\text{CG, system from base,} &= 0.488 \text{ ft} \\
x &= 0.027 \text{ ft} \\
M_f x^2 &= 0.0003 \text{ slug-ft}^2 \\
i_{y0} + M_f x^2 &= 0.0143 \text{ slug-ft}^2 \\
I_{y0} - \frac{M_f x^2}{c/a} &= 0.1405, \text{ slug-ft}^2 \\
c/a &= 1.56 \\
\beta &= 0.37 \\
\beta i_{y0} &= 0.0052, \text{ slug-ft}^2 \\
\bar{I}_y = \beta i_{y0} &= 0.0055, \text{ slug-ft}^2 \\
I_{y0} + \bar{I}_y &= 0.1460, \text{ slug-ft}^2 \\
\frac{I_y}{I_{y0} + \bar{I}_y} &= 1.06
\end{aligned}$$

Previously we have found that the gyroscopic stability factor for the **XM410** as a rigid projectile, at Mach 1.5, was 2.14. Therefore, if the WP is liquid, then by Eq. 2-16, the actual gyroscopic stability factor at the muzzle is

$$(s_g)_L = (2.14)(0.69)(1.06) = 1.57$$

i.e., 27% less. Examination of the spin decay shows that with WP liquid filler in the **XM410** Projectile, D is positive and the above value of the stability factor at the muzzle is a minimum.

In practice it may be adequate, in estimating the degradation of the gyroscopic stability factor with a liquid filler, simply to multiply its rigid value by the first factor and ignore the ratio of the unmodified to modified transverse moments of inertia. The error will be less than 10%.

2-6 THE GYROSCOPE

As we shall see later, if the liquid in the cavity contains a fundamental fluid frequency which is in resonance with the nutational frequency of the projectile, then the

projectile may become dynamically unstable. For dynamic stability, therefore, the nutational yaw damping rate must now satisfy a more stringent condition:

$$\tau_n \lambda_{\text{liq}} < 0$$

Our task shall be to show how to compute λ_{liq} and how to suppress, if need be, the offending fluid frequency. Unfortunately, at present an *a priori* computation of fluid frequencies can be done only for cylindrical cavities or for cavities not departing too far from the cylindrical. For cavities of other geometries it is most economical, at present, to resort to laboratory experiments. A properly designed gyroscope is an excellent tool for this latter purpose. The equation describing the gyroscope's oscillatory motion is analogous to that describing the yawing motion of the projectile. Hence, inferences from the behavior of the liquid-filled gyroscope are at once transferable to the behavior of the liquid-filled projectile provided that the gyroscope is designed to simulate the projectile's nutational frequency τ_n .

A description of various types of gyroscopes and their properties and uses can be found in many books; see, for example, Ref. 9.

The gyroscope is essentially a rotor which, for liquid-filled experiments, should be hollow. The rotor is mounted on an inner gimbal which, in turn, is mounted on an outer gimbal. The outer gimbal is supported by a rigid frame. A successful instrument, developed at the Ballistic Research Laboratories, is shown in Fig. 5-2. It will be described in detail in Chapter 5 in connection with the description of some experiments.

The elementary theory of the gyroscope's motion will be sketched only briefly. Let the x -axis coincide with the axis of symmetry of the rotor, the y -axis pass through the pivots of the inner gimbal, and the z -axis pass through those of the outer gimbal. Thus the rotor spins about the x -axis

but can oscillate about the y- and z-axes. The inner gimbal can oscillate also about the y- and z-axes, but the outer gimbal can oscillate only about the z-axis. Let θ be the angle of deflection of the x-axis from the vertical. In the projectile analogy, this angle is equivalent to the yaw. Angular displacements about the y- and z-axes are θ_y and θ_z , respectively. Let Ω be the constant spin of the rotor in rad/sec. Also let

I_x be the axial moment of inertia of the rotor

I_Y, I'_Y, I''_Y be the transverse moments of inertia of the rotor, inner, and outer gimbals, respectively, about the y-axis.

I_z, I'_z, I''_z be the transverse moments of inertia of the rotor, inner, and outer gimbals, respectively, about the z-axis.

All transverse moments of inertia are about the origin, i.e., about a common pivot point.

Let

$$I_{Y0} = I_Y + I'_Y$$

$$I_{Z0} = I_z + I'_z + I''_z$$

I''_Y does not appear in the equation of I_{Y0} because the outer gimbal cannot turn about the y-axis. Further analysis is markedly simplified if the gyroscope is designed so that $I_{Y0} \approx I_{Z0}$, i.e., so that the outer gimbal is very light. Then one can replace I_{Y0} and I_{Z0} by, say, $I = \sqrt{I_{Y0} I_{Z0}}$ as the moment of inertia about either axis.

Further assume that the bearing friction in the gimbals can be represented by $f \dot{\theta}_y$ and $f \dot{\theta}_z$ (viscous friction) where f is a constant. Then it can be shown that the differential equations of motion in the y- and z-components can be written (see Ref. 9) as

$$I \ddot{\theta}_y + f \dot{\theta}_y + I_x \Omega \dot{\theta}_z - K_0 \theta_y = 0$$

$$I \ddot{\theta}_z + f \dot{\theta}_z - I_x \Omega \dot{\theta}_y - K_0 \theta_z = 0$$

The independent variable is time. $K_0 = Mgh$ is the gravitational moment where M is the mass of the rotor and the inner gimbal, h is the separation of the center of mass (CM) and the pivot-point, and g is the acceleration due to gravity. For the unstable position, i.e., when the center of mass is above the pivot-point, $K_0 > 0$. This situation is analogous to the positive static moment for a statically unstable projectile when the center of pressure is ahead of the center of mass. Define

$$\theta = \theta_y + i \theta_z$$

The two equations above can be combined to give a single equation in a complex variable θ

$$I \ddot{\theta} + (f - i I_x \Omega) \dot{\theta} - K_0 \theta = 0 \quad (2-18)$$

The roots of the characteristic equation of Eq. 2-18 are complex, giving two frequencies and two damping rates. With the assumption that $f/I_x \Omega \ll 1$, we have

	<u>Frequency</u>	$\frac{I}{2I} \left(1 + \frac{1}{\sigma} \right)$
Nutation	$\frac{I_x \Omega}{2I} (1 + \sigma)$	$\left. \begin{array}{l} -\frac{f}{2I} \left(1 + \frac{1}{\sigma} \right) \\ -\frac{f}{2I} \left(1 - \frac{1}{\sigma} \right) \end{array} \right\}$
Precession	$\frac{I_x \Omega}{2I} (1 - \sigma)$	$\left. \begin{array}{l} -\frac{f}{2I} \left(1 - \frac{1}{\sigma} \right) \\ -\frac{f}{2I} \left(1 + \frac{1}{\sigma} \right) \end{array} \right\}$

(2-19)

where

$$\sigma = \sqrt{1 - \frac{1}{s_g}} = 1 - \frac{1}{2s_g} + \dots$$

and the gyroscopic stability factor:

$$s_g = \frac{I_x^2 \Omega^2}{4IK_0}$$

The nondimensional frequencies are

$$\tau_n = \frac{I_x}{2I} (1 + \sigma)$$

$$\tau_p = \frac{I_x}{2I} (1 - \sigma)$$

If s_g is large, as is usual with the gyroscope, then

$$\sigma \approx 1 - \frac{1}{2s_g}$$

and

$$\begin{aligned} \tau_n &\approx \frac{I_x}{I} \\ \tau_p &\approx \frac{K_0}{I_x \Omega^2} \end{aligned} \quad (2-20)$$

It should be noted that for statically unstable position $K_0 > 0$, we have $s_g > 0$, $\sigma < 1$, and the precessional amplitude has a tendency to diverge at a rate depending on the quality of the bearing or on the value of f . For statically stable position $K_0 < 0$, $s_g < 0$ and $\sigma > 1$ — friction in the bearings damps both components. It is desirable, therefore, to have frictionless bearings. Also, it is desirable to design the gyroscope to have only pure nutation, i.e., to provide the means of adjusting its center of mass location to the pivot-point. This suppresses the precessional motion by making $K_0 = 0$. Since the liquid affects only the nutational amplitude, and not the precession, the observations of the effect of the liquid are considerably simplified.

2-7 THE PROJECTILE AND THE GYROSCOPE

To obtain the equations which we shall use in the next chapter for adding the hydrodynamic moment, let us return to Eq. 2-1 and let $H=T=G=0$. The resulting equation

$$\xi'' - iP \xi' - M \xi = 0 \quad (2-21)$$

describes a neutrally stable oscillation, i.e., the amplitudes k_{10} and k_{20} remain constant. Assume, also, that the velocity of the projectile V is a constant V_0 . Then we can easily change the independent variable from distance, in calibers, to time since by Eq. 2-2

$$s = \frac{V_0}{d} t$$

Eq. 2-21 becomes

$$\ddot{\xi} - i \frac{I_x}{I_y} p \dot{\xi} - \frac{MV_0^2}{d^2} \xi = 0 \quad (2-22)$$

Now

$$M \frac{V_0^2}{d^2} = \frac{\rho_a S' d m d^2}{2m} C_{M\alpha} \frac{V_0^2}{d^2}$$

by definition of M , Eq. 2-3.

Since $\hat{M} = \frac{1}{2} \rho_a V_0^2 S' d C_{M\alpha}$ is defined as the aerodynamic moment,

$$\frac{MV_0^2}{d^2} = \frac{\hat{M}}{I_y}$$

Let us also change the axial spin p rad/sec to Ω rad/sec. Then the two equations for the projectile and the gyroscope become, respectively:

$$\begin{aligned} I_y \ddot{\xi} - i I_x \Omega \dot{\xi} - \hat{M} \xi &= 0 \\ I \ddot{\theta} - i I_x \Omega \dot{\theta} - K_0 \theta &= 0 \end{aligned} \quad (2-23)$$

where we let $f=0$ in the gyroscope Eq. 2-18. The only difference between the two equations is that the projectile is being acted upon by the aerodynamic moment

\hat{M} ; whereas the gyroscope, by the gravitational moment K_0 . The solution for each equation is the sum of two exponentials. To obtain the characteristic equation let

$$\xi \text{ or } \theta \propto e^{i\tau\Omega t} \quad (2-24)$$

The characteristic equation for the projectile, for example, becomes

$$I_y \tau^2 - I_x \tau + \frac{I_x^2}{4I_y s_g} = 0 \quad (2-25)$$

The roots are:

For stability of the system, in view of the definition of τ by Eq. 2-24, τ must be real.

We shall introduce the hydrodynamic moment, which arises from the disturbed fluid oscillations in the cavity, into Eq. 2-23 rather than the full Eq. 2-1. The former is algebraically simpler to work with. Since we are dealing with a linearized system of equations, whatever one finds with Eq. 2-23, such as a divergence of one of its amplitudes (instability), this rate of divergence is simply to be added algebraically to the aerodynamic damping of corresponding amplitude as found from Eq. 2-4.

As we shall see in Chapter 3, the method of analysis of the stability of the liquid-filled projectile system is to disturb initially undisturbed flight by causing small amplitude oscillations, about the CG, of the form $e^{i\tau\Omega t}$. Such a disturbance excites the natural fluid oscillations, causing pressure pulses on the walls of the cavity. When these pressure pulses associated with various fluid frequencies are integrated over the cavity, it is found that some produce no moments while others do. These hydrodynamic moments, acting as external moments, are added to aerodynamic moments in Eq. 2-23. The stability of the system is determined from the nature of the roots of the characteristic equation of the whole system. For the system to be stable, the roots must be real.

REFERENCES

1. C. H. Murphy, *Free Flight Motion of Symmetric Missiles*, BRL Report 1216, Aberdeen Proving Ground, Md., July 1963.
2. E. J. McShane, J. L. Kelley, and F. Reno, *Exterior Ballistics*, University of Denver Press, Denver, Colorado, 1953.
3. W. E. Scott, *The Free Flight Stability of a Liquid Filled Spinning Shell*, Part 1a, BRL Report 1120, Aberdeen Proving Ground, Md., Dec. 1960.
4. W. E. Scott, *The Free Flight Stability of a Liquid Filled Spinning Shell*, Part 1b, BRL Report 1135, Aberdeen Proving Ground, Md., July 1961.
5. AMCP 706-242, Engineering Design Handbook, *Design for Control of Projectile Flight Characteristics*.
6. C. H. Murphy, *On the Stability Criteria of the Kelley-McShane Linearized Theory of Yawing Motion*, BRL Report 853, Aberdeen Proving Ground, Md., April 1953.
7. N. G. Chetaev, *On the Stability of Rotating Movements of a Solid Body the Cavity of Which is Filled With an Ideal Fluid*, December 1960, AD-255 359.
8. E. Widmayer, Jr., and J. R. Reese, *Moments of Inertia and Damping of Fluid in Tanks Undergoing Pitching Oscillations*, NACA RM L53E01a, June 1953.
9. R. N. Arnold and L. Maunder, *Gyrodynamics and Its Engineering Applications*, Academic Press, 1961.

CHAPTER 3

DYNAMICS OF A LIQUID-FILLED PROJECTILE

3-0 LIST OF SYMBOLS*

2a	= diameter of cylindrical cavity	M_{yz}, M_{zx}, M_{xy}	= components of \bar{M} about x-, y-, z- axes, respectively
b	= a constant depending on fill-ratio	M_f	= mass of liquid filler
2b	= diameter of cylindrical air column for a partially filled cylindrical cavity	n	= radial mode number
C	= aerodynamic coefficient	P	= hydrodynamic pressure
Cl	= component of aerodynamic moment of empty projectile	P_b	= pressure due to basic flow
Cm	= component of aerodynamic moment of empty projectile	P	= perturbation pressure
2c	= height of cylindrical cavity	r, θ , z	= cylindrical system of coordinates with the z-axis along the direction of flight
C_1	= Bessel function	S	= $-4D(\tau_{nj}) / (L d e)$ Stewartson's parameter
d	= deceleration of projectile	T	= transverse moment of inertia of empty projectile
$F(\bar{r}, t) = 0$	= equation of surface bounding the liquid	T_e	= "effective" transverse moment of inertia of liquid
$G(\bar{r}, t) = 0$	= equation of a free surface	t	= time
h	= distance from point on axis of projectile to CG; distance between center of cavity and center of rotation	U, V, W	= velocity components of basic flow along r, θ , z, respectively
i	= $\sqrt{-1}$	u, v, w	= velocity components of perturbed flow along r, θ , z, respectively
J_1	= Bessel function	\bar{V}	= flow velocity vector
J	= axial mode number	\bar{V}_b	= velocity vector of basic flow
K	= c/a fineness ratio; a constant	\bar{v}	= perturbation velocity vector
L	= axial (longitudinal) moment of inertia of empty projectile	Y_1	= Bessel function
l, m, n	= components of the unit vector z' along the x-, y-, z- axes, respectively (direction cosines)	x, y, z	= inertial system of coordinates with z-axis along the direction of flight
M	= hydrodynamic moment on projectile	x', y', z'	= body-fixed coordinate system of projectile located at its center of mass with z' -axis along axis of symmetry of projectile
\bar{M}	= hydrodynamic moment vector		

*Dimensions are omitted since there are no engineering applications in this chapter. If the given formulas using these symbols are to be applied, any consistent set of units may be employed.

GREEK LETTERS

α	= yaw angle
β	= $1/s_g$ reciprocal of gyroscopic stability factor

γ	= ωt azimuthal angle
η	= displacement of a free surface
ν	= kinematic viscosity of fluid
ξ	= $1 + \sin$ of yaw, for small yaw ξ is yaw angle
ρ	= density of fluid
τ_n	= ω/Ω nondimensional nutational frequency
τ_0 or τ_{ni}	= ω_{ni}/Ω nondimensional eigenfrequency
τ_p	= nondimensional precessional frequency
Ω	= axial spin rate
ω	= nutational (or precessional) frequency

MATH SYMBOLS

\sim	= approximately
\sim	= of the order
\propto	= proportional

3-4 INTRODUCTION

The dynamic equations of a spinning projectile become very complicated when the projectile is filled with liquid. In fact, it is not generally possible to describe the behavior of a liquid-filled projectile by a simple dynamic equation as Eq. 2-1 for the rigid projectile. The liquid within the cavity of the projectile, as it moves about, exerts pressure forces on the inner walls of the cavity, producing a moment on the projectile. This external moment must be considered in the dynamics of the projectile in a manner similar to the moment due to aerodynamic forces. However, the motion of the liquid and, therefore, the moment produced by this motion are not completely determined by the instantaneous motion of the confining casing but rather by the entire history of the projectile's motion. When, for example, the projectile is at rest, this

does not imply that the liquid within the cavity is at rest; it only implies that, if there is a flow of liquid inside the cavity, the flow velocity near the wall must be directed parallel to the wall.

When the projectile undergoes any motion, it is necessary that the liquid follow this motion to a certain extent. Precisely, the flow must adjust to the motion of the cavity walls so that, at any point on the wall, the flow velocity has a normal component equal to that of the wall. Certainly, these "boundary conditions" are insufficient to determine the state of the fluid motion which is determined by the previous motion of the boundaries as well.

For the reasons given above it is clear that the stability of a liquid-filled projectile depends not only on the design properties of the projectile and the physical properties of the liquid but, in a sense, on the flight history, too. It is possible that a spin-stabilized liquid-filled projectile will be quite stable at the beginning of its trajectory and become suddenly unstable as the liquid within the cavity attains a certain amount of rotation, and vice versa.

From the preceding discussion it should be clear that the dynamics of a liquid-filled projectile system involves an extremely complex interaction between the motion of the casing and the motion of the liquid within the cavity. It is not surprising then that the problem of predicting the dynamic behavior of a liquid-filled projectile can be solved — exactly — only for certain special cases or under very restrictive conditions, or both. Other cases require simplifications and approximations in order to be mathematically tractable.

It is very fortunate that the limitations dictated by mathematical tractability do not greatly restrict the application of the theory to the more important practical problems as, for example, the prediction of stability of the liquid-filled projectile system.

The main limitation of the present theory is the following: it is assumed that the projectile moves with essentially constant speed and eventually spins about its axis of symmetry. Superimposed on this basic translational and rotational motion is a small yawing motion, i.e., only small perturbations about the state of uniform motion of the projectile are considered. The assumption of a small perturbation is completely appropriate when one is concerned with the question of stability. As in the case of a rigid projectile, a liquid-filled projectile is considered unstable when a small perturbation increases in time and, vice versa, the projectile is stable when the perturbed motion is damped. As a consequence of the small perturbation assumption, one can assume that the motion of the liquid consists of an essentially steady basic flow, superimposed on which is an oscillatory flow of small amplitude. The smallness of the superimposed oscillatory flow permits linearization of the equations for the perturbed fluid motion as well as the dynamic equations of the projectile.

The linearization of the fluid dynamic equations is essential for the tractability of the whole problem. While the nonlinear equations for the spinning rigid projectile can be handled, it appears to be quite hopeless to solve the nonlinear fluid dynamic problem.

The division of the flow field into a steady basic flow and a superimposed oscillatory flow is an idealization, justified only under the assumption of small yaw amplitude. When a small yaw can be assumed, then and only then is it possible to treat the basic flow and the superimposed oscillatory flow separately.

The basic flow is generated by the unperturbed motion of the casing, i.e., by its translational and rotational motions. When the projectile spins, the liquid within the cavity is taken along with the walls by friction and starts to rotate. As the time elapses, the liquid acquires more and more rotation until finally all of the liquid rotates with the casing as if it were solid.

The basic flow, thus, consists of a more or less uniform rotation depending on the spin of the projectile and the time elapsed after the firing; it is, however, not affected by an eventual yawing motion of the projectile.

Once the basic flow is given, the superimposed oscillatory flow consequent to the yawing motion of the projectile depends only on this yawing motion, i.e., on the frequency and amplitude of yaw. It should be mentioned that the independence of the oscillatory flow from the previous motion of the projectile rests on the reasonable assumption that both the basic flow and the yaw amplitude are "almost" stationary, i.e., that their characteristic time of change is large compared to the inverse of the yaw frequency.

A consequence of this independence from the previous motion of the projectile is that the moment due to liquid oscillations can be related directly to the instantaneous motion of the projectile. This fact is very important for the writing of the dynamic equations which take the simple form of differential equations only when the acting forces are determined solely by the instantaneous motion, i.e., the yaw angle and its derivatives rather than by previous events.

The period during which the liquid achieves full spin — denoted as the "spin-up" period — is usually short compared with total time of flight. The duration of the spin-up period depends on the liquid viscosity, the geometrical dimensions of the cavity, and on the spin rate itself. Some problems regarding the attainment of liquid rotation and dynamic stability during the spin-up period are discussed in Chapter 8.

For the present it may be sufficient to note that in practice the state of solid rotation is the most important one to consider since the spin-up period is usually rather short. In typical cases, a state of substantially solid rotation is achieved within a distance of a few thousand calibers of travel from the muzzle.

If we omit the earliest part of the projectile's trajectory from present consideration, we can assume that the basic flow of the liquid within the cavity of a spinning projectile is a solid rotation having the angular velocity of the projectile. The superimposed oscillatory flow is regarded as a perturbation about the state of solid rotation. It is again very fortunate that the most important practical case, in which the liquid has achieved full spin, is comparatively simple from the analytical point of view. In fact, if full spin of the liquid is assumed, exact solutions of the stability problem can be obtained for special cavity shapes. The earliest example — Greenhill's solution for the spheroidal cavity — is characterized by mathematical simplicity. However, its practical application is rather limited. The second example — Stewartson's solution for the cylindrical cavity — has become the most important tool for the prediction of stability and the basis on which further refinements have been built. Both of these examples will be discussed in greater detail — Greenhill's solution because of its mathematical simplicity and Stewartson's solution because of its practical relevancy.

3-2 EQUATIONS OF PERTURBED FLUID MOTION

The motion of the liquid within the cavity of the projectile is described by the Navier-Stokes Equations together with certain boundary conditions. Throughout the analysis which follows it is assumed that the liquid is incompressible. Then the Navier-Stokes Equations, in vector notation, reduce to:

$$\frac{\partial \bar{\mathbf{v}}}{\partial t} + \bar{\mathbf{v}} \cdot \nabla \bar{\mathbf{v}} + \nabla p = \nu \nabla^2 \bar{\mathbf{v}} \quad (3-1)$$

$$\nabla \cdot \bar{\mathbf{v}} = 0 \quad (3-2)$$

Here $\bar{\mathbf{v}}$ denotes the flow velocity vector, p the hydrodynamic pressure, ρ the density and ν the kinematic viscosity of the liquid, t the time, and ∇ the differential operator nabla (del) which, in Cartesian coordinates,

is defined as: $\nabla = \left(\frac{\partial}{\partial x}, \frac{\partial}{\partial y}, \frac{\partial}{\partial z} \right)$. The flow velocity vector $\bar{\mathbf{v}}(x,y,z,t)$ and the pressure $p(x,y,z,t)$ must satisfy not only the partial differential Eqs. 3-1 and 3-2 but also the boundary conditions which, in their most general form, are as follows:

- (1) Condition on any surface bounding the liquid (solid wall, free surface, interface): the component of the flow velocity normal to the surface must equal the normal component of the surface velocity.
- (2) Condition on a free surface: the pressure must be constant on a free surface.
- (3) Condition on a solid wall: the tangential component of the flow velocity must equal the tangential component of the velocity of the wall.

Frequently, the term $\nu \nabla^2 \bar{\mathbf{v}}$ in Eq. 3-1, which represents viscous forces, is neglected. With this "inviscid approximation" the boundary condition (3) is disregarded (see pars. 3-2.2 and 3-2.3).

As outlined above, the flow is thought to consist of two parts: (1) an essentially steady basic flow, the components of which may be denoted by $\bar{\mathbf{v}}_b$, p_b , and (2) a small perturbation $\bar{\mathbf{v}}$, p . The basic flow $\bar{\mathbf{v}}_b$, p_b is generated by the undisturbed motion of the cavity walls, i.e., by the simple spinning motion. Thus the basic flow alone is a solution of the Navier-Stokes Equations (viz. the solution with the appropriate boundary conditions imposed by the pure spinning motion of the walls). Inserting the total flow vector $\bar{\mathbf{v}} = \bar{\mathbf{v}}_b + \bar{\mathbf{v}}$ and pressure $p_b + p$ into Eqs. 3-1 and 3-2 and considering that the basic flow $\bar{\mathbf{v}}_b$, p_b solves the equations, one obtains:

$$\frac{\partial \bar{\mathbf{v}}}{\partial t} + \bar{\mathbf{v}} \cdot \nabla \bar{\mathbf{v}}_b + \bar{\mathbf{v}}_b \cdot \nabla \bar{\mathbf{v}} + \nabla p = \nu \nabla^2 \bar{\mathbf{v}} \quad (3-3)$$

$$\nabla \cdot \bar{\mathbf{v}} = 0 \quad (3-4)$$

Here the second order term $\bar{\mathbf{v}} \cdot \nabla \bar{\mathbf{v}}$ has been neglected in accordance with the assumption that the perturbation $\bar{\mathbf{v}}, p$ is small in comparison with $\bar{\mathbf{V}}_b, P_b$.

The boundary conditions (1), (2), and (3) apply, naturally, to the sum of the two flow fields: $\bar{\mathbf{V}}_b \pm \bar{\mathbf{v}}, P_b \pm p$.

The basic flow velocity $\bar{\mathbf{V}}_b$ which occurs in Eq. 3-3 is not yet specified, except that $\bar{\mathbf{V}}_b$ must solve the Navier-Stokes Equations. As stated before, $\bar{\mathbf{V}}_b$ may be a rigid rotation about the spin axis, a motion which is actually attained after a sufficiently long time after firing. Whatever the basic flow is, it must be specified before the perturbed motion can be computed.

3-21 INVISCID APPROXIMATION

In the previous paragraph the equations of perturbed fluid motion are derived in full generality for future application. Here an important simplification of the general equations will be considered, namely, the equations of inviscid flow, which result when the viscous term on the right hand side of Eq. 3-3 is neglected. The resulting inviscid equations are substituted for the full viscous equations on the usual assumption that the viscous, or frictional, forces which are represented by the term on the right hand side of Eq. 3-3 are negligibly small.

It should be emphasized at this point that although viscosity plays an important role in the attainment of liquid spin, it may — and frequently does — have a negligible influence on the oscillatory motion of the liquid. But even when the influence of viscosity on the oscillatory motion is not negligible, the inviscid solution provides an approximation which can be improved by the methods discussed in Chapter 6. Accordingly, throughout the following paragraphs of this chapter the liquid within the cavity of the projectile is considered as inviscid, i.e., the viscous term $\nu \nabla^2 \bar{\mathbf{v}}$ in Eq. 3-3 is neglected.

In conjunction with the reduction of the second order viscous equations to first order inviscid equations, the boundary conditions reduce to conditions (1) and (2) of par. 3-2.

An equivalent formulation of the boundary conditions (1) and (2) can be given as follows:

- (1) If $F(\bar{\mathbf{r}}, t) = 0$ is the equation of a surface bounding the liquid, the condition on $F(\bar{\mathbf{r}}, t) = 0$ is

$$\frac{\partial F}{\partial t} + \bar{\mathbf{V}} \cdot \nabla F = 0 \quad \text{when } F(\bar{\mathbf{r}}, t) = 0 \quad (3-5)$$

- (2) If $G(\bar{\mathbf{r}}, t) = 0$ is the equation of a free surface, the condition is

$$P = P_b \pm p = 0 \quad \text{when } G(\bar{\mathbf{r}}, t) = 0 \quad (3-6)$$

Eq. 3-5 is a consequence of the boundary condition (1): a fluid particle which at time t is located at a point $\bar{\mathbf{r}}$ of a bounding surface moves so that at time $t + dt$ its location $\bar{\mathbf{r}} + \bar{\mathbf{V}} dt$ is again on the bounding surface; i.e., when $F(\bar{\mathbf{r}}, t) = 0$, it follows that $F(\bar{\mathbf{r}} + \bar{\mathbf{V}} dt, t + dt) = 0$ or $\frac{\partial F}{\partial t} + \bar{\mathbf{V}} \cdot \nabla F = 0$.

3-22 EQUATIONS OF PERTURBED FLUID MOTION IN CYLINDRICAL COORDINATES

Cavities of liquid-filled projectiles have, with rare exceptions, the shape of bodies of revolution with a symmetry axis coincident with the symmetry axis of the projectile. It is convenient, therefore, to introduce a cylindrical system of coordinates (r, θ, z) such that the z -axis is along the direction of flight which, for zero yaw, coincides with the spin — and symmetry axis. Here r is the radial distance from the axis and θ is the polar angle. The velocity components of the basic flow and the perturbation in the (r, θ, z) system are, respectively:

$$\bar{\mathbf{V}}_b = (U, V, W) \quad \text{and} \quad \bar{\mathbf{v}} = (u, v, w).$$

The origin of the coordinate system (r, θ, z) is fixed to the moving projectile, i.e., the coordinate system is assumed to move uniformly but not to rotate with the projectile. (Rotating coordinates are introduced by Stewartson' and other authors; such coordinates offer slight advantage when the basic flow \bar{V}_b is a solid rotation. For economic use of notation and to avoid confusion, rotating coordinates will not be used in the analysis which follows unless it is explicitly so stated.)

When the cavity is a body of revolution, it is possible to specify, to a certain extent, the basic flow \bar{V}_b . Obviously, because of the rotational symmetry of the cavity, the generated flow field must have rotational symmetry, i.e., V_b must be independent of the polar angle θ . Moreover, as is shown in Chapter 8, \bar{V}_b is also independent of z and only its circumferential component V is different from zero. Thus the basic flow reduces to only one component which depends on r and t only:

$$\bar{V}_b = (0, V(r, t), 0). \quad (3-7)$$

It can also be shown (see Chapter 8) that $V(r, t)$ depends only very weakly on time, so that $V(r, t)$ undergoes a negligibly small change during each cycle of the yawing motion of the projectile. Consequently, V may be treated as quasi-steady, i.e., the time dependence of V may be ignored as far as the solution of Eqs. 3-3 and 3-4 is concerned. With V specified in this way, and with viscous terms neglected, Eqs. 3-3 and 3-4 become, in cylindrical coordinates

$$\frac{\partial u}{\partial t} + \frac{V}{r} \frac{\partial u}{\partial \theta} - \frac{2V}{r} v + \frac{\partial p/\rho}{\partial r} = 0 \quad (3-8)$$

$$\frac{\partial v}{\partial t} + \frac{V}{r} \frac{\partial v}{\partial \theta} + \left(\frac{dV}{dt} + \frac{V}{r} \right) u + \frac{1}{r} \frac{\partial p/\rho}{\partial \theta} = 0 \quad (3-9)$$

$$\frac{\partial w}{\partial t} + \frac{V}{r} \frac{\partial w}{\partial \theta} + \frac{\partial p/\rho}{\partial z} = 0 \quad (3-10)$$

$$\frac{\partial u}{\partial r} + \frac{u}{r} + \frac{1}{r} \frac{\partial v}{\partial \theta} + \frac{\partial w}{\partial z} = 0 \quad (3-11)$$

With \bar{V}_b specified by Eq. 3-7, the boundary conditions, Eqs. 3-5 and 3-6, become in cylindrical coordinates

$$\frac{\partial F}{\partial t} + u \frac{\partial F}{\partial r} + (V + v) \frac{1}{r} \frac{\partial F}{\partial \theta} + w \frac{\partial F}{\partial z} = 0$$

when $F(r, \theta, z, t) = 0 \quad (3-12)$

$$P = P_b + p = 0 \text{ when } G(r, \theta, z, t) = 0 \quad (3-13)$$

3-2.3 BOUNDARY CONDITIONS IMPOSED BY THE YAWING MOTION OF THE PROJECTILE

An explicit formulation of the boundary conditions of perturbed fluid motion can be given only when the shape of the cavity and the motion of the projectile are known. It is, however, possible to compile the boundary conditions in a rather general form which can be easily adapted to cases of special interest.

It is assumed that the cavity has rotational symmetry and that the spinning projectile performs a pure nutational or precessional motion. (The general yawing motion can always be made up from each pure motion — nutation and precession — by superposition. It is thus sufficient here to consider a pure circular motion which can be either nutation or precession.)

The liquid is assumed to rotate, initially, with velocity $V(r)$ about the axis of symmetry. Obviously, $V(r)$ satisfies the boundary conditions for zero yaw. When, however, the projectile undergoes a small yawing motion in addition to its spin, a pure rotation of the liquid is no longer compatible with the boundary conditions. The perturbed motion of the projectile is communicated, through the cavity walls, to the rotating liquid, causing it to perform a perturbed motion also.

To describe the yawing motion of the cavity walls, it is convenient to introduce two coordinate systems. (For the benefit of those who wish to study the original

Stewartson's paper¹ and to follow more detailed development by Ash and Gundersen⁶ we shall follow Stewartson's notation and his coordinate system. This differs from that of Chapter 2 in that the z -axis lies along the axis of symmetry of the projectile rather than the x -axis as in Chapter 2.) The two coordinate systems are: inertial system (x,y,z) where the z -axis lies along the direction of flight, and a body-fixed coordinate system (x',y',z') so that z' lies along the axis of symmetry of the projectile. The (x',y',z') system is obtained when the (x,y,z) system is rotated by the

amount and in the direction of the yaw angle α .

The relations which follow are most easily derived by referring to Fig. 3-1. In this figure the z -axis is shown upward and the z' -axis forms the yaw angle α with the z -axis. (In order not to confuse the diagram, the x',y' -axes are not shown.) Also shown in Fig. 3-1 is the unit vector \bar{z}' which points into the direction of the z' -axis. The projections of \bar{z}' on the (x,y,z) -axes are, respectively: $(l,m,n) = (\sin \alpha \cos \gamma, \sin \alpha \sin \gamma, \cos \alpha)$ where γ is the azimuthal

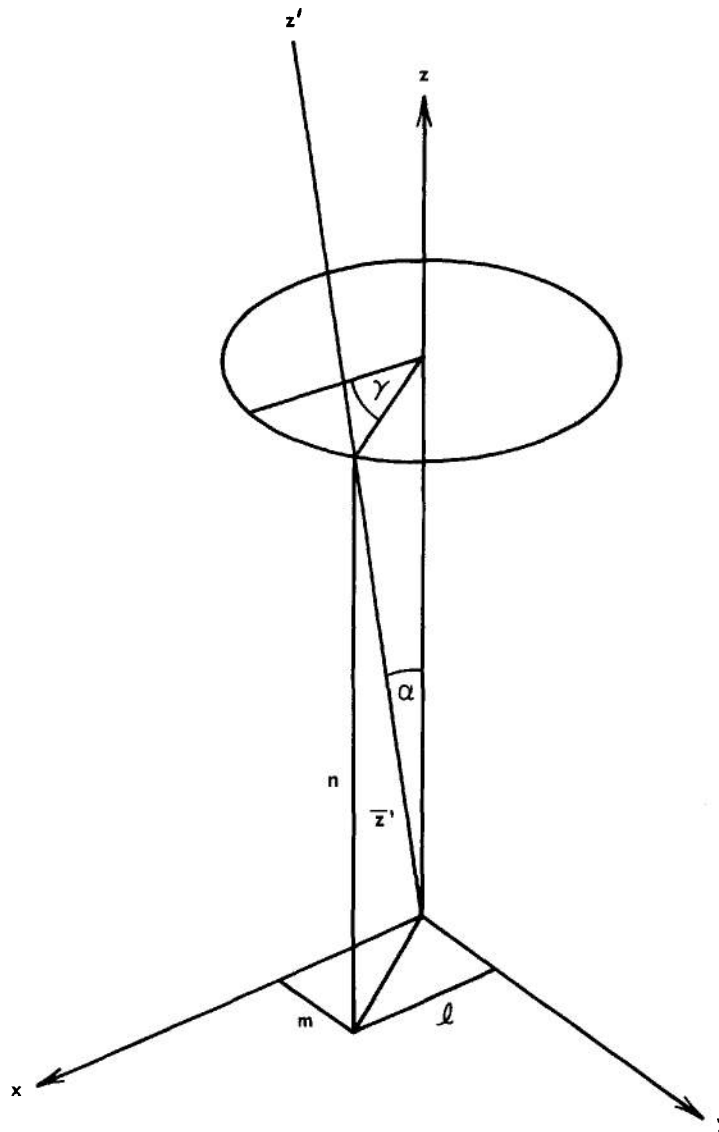


FIGURE 3-1. SCHEMATIC OF COORDINATES

angle shown in the figure. (It may be noted that in the notation of Chapter 2, v/V , $m = w/V$, and $n = u/V$ where V is the velocity of the projectile and u, v, w , are its velocity components on the projectile-fixed coordinate system.) If now the projectile precesses (or nutates) with the precessional (or nutational) frequency ω , the end point of the unit-vector \bar{z}' describes a circle as indicated in the diagram and the azimuthal angle γ changes according to the relation: $\gamma = \omega t$. The components of the unit vector \bar{z}' are then

$$z' = (l, m, n) = (\sin \alpha \cos \omega t, \sin \alpha \sin \omega t, \cos \alpha).$$

In accordance with the assumption that the yaw angle α is very small compared to unity, it is permissible to neglect terms of the second and higher orders in α , i.e.,

$$(l, m, n) = (\alpha \cos \omega t, \alpha \sin \omega t, 1) \quad (3-14)$$

The transformation rules between the (x, y, z) -system and the (x', y', z') -system are (neglecting terms of higher than first order)

$$\begin{aligned} x' &= x - \alpha y \\ y' &= y + \alpha x \\ z' &= z + \alpha (lx + my) \end{aligned} \quad (3-15)$$

The liquid within the cavity of the projectile is bounded by the solid walls of the cavity and — if the cavity is only partially filled — by a free surface. In the analysis which follows it is assumed that the liquid is rotating sufficiently rapidly so that the free surface — prior to perturbation — is a cylinder parallel to the axis of symmetry. (In other words, gravity and deceleration are assumed to be negligible in comparison with the centripetal forces.)

The boundary condition on the cavity surface can be derived from Eq. 3-12. For a cavity of rotational symmetry, the equation of the cavity surface in body-fixed coordinates is

$$r'^2 = x'^2 + y'^2 = R^2(z') = 0 \quad (3-16)$$

where $R(z')$ is the cavity radius at z' . The same equation in space-fixed coordinates (x, y, z) is obtained by substituting x', y' and z' according to Eq. 3-15. Neglecting, again, higher order terms and considering that

$R^2(z + \alpha (lx + my)) = R^2(z) + \frac{dR^2}{dz}(\alpha (lx + my)) + \text{higher order terms}$, we obtain

$$\begin{aligned} x^2 + y^2 - R^2(z) - \left(2z + \frac{dR^2}{dz}\right) \alpha (lx + my) &= 0 \end{aligned} \quad (3-17)$$

Finally, Eq. 3-17 may be expressed in polar coordinates (r, θ, z) . It is

$$x = r \cos \theta; \quad y = r \sin \theta \quad (3-18)$$

Substituting for x, y according to Eq. 3-18 and for l, m according to Eq. 3-14 yields

$$\begin{aligned} lx + my &= \alpha r \cos(\omega t - \theta) \\ x^2 + y^2 &= r^2 \end{aligned} \quad (3-19)$$

With Eq. 3-19, Eq. 3-17 becomes

$$r^2 - R^2(z) - \alpha \left(2z + \frac{dR^2}{dz}\right) r \cos(\omega t - \theta) = 0 \quad (3-20)$$

Eq. 3-20 is the differential equation of the cavity surface in space-fixed polar coordinates. The boundary condition on the cavity wall can now be easily derived by substituting the left-hand side of Eq. 3-20 for $F(r, \theta, z, t)$ in Eq. 3-12.

Considering that the perturbation velocity components (u, v, w) are — like the yaw angle α — small compared to the basic flow (U, V, W) and neglecting higher than the first order terms, one obtains

$$\begin{aligned} 2ru - \frac{dR^2}{dz} w &= \alpha r \left(\frac{V}{r} - \omega\right) \left(2z + \frac{dR^2}{dz}\right) \sin(\omega t - \theta) \end{aligned} \quad (3-21)$$

when $r = R(z)$

In accordance with the linearization and neglect of higher order terms, the boundary conditions, Eq. 3-21, will be satisfied on the cavity surface of the undisturbed spinning projectile, i.e., at $r = R(z)$.

3-2.4 BOUNDARY CONDITIONS ON A FREE SURFACE

To determine the boundary conditions on the free surface of the liquid, it is important to remember that the free surface is displaced relative to its undisturbed position. It can, however, be assumed that the displacement is small.

For the undisturbed projectile, the free surface is assumed to be a cylinder parallel to the axis, its equation being $r = b$ where b is a constant depending on the fill-ratio. The displaced free surface, then, is given by the equation

$$r = b + \eta(\theta, z, t)$$

$$\text{or } G(r, \theta, z, t) = r - b - \eta(\theta, z, t) = 0 \quad (3-22)$$

where η is the displacement of the free surface from its equilibrium position. It can be assumed that $\eta/b \ll 1$.

Since the free surface $G(r, \theta, z, t) = 0$ is a surface bounding the liquid, $G(r, \theta, z, t)$ must satisfy Eq. 3-12, i.e.,

$$\frac{\partial G}{\partial t} + u \frac{\partial G}{\partial r} + \left(\frac{V + v}{r} \right) \frac{\partial G}{\partial \theta} + w \frac{\partial G}{\partial z} = 0 \quad (3-23)$$

Substituting Eq. 3-22 into Eq. 3-23 and neglecting higher order terms, we obtain a condition for η

$$\frac{\partial \eta}{\partial t} + \frac{V}{r} \frac{\partial \eta}{\partial \theta} = u \quad (3-24)$$

The dynamic condition on the free surface, Eq. 3-13, becomes

$$P_b(b + \eta) + p(b + \eta) = 0$$

or, neglecting higher order terms

$$P_b(b) + \eta \left(\frac{\partial P_b}{\partial r} \right) + p(b) = 0 \quad (3-25)$$

According to the dynamic equations

$$\frac{\partial P_b}{\partial r} = \rho \frac{V^2}{r} \quad (3-26)$$

Eq. 3-26 evaluated at $r = b$ and substituted in Eq. 3-25 gives

$$P_b(b) + \rho \frac{V^2(b)}{b} \eta + p(b) = 0 \quad (3-27)$$

Finally, η can be eliminated by applying the operator $\frac{d}{dt} + \frac{V}{r} \frac{\partial}{\partial \theta}$ to Eq. 3-27. One obtains

$$\frac{V^2(b)}{b} u + \frac{1}{\rho} \left(\frac{\partial p}{\partial t} + \frac{V}{r} \frac{\partial p}{\partial \theta} \right) = 0, \quad \text{when } r = b \quad (3-28)$$

Eq. 3-28 is the boundary condition on a free surface of the rotating liquid. In contrast to the boundary condition on the cavity wall, Eq. 3-28 is a homogeneous boundary condition, i.e., the yaw angle σ_y does not enter into it.

3-3 REACTION OF THE LIQUID UPON THE PROJECTILE

The dynamics of a liquid-filled projectile involve a coupling of the equations of fluid motion and the equations of yawing motion of the projectile. Precisely, the fluid motion depends on the motion of the projectile and the motion of the projectile depends on the reaction of the fluid motion. To uncouple the two sets of equations it is assumed that the liquid-filled Projectile describes a yawing motion of the same type as a rigid projectile. In combined motion, however, the frequency and damping rate may be changed relative to the values for the rigid

projectile. Thus the first step is to compute the fluid motion consequent to a yawing motion of — for the present — an unspecified frequency and damping rate. Once the fluid motion is known, the reaction of the liquid can be computed and introduced into the equations of yawing motion. Finally the equations of yawing motion yield a condition for frequency and damping rate of the liquid-filled projectile system.

3-3.1 MOMENTS DUE TO THE LIQUID

The perturbed fluid motion produces pressure forces on the cavity surface which in turn give rise to a moment on the projectile. When the pressure P is known, the resulting hydrodynamic moment \bar{M} is found by integration:

$$\bar{M} = \iint_A P \bar{r} \times d\bar{A} \quad (3-29)$$

where $d\bar{A}$ denotes the vectorial surface element (pointing in a direction normal to the surface and away from the inside), \bar{r} is the radial vector from the moment-reference point to the surface element, and $\bar{r} \times d\bar{A}$ is the cross-product between \bar{r} and $d\bar{A}$. The integral is taken over the wetted part of the cavity surface.

The components of \bar{M} may be denoted by $\bar{M} = (M_{yz}, M_{zx}, M_{xy})$ where, for example, M_{zx} is a moment about the y -axis which is directed so that — for positive M_{zx} — it tends to turn the z -axis toward the direction of the x -axis. (The use of double subscripts (yz, zx, xy) instead of (x, y, z) is convenient here as it designates the direction of the torque and also accounts for the fact that \bar{M} is really an antisymmetric tensor with components $M_{yz} = -M_{zy}$, etc.)

(M_{yz}, M_{zx}, M_{xy}) are the components of \bar{M} in the inertial system (x, y, z). In practice it is easier to compute the components of \bar{M} in the body-fixed coordinate system (x', y', z'). Let the components of \bar{M} in the body-fixed system be: $(M'_{yz}, M'_{zx}, M'_{xy})$. Then,

since \bar{M} is of first order in α , we find that, within first order

$$M'_{yz} = M_{yz}; \quad M'_{zx} = M_{zx}; \quad M'_{xy} = M_{xy}.$$

Thus, we can use the components of \bar{M} in the primed system as the components in the unprimed system.

Of special interest is the cavity of rotational symmetry. Assume that the shape of the cavity surface is given by an equation $r' = R(z')$. Then for $z_1 < z' < z_2$ the integral, Eq. 3-29, assumes the special form

$$M_{zx} = \int_{z_1}^{z_2} \int_0^{2\pi} P \left(z' + R \frac{dR}{dz'} \right) R \cos \theta' d\theta' dz' \quad (3-30)$$

$$M_{yz} = \int_{z_1}^{z_2} \int_0^{2\pi} P \left(z' + R \frac{dR}{dz'} \right) R \sin \theta' d\theta' dz' \quad (3-31)$$

$$M_{xy} = 0 \quad (3-32)$$

If $\frac{dR}{dz'}$ becomes infinite, as is the case at a plane endwall of the cavity, the expressions on the right-hand sides of Eqs. 3-30 and 3-31 degenerate. Let us assume, for example, that the cavity has a plane endwall at $z' = z_1$ and let us denote the portion of the moments contributed by the plane endwall by $(M_{zx})_{z_1}$ and $(M_{yz})_{z_1}$, respectively. Then, considering that $R(z') = r'$, $\frac{dR}{dz'} dz' = dr'$, we may write

$$(M_{zx})_{z_1} = \int_0^{R(z_1)} \int_0^{2\pi} P r'^2 \cos \theta' d\theta' dr' \quad (3-30a)$$

$$(M_{yz})_{z_1} = \int_0^{R(z_1)} \int_0^{2\pi} P r'^2 \sin \theta' d\theta' dr' \quad (3-31a)$$

3-3.2 EQUATIONS OF YAWING MOTION

The dynamic equations of the yawing motion of a liquid-filled projectile have a similar form as the corresponding equations of a rigid projectile (Eq. 2-23); the only difference being that the moments due to liquid oscillations must be included in the "external" moment. Thus, the dynamic equations may be written

$$T \frac{d^2 \xi}{dt^2} + L \Omega \frac{d \xi}{dt} - C \xi = M_{zx} \quad (3-33)$$

$$T \frac{d^2 \eta}{dt^2} + L \Omega \frac{d \eta}{dt} - C \eta = M_{yz} \quad (3-34)$$

where C_x , C_y are the components of the aerodynamic moment, T and L the transverse and longitudinal moments of inertia of the empty projectile, respectively, and Ω the spin frequency. M_{zx} and M_{yz} are the moments due to the liquid as defined by Eqs. 3-30 and 3-31.

Eqs. 3-33 and 3-34 can be combined as usual into one complex equation. Writing $\xi + i\eta = \xi$; $M_{zx} + iM_{yz} = M$ gives

$$T \frac{d^2 \xi}{dt^2} + iL\Omega \frac{d \xi}{dt} - C \xi = M \quad (3-35)$$

3-4 NONSPINNING LIQUID

The assumption of a nonspinning liquid seems to be relevant only in connection with a nonspinning projectile. For a spinning projectile, the fluid near the wall attains spin quite rapidly, a fact that precludes the assumption of nonspinning liquid. In typical cases the liquid has achieved about 10% of spin when the projectile leaves the muzzle (see Ch. 5).

For a nonspinning projectile, however, the assumption of nonspinning liquid is valid and the results outlined in the paragraphs which follow are applicable.

The effects of a nonspinning liquid on the dynamics of a projectile are summarized in pars. 3-4.1 and 3-4.2.

3-4.1 COMPLETELY FILLED CAVITY

When the cavity is completely filled so that no free surface is formed, the presence of the liquid only influences the weight, center of gravity, and moments of inertia of the projectile. The proper weight and center of gravity of the projectile-liquid system are to be taken just as though the liquid were replaced by a solid of identical specific weight. The moments of inertia, however, are different from those which one would obtain by treating the liquid as a solid. The liquid follows less than a solid the yawing or pitching motion of the projectile and, therefore, contributes less to the moments of inertia than a solid of equal weight occupying the same volume. The presence of the liquid can be accounted for by attributing to the liquid "effective" moments of inertia. The effective moments are fractions of the rigid moments of inertia.

The inviscid liquid within a spherical cavity, for example, is not constrained to follow any rotation of the casing about the center; therefore, all effective moments of inertia taken about the center are zero. Similarly, for a liquid-filled cavity of rotational symmetry, the effective moment of inertia about the symmetry-axis is zero. Once the effective moments about a certain point are given, one can recompute their values for any other point in the same way as for a solid.

In particular, if the effective transverse moment of inertia about the center of gravity is T_e , the effective transverse moment about a point on the axis at a distance h from the center of gravity is: $(T_e)_h = T_e + M_l h^2$, where M_l is the mass of the liquid.

If necessary, the effective moments of inertia can be computed by methods outlined in the following. An example is given

in par. 3-6 for the spheroidal cavity. Generally, a computation of the moments of inertia is not necessary since the stability of a nonspinning projectile does not depend on it. Moreover, the contribution of the liquid to the total moments of inertia is usually very small. For the stability of a nonspinning projectile, it is necessary and sufficient that the center of gravity lies ahead of the center of pressure. For the design of a stable projectile, therefore, the shift of the center of gravity due to the liquid should be calculated.

3-4.2 PARTIALLY FILLED CAVITY

When the cavity is only partially filled, the reaction of the liquid upon the yawing motion of the projectile is less simple. Some time after firing the liquid forms a free surface, the shape of which depends on the joint action of gravity and deceleration. (Immediately after firing, the liquid is likely to undergo a violent splashing motion which, however, subsides quickly by the action of strong deceleration.) If we assume that the deceleration of the projectile is many times larger than gravity, the action of gravity may be neglected. The liquid, then, moves into the most forward position and forms — prior to perturbation — a plane free surface which is perpendicular to the direction of deceleration, i.e., the direction of flight.

The yawing motion of the projectile causes oscillations of the liquid with waves forming on the free surface (analogous to gravity waves). Usually the mass of the liquid is relatively small and hence the reaction of the wave motion on the casing is negligible. An exception arises when the yaw frequency is close to a natural frequency of free oscillation of the liquid. In this case the wave amplitude can rise very high and cause a noticeable interaction with the casing. (For the basic mode of free oscillation the natural frequency is roughly $\omega_0 = 2\pi n_0 = \sqrt{d/a}$ where d is the deceleration of the projectile, and $2a$ the diameter of the cavity at the location of the

free surface.) Due to the strong interaction at resonance, the yawing frequency may be shifted somewhat. However, in contrast to the case of a rotating liquid, the oscillatory motion has no detrimental effect on the stability of the projectile. In any instance of instability, energy is transferred to the perturbed motion. When aerodynamic forces are not destabilizing, the perturbation energy must have its origin in the projectile-liquid system itself. However, if the projectile and liquid have no spin, the energy of the unperturbed system is at its lowest value and hence no energy can be transferred to the perturbation. This is different for the spinning projectile where a large amount of rotational energy is stored in the system.

3-4.3 COMPUTATION OF EFFECTIVE MOMENTS OF INERTIA

For a nonspinning liquid the equations of perturbed fluid motion, Eqs. 3-3 and 3-4, reduce to

$$\frac{\partial \mathbf{v}}{\partial t} + \nabla \frac{p}{\rho} = 0 \quad (3-36)$$

$$\nabla \cdot \mathbf{v} = 0 \quad (3-37)$$

In order to compute the perturbed flow, it is often convenient to eliminate \mathbf{v} . Taking the divergence of Eq. 3-36 and making use of Eq. 3-37 yields

$$\nabla^2 p = 0 \quad (3-38)$$

In polar coordinates Eq. 3-38 reads

$$\frac{\partial^2 p}{\partial r^2} + \frac{1}{r} \frac{\partial p}{\partial r} + \frac{1}{r^2} \frac{\partial^2 p}{\partial \theta^2} = 0 \quad (3-39)$$

In the discussion which follows some basic results for cavities of rotational symmetry are presented. It is assumed that the cavity is given — in body-fixed coordinates — by an equation: $r'^2 = x'^2 + y'^2 = R^2(z')$ or, according to Eq. 3-17, in space-fixed coordinates

$$F(r, \theta, z, t) = r^2 - R^2(z) - (2z + \frac{dR^2}{dz})r(1 \cos \theta + m \sin \theta) = 0 \quad (3-40)$$

The boundary conditions follow when Eq. 3-40 is substituted in Eq. 3-12 and second order terms are neglected

$$(1 \cos \theta + m \sin \theta)(z + R \frac{dR}{dz}) = u - w \frac{dR}{dz} \quad (3-41)$$

when $r = R(z)$

Taking the derivative of Eq. 3-41 with respect to t and substituting

$$\frac{\partial u}{\partial t} = -\frac{1}{\rho} \frac{\partial p}{\partial x} \quad \text{and} \quad \frac{\partial w}{\partial t} = -\frac{1}{\rho} \frac{\partial p}{\partial z}$$

according to Eq. 3-36 yields the following condition for p

$$(\ddot{t} \cos \theta + \ddot{m} \sin \theta) \left(z + R \frac{dR}{dz} \right) = \frac{1}{\rho} \left(\frac{dR}{dz} \frac{\partial p}{\partial z} - \frac{\partial p}{\partial r} \right) \quad (3-42)$$

when $r = R(z)$

The form of Eq. 3-42 of the boundary condition and the differential equation, Eq. 3-39, suggest that the factor $(\ddot{t} \cos \theta + \ddot{m} \sin \theta)$ should be separable from the solution of p . Thus, the solution is sought in the form

$$p = -\rho(\ddot{t} \cos \theta + \ddot{m} \sin \theta) \cdot f(r, z) \quad (3-43)$$

where $f(r, z)$ satisfies the equation

$$\frac{\partial^2 f}{\partial r^2} + \frac{1}{r} \frac{\partial f}{\partial r} - \frac{f}{r^2} + \frac{\partial^2 f}{\partial z^2} = 0 \quad (3-44)$$

and the boundary condition

$$\left(z + R \frac{dR}{dz} \right) = \left(\frac{\partial f}{\partial r} - \frac{dR}{dz} \frac{\partial f}{\partial z} \right) \quad (3-45)$$

when $r = R(z)$

The fluid dynamic problem thus is reduced to the problem of solving Eq. 3-44 with

boundary condition Eq. 3-45 for the function f of the two variables r and z . Further computation of flow and pressure fields can be performed only when the shape of the cavity, i.e., the function $r = R(z)$, is given. As an example, the solution of Eqs. 3-44 and 3-45 for the spheroidal cavity is given in par. 3-5. Without the final determination of $f(r, z)$, an important result can be derived from Eq. 3-43. Substituting Eq. 3-43 into Eqs. 3-30 and 3-31, one obtains

$$M_{zx} = -\ddot{t} T_e, \quad M_{yz} = -\ddot{m} T_e \quad (3-46)$$

$$\text{with } T_e = \rho \pi \int_{z_1}^{z_2} f(a, z) \left[z + R \frac{dR}{dz} \right] R dz \quad (3-47)$$

The components of the moment, according to Eq. 3-46, are proportional to the acceleration of the corresponding components of the yaw angle. Substituting Eq. 3-46 into Eq. 3-35 yields

$$(\ddot{T} + T_e) \ddot{\xi} - i \Omega L \xi - C \xi = 0 \quad (3-48)$$

Eq. 3-48 shows that the reaction of the liquid upon the projectile can be described by attributing to the liquid an "effective" moment of inertia T_e given by Eq. 3-47.

This result is derived here for the approximate linearized equations of motion but it is valid also within the exact theory, as shown by Zhukovskii⁴ in 1948.

3-5 SPINNING LIQUID

3-5.1 INTRODUCTION

Except for a short "spin-up" period the liquid within the cavity of a spinning projectile can be assumed to rotate with the projectile as if solid. For this state of solid rotation, the equations of perturbed fluid motion assume a particularly simple form.

Setting $V = \Omega r$, where Ω is the axial spin, Eqs. 3-8 to 3-11 reduce to

$$\frac{\partial}{\partial t} \left(\frac{\partial v}{\partial r} + \frac{v}{r} \right) - 2\Omega u + \frac{1}{r} \frac{\partial p}{\partial r} = 0 \quad (3-49)$$

$$\frac{\partial v}{\partial t} + \Omega \frac{\partial v}{\partial \theta} + 2\Omega u + \frac{1}{r} \frac{\partial p}{\partial \theta} = 0 \quad (3-50)$$

$$\frac{\partial w}{\partial t} + \Omega \frac{\partial w}{\partial \theta} + \frac{\partial p}{\partial z} = 0 \quad (3-51)$$

$$\frac{\partial u}{\partial r} + \frac{u}{r} + \frac{1}{r} \frac{\partial v}{\partial \theta} + \frac{\partial w}{\partial z} = 0 \quad (3-52)$$

As for the perturbed motion of the non-spinning liquid (par. 3-4), solutions of Eqs. 3-49 to 3-52 are sought by the method of separation of variables. In the nonspinning case, it was possible to separate from the solution the t - and θ -dependence in form of a factor $(i \cos \theta + \dot{m} \sin \theta)$ (see Eq. 3-43). It can be shown that in the case of a spinning liquid a separation of the t - and θ -dependence is not possible except for special motions of the projectile. The special motions for which separation is possible are described by

$$(1 + im) = \alpha_0 e^{i\omega t} \quad (3-53)$$

where ω may be complex, while α_0 — the initial yaw angle — is a real constant. For complex ω , i.e., if $\omega = \omega_R + i\omega_I$, Eq. 3-53 describes a damped ($\omega_I > 0$) or undamped ($\omega_I < 0$) nutational or precessional motion. It is well known that the actual yawing motion of a spin-stabilized solid projectile is of the type given by Eq. 3-53 and, it will be shown later, that the presence of the liquid does not alter the character of the motion although it may alter the frequencies of nutation and precession and — most noteworthy — the damping rates.

Although the particular motions, Eq. 3-53, suffice to describe the stability behavior of the projectile, it should be mentioned that any motion can be represented as superposition of particular motions so that the expressions, Eq. 3-53, may be considered as Fourier components of the

general motion. For example, a pure pitching motion at fixed frequency ω is $l = \alpha_0 \cos \omega t$, $m = 0$. This pitching motion is obtained by superposition of two precessional motions with frequencies ω and $-\omega$: $(1 + im) = \alpha_0 \cos \omega t = \frac{1}{2} (\alpha_0 e^{i\omega t} + \alpha_0 e^{-i\omega t})$.

Due to the linearity of the perturbation equations, the perturbed flow and the moments on the casing consequent to the general yawing motion can be obtained by superposition of the particular flows and moments, respectively.

3-5.2 THE BOUNDARY VALUE PROBLEM

In this paragraph some basic results are presented which rest on the following assumptions:

- (1) The cavity has the shape of a body of revolution; the equation of the cavity surface is: $r' = R(z')$
- (2) The liquid has achieved full spin, $V = \Omega r$
- (3) If the cavity is only partially filled, the liquid forms — prior to perturbation — a cylindrical free surface. The equation of the free surface is $r = b$; the radius of the cavity $R(z')$ is everywhere larger than the radius of the void b .
- (4) The projectile describes a yawing motion of the type: $l + im = \alpha_0 e^{i\omega t}$.

The boundary value problem can be formulated most conveniently using complex notation. It is understood that, when complex notation is used, only the real part of an expression shall have physical significance; exceptions are equations like 3-35 and 3-53 where two real components of a vector are united into one complex quantity $(l + im)$, etc. Under the assumptions (1) to (4) the boundary conditions — Eqs. 3-21 and 3-28 — assume the special form

$$\left(u - \frac{dR}{dz} w \right) = -i\alpha (\Omega - \omega) \left(z + R \frac{dR}{dz} \right) e^{i(\omega t - \theta)} \quad \text{when } r = R(z) \quad (3-54)$$

$$\Omega^2 bu + \frac{1}{\rho} \left(\frac{\partial p}{\partial t} + \Omega \frac{\partial p}{\partial \theta} \right) = 0 \quad (3-55)$$

when $r = b$

The above boundary conditions suggest that the solution of Eqs. 3-49 to 3-52 is of the form

$$\left. \begin{aligned} u &= \underline{u}(r, z) e^{i(\omega t - \theta)} \\ v &= \underline{v}(r, z) e^{i(\omega t - \theta)} \\ w &= \underline{w}(r, z) e^{i(\omega t - \theta)} \\ \frac{p}{\rho} &= f(r, z) e^{i(\omega t - \theta)} \end{aligned} \right\} \quad (3-56)$$

In terms of these quantities, Eqs. 3-41 to 3-52 can be put into the following form

(writing: $f' = \frac{\partial f}{\partial r}$, $f_z = \frac{\partial f}{\partial z}$):

$$-i\underline{u} = \frac{(\Omega - \omega)f' + 2\Omega f/r}{4\Omega^2 - (\Omega - \omega)^2} \quad (3-57)$$

$$\underline{v} = \frac{2\Omega f' + (\Omega - \omega)f/r}{4\Omega^2 - (\Omega - \omega)^2} \quad (3-58)$$

$$\underline{w} = -i \frac{f_z}{\Omega - \omega} \quad (3-59)$$

$$\frac{\partial^2 f}{\partial r^2} + \frac{1}{r} \frac{\partial f}{\partial r} - \frac{f}{r^2} - \left[\frac{4\Omega^2}{(\Omega - \omega)^2} - 1 \right] \frac{\partial^2 f}{\partial z^2} = 0 \quad (3-60)$$

The boundary conditions, Eqs. 3-54 and 3-55, become

$$\begin{aligned} & \frac{(\Omega - \omega)f' + 2\Omega f/r}{4\Omega^2 - (\Omega - \omega)^2} + \frac{dR}{dz} \frac{f_z}{(\Omega - \omega)} \\ &= -\alpha (\Omega - \omega) \left(z + R \frac{dR}{dz} \right) \end{aligned} \quad (3-61)$$

when $r = R(z)$

$$\Omega^2 b \frac{(\Omega - \omega)f' + 2\Omega f/r}{4\Omega^2 - (\Omega - \omega)^2} - (\Omega - \omega)f = 0 \quad (3-62)$$

when $r = b$

As a special case we consider the boundary condition on the walls of a cylindrical cavity with radius a and two plane endwalls at $z = z_1, z_2$. At the cylindrical sidewalls the boundary condition is: $\frac{dR}{dz} = 0$ and Eq. 3-61 becomes

$$\frac{(\Omega - \omega)f' + 2\Omega f/r}{4\Omega^2 - (\Omega - \omega)^2} = -\alpha z (\Omega - \omega) \quad (3-61a)$$

when $r = a$

At the plane endwalls $\frac{dR}{dz}$ becomes infinite and Eq. 3-61 reduces to

$$\frac{f_z}{\Omega - \omega} = -\alpha r (\Omega - \omega), \quad (3-61b)$$

when $z = z_1, z_2$

3-6 GREENHILL'S SOLUTION FOR SPHEROIDAL CAVITY

The stability problem for the completely filled spheroidal cavity was solved by Greenhill² in 1880. In 1940 Greenhill's solution was applied to a liquid-filled spinning projectile by Milne, who exhibited the stability criterion in form of a simple diagram (Milne's graph). Milne also compared theoretical predictions with experimental data of free flight firings. The stability criterion of Milne is discussed in Chapter 4.

Greenhill's solution requires relatively little computational effort; nevertheless, the solution displays the essential features of the liquid-filled projectile problem. For these reasons the solution is discussed in this paragraph in detail.

It is assumed that the cavity is spheroidal; its equation is

$$r^2 = R^2(z) = a^2(1 - z^2/c^2) \quad (3-63)$$

where $2a$, $2c$ are the lengths of the principal axes of the spheroid. A simple solution of Eq. 3-60 is

$$f = krz \quad (3-64)$$

where k is a constant yet to be determined.

Evaluating the boundary condition Eq. 3-61 with $R(z)$ and $f(r,z)$ given by Eqs. 3-63 and 3-64, respectively, yields for k

$$k = \alpha (K^2 - 1) \frac{(\Omega - \omega)^2 (\Omega + \omega)}{(\Omega + \omega) - K^2 (\Omega - \omega)} \quad (3-65)$$

where $K = \frac{c}{a}$.

It is thus shown that Eq. 3-64 with Eq. 3-65 solves the boundary value problem for a spheroidal completely filled cavity. The perturbation pressure and velocity components of the perturbed fluid motion follow from Eqs. 3-64 and 3-59. The perturbation pressure is

$$p = \alpha krz e^{i(\omega t - \theta)} \quad (3-66)$$

When the frequency ω is equal to $\Omega \left(\frac{K^2 - 1}{K^2 + 1} \right)$,

the right-hand side of Eq. 3-65 becomes infinite or the yaw amplitude α is zero. In fact, at this frequency the solution, Eq. 3-64, satisfies the homogeneous boundary condition which is obtained from Eq. 3-61 when α is set equal to zero. This means that the liquid can undergo free oscillations at the discrete frequency $\omega_0 = \Omega \left(\frac{K^2 - 1}{K^2 + 1} \right)$.

A frequency of free oscillation is usually referred to as "natural frequency" or "eigenfrequency". It is shown later that frequencies of free oscillation play an important role in the stability theory of a liquid-filled projectile; generally the projectile becomes unstable when the frequency of nutation of the projectile is sufficiently close to a natural frequency. Usually the mass of the liquid is small compared to the

mass of the projectile; and, hence, the reaction of the liquid upon the projectile is small. When, however, the frequency of yaw approaches a natural frequency, the liquid oscillations attain very high amplitudes and the reaction of the liquid upon the projectile becomes significant. This effect is discussed in the paragraph which follows for the case of the spheroidal cavity.

3-6.1 THE MOMENT ON A PROJECTILE WITH SPHEROIDAL CAVITY

3-6.1.1 Center of Rotation Coincides With Center of Cavity

The moment on the projectile is obtained by evaluation of the integrals, Eqs. 3-30a and 3-31a. The pressure in the liquid is

$$P = \left(\frac{\rho}{2} \right) \Omega^2 r^2 + p \quad (3-67)$$

where the first part $\left(\frac{\rho}{2} \right) \Omega^2 r^2$ is the pressure due to the basic flow, and the second part p is the pressure due to the perturbed fluid motion.

At the cavity surface we have

$$r^2 = R^2(z') + 2 \alpha z' R(z') e^{i(\omega t - \theta)} \quad (3-68)$$

Eq. 3-67 evaluated at the cavity surface yields

$$\begin{aligned} P(z', \theta, t) &= \frac{\rho}{2} \Omega^2 R^2(z') \\ &+ \alpha \rho \Omega^2 z' R(z') e^{i(\omega t - \theta)} \\ &+ p(z', \theta, t) \end{aligned} \quad (3-69)$$

with

$$p(z', \theta, t) = \rho k z' R(z') e^{i(\omega t - \theta)} \quad (3-70)$$

(Eq. 3-70 follows when Eq. 3-66 is evaluated at the cavity surface and higher order terms are neglected.) Substituting Eq. 3-69 into Eqs. 3-30 and 3-31, and integrating yields for the hydrodynamic moment on the projectile (setting $\alpha e^{i\omega t - i\theta} = 1$)

$$\begin{aligned}
 M &= M_{zx} + iM_{yz} \\
 &= (l \text{im}) \Omega^2 \frac{a^2 M_f}{5} (K^2 - 1) \tau \frac{1 - \tau_0(1 + \tau - \tau^2)}{\tau - \tau_0}
 \end{aligned}
 \quad (3-71)$$

where

$$M_f = \rho \frac{4\pi}{3} a^2 c, \text{ mass of the liquid}$$

$$\tau = \frac{\omega}{\Omega}, \text{ dimensionless yawing frequency}$$

$$\tau_0 = \frac{\omega_0}{\Omega} = \frac{K^2 - 1}{K^2 + 1}, \text{ dimensionless eigenfrequency}$$

$$K = c/a, \text{ fineness-ratio}$$

It should be emphasized that both the basic pressure and the pressure perturbation p contribute to the moment on the projectile. The basic pressure — represented by the first two terms of Eq. 3-69 — is rotationally symmetrical about the z -axis; about z' , however, it contains a small antisymmetrical part in addition to the large symmetrical part. Clearly, the symmetrical part gives no contribution to the moment. The antisymmetrical part, however, which is of first order in the yaw angle, must be considered.

Eq. 3-71 was derived under the assumption that the center of rotation coincides with the center of the cavity. This restriction can easily be removed as shown in the discussion which follows.

3-6.1.2 Change of the Center of Rotation

Let us consider the case that the center of the cavity lies a distance h above the center of rotation and the latter is kept at $z = 0$. Generally, a rotation about the point $z = 0$ is composed of a rotation about $z = h$ and a translational motion of the point $z = h$. Because of the principle of superposition, the pressure field produced by the combined motion is the sum of the pressure fields due to rotation and translation.

The solution of the boundary value problem for the combined motion is, instead of Eq. 3-64,

$$f = kr(z - h) + \alpha h(\omega^2 - \Omega^2)r \quad (3-71a)$$

The part $kr(z - h)$ represents the pressure field due to rotation about $z = h$, and $\alpha h(\omega^2 - \Omega^2)r$ is the part due to the translational motion. It can be shown readily that the second part, $\alpha h(\omega^2 - \Omega^2)r$, is independent of the cavity shape. Precisely, if $f(r, z)$ solves the boundary value problem for a completely filled cavity of rotational symmetry, then $f(r, z - h) + \alpha h(\omega^2 - \Omega^2)r$

is the solution for the case that the center of rotation is changed in the way described above.

For the moment M , on the projectile, one finds in a generalization of Eq. 3-71

$$M = M + h^2 \omega^2 M_f (l \text{im}) \quad (3-71b)$$

where M is given by Eq. 3-71 and M_f is the mass of the liquid.

It can be shown that the last equation has general validity if M is interpreted as the moment on the projectile consequent to rotation about the center of gravity.

The above formula for M_h shows that — with respect to the superposed translational motion — the liquid reacts in the same way as a rigid body. In fact, the liquid moves like a rigid body, provided the casing is not rotated about a transverse axis and no free surface is present. If the cavity is only partially filled, the free surface bounding the liquid is being deformed when subjected to a lateral acceleration and, consequently, the reaction on the casing is different from that of a rigid body. The motion of the liquid in this case is more complex and depends on the cavity shape. If the cavity is almost completely filled — as usual in practice — Eq. 3-71b is still a good approximation.

3-6.2 THE MOTION OF THE PROJECTILE

Substituting Eq. 3-71 into the dynamic equation, Eq. 3-35, and recalling that $\xi = (1 + im) = \alpha_0 e^{i\omega t}$, yields the following condition for τ

$$T\tau^2 - L\tau + \frac{L^2}{4T}\beta = \frac{D}{\tau - \tau_0} \quad (3-72)$$

$$\text{where } \beta = \frac{4TC}{L^2\Omega^2} \quad (3-73)$$

$$\text{and } D = \frac{-a^2 M_f}{5} (K^2 - 1) \tau [1 - \tau_0(1 + \tau - \tau^2)] \quad (3-74)$$

For the empty projectile the right-hand side of Eq. 3-72 is zero and one has the well-known solution

$$\tau = \frac{L}{2T} \left[1 \pm \sqrt{1 - \beta} \right] \quad (3-75)$$

where β is the reciprocal of the gyroscopic stability factor. When $\beta < 1$ the projectile is stable and its nutational and precessional frequencies are, respectively,

$$\frac{L}{2T} (1 + \sqrt{1 - \beta}) = \tau_n \quad (3-76)$$

$$\frac{L}{2T} (1 - \sqrt{1 - \beta}) = \tau_p \quad (3-77)$$

Instability occurs only when $\beta > 1$, i.e., when the roots of Eq. 3-75 are complex. Similarly, the liquid-filled projectile is unstable when a root of the complete Eq. 3-72 is complex. (Since Eq. 3-72 is a cubic with real coefficients, it has either three real roots or one real and two conjugate complex roots.)

The usual procedure for removing the gyroscopic instability is to increase the spin of the projectile, which has the effect of decreasing β .

It was noted by Stewartson¹ that the instability caused by liquid oscillations is of a different kind; the latter cannot be re-

moved by increasing the spin. Eq. 3-71 shows that the moment due to the liquid is proportional to Ω^2 . Increasing the spin, increases the moment so that the ratio of liquid forces and inertia forces is independent of the spin. This fact is also displayed by Eq. 3-72; only the term containing β is influenced by a change of spin.

A further discussion of Eq. 3-72 may be limited here to two extreme cases:

- (1) A spheroidal mass of liquid contained in a thin-walled casing.
- (2) A heavy top with a small liquid-filled cavity.

The first case had found the attention of Kelvin⁵ who had demonstrated that a thin-walled spheroidal top full of liquid which is pivoted at the center of the spheroid can be made unstable by changing the shape of the casing from an oblate into a slightly prolate form. Greenhill's solution² gave the mathematical explanation of this phenomenon. The assumption that the left-hand side of Eq. 3-72 is zero, requires $D = 0$, or

$$\tau_0(1 + \tau - \tau^2) = 1 \quad (3-78)$$

The roots of Eq. 3-78 are complex and the top is unstable when

$$0 < \tau_0 < \frac{4}{5} \quad \text{or} \quad 1 < K < 3 \quad (3-79)$$

Eq. 3-79 is the criterion for instability of a spinning liquid mass enclosed in a prolate spheroidal thin-walled cavity. The spheroidal mass is stable for $K < 1$ —i.e., when the spheroid has an oblate shape—while it becomes unstable for a slightly prolate shape.

Generally, the problem of liquid-filled projectiles is more relevant to the other extreme case (case 2): the mass of the liquid is small compared to the mass of the projectile. Then the right-hand side of Eq. 3-72 is negligible except near $\tau = \tau_0$

where $\frac{D}{\tau - \tau_0}$ has a pole. D is a slowly varying function of τ . Thus, since $D/\tau - \tau_0$ is important only when a root of Eq. 3-72 occurs near τ_0 , $D(\tau)$ may be replaced by $D(\tau_0)$ the residue of the pole.

It can be seen readily that, when D is small, the three roots of Eq. 3-72 are near τ_p , τ_n , and τ_0 , respectively. If D is negative, the root near τ_p is always real, while the roots near τ_n and τ_0 can become complex conjugates when τ_n is sufficiently close to τ_0 . If $\tau_n \approx \tau_0$ the left-hand side of Eq. 3-72 may be expanded about τ_n and one has approximately

$$(\tau - \tau_n)(\tau - \tau_0) = \frac{D}{L \sqrt{1 - \beta}} \quad (3-80)$$

$$\text{or } \tau = \frac{\tau_n + \tau_0}{2} \pm \sqrt{\frac{(\tau_n - \tau_0)^2}{4} + \frac{D/L}{\sqrt{1 - \beta}}} \quad (3-81)$$

Thus, if D is negative, the criterion for instability is

$$|\tau_n - \tau_0| < \left[\frac{-4D(\tau_0)}{L \sqrt{1 - \beta}} \right]^{\frac{1}{2}} \quad (3-82)$$

Eq. 3-82 shows that the projectile becomes unstable when D is negative and τ_0 falls within a small bandwidth about the nutational frequency.

Similarly, when D is positive, instability occurs when τ_0 falls within a small bandwidth about the precessional frequency. The criterion for instability then is

$$|\tau_p - \tau_0| < \left[\frac{4D(\tau_0)}{L \sqrt{1 - \beta}} \right]^{\frac{1}{2}} \quad (3-82a)$$

However, according to Eq. 3-74, $D(\tau_0)$ is always negative, so that only the nutational component of the yaw can become divergent. Eq. 3-82 describes the complete range of instability.

Eq. 3-82 also shows that the bandwidth of instability cannot be decreased below the value $\sqrt{-4D(\tau_0)/L}$ however large the stability factor $1/\beta$ is.

If the center of rotation does not coincide with the center of the cavity, the right-hand side of Eq. 3-72 must be supplemented — according to Eq. 3-71b — by the additional term $-h^2 M_f \tau^2$, where h is the distance between the center of the cavity and the center of rotation. This additional term is usually very small. The additional term does not alter the residue $D(\tau_0)$, i.e., the stability of the projectile is not affected by a change of the center of rotation.

The stability criterion Eq. 3-82 can be put, alternatively, into the following form proposed by Milne³ by defining

$$x = \sqrt{\frac{\tau_0}{\tau_n}} = \sqrt{\left(\frac{K^2 - 1}{K^2 + 1} \right) \frac{T}{L}}$$

$$y = \frac{2K}{K^2 + 1} \sqrt{\frac{2a^2 M_f}{5L}}$$

Milne's criterion for instability is

$$|1 - x| < y \quad (3-83)$$

In deriving Eq. 3-83, use is made of the approximation

$$\tau_0 \approx \tau_n \quad \text{or} \quad x \approx 1.$$

3-6.3 EFFECTIVE MOMENTS OF INERTIA OF A SPHEROIDAL MASS OF LIQUID

For the case of a nonspinning liquid, Eq. 3-71 may be specialized by setting $\Omega = 0$ but $\Omega \tau = \omega = \text{finite}$. One obtains

$$M = (1 + i m) \frac{\omega^2 a^2 M_f (K^2 - 1)^2}{5 (K^2 + 1)} \quad (3-84)$$

Recalling that $(1 + i m) = \xi = \alpha_0 e^{i \omega t}$ yields:

$$M = -T_e \frac{d^2 \xi}{dt^2} \quad \text{with}$$

$$T_e = \frac{a^2 M_f (K^2 - 1)^2}{5 (K^2 + 1)} \quad (3-85)$$

T_e is the effective transverse moment of inertia of a spheroidal mass of liquid, relative to the center of gravity. As shown in par. 3-4, a liquid-filled nonspinning projectile behaves as though the liquid is replaced by an "equivalent rigid body" having the same mass but effective moments of inertia which are smaller than the moments of inertia of the frozen liquid. The effective axial moment of inertia is for an inviscid fluid for all bodies of revolution. Eq. 3-85 shows that for a sphere ($K = 1$) also the transverse effective moment is zero. For small deviations from a sphere ($K \approx 1$) the effective moment of inertia is still very small since it varies like $(K^2 - 1)^2$. In the limit $K \rightarrow \infty$, the effective moment of inertia agrees with that of a solid body

$$T_e = \lim_{K \rightarrow \infty} \frac{a^2 M_f (K^2 - 1)^2}{5 (K^2 + 1)} = \frac{c^2 M_f}{5} \quad (3-85a)$$

When the center of rotation does not coincide with the center of gravity, the effective moment of inertia follows from Eq. 3-71b

$$(T_e)_h = T_e + h^2 M_f \quad (3-86)$$

where T_e and $(T_e)_h$ are the respective moments of inertia about the center of gravity and about a point which is a distance h above the center of gravity, and M_f is the mass of the liquid. Eq. 3-86 is completely analogous to the corresponding relation for a rigid body.

3-7 STEWARTSON'S SOLUTION FOR A CYLINDRICAL CAVITY

3-7.1 INTRODUCTION

Stewartson's solution for the cylindrical cavity is certainly the most important contribution to the theory of liquid-filled projectiles, at least from the projectile designer's point of view. Cylindrical cavities are favored by various design considerations; in fact, most of the existing liquid-filled projectiles have cylindrical or nearly cylindrical cavities. On the other hand the solution for cylindrical cavity includes the practically important case of partially filled cavity, while Greenhill's solution for the spheroidal cavity cannot easily be extended to the partial fill conditions. Stewartson's solution is the only known exact solution for partially filled cavities and there seems to be little hope that exact solutions can be obtained for other cavity shapes.

For a cylindrical cavity, the boundary conditions assume a particularly convenient form, and the boundary value problem becomes amenable to methods of solution which are briefly outlined in par. 3-7.2. A discussion of the main results of Stewartson's analysis is given below. For further information the reader is referred to Stewartson's original paper¹ and a more detailed analysis by Ash and Gundersen².

The calculations show that, in a generalization of the results for the spheroidal cavity, the projectile becomes unstable whenever the frequency of nutation of the projectile is sufficiently near to one of a number of natural frequencies of the liquid. The completely filled spheroidal cavity appears to be a special case, as only one

mode of free oscillation is related to instability. (There are other modes of free oscillations of the liquid in a spheroidal cavity which, however, do not produce a moment nor are they induced by the yawing motion of the casing.)

For the cylindrical cavity a doubly infinite number of modes of free oscillation occur in contrast to the one mode for the spheroidal cavity. The different modes of oscillation can be characterized by pairs of numbers (n, j) where n and j relate to the number of radial and axial half-waves of the respective mode of oscillation. Associated with each mode (n, j) is a natural frequency ω_{nj} and a residue D determining the bandwidth of instability.

Similarly as for the spheroidal cavity, the moment due to the liquid is small except when the yawing frequency of the projectile ω approaches a natural frequency ω_{nj} .

Mathematically, the moment is a very complicated function of the yawing frequency ω , having poles at all frequencies ω_{nj} . If ω is not near a pole, the moment is small and may be neglected. If, however, ω approaches a natural frequency, say ω_{nj} , the moment becomes large as $D/(\omega - \omega_{nj})$ and the equation of yawing motion, Eq. 3-35, reduces to

$$T \tau^2 - L \tau + \frac{L^2}{4T} \beta = \frac{D(\tau_{nj})}{\tau - \tau_{nj}} + \text{small terms} \quad (3-87)$$

where $\tau = \frac{\omega}{\Omega}$, $\tau_{nj} = \frac{\omega_{nj}}{\Omega}$ and D is the residue at the pole.

In analogy to the results for the spheroidal cavity, Eq. 3-87 yields as condition for instability

$$|\tau_n - \tau_{nj}| < \sqrt{S}; \quad S = \frac{-4D(\tau_{nj})}{L \sqrt{1 - \beta}} \quad (3-88)$$

where τ_n is the nutational frequency of the projectile.

The quantity $\frac{-4D}{L \sqrt{1 - \beta}} = S$ will be denoted as "Stewartson's parameter" in the discussion which follows.

The derivation of Eq. 3-88 is analogous to the derivation of the corresponding Eq. 3-82 for the spheroidal cavity. Eq. 3-88 also rests on the assumption that D/L is a small negative quantity. Computations have shown that D is always negative and that $|D|/L \ll 1$ when the liquid mass is small relative to the mass of the projectile.

The analogy of the solutions for spheroidal and cylindrical cavities as well as considerations concerning the general nature of the boundary value problem suggest that the stability criterion for any cavity of rotational symmetry can be put into the form of Eq. 3-88. The eigenfrequencies ω_{nj} and residues $D(\omega_{nj})$ take on values characteristic of cavity shape and dimension. In particular, the dimensionless eigenfrequencies τ_{nj} depend only on the cavity shape and fill-ratio; i.e., the τ_{nj} are independent of spin, absolute dimensions of the cavity, and properties of the liquid. (This is no longer the case when liquid viscosity is taken into account; see Chapter 6.)

In the light of the aforementioned relations, the spheroidal cavity appears to be a limiting case for which all except one residue are zero. Computations for a cylindrical cavity show that the absolute values of the residues decrease rapidly with mode numbers (n, j) so that in practical applications only the lowest modes are important (see Chapter 9).

For the lowest radial mode numbers, eigenfrequencies and residues have been computed and presented in tabulated form. The tables are briefly referred to as "Stewartson's Tables".

It turned out that tables for higher axial mode numbers ($j=1, 2, 3 \dots$) could be absorbed into the table for $j=0$ because j occurs only

in a product: $\frac{c/a}{(2j+1)}$ where c/a is the fineness-ratio of the cylinder ($2c$ = length, $2a$ = diameter). In other words τ_{nj} is — for fixed radial mode number n — only a function of $\frac{c/a}{(2j+1)}$.

It should be mentioned that the absorption of j into the factor $\frac{c/a}{2j+1}$ is a peculiarity for the cylindrical cavity — a result of the periodicity of waves in an axial direction.

For the tabulation it was convenient to separate from D a dimensional factor and introduce a new dimensionless quantity R .

$$D \pm \frac{\rho a^6}{c} R^2 = 0 \quad (3-89)$$

Extended Stewartson Tables for $c/[a(2j+1)]$ and $2R$ versus eigenfrequencies τ_0 are presented in Chapter 4.

3-7.2 METHOD OF SOLUTION OF THE BOUNDARY VALUE PROBLEM

It is readily seen that a particular solution of Eq. 3-60 is

$$f(r, z) = C_1(\gamma kr) e^{ikz} \quad (3-90)$$

$$\text{where } \gamma^2 = \left[\frac{4\Omega^2}{(\Omega - \omega)^2} - 1 \right] \quad (3-91)$$

and C_1 is a Bessel function of order one with argument γkr . The solution of the boundary value problem may be constructed by superposition of particular solutions of the type Eq. 3-90. For the cylindrical cavity Stewartson obtains (the notation used here is slightly different from Stewartson's notation)

$$f(r, z) = -\alpha (\Omega - \omega)^2 r (z - h) \pm X_0 r \pm \frac{Z_0}{r} + \sum_{j=0}^{\infty} \left[X_{2j+1} J_1(\gamma kr) + Z_{2j+1} Y_1(\gamma kr) \right] \cos k(z - h \pm c) \quad (3-92)$$

J_1, Y_1 are Bessel functions of the first and second kind, respectively, and $k = \frac{\pi}{2c} (2j + 1)$.

The length of the cylinder is $2c$ and its center is a distance h above the center of rotation, which is at $z = 0$. The first term of Eq. 3-92 has the effect that the solution satisfies the boundary condition, Eq. 3-61b, at the plane endwalls $z - h = \pm c$ of the cylindrical cavity. The boundary conditions at the curved sidewall, Eq. 3-61a, and at the free surface, Eq. 3-62, lead to two conditions of the form

$$z - h = \sum_{j=0}^{\infty} C_{2j+1}^{(i)} \cos k(z - h \pm c) ; i = 1, 2 \quad (3-93)$$

where the constant coefficients $C_{2j+1}^{(1)}$ and $C_{2j+1}^{(2)}$ are linear combinations of the X_{2j+1} and Z_{2j+1} . On the other hand, the $C_{2j+1}^{(i)}$ are the coefficients of a Fourier expansion of $(z - h)$ and are $C_{2j+1}^{(i)} = -\frac{2}{\pi}$. Thus one obtains two linear equations for each pair (X_{2j+1}, Z_{2j+1}) which suffice to determine the X_{2j+1} and Z_{2j+1} .

The term $X_0 r \pm Z_0/r$ of Eq. 3-92 takes care of the lateral motion of the cavity; it is zero when $h = 0$, i.e., when the center of rotation coincides with the center of the cavity.

When the cavity is completely filled, i.e., when $b = 0$, $Z_0 = 0$, $Z_{2j+1} = 0$ and only the X_{2j+1} must be computed. (That $Z_{2j+1} = 0$ when $b = 0$ follows readily from the fact that Y_1 (Y_{kb}) becomes infinite for $b = 0$.)

Obviously, the method outlined above is not applicable when the cavity surface or the free surface is noncylindrical. In either case the coefficients $C_{2j+1}^{(i)}$ of Eq. 3-93 would depend on z , and the elimination of the X_{2j+1} , Z_{2j+1} becomes impractical.

The special simplification achieved when the boundaries are cylindrical renders possible the solution of another problem, namely, the completely filled cylindrical cavity with a cylindrical central body (burster). At the surface of the immersed cylindrical body the boundary condition is that of a solid wall, i.e., Eq. 3-61 must be satisfied at $r = a$ and $r = b$ when b is the radius of the central body. This yields again two conditions for X_{2j+1} , Z_{2j+1} .

Eigenfrequencies and residues for the cavity with central burster have been computed and tabulated. Tables for various ratios b^2/a^2 are presented in Chapter 4.

Calculations show that the j th terms under the sum of Eq. 3-92 solve the homogeneous boundary conditions (Eqs. 3-61b and 3-62 with $1 \pm im = 0$) when Yka assumes one of an infinite series of discrete eigenvalues y_n ($n = 1, 2, 3, \dots$).

This leads to the eigenvalue-condition

$$Yka = \sqrt{\frac{4}{(1 - \tau_0)^2} - 1} \cdot \frac{\pi a(2j \pm 1)}{2c} = y_n(\tau_0, b^2/a^2) \quad (3-94)$$

$$n = 1, 2, 3, \dots$$

$$j = 0, 1, 2, 3, \dots$$

The y_n depend on τ_0 and b^2/a^2 . The eigenfrequencies τ_0 can now—in principle—be found solving Eq. 3-94. It is, however, difficult and not even practical to eliminate τ_0 from Eq. 3-94. Instead, τ_0 is considered as the independent variable (first column in Stewartson's Tables) and $c/[a(2j+1)]$ is tabulated as function of τ_0 (second column in Stewartson's Tables). It is

$$\frac{c}{a(2j+1)} = \frac{\pi/2 \sqrt{\frac{4}{(1 - \tau_0)^2} - 1}}{y_n(\tau_0, b^2/a^2)}; \quad (3-95)$$

$$n = 1, 2, 3, \dots$$

Once the amplitudes X_{j+1} , Z_{2j+1} of the pressure fluctuations are known, the moments on the projectile can be computed through integration (inserting Eq. 3-92 into Eqs. 3-30 and 3-31 and integrating). By a similar argument as for the spheroidal cavity (par. 3-6) it follows that, near resonance, the moment on the projectile becomes large as $\frac{D}{\tau - \tau_0} \Omega^2$ ($1 \pm im$).

3-8 THE EIGENVALUE PROBLEM

The importance of eigenfrequencies for the stability of a liquid-filled projectile was discussed in pars. 3-6 and 3-7. For a heavy projectile filled with a comparatively small mass of liquid, the stability problem reduces to the problem of calculating the eigenfrequencies and associated residues.

Frequently, an exact knowledge of the eigenfrequencies appears to be of primary interest while approximate values for the residues are sufficient. The residue determines the bandwidth of instability. Even when the value of the residue is only approximately known, it is still possible to avoid instability when the frequency of

nutational frequency is chosen sufficiently remote from any one of the eigenfrequencies or the cylindrical cavity is so constructed as to have its eigenfrequencies sufficiently remote from the nutational frequency of the projectile.

On the other hand, the calculation of eigenfrequencies is usually far easier than the solution of the complete stability problem. For the reasons given above one is very often content to know just the eigenfrequencies for a given cavity shape and to estimate the value of the residue. It was shown experimentally⁷ that for small changes of cavity shape there may be significant changes of the eigenfrequencies while the associated bandwidths change very little. Precisely, when the eigenfrequency is shifted by an amount equal to the bandwidth, the bandwidth itself remains practically unchanged. It is clear, then, that the eigenfrequencies should be known with a much higher degree of accuracy than the residues. These considerations play an important role in computation of eigenfrequencies in noncylindrical cavities, Chapter 7.

An impression of how frequency and residue depend on cavity shape is furnished by Table 3-1 which shows comparison of data for cylindrical and spheroidal cavities.

TABLE 3-1. EIGENFREQUENCIES AND RESIDUES OF THE BASIC MODE ($n = 1, j = 0$) FOR CYLINDER AND SPHEROIDAL CAVITY

τ_0	c/a		2R	
	cyl. cav.	spher. cav.	cyl. cav.	spher. cav.
0.00	0.995	1.000	0	0
0.10	1.117	1.185	0.343	0.248
0.20	1.262	1.225	0.682	0.540

The problem of calculating the eigenfrequencies — briefly denoted as the eigenvalue problem — is described below.

The equations of perturbed fluid motion in connection with homogeneous boundary

conditions ($l + im = 0$) have solutions representing liquid oscillations at discrete frequencies (eigenfrequencies). The problem is to find the frequencies for which solutions exist. For the stability problem only those solutions are of interest which produce a moment on the projectile.

For cavities of rotational symmetry the free oscillations are of the form

$$(\bar{v}, p/\rho) = [\underline{v}(r, z), f(r, z)] e^{i(\omega t - m\theta)}$$

$$(m = 0, \pm 1, \pm 2, \pm 3, \dots)$$

Only the modes with $m = 1, \omega > 0$ are of interest for the stability problem since modes with $|m| \neq 1$ cannot produce a moment, and modes with $m = -1, \omega > 0$ cannot be in resonance with the nutational motion of the projectile. The case $m = -1, \omega > 0$ is physically the same as $m = 1, \omega < 0$ and corresponds to waves traveling retrograde relative to the spin. Although such waves exist, they can be excluded here from consideration since they cannot cause instability. For a liquid-filled projectile it is possible that one of its frequencies is negative, i.e., that the yawing motion is reversed. An example is the oblate spheroidal cavity. Its only eigenfrequency is negative and, as a consequence, the root nearest to τ_0 of the characteristic equation may be negative. It can, however, never become complex and thus does not lead to instability.

For the reasons given above, only positive eigenfrequencies are of interest. In practice, nutational frequencies are small and rarely exceed $1/3$ of the spin frequency. It is, therefore, sufficient to calculate eigenfrequencies only up to about $1/2$ of the spin frequency. The domain of interest of τ_0 is: $0 < \tau_0 < 0.5$.

For a cylindrical cavity the theory shows that residues associated with higher radial modes become very small and it is reasonable to assume a similar behavior for other cavities, too. It is sufficient then to calculate only the eigenfrequencies of the lowest

modes. It should be noted that — in contrast to acoustic or elastic vibrations, etc. — higher modes of liquid oscillations do not necessarily correspond to larger eigenfrequencies.

Exact solutions of the eigenvalue problem are known only for ellipsoidal and cylindrical cavities; it is, however, possible to compute eigenfrequencies for a variety of other cavity shapes by approximate methods⁸. Practical computations of eigenfrequencies for nearly cylindrical cavities and methods for the approximate solution of the eigenvalue problem are discussed in Chapter 7.

REFERENCES

1. K. Stewartson, "On the Stability of a Spinning Top Containing Liquid", *J. Fluid Mech.* **5**, Part 4 (1959).
2. A. G. Greenhill, *Proc. Camb. Phil. Soc.* **4**, 4 (1880).
3. E. A. Milne, *Report on the Stability of Liquid-Filled Shell* (U), EBD Report No. 6, 1940 (Confidential).
4. N. E. Zhukovskii, "Odvizhenii tverdogo, tela, imeiushchego polosti, napolnennye odnorodnoi kapel'noi zhidkost'iu", "On the Motion of a Rigid Body, Containing a Cavity Filled With a Homogeneous Liquid, *Sobr. Soch.* Vol. 2, Gos-tekhnizdat (1948).
5. Lord Kelvin, *Nature*, London, **15**, 297 (1877).
6. J. E. Ash and R. M. Gundersen, *Investigations in the Exterior Ballistics of Shell With Nonsolid Fillers, Final Report*, Armour Research Foundation (now IIT Research Inst.), Project 4187, 1960.
7. B. G. Karpov, *Dynamics of Liquid Filled Shell: Resonance in Modified Cylindrical Cavities*, BRL Report 1332, Aberdeen Proving Ground, Md., 1966.
8. E. H. Wedemeyer, *Dynamics of Liquid-Filled Shell: Non Cylindrical Cavity*, BRL Report 1326, Aberdeen Proving Ground, Md., 1966.
9. J. T. Frasier and W. E. Scott, *Dynamics of Liquid-Filled Shell: Cylindrical Cavity With Central Rod*, BRL Report 1391, Aberdeen Proving Ground, Md., 1967.

CHAPTER 4

MILNE'S STABILITY GRAPH, STEWARTSON'S AND
CENTRAL COLUMN TABLES

4-0 LIST OF SYMBOLS*

d	= exterior diameter of projectile, ft
$F(\tau)$	= function of fineness-ratio c/a and of fractional air volume b^2/a^2
I_x	= axial moment of inertia of a loaded projectile, slug-ft ²
I_y	= transverse moment of inertia of a loaded projectile, slug-ft ²
M	= mass of loaded projectile, slug
n	= twist of rifling, cal/turn
$2R$	= residue at the pole, obtained from Stewartson's Tables
s_g	= gyroscopic stability factor
V	= velocity of projectile, ft/sec
V_c	= volume of cylindrical cavity, ft ³

GREEK LETTERS

λ_1	= aerodynamic nutational yaw damping rate, per cal or per ft
λ_{liq}	= nutational yaw damping rate due to liquid, per cal or per ft
λ_{max}	= maximum rate of divergence of nutational amplitude, per sec
σ	= $\sqrt{1 - 1/s_g}$

MILNE'S STABILITY GRAPH

4-1.1 INTRODUCTION

E. A. Milne¹ working (1940) under the auspices of the British Liquid-Filled Shell Panel of the Ministry of Supply was concerned with finding some rationale behind the unpredictable behavior of liquid-filled

projectiles in flight. For this purpose he had collected all available data from field trials conducted by British Services between 1926 and 1940. These data presented a "bewildering complexity" — all attempts at discovering a common cause for instability proved unavailing. Numerous attempts at various correlations between intuitively "reasonable" parameters also proved unsuccessful.

In 1880 Greenhill² developed a theory for instability of a spinning top containing liquid which completely filled a spheroidal cavity — the liquid spinning with the full spin of the top. He showed that only a prolate spheroidal cavity led to instability. Milne has reexamined this theory and derived a condition for instability for the projectile containing such liquid-filled cavity. The development of this theory is given in Ch. 3.

4-1.2 INSTABILITY CRITERIA

It is shown in Ch. 3 that the condition for instability of the projectile containing a prolate spheroidal cavity full of liquid is by Eq. 3-82

$$(\tau_n - \tau_0)^2 < \frac{-4D(\tau_0)}{I_x \sigma} \quad (4-1)$$

where, to be consistent with the notation of Ch. 2 which notation is more familiar to the American designers, we have replaced the axial moment of inertia L by I_x , and

$\sqrt{1 - \beta}$ by $\sigma = \sqrt{1 - 1/s_g}$.^{*} The expression

* L and T , Chapter 3, are defined for an empty projectile. We replace L and T by I_x and I_y , respectively, for a loaded projectile. It can be shown that the end results, i.e., instability criteria, are identical whether written for an empty or loaded projectile. Since Milne uses the inertial properties of a loaded projectile, Eqs. 4-4 and 4-5 were written for the loaded case.

*For identification of other symbols in this chapter, refer to Chapter 3.

for $D(\tau_0)$ — a residue at the pole τ_0 — is

$$D(\tau_0) = \frac{8M_f a^2}{5} \frac{K^2}{(K^2+1)^2} (\tau_0)^2 \quad (4-2)$$

which is obtained by replacing τ by τ_0 in Eq. 3-74 and substituting for τ_0 — the eigenfrequency of the liquid — its value

$$\tau_0 = \frac{K^2 - 1}{K^2 + 1} \quad (4-3)$$

Thus replacing $D(\tau_0)$ in Eq. 4-1 by its value, Eq. 4-2, and after some slight rearrangement the instability criteria becomes

$$\left(\frac{\tau_0}{\tau_n} - 1 \right)^2 < 4 \left[\frac{4K^2}{(K^2+1)^2} \frac{2M_f a^2}{5I_x \sigma} \right] \left(\frac{\tau_0}{\tau_n} \right)^2 \quad (4-4)$$

To simplify the writing, define

$$\left. \begin{aligned} x &= \sqrt{\frac{\tau_0}{\tau_n}} = \sqrt{\left(\frac{K^2 - 1}{K^2 + 1} \right) \left(\frac{I_y}{I_x} \right) \frac{2}{1 + \sigma}} \\ y &= \frac{2K}{K^2 + 1} \sqrt{\frac{2M_f a^2}{5I_x \sigma}} \end{aligned} \right\} \quad (4-5)$$

In terms of the variables x and y , the instability criteria become

$$\begin{aligned} (x^2 - 1)^2 &< 4y^2 x^4 \\ \text{or} \\ |x^2 - 1| &< 2yx^2 \end{aligned} \quad (4-6)$$

Eq. 4-6 readily reduces to Eq. 3-83, i.e., $|x^2 - 1| = |(x - 1)(x + 1)|$ and if near resonance $\tau_n \approx \tau_0$, $x \approx 1$, Eq. 3-83 follows.

4-2

4-1.3 MILNES STABILITY GRAPH

Milne has expressed the instability criteria as

$$x - y < 1 < x + y \quad (4-7)$$

which form can be obtained from Eq. 4-6. He defined x and y as

$$\left. \begin{aligned} x &= \sqrt{\left(\frac{K^2 - 1}{K^2 + 1} \right) \left(\frac{I_y}{I_x} \right)} \\ y &= \frac{2K}{K^2 + 1} \sqrt{\frac{2M_f a^2}{5I_x}} \end{aligned} \right\} \quad (4-8)$$

which are identical to x and y defined by Eq. 4-5 if $\sigma = 1$.

In Milne's analysis of actual firings it was very difficult to reconstruct the moments of inertia of fired projectiles from their drawings. He used, therefore, the following approximate relationships

$$I_x = 0.14Md^2$$

$$I_y = 0.06Md^2 L^2$$

where

M = mass of loaded projectile, slug

d = projectile exterior diameter, ft

L = overall length of fuze projectile, cal

The use of these approximate relations had the virtue of consistency.

By use of these relations in Eq. 4-8, the x and y become

$$\left. \begin{aligned} x &= 0.67L \sqrt{\frac{K^2 - 1}{K^2 + 1}} \\ y &= \frac{5.4K}{K^2 + 1} \sqrt{\frac{2M_f a^2}{5Md^2}} \end{aligned} \right\} \quad (4-9)$$

When these coordinates were computed for each projectile and plotted x vs y with each projectile being marked whether stable or unstable — i.e., going full range or falling short — a clear separation was exhibited between these regions. A fairly unambiguous curve could be drawn between stable and unstable regions. Milne's stability graph with Eq. 4-9 as coordinates is reproduced in Fig. 4-1.

As can be seen, most of the curve is empirical and appears to be only tangent to the theoretical curve defining the region of instability at $x - y = 1$ near $y = 0$. Nevertheless, it is remarkable that although the mathematical model was clearly inadequate — since probably none of the actual projectiles had spheroidal cavities and were completely filled — the theory indicated proper correlating parameters. With these parameters a heterogeneous collection of projectiles and their bewilderingly unpredictable behavior in flight fell into order, delineating the regions of stability and instability.

Now the graph is probably only of historical interest. But in its time it served a very useful purpose. If it is to be used now for cavity shapes which, as yet, cannot be treated theoretically or tested experimentally, Milne's paper should be consulted for other details and fuller appreciation of the limitations of his empirical curve.

4-4.4 RATE OF DIVERGENCE

of the instability unstable is satisfied the precessional amplitude may grow at a certain rate. What is this rate?

The solution of the yaw equation, Eq. 3-35, with hydrodynamic moment Eq. 3-71 added, is a sum of exponentials of the form

$$e^{i\tau\Omega t}$$

The values of τ are the roots of the characteristic equation, Eq. 3-72. In the notation of Ch. 2 the characteristic equation is

$$I_y \tau^2 - I_x \tau + \frac{I_x^2}{4I_y s_g} = -\frac{D(\tau_0)}{\tau - \tau_0} \quad (4-10)$$

which is cubic in τ . For unstable projectile, the three roots are one real and two complex conjugate. As was shown in Ch. 3 the latter are

$$\tau_{1,2} = \frac{\tau_n + \tau_0}{2} \pm \frac{i}{2} \sqrt{\frac{4D}{I_x s_g} - (\tau_n - \tau_0)^2} \quad (4-11)$$

These are of the form

$$\tau_1 = a + ib$$

$$\tau_2 = a - ib$$

Hence the solution of the yaw equation, i.e., Eq. 3-35 with Eq. 3-71 added, is

$$\xi = k_{10} e^{i\Omega_0 t} [e^{-\Omega b t} + e^{\Omega b t}] + k_{20} e^{i\tau_p \Omega t} \quad (4-12)$$

where τ_p is the precessional frequency

$$\tau_p = \frac{I_x}{2I_y} (1 - \sigma)$$

Clearly, the second term in the bracket will lead to the divergence of the nutational component k_{10} . The rate of divergence is Ωb per sec, or

$$\lambda_{liq} = \frac{\Omega}{2} \sqrt{\frac{4D}{I_x s_g} - (\tau_n - \tau_0)^2}, \text{ per sec} \quad (4-13)$$

It is to be recalled that the hydrodynamic moment was added to the simplified yaw equation, Eq. 2-23 (or Eq. 3-35). Therefore, for a complete description of the yawing motion of the projectile, the aerodynamic damping rates — as obtained from the solution of Eq. 2-1 — should be added. There is no change in the precessional yaw

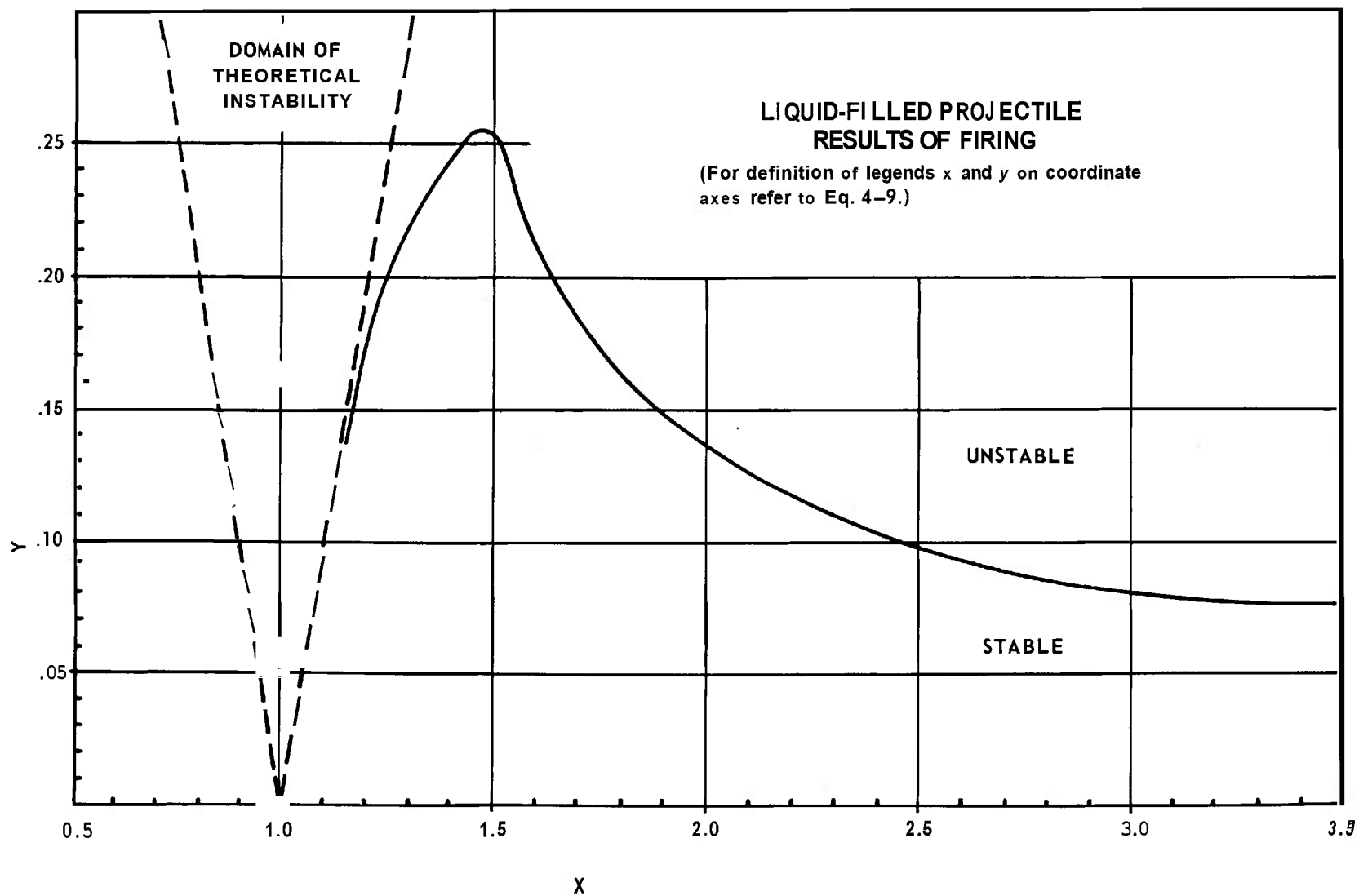


FIGURE 4-1. MILNE'S STABILITY GRAPH

damping rate λ_2 . However, the nutational damping rate becomes $\lambda_1 \approx \lambda_{liq}$.

To express λ_{liq} in other units than per sec — as per foot, for example — divide Eq. 4-13 by the velocity V . However,

$$\frac{\Omega}{V} = \frac{2\pi}{nd}$$

Therefore,

$$\lambda_{liq} = \frac{\pi}{nd} \sqrt{\frac{14D}{I_x \sigma} - (\tau_n - \tau_0)^2}, \text{ per ft} \quad (4-13a)$$

or

$$\lambda_{liq} = \frac{\pi}{n} \sqrt{\frac{4D}{I_x \sigma} - (\tau_n - \tau_0)^2}, \text{ per cal} \quad (4-13b)$$

The nutational amplitude will either grow or diminish as

$$k_1 = k_{10} e^{(\lambda_1 + \lambda_{liq})t}$$

4-2 STEWARTSON'S TABLES

4-2.1 INTRODUCTION

Stewartson's theory and his instability criteria for the projectile containing a cylindrical cavity of height $2c$ and diameter $2a$, which is either partially or completely filled, were discussed in Ch. 3. As a preliminary to the consideration of Stewartson's Tables, we may add a few more comments which might be useful to the designer.

It has been shown that for the cylindrical cavity a doubly infinite number of modes of free oscillations occur, in contrast to the one mode for the spheroidal cavity. The different modes of oscillations can be characterized by a pair of numbers (n, j) where n and j relate to the number of radial and axial half-waves of the respective modes of oscillations. Thus the hydrodynamic moment is much more complicated

than was the case for the spheroidal cavity. Nevertheless, the characteristic equation of the yawing motion with hydrodynamic moment added can be written formally as

$$I_y \tau^2 - I_x \tau + \frac{I_x^2}{4I_y s_g} = M_f c^2 F(\tau) \quad (4-14)$$

where M_f is the mass of the fluid, and $F(\tau)$ is a function of the fineness-ratio of the cavity c/a and the amount of fluid $1 - b^2/a^2$ in it where $2b$ is the diameter of the air column for a partially filled cavity. $F(\tau)$ contains a double infinity of poles corresponding to all the eigenfrequencies τ_{nj} .

It can be shown that if the mass of the fluid in a cavity is small relative to the mass of the projectile, $F(\tau)$ can be expanded into a series of terms of the form

$$\frac{D(\tau_{nj})}{\tau - \tau_{nj}}$$

where $D(\tau_{nj})$ are the residues at corresponding poles $\tau = \tau_{nj}$. It also can be shown that all terms are negligibly small except those for which τ_{nj} is close to either the nutational or the precessional frequencies of the projectile. Therefore, if one of τ_{nj} is close to the nutational frequency τ_n , for example, Eq. 4-14 can be written as

$$I_y \tau^2 - I_x \tau + \frac{I_x^2}{4I_y s_g} = \frac{D(\tau_{nj})}{\tau - \tau_{nj}} \quad (4-15)$$

Eq. 4-15 is of the same form as Eq. 4-10. To stress the analogy of further analysis with that of the spheroidal cavity, we designate $\tau_{nj} = \tau_0$ with the understanding that τ_0 will stand for any τ_{nj} .

As before, we expand the left-hand side of Eq. 4-15 in a Taylor's series about τ_n ,

which is the root of the left-hand side, retaining only the first order term. Eq. 4-15 becomes

$$I_{x\sigma}(\tau - \tau_n) = \frac{D(\tau_0)}{\tau - \tau_0} \quad (4-16)$$

which is quadratic in τ . The solution of Eq. 4-16 is

$$\tau = \frac{\tau_n + \tau_0}{2} \pm \frac{1}{2} \sqrt{(\tau_n - \tau_0)^2 + \frac{4D}{I_{x\sigma}}}$$

It is to be recalled that the solution of the yaw equation, Eq. 3-35 with hydrodynamic moment added, is a sum of exponentials of the form $e^{i\tau\Omega t}$. For stability τ must be real; for instability τ must be complex conjugate. For instability, therefore, the discriminant in Eq. 4-17 must be negative, i.e.,

$$(\tau_n - \tau_0)^2 + \frac{4D}{I_{x\sigma}} < 0$$

This can happen only if $D < 0$. Computations of the residues show that all $D(\tau_{nj})$ are real and negative. Therefore, the condition for instability of the nutational amplitude becomes

$$(\tau_n - \tau_0)^2 - \frac{4|D|}{I_{x\sigma}} < 0$$

The residue D has the dimensions of moment of inertia. For tabulation of the residue it is more convenient to separate D into two factors: (1) a quantity ρ which has the dimensions of moment of inertia where ρ is the density of the fluid, and $2a$ and $2c$ are the diameter and the height of the cavity, respectively, and (2) a non-dimensional positive function, say R^2 , which — as the residue D — depends only on c/a and b^2/a^2 , i.e.,

$$|D| \equiv \rho \frac{a^6}{c} R^2$$

For simplicity of writing define a new quantity

$$S \equiv \frac{\rho (2R)^2 a^5}{I_{x\sigma} (c/a)} \quad (4-19)$$

and call it "Stewartson's parameter". With this parameter the instability condition, Eq. 4-18, becomes

$$(\tau_n - \tau_0)^2 < S \quad (4-20)$$

which can be written in a more familiar form as Stewartson's instability criteria

$$-1 < \frac{\tau_n - \tau_0}{\sqrt{S}} < 1 \quad (4-21)$$

It is to be noted that the factor 4 in front of D in Eq. 4-18 was absorbed in $(2R)^2$.

By following arguments similar to those for the spheroidal cavity, par. 4-1.4, the rate of divergence of the nutational amplitude of yaw is

$$\lambda_{liq} = \frac{\Omega}{2} \sqrt{S - (\tau_n - \tau_0)^2}, \text{ per sec} \quad (4-22)$$

or

$$\lambda_{liq} = \frac{\pi}{nd} \sqrt{S - (\tau_n - \tau_0)^2}, \text{ per ft} \quad (4-22a)$$

The algebraic sum of λ and the aerodynamic damping λ_1 will control the nutational amplitude.

At exact resonance $\tau_n = \tau_0$, the rate of divergence is maximum

$$\lambda_{max} = \frac{\Omega}{2} \sqrt{S}, \text{ per sec} \quad (4-23)$$

The width of the resonance band, on the frequency scale, is obtained by setting

$\lambda_{liq} = 0$ in Eq. 4—22. The width is

$$\Delta\tau_0 = \pm \sqrt{S}$$

or the width is $2\sqrt{S}$.

It can be readily seen that Eq. 4—22 is an equation of an ellipse with semi-major axis $= \frac{\Omega}{2} \sqrt{S}$ and semi-minor axis \sqrt{S} .

The elliptical shape of the resonance band is clearly shown in Fig. 4—2. As we shall see later, the introduction of viscosity markedly alters the shape of this band.

4—2.2 THE TABLES AND THEIR APPLICATION

In order to use Stewartson's instability criteria, Eq. 4—21, it is necessary to know the poles τ_0 and the residues $2R$ at these poles. These are functions of the geometry of the cavity c/a and the amount of fluid as determined by b^2/a^2 . Special tables, therefore, were prepared to facilitate the use of Eq. 4—21 for design purposes.

Let V_c be the volume of the cylindrical cavity. If it is filled to β fraction of its volume, then $\beta V_c = V_c(1 - b^2/a^2)$. b^2/a^2 is fractional volume of cylinder of air of diameter $2b$.

Each table is computed for a specific air volume ratio b^2/a^2 at 0.05 intervals. In each table — i.e., for a given b^2/a^2 — the first column, or the argument, gives the values of the fluid frequencies $\tau_0(n)$. This column is followed by a column pair, one headed by the quantity $c/[a(2j + 1)]$ and another by $2R$. The physical significance of the quantity $c/[a(2j + 1)]$, see Ch. 3, is that it is associated with longitudinal number of half-wave lengths of pressure fluctuations. Thus for $j = 0$ there is one-half of the full cosine wave in the cavity; $j = 1$ corresponds to $3/2$ waves; $j = 2$ to $5/2$ waves, etc.

It is to be noted that only antisymmetrical pressure waves give rise to hydrodynamic moments. The next column headed by $2R$ shows the residues corresponding to the associated frequencies. The first column pair corresponds to the radial mode $n = 1$. The succeeding column pairs, i.e., headed by $c/[a(2j + 1)]$ and $2R$, correspond to higher radial modes, $n = 2, 3$. Because the hydrodynamic moment is proportional to the residue at the corresponding pole, and these decrease very rapidly at higher radial modes, the Tables terminate at $n = 3$. In practice it is found (see Ref. 5 of Ch. 5) that the designer will usually be concerned only with the first column pair for $n = 1$. Other radial modes, unless unusual circumstances prevail such as an exceptionally high specific gravity of the fluid, lead to negligible moments and could be ignored. If desirable for peace of mind, they always can be computed and the resulting instability can be compared with the aerodynamic damping.

We shall make more extensive use of these Tables in Chapter 9. Here, we briefly illustrate their use as an introduction to the next paragraph where we shall apply Stewartson's instability criteria to the XM410 Projectile.

Problem 1. In designing a new projectile containing a cylindrical cavity, liquid-filled to 95%, we have to select the fineness-ratio of the cavity c/a in such a way that the cavity will contain no fluid frequencies in close proximity to the nutational frequency of the projectile. Let us assume that the nutational frequency of a loaded projectile is $\tau_n = 0.10$. From Stewartson's Tables we can readily find all c/a of cavities which contain fluid frequency $\tau_0 = 0.10$. In our design we should avoid all these fineness-ratios.

To find c/a of resonating cavities we go to the Tables to page marked $b^2/a^2 = 0.05$ (95% fill). On the line $\tau_0 = 0.10$, in the column headed by $c/[a(2j + 1)]$ for $n = 1$, we

find the following number 1.114. This number signifies that the following cavities, as defined by their fineness-ratios c/a , will contain fluid frequency $\tau_0 = 0.10$:

$$c/a = 1.114(2j + 1) \quad j = 0, 1, 2, \dots$$

j	c/a
0	1.114
1	3.34
2	5.57

etc.

Similarly for $n = 2$

$$c/a = 0.530(2j + 1) \quad j = 0, 1, 2, \dots$$

Avoid such cavities. The width of the resonance band also has to be taken into account. But such details will be discussed in Chapter 9.

Problem 2. Suppose a WP-loaded projectile with a cylindrical cavity filled to 95% is to be shipped to a hot climate where WP may become liquid. The fineness-ratio of the cavity is 2.1. The nutational frequency of the loaded system is $\tau_n = 0.10$. Is there a possibility that the projectile with liquid WP will become dynamically unstable? To answer this question we compute the following table by referring to the fluid frequencies and corresponding residues in Stewartson's Tables for $b^2/a^2 = 0.05$ (linear interpolation is used):

j	$\frac{2.1}{2j + 1}$	$\tau_0(nj)$	$2R$
0	2.10	0.48(1,0)	1.945
1	0.700	0.29(2,1)	0.141
2	0.420	0.26(3,2)	0.035
3	0.300	0.02(3,3)	0.002

Then compute the "Stewartson's parameter" S and perform the necessary test for instability by applying Eq. 4-21. Since none of the fluid frequencies is close to the nutational frequency $\tau_n = 0.10$, the projec-

tile appears to be safe. But the instability test has to be performed to assure one that this is so.

4-3 AN EXAMPLE: 152 MM WP PROJECTILE, XM410

The cavity of the XM410 Projectile, as shown in Fig. 2-1, is not cylindrical. Later we shall learn how to deal with such a cavity. For the present, however, let us assume that the cavity is cylindrical and is defined by its fineness-ratio $c/a = 1.56$, and its radius $a = 2.68$ inches.

The pertinent physical information needed for applying Stewartson's instability criteria to this projectile is

$$\begin{aligned} \text{Density of liquid WP } \rho &= 3.49 \text{ slug/ft}^3 \\ I_x &= 0.0446 \text{ slug-ft}^2 \\ a &= 0.223 \text{ ft} \\ \sigma &= 0.73 \\ \tau_n &= 0.25 \end{aligned}$$

Thus, by Eq. 4-19

$$S = 3.81 \times 10^{-2}(2R)^2$$

Suppose the cavity is to be filled to 95%, i.e., $b^2/a^2 = 0.05$. What fluid frequencies are present in this cavity with this percent of fill? To find this, we compute the following table

j	$\frac{1.56}{2j + 1}$	$\tau_0(nj)$	$2R$
0	1.56	0.343(1,0)	1.300
1	0.52	0.087(2,1)	0.0312
2	0.312	0.050(3,2)	0.0047

The last two columns in the above table were obtained from Stewartson's Tables by referring to the page corresponding to $b^2/a^2 = 0.05$ and finding the frequencies and the residues corresponding to $\frac{c}{a(2j + 1)} = 1.56, 0.52$, etc. One finds, for example, for

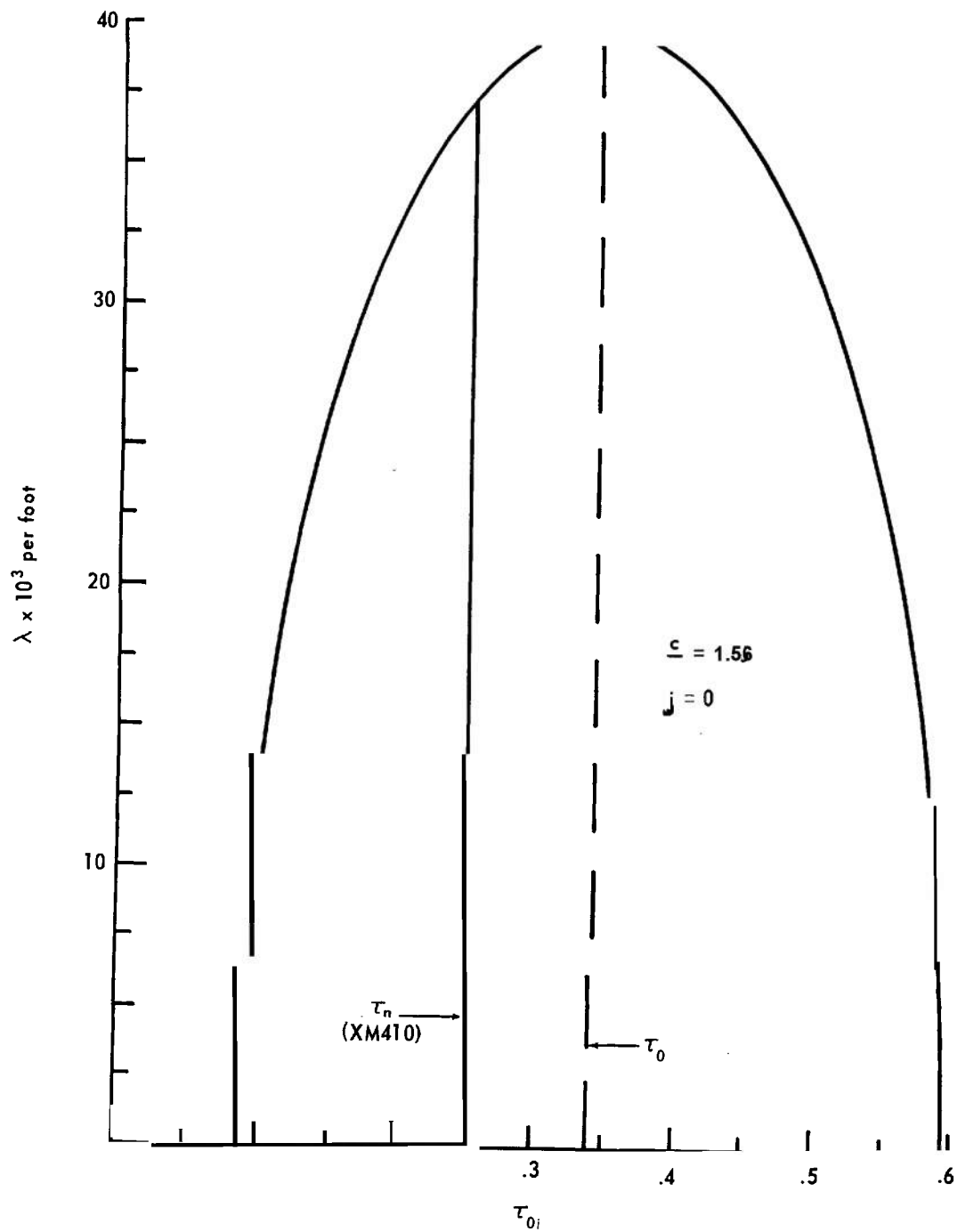


FIGURE 4-2. RESONANCE BAND IN THE CYLINDRICAL CAVITY OF THE XM410 PROJECTILE

1.56 the following

τ_0	$\frac{c}{a(2j+1)}$	$2R$
0.34	1.551	1.286
0.36	1.605	1.381

By simple linear interpolation the value of τ_0 for 1.56 is 0.343; other entries in the above table are similarly determined. Clearly, since $\tau_n = 0.25$, there is no need to consider higher values of j . Even $j = 2$ is unnecessary; τ_0 is too far removed from the resonance. With the residues we compute S and the middle term in Stewartson's inequality.

j	S	\sqrt{S}	$\tau_0 - \tau_n$	$\frac{\tau_0 - \tau_n}{\sqrt{S}}$
0	6.45×10^{-2}	0.254	0.093	0.37
1	0.37×10^{-4}	0.0061	-0.163	-26.7

For *instability*

$$-1 < \frac{\tau_0 - \tau_n}{\sqrt{S}} < 1$$

Therefore, this projectile is unstable because there is a fluid frequency $\tau_0 = 0.34$ for $j = 0$ which satisfies the instability condition.

It is interesting to note that for this projectile, although the fundamental fluid frequency $\tau_0 = 0.34$ is fairly far removed from the nutational frequency $\tau_n = 0.25$, the projectile is still unstable. The reason for this is the exceptional width of the band of frequencies present in this cavity

$$\tau_0 \pm \sqrt{S} = 0.34 \pm 0.25$$

or, from $\tau_{01} = 0.09$ to $\tau_{02} = 0.59$. This is shown in Fig. 4-2.

It is to be noted, however, that fluid frequencies $\tau_0 \pm \sqrt{S}$ are properties of the fluid

and the cavity. To be unstable, the projectile must satisfy the instability condition, see Eq. 4-20,

$$S - (\tau_0 - \tau_n)^2 > 0$$

Thus relative to the nutational frequency, the response of the projectile to the above range of fluid frequencies will be, on the high side, from

$$\tau_{01} = \tau_n + \sqrt{S} = 0.25 + 0.25 = 0.50$$

but on the low side, it cannot reach the computed value

$$\tau_{02} = \tau_n - \sqrt{S} = 0.25 - 0.25 = 0.00$$

because the lower limit of the frequency band present in the cavity is only $\tau_{02} = 0.09$.

Therefore, the resonance band, for this projectile, is assymmetric.

Such broadness of the frequency band is usually characteristic of the thin-walled, small fineness-ratio cavities. As we shall see later, to design such projectiles free of resonance instability usually presents very severe design problems.

The rate of divergence of the nutational amplitude, due to the liquid, is:

$$\lambda_{liq} = \frac{\Omega}{2} \sqrt{S - (\tau_0 - \tau_n)^2}, \text{ per sec}$$

or, as before:

$$\lambda_{liq} = \frac{\pi}{nd} \sqrt{S - (\tau_0 - \tau_n)^2}, \text{ per ft}$$

Using the above values of S and τ_0 for $j = 0$, we find

$$\lambda_{liq} = 37.2 \times 10^{-3}, \text{ per ft}$$

This is to be added to the aerodynamic damping of the nutational component $\lambda_1 = -1.60 \times 10^{-3}$ per ft. Therefore, the nutational amplitude initially will grow very rapidly.

4-4 CENTRAL COLUMN TABLES

As was pointed out in Chapter 3, the special simplification achieved when the boundaries are cylindrical renders possible the solution of another problem, namely, the completely filled cylindrical cavity with a cylindrical central body (burster). Central bursters are frequently employed in the design of WP projectiles.

However, to fill the cavity 100% is usually difficult to achieve in practice and, moreover, some space must always be provided for the expansion of the fluid when heated. Thus practical usefulness of this solution is limited. Nevertheless, special tables have been prepared to handle this problem when needed.

The tables, in their structure, are identical to Stewartson's Tables. The diameter of the central column is designated $2r$. Hence, the central column occupies r^2/a^2 fraction of the total volume. The ratio r^2/a^2 formally plays the same role as b^2/a^2 in Stewartson's Tables, i.e., each table is constructed for a specified r^2/a^2 . The remaining volume is always 100% full.

REFERENCES

1. E. A. Milne, *Report on the Stability of Liquid-Filled Shell* (U), EBD Report No. 6, 1940 (Confidential).
2. A. G. Greenhill, Proc. Camb. Phil. Soc. **4**, 4 (1880).

TABLE 4-1. STEWARTSON'S TABLES

FLUID FREQUENCIES AND RESIDUES FOR VARIOUS CYLINDRICAL CAVITIES OF HEIGHT $2c$ AND DIAMETER $2a$, AND VARIOUS FILL-RATIOS b^2/a^2 WHERE $2b$ IS THE DIAMETER OF THE AIR COLUMN

$b^2/a^2 = 0.00$						
τ_0	$n = 1$		$n = 2$		$n = 3$	
	$\frac{c}{a(2j+1)}$	$2R$	$\frac{c}{a(2j+1)}$	$2R$	$\frac{c}{a(2j+1)}$	$2R$
.00	.995	.000	.478	.0000	.310	.0000
.02	1.018	.058	.490	.0070	.319	.0019
.04	1.042	.118	.503	.0144	.327	.0040
.06	1.066	.181	.516	.0223	.336	.0062
.08	1.091	.246	.530	.0307	.345	.0086
.10	1.117	.313	.544	.0396	.355	.0111
.12	1.144	.382	.559	.0491	.364	.0139
.14	1.172	.454	.574	.0591	.375	.0168
.16	1.201	.528	.590	.0697	.385	.0198
.18	1.231	.604	.607	.0809	.397	.0231
.20	1.262	.682	.624	.0928	.408	.0266
.22	1.294	.762	.642	.1054	.420	.0304
.24	1.328	.845	.661	.1187	.433	.0344
.26	1.363	.930	.680	.1328	.446	.0387
.28	1.399	1.017	.700	.1478	.460	.0433
.30	1.437	1.107	.722	.1636	.475	.0481
.32	1.478	1.200	.745	.1804	.490	.0533
.34	1.521	1.295	.769	.1981	.506	.0589
.36	1.565	1.392	.794	.2169	.523	.0649
.38	1.612	1.491	.820	.2369	.541	.0714
.40	1.662	1.593	.848	.2581	.561	.0783
.42	1.715	1.698	.878	.2805	.582	.0858
.44	1.771	1.805	.910	.3043	.603	.0938
.46	1.831	1.914	.944	.3296	.626	.1024
.48	1.895	2.026	.980	.3566	.651	.1118
.50	1.963	2.142	1.019	.3853	.678	.1220

TABLE 4-1. STEWARTSON'S TABLES (CONT)

$$b^2/a^2 = 0.02$$

τ_0	$n = 1$		$n = 2$		$n = 3$	
	$\frac{c}{a(2j+1)}$	2R	$\frac{c}{a(2j+1)}$	2R	$\frac{c}{a(2j+1)}$	2R
.00	.994	.000	.475	.0000	.305	.0000
.02	1.017	.058	.488	.0068	.314	.0020
.04	1.041	.118	.501	.0141	.322	.0040
.06	1.066	.180	.514	.0219	.331	.0062
.08	1.091	.245	.528	.0302	.340	.0085
.10	1.117	.312	.542	.0389	.349	.0110
.12	1.144	.381	.556	.0481	.359	.0136
.14	1.173	.453	.572	.0578	.369	.0165
.16	1.202	.526	.588	.0680	.380	.0195
.18	1.232	.602	.605	.0788	.391	.0228
.20	1.264	.680	.623	.0902	.403	.0264
.22	1.297	.760	.642	.1023	.416	.0302
.24	1.332	.843	.662	.1151	.429	.0343
.26	1.369	.928	.682	.1285	.443	.0386
.28	1.407	1.014	.704	.1428	.458	.0433
.30	1.448	1.103	.727	.1579	.473	.0483
.32	1.491	1.194	.752	.1738	.490	.0538
.34	1.537	1.286	.778	.1906	.507	.0596
.36	1.586	1.380	.806	.2083	.526	.0660
.38	1.638	1.475	.837	.2268	.547	.0730
.40	1.695	1.570	.871	.2462	.569	.0807
.42	1.757	1.664	.909	.2665	.593	.0892
.44	1.825	1.755	.951	.2876	.620	.0985
.46	1.902	1.839	.998	.3095	.650	.1090
.48	1.990	1.909	1.051	.3321	.683	.1207
.50	2.097	1.953	1.112	.3553	.719	.1338
.52	2.234	1.951	1.191	.3811	.762	.1500
.54	2.439	1.877	1.295	.4160	.812	.1700
.56	2.841	1.759	1.441	.4820	.869	.1961
.58			1.647	.6419	.936	.2311
.60			1.893	.9860	1.012	.2774
.62			2.117	1.4607	1.094	.3348
.64			2.309	1.9151	1.181	.4001
.66			2.488	2.2961	1.272	.4694
.68			2.667	2.6144	1.368	.5400
.70			2.855	2.8913	1.471	.6116

TABLE 4-1. STEWARTSON'S TABLES (CONT)

$$b^2/a^2 = 0.05$$

τ_0	$n = 1$		$n = 2$		$n = 3$	
	$\frac{c}{a(2j+1)}$	2R	$\frac{c}{a(2j+1)}$	2R	$\frac{c}{a(2j+1)}$	2R
.00	.991	.000	.465	.0000	.291	.0000
.02	1.014	.058	.477	.0067	.299	.0018
.04	1.038	.118	.490	.0138	.307	.0037
.06	1.062	.180	.503	.0212	.316	.0057
.08	1.088	.245	.516	.0292	.324	.0078
.10	1.114	.311	.530	.0373	.333	.0101
.12	1.141	.381	.545	.0460	.343	.0126
.14	1.169	.452	.560	.0552	.353	.0153
.16	1.199	.525	.576	.0650	.363	.0182
.18	1.231	.601	.593	.0753	.374	.0213
.20	1.264	.679	.611	.0863	.385	.0246
.22	1.299	.759	.630	.0979	.397	.0282
.24	1.335	.841	.650	.1101	.410	.0321
.26	1.373	.926	.671	.1231	.423	.0362
.28	1.413	1.013	.693	.1368	.437	.0407
.30	1.456	1.102	.717	.1514	.452	.0455
.32	1.502	1.193	.742	.1668	.468	.0508
.34	1.551	1.286	.769	.1833	.485	.0565
.36	1.605	1.381	.798	.2009	.503	.0627
.38	1.663	1.477	.830	.2199	.522	.0696
.40	1.727	1.574	.865	.2405	.543	.0771
.42	1.799	1.670	.903	.2625	.566	.0855
.44	1.880	1.765	.946	.2867	.591	.0948
.46	1.974	1.857	.994	.3134	.617	.1051
.48	2.087	1.944	1.048	.3433	.647	.1167
.50	2.229	2.026	1.109	.3778	.679	.1296
.52	2.421	2.105	1.183	.4198	.715	.1447
.54	2.711	2.213	1.271	.4742	.755	.1622
.56	3.255	2.493	1.379	.5503	.800	.1828
.58	4.949	4.128	1.510	.6627	.851	.2072
.60			1.665	.8314	.907	.2363
.62			1.837	1.0676	.971	.2712
.64			2.016	1.3576	1.042	.3122
.66			2.198	1.6702	1.121	.3596
.68			2.382	1.9800	1.209	.4132
.70			2.575	2.2757	1.305	.4726

TABLE 4-1. STEWARTSON'S TABLES (CONT)

$$b^2/a^2 = 0.10$$

τ_0	$n = 1$		$n = 2$		$n = 3$	
	$\frac{c}{a(2j+1)}$	2R	$\frac{c}{a(2j+1)}$	2R	$\frac{c}{a(2j+1)}$	2R
.00	.981	.000	.441	.0000	.267	.0000
.02	1.003	.057	.453	.0061	.274	.0015
.04	1.027	.117	.465	.0125	.282	.0031
.06	1.051	.179	.477	.0193	.289	.0047
.08	1.078	.243	.490	.0265	.297	.0065
.10	1.103	.309	.503	.0339	.306	.0085
.12	1.130	.377	.517	.0417	.314	.0106
.14	1.158	.447	.532	.0500	.323	.0128
.16	1.189	.521	.547	.0588	.333	.0153
.18	1.221	.596	.563	.0682	.343	.0179
.20	1.255	.675	.580	.0781	.353	.0207
.22	1.290	.756	.598	.0886	.364	.0238
.24	1.328	.839	.617	.0998	.375	.0270
.26	1.368	.925	.637	.1116	.387	.0306
.28	1.410	1.014	.659	.1242	.400	.0344
.30	1.454	1.105	.681	.1376	.414	.0385
.32	1.502	1.199	.705	.1520	.428	.0430
.34	1.555	1.296	.731	.1675	.443	.0479
.36	1.612	1.397	.759	.1843	.459	.0531
.38	1.676	1.502	.789	.2025	.476	.0589
.40	1.749	1.611	.821	.2225	.495	.0653
.42	1.829	1.723	.857	.2443	.515	.0723
.44	1.921	1.841	.896	.2683	.537	.0800
.46	2.029	1.968	.940	.2950	.560	.0885
.48	2.160	2.107	.988	.3253	.585	.0979
.50	2.327	2.268	1.041	.3602	.612	.1084
.52	2.549	2.472	1.102	.4011	.643	.1203
.54	2.876	2.779	1.172	.4502	.676	.1337
.56	3.434	3.384	1.253	.5106	.712	.1489
.58	4.773	5.366	1.346	.5869	.753	.1663
.60			1.454	.6860	.798	.1865
.62			1.578	.8133	.849	.2097
.64			1.718	.9758	.906	.2368
.66			1.873	1.1707	.971	.2682
.68			2.041	1.3947	1.044	.3047
.70			2.222	1.6378	1.126	.3469

TABLE 4-1. STEWARTSON'S TABLES (CONT)

$$b^2/a^2 = 0.15$$

τ_0	$n = 1$		$n = 2$		$n = 3$	
	$\frac{c}{a(2j+1)}$	2R	$\frac{c}{a(2j+1)}$	2R	$\frac{c}{a(2j+1)}$	2R
.00	.966	.000	.415	.0000	.245	.0000
.02	.988	.057	.425	.0054	.251	.0012
.04	1.011	.115	.436	.0111	.258	.0025
.06	1.035	.176	.448	.0170	.265	.0039
.08	1.060	.239	.460	.0233	.272	.0054
.10	1.086	.304	.473	.0299	.280	.0070
.12	1.113	.371	.486	.0368	.288	.0087
.14	1.141	.441	.500	.0441	.296	.0106
.16	1.171	.514	.514	.0519	.305	.0126
.18	1.203	.590	.529	.0601	.314	.0148
.20	1.237	.668	.545	.0689	.323	.0171
.22	1.273	.750	.562	.0782	.333	.0196
.24	1.311	.834	.580	.0880	.343	.0223
.26	1.351	.921	.598	.0985	.354	.0253
.28	1.394	1.011	.618	.1097	.366	.0284
.30	1.439	1.104	.639	.1217	.378	.0318
.32	1.488	1.201	.662	.1346	.391	.0355
.34	1.542	1.303	.685	.1484	.405	.0395
.36	1.601	1.410	.711	.1635	.419	.0439
.38	1.668	1.523	.739	.1799	.435	.0487
.40	1.743	1.645	.769	.1978	.451	.0539
.42	1.826	1.773	.801	.2173	.469	.0596
.44	1.922	1.911	.836	.2389	.488	.0658
.46	2.035	2.064	.875	.2630	.509	.0727
.48	2.172	2.241	.918	.2900	.531	.0803
.50	2.343	2.458	.964	.3205	.556	.0887
.52	2.569	2.739	1.017	.3556	.582	.0981
.54	2.888	3.149	1.076	.3964	.611	.1087
.56	3.400	3.885	1.142	.4447	.643	.1206
.58	4.448	5.768	1.218	.5029	.678	.1340
.60	9.421	21.765	1.305	.5735	.717	.1493
.62			1.404	.6607	.760	.1668
.64			1.517	.7689	.809	.1870
.66			1.646	.9006	.864	.2103
.68			1.790	1.0582	.927	.2373
.70			1.951	1.2408	.998	.2688

TABLE 4-1. STEWARTSON'S TABLES (CONT)

$$b^2/a^2 = 0.20$$

τ_0	$n = 1$		$n = 2$		$n = 3$	
	$\frac{c}{a(2j+1)}$	2R	$\frac{c}{a(2j+1)}$	2R	$\frac{c}{a(2j+1)}$	2R
.00	.947	.000	.387	.0000	.224	.0000
.02	.968	.055	.398	.0048	.230	.0010
.04	.991	.113	.408	.0097	.236	.0020
.06	1.015	.172	.419	.0149	.242	.0032
.08	1.039	.234	.430	.0202	.249	.0044
.10	1.065	.298	.442	.0259	.256	.0057
.12	1.091	.364	.454	.0313	.263	.0071
.14	1.119	.433	.467	.0382	.271	.0086
.16	1.149	.504	.480	.0450	.279	.0103
.18	1.180	.579	.494	.0521	.287	.0121
.20	1.214	.657	.509	.0597	.295	.0140
.22	1.249	.739	.525	.0677	.305	.0160
.24	1.287	.823	.541	.0762	.314	.0183
.26	1.327	.910	.558	.0853	.324	.0207
.28	1.369	1.001	.577	.0951	.334	.0232
.30	1.415	1.096	.596	.1055	.346	.0260
.32	1.464	1.195	.617	.1167	.357	.0291
.34	1.518	1.299	.639	.1288	.370	.0323
.36	1.577	1.411	.662	.1419	.383	.0359
.38	1.644	1.530	.688	.1561	.397	.0398
.40	1.719	1.660	.715	.1717	.412	.0440
.42	1.803	1.800	.744	.1888	.428	.0487
.44	1.899	1.954	.776	.2077	.445	.0537
.46	2.011	2.129	.811	.2285	.464	.0593
.48	2.147	2.331	.849	.2516	.484	.0654
.50	2.315	2.576	.890	.2774	.505	.0722
.52	2.532	2.897	.937	.3070	.529	.0797
.54	2.831	3.358	.988	.3409	.555	.0881
.56	3.287	4.128	1.045	.3799	.583	.0976
.58	4.114	5.781	1.110	.4257	.614	.1082
.60	6.509	12.660	1.183	.4801	.648	.1202
.62			1.266	.5454	.687	.1338
.64			1.360	.6239	.729	.1495
.66			1.469	.7193	.778	.1674
.68			1.592	.8342	.832	.1883
.70			1.733	.9706	.894	.2125

TABLE 4-1. STEWARTSON'S TABLES (CONT)

$$b^2/a^2 = 0.25$$

τ_0	$n = 1$		$n = 2$		$n = 3$	
	$\frac{c}{a(2j+1)}$	2R	$\frac{c}{a(2j+1)}$	2R	$\frac{c}{a(2j+1)}$	2R
.00	.925	.000	.360	.0000	.205	.0000
.02	.946	.054	.370	.0041	.210	.0008
.04	.968	.110	.379	.0083	.216	.0016
.06	.991	.168	.389	.0127	.222	.0026
.08	1.015	.229	.400	.0173	.228	.0035
.10	1.039	.290	.411	.0221	.234	.0046
.12	1.065	.354	.422	.0272	.241	.0058
.14	1.092	.422	.434	.0326	.248	.0070
.16	1.122	.492	.446	.0383	.255	.0083
.18	1.153	.565	.459	.0444	.262	.0098
.20	1.185	.642	.473	.0509	.270	.0113
.22	1.220	.722	.488	.0577	.278	.0130
.24	1.257	.806	.503	.0650	.287	.0148
.26	1.296	.893	.519	.0728	.296	.0168
.28	1.338	.983	.536	.0811	.306	.0189
.30	1.383	1.078	.553	.0900	.316	.0211
.32	1.432	1.178	.572	.0996	.326	.0236
.34	1.485	1.285	.593	.1100	.338	.0263
.36	1.543	1.398	.614	.1211	.350	.0291
.38	1.609	1.522	.637	.1333	.362	.0323
.40	1.683	1.657	.662	.1466	.376	.0357
.42	1.765	1.803	.689	.1612	.390	.0395
.44	1.859	1.966	.718	.1772	.406	.0436
.46	1.970	2.150	.749	.1949	.423	.0481
.48	2.100	2.366	.783	.2144	.441	.0530
.50	2.261	2.630	.820	.2361	.460	.0584
.52	2.465	2.970	.861	.2607	.481	.0645
.54	2.739	3.443	.907	.2887	.504	.0712
.56	3.138	4.190	.957	.3206	.530	.0787
.58	3.802	5.616	1.013	.3573	.557	.0871
.60	5.307	9.816	1.076	.4004	.588	.0966
.62			1.148	.4511	.622	.1074
.64			1.229	.5111	.660	.1197
.66			1.322	.5834	.703	.1339
.68			1.428	.6695	.751	.1502
.70			1.550	.7727	.806	.1692

TABLE 4-1. STEWARTSON'S TABLES (CONT)

$$b^2/a^2 = 0.30$$

τ_0	$n = 1$		$n = 2$		$n = 3$	
	$\frac{c}{a(2j+1)}$	2R	$\frac{c}{a(2j+1)}$	2R	$\frac{c}{a(2j+1)}$	2R
.00	.900	.000	.333	.0000	.187	.0000
.02	.920	.052	.342	.0034	.192	.0006
.04	.941	.106	.351	.0070	.197	.0013
.06	.963	.162	.360	.0106	.202	.0020
.08	.987	.220	.370	.0145	.208	.0028
.10	1.011	.281	.380	.0186	.213	.0037
.12	1.036	.343	.391	.0229	.219	.0046
.14	1.063	.408	.402	.0274	.226	.0056
.16	1.091	.476	.413	.0322	.232	.0067
.18	1.121	.548	.425	.0373	.239	.0079
.20	1.153	.623	.438	.0428	.246	.0091
.22	1.187	.701	.451	.0485	.254	.0105
.24	1.223	.783	.465	.0547	.262	.0119
.26	1.261	.869	.480	.0612	.270	.0135
.28	1.302	.958	.495	.0682	.279	.0152
.30	1.346	1.052	.512	.0757	.288	.0170
.32	1.393	1.152	.529	.0838	.297	.0190
.34	1.445	1.258	.548	.0925	.308	.0211
.36	1.502	1.372	.567	.1019	.318	.0235
.38	1.565	1.496	.588	.1122	.330	.0260
.40	1.637	1.633	.611	.1234	.342	.0288
.42	1.717	1.781	.635	.1356	.356	.0318
.44	1.808	1.948	.661	.1490	.370	.0351
.46	1.913	2.138	.690	.1638	.385	.0387
.48	2.037	2.360	.720	.1801	.401	.0426
.50	2.188	2.629	.754	.1982	.419	.0470
.52	2.378	2.972	.790	.2185	.438	.0518
.54	2.625	3.437	.831	.2415	.458	.0571
.56	2.973	4.134	.875	.2676	.481	.0631
.58	3.517	5.361	.925	.2974	.506	.0698
.60	4.564	8.244	.980	.3319	.533	.0774
.62	8.380	24.961	1.042	.3718	.564	.0859
.64			1.113	.4189	.598	.0957
.66			1.193	.4746	.636	.1068
.68			1.286	.5410	.679	.1197
.70			1.391	.6197	.728	.1346

TABLE 4-7. STEWARTSON'S TABLES (CONT)

$$b^2/a^2 = 0.35$$

τ_0	$n = 1$		$n = 2$		$n = 3$	
	$\frac{c}{a(2j+1)}$	2R	$\frac{c}{a(2j+1)}$	2R	$\frac{c}{a(2j+1)}$	2R
.00	.872	.000	.307	.0000	.170	.0000
.02	.892	.050	.315	.0028	.174	.0005
.04	.912	.102	.323	.0057	.179	.0010
.06	.934	.155	.332	.0088	.184	.0016
.08	.957	.211	.341	.0120	.189	.0023
.10	.980	.269	.350	.0154	.194	.0029
.12	1.004	.329	.360	.0189	.200	.0037
.14	1.030	.392	.370	.0227	.205	.0045
.16	1.057	.458	.380	.0267	.211	.0053
.18	1.086	.527	.391	.0309	.217	.0063
.20	1.117	.600	.403	.0354	.224	.0073
.22	1.150	.676	.415	.0402	.231	.0083
.24	1.184	.755	.428	.0453	.238	.0095
.26	1.221	.838	.441	.0507	.245	.0108
.28	1.261	.926	.456	.0565	.253	.0121
.30	1.303	1.018	.471	.0628	.261	.0136
.32	1.349	1.116	.487	.0695	.270	.0151
.34	1.399	1.220	.503	.0767	.280	.0169
.36	1.454	1.333	.521	.0845	.289	.0187
.38	1.515	1.457	.541	.0930	.300	.0207
.40	1.584	1.593	.561	.1023	.311	.0229
.42	1.659	1.741	.583	.1124	.323	.0253
.44	1.746	1.908	.607	.1235	.336	.0279
.46	1.846	2.097	.632	.1357	.349	.0308
.48	1.963	2.317	.660	.1492	.364	.0339
.50	2.104	2.582	.690	.1640	.380	.0374
.52	2.277	2.916	.723	.1807	.397	.0412
.54	2.500	3.359	.759	.1995	.416	.0455
.56	2.802	3.996	.799	.2207	.436	.0502
.58	3.250	5.039	.843	.2448	.458	.0555
.60	4.022	7.143	.892	.2724	.483	.0615
.62	5.920	14.119	.946	.3043	.510	.0682
.64			1.008	.3415	.541	.0759
.66			1.078	.3851	.575	.0847
.68			1.159	.4366	.613	.0948
.70			1.251	.4980	.657	.1065

TABLE 4-1. STEWARTSON'S TABLES (CONT)

$$b^2/a^2 = 0.40$$

τ_0	$n = 1$		$n = 2$		$n = 3$	
	$\frac{c}{a(2j+1)}$	2R	$\frac{c}{a(2j+1)}$	2R	$\frac{c}{a(2j+1)}$	2R
.00	.842	.000	.281	.0000	.154	.0000
.02	.861	.047	.288	.0023	.158	.0004
.04	.881	.097	.296	.0047	.162	.0008
.06	.901	.148	.304	.0072	.166	.0013
.08	.923	.201	.312	.0098	.171	.0018
.10	.945	.256	.320	.0125	.176	.0023
.12	.969	.313	.329	.0154	.181	.0029
.14	.994	.373	.338	.0185	.186	.0035
.16	1.020	.436	.348	.0218	.191	.0042
.18	1.048	.503	.358	.0252	.197	.0049
.20	1.077	.572	.369	.0289	.203	.0057
.22	1.109	.645	.380	.0328	.209	.0066
.24	1.142	.722	.392	.0369	.215	.0075
.26	1.178	.802	.404	.0414	.222	.0085
.28	1.215	.886	.417	.0461	.229	.0095
.30	1.256	.975	.431	.0512	.237	.0107
.32	1.300	1.070	.445	.0567	.245	.0119
.34	1.348	1.172	.460	.0626	.253	.0133
.36	1.401	1.282	.477	.0690	.262	.0147
.38	1.459	1.402	.494	.0759	.271	.0163
.40	1.524	1.535	.513	.0835	.281	.0181
.42	1.596	1.680	.533	.0917	.292	.0199
.44	1.677	1.842	.554	.1008	.304	.0220
.46	1.771	2.026	.577	.1107	.316	.0243
.48	1.881	2.240	.602	.1217	.329	.0267
.50	2.010	2.497	.629	.1337	.343	.0294
.52	2.168	2.814	.658	.1473	.359	.0324
.54	2.367	3.226	.691	.1624	.376	.0358
.56	2.629	3.799	.726	.1795	.394	.0395
.58	3.000	4.675	.765	.1989	.414	.0436
.60	3.591	6.270	.809	.2210	.436	.0483
.62	4.764	10.204	.857	.2463	.460	.0536
.64	9.819	39.504	.911	.2757	.488	.0596
.66			.973	.3100	.518	.0664
.68			1.043	.3502	.552	.0744
.70			1.124	.3980	.592	.0835

TABLE 4-1. STEWARTSON'S TABLES (CONT)

$$b^2/a^2 = 0.45$$

τ_0	$n = 1$		$n = 2$		$n = 3$	
	$\frac{c}{a(2j+1)}$	2R	$\frac{c}{a(2j+1)}$	2R	$\frac{c}{a(2j+1)}$	2R
.00	.810	.000	.255	.0000	.138	.0000
.02	.828	.045	.262	.0018	.142	.0003
.04	.847	.092	.269	.0037	.146	.0006
.06	.866	.140	.276	.0057	.150	.0010
.08	.887	.190	.284	.0078	.154	.0014
.10	.908	.242	.291	.0100	.158	.0018
.12	.931	.296	.299	.0123	.163	.0022
.14	.954	.353	.308	.0148	.167	.0027
.16	.979	.412	.317	.0174	.172	.0032
.18	1.006	.475	.326	.0202	.177	.0038
.20	1.034	.541	.335	.0231	.182	.0044
.22	1.064	.610	.346	.0263	.188	.0051
.24	1.096	.683	.356	.0296	.194	.0058
.26	1.130	.759	.367	.0332	.200	.0066
.28	1.166	.840	.379	.0370	.206	.0074
.30	1.205	.925	.391	.0410	.213	.0083
.32	1.247	1.016	.405	.0454	.220	.0092
.34	1.292	1.114	.418	.0502	.228	.0103
.36	1.342	1.220	.433	.0553	.236	.0114
.38	1.397	1.335	.449	.0609	.244	.0127
.40	1.459	1.462	.466	.0669	.253	.0140
.42	1.528	1.604	.484	.0735	.263	.0155
.44	1.603	1.760	.503	.0808	.273	.0171
.46	1.691	1.937	.524	.0888	.284	.0188
.48	1.792	2.141	.546	.0975	.296	.0207
.50	1.910	2.380	.570	.1072	.309	.0228
.52	2.052	2.676	.596	.1180	.323	.0252
.54	2.229	3.052	.625	.1301	.338	.0277
.56	2.456	3.560	.657	.1437	.354	.0306
.58	2.766	4.299	.691	.1590	.372	.0338
.60	3.227	5.527	.730	.1765	.392	.0374
.62	4.028	8.043	.773	.1965	.413	.0415
.64	6.051	16.751	.821	.2196	.438	.0461
.66			.875	.2464	.465	.0514
.68			.937	.2778	.495	.0576
.70			1.007	.3148	.530	.0646

TABLE 4-1. STEWARTSON'S TABLES (CONT)

$$b^2/a^2 = 0.50$$

τ_0	$n = 1$		$n = 2$		$n = 3$	
	$\frac{c}{a(2j+1)}$	2R	$\frac{c}{a(2j+1)}$	2R	$\frac{c}{a(2j+1)}$	2R
.00	.775	.000	.230	.0000	.123	.0000
.02	.792	.042	.236	.0014	.127	.0002
.04	.810	.085	.243	.0029	.130	.0005
.06	.828	.131	.249	.0045	.134	.0007
.08	.848	.178	.256	.0061	.137	.0010
.10	.869	.226	.263	.0078	.141	.0014
.12	.890	.277	.270	.0097	.145	.0017
.14	.912	.330	.278	.0116	.149	.0021
.16	.936	.386	.286	.0137	.154	.0025
.18	.961	.444	.294	.0158	.158	.0029
.20	.988	.506	.303	.0181	.163	.0034
.22	1.017	.571	.312	.0206	.168	.0039
.24	1.047	.640	.321	.0232	.173	.0044
.26	1.079	.712	.331	.0260	.179	.0050
.28	1.113	.788	.342	.0290	.184	.0056
.30	1.150	.869	.353	.0322	.190	.0063
.32	1.190	.955	.365	.0357	.197	.0070
.34	1.233	1.047	.377	.0394	.203	.0078
.36	1.280	1.147	.391	.0434	.211	.0087
.38	1.331	1.256	.405	.0478	.218	.0096
.40	1.389	1.377	.420	.0526	.226	.0107
.42	1.453	1.510	.436	.0578	.235	.0118
.44	1.525	1.659	.453	.0635	.244	.0130
.46	1.606	1.828	.472	.0697	.254	.0143
.48	1.698	2.018	.492	.0766	.264	.0158
.50	1.803	2.236	.513	.0842	.276	.0174
.52	1.931	2.507	.537	.0926	.288	.0191
.54	2.088	2.847	.562	.1021	.301	.0211
.56	2.284	3.290	.590	.1127	.316	.0233
.58	2.543	3.910	.621	.1247	.332	.0257
.60	2.909	4.866	.655	.1383	.349	.0285
.62	3.487	6.588	.693	.1539	.369	.0316
.64	4.625	10.812	.735	.1718	.390	.0351
.66	9.260	39.918	.783	.1926	.414	.0391
.68			.836	.2167	.442	.0438
.70			.898	.2453	.472	.0492

TABLE 4-1. STEWARTSON'S TABLES (CONT)

$$b^2/a^2 = 0.60$$

T_0	$n = 1$		$n = 2$		$n = 3$	
	$a(2j + 1)$	$2R$	$a(2j + 1)$	$2R$	$a(2j + 1)$	$2R$
.00	.697	.000	.182	.0000	.096	.0000
.02	.712	.035	.186	.0008	.098	.0001
.04	.728	.071	.191	.0017	.101	.0003
.06	.744	.109	.196	.0025	.104	.0004
.08	.762	.149	.202	.0035	.107	.0006
.10	.780	.190	.207	.0044	.110	.0007
.12	.799	.233	.213	.0055	.113	.0009
.14	.819	.278	.219	.0066	.116	.0011
.16	.840	.325	.225	.0077	.119	.0013
.18	.862	.375	.232	.0090	.123	.0016
.20	.886	.427	.239	.0103	.126	.0018
.22	.911	.482	.246	.0117	.130	.0021
.24	.937	.541	.254	.0132	.134	.0024
.26	.966	.602	.261	.0147	.138	.0027
.28	.996	.667	.270	.0164	.143	.0030
.30	1.028	.736	.278	.0183	.148	.0034
.32	1.063	.810	.288	.0202	.152	.0038
.34	1.100	.889	.298	.0224	.158	.0042
.36	1.141	.975	.308	.0247	.163	.0047
.38	1.185	1.068	.319	.0272	.169	.0052
.40	1.234	1.170	.331	.0299	.175	.0057
.42	1.288	1.283	.343	.0328	.182	.0063
.44	1.348	1.409	.357	.0361	.189	.0070
.46	1.416	1.549	.371	.0397	.197	.0077
.48	1.491	1.708	.387	.0436	.205	.0085
.50	1.577	1.886	.403	.0479	.214	.0093
.52	1.678	2.102	.422	.0527	.223	.0103
.54	1.798	2.364	.441	.0581	.233	.0113
.56	1.942	2.689	.463	.0642	.245	.0125
.58	2.124	3.114	.487	.0710	.257	.0138
.60	2.360	3.702	.513	.0787	.270	.0153
.62	2.687	4.585	.541	.0875	.285	.0170
.64	3.191	6.133	.574	.0976	.302	.0189
.66	4.116	9.591	.610	.1092	.320	.0210
.68	6.948	25.388	.650	.1228	.341	.0235
.70			.697	.1388	.365	.0264

TABLE 4-1. STEWARTSON'S TABLES (CONT)

$$b^2/a^2 = 0.70$$

τ_0	$n = 1$		$n = 2$		$n = 3$	
	$\frac{c}{a(2j+1)}$	$2R$	$\frac{c}{a(2j+1)}$	$2R$	$\frac{c}{a(2j+1)}$	$2R$
.00	.606	.000	.134	.0000	.070	.0000
.02	.619	.028	.138	.0004	.072	.0001
.04	.633	.057	.142	.0008	.074	.0001
.06	.647	.086	.145	.0012	.076	.0002
.08	.661	.117	.149	.0017	.078	.0003
.10	.677	.149	.154	.0021	.080	.0003
.12	.693	.183	.158	.0026	.082	.0004
.14	.710	.218	.162	.0032	.084	.0005
.16	.728	.256	.167	.0037	.087	.0006
.18	.747	.295	.172	.0043	.090	.0007
.20	.767	.336	.177	.0050	.092	.0008
.22	.788	.380	.182	.0056	.095	.0009
.24	.811	.426	.188	.0063	.098	.0011
.26	.835	.474	.194	.0071	.101	.0012
.28	.860	.526	.200	.0079	.104	.0014
.30	.887	.580	.206	.0088	.108	.0016
.32	.916	.639	.213	.0098	.111	.0017
.34	.948	.702	.220	.0108	.115	.0019
.36	.981	.769	.228	.0119	.119	.0021
.38	1.018	.843	.236	.0131	.123	.0024
.40	1.058	.923	.245	.0145	.128	.0026
.42	1.102	1.012	.254	.0159	.133	.0029
.44	1.151	1.109	.264	.0175	.138	.0032
.46	1.204	1.217	.275	.0192	.143	.0035
.48	1.264	1.338	.286	.0211	.149	.0039
.50	1.330	1.473	.298	.0232	.156	.0043
.52	1.407	1.632	.312	.0256	.163	.0047
.54	1.496	1.818	.326	.0282	.170	.0052
.56	1.600	2.042	.342	.0312	.178	.0058
.58	1.725	2.319	.359	.0345	.187	.0064
.60	1.878	2.674	.378	.0382	.197	.0070
.62	2.074	3.152	.399	.0425	.208	.0078
.64	2.337	3.845	.422	.0474	.220	.0087
.66	2.718	4.960	.448	.0531	.233	.0097
.68	3.347	7.116	.478	.0597	.248	.0108
.70	4.729	13.311	.511	.0675	.265	.0122

TABLE 4-7. STEWARTSON'S TABLES (CONT)

$$b^2/a^2 = 0.80$$

τ_0	$n = 1$		$n = 2$	
	$\frac{c}{a(2j+1)}$	2R	$\frac{c}{a(2j+1)}$	2R
.00	.496	.000	.088	.0000
.02	.507	.019	.091	.0001
.04	.517	.039	.093	.0003
.06	.529	.060	.096	.0004
.08	.541	.081	.098	.0006
.10	.553	.104	.101	.0008
.12	.566	.127	.104	.0009
.14	.580	.152	.107	.0011
.16	.594	.178	.110	.0013
.18	.609	.205	.113	.0016
.20	.625	.234	.117	.0018
.22	.642	.264	.120	.0020
.24	.660	.296	.124	.0023
.26	.679	.330	.128	.0026
.28	.699	.366	.132	.0029
.30	.720	.405	.136	.0032
.32	.743	.445	.141	.0035
.34	.768	.489	.145	.0039
.36	.794	.536	.150	.0043
.E	.822	.587	.156	.0048
.E	.853	.643	.162	.0052
.42	.887	.703	.168	.0058
.44	.923	.770	.174	.0063
.46	.963	.843	.181	.0070
.48	1.007	.924	.189	.0077
.50	1.056	1.013	.197	.0084
.52	1.110	1.116	.205	.0093
.54	1.172	1.234	.215	.0102
.56	1.243	1.371	.225	.0113
.58	1.325	1.534	.237	.0125
.60	1.422	1.731	.249	.0139
.62	1.537	1.975	.263	.0154
.64	1.681	2.294	.278	.0172
.66	1.863	2.721	.295	.0193
.68	2.108	3.346	.314	.0217
.70	2.466	4.367	.335	.0246

TABLE 4-2. TABLES FOR CYLINDRICAL CAVITIES WITH CENTRAL COLUMN

FLUID FREQUENCIES AND RESIDUES FOR VARIOUS CYLINDRICAL CAVITIES OF HEIGHT $2c$ AND DIAMETER $2a$, WITH CYLINDRICAL CENTRAL COLUMN OF DIAMETER $2t$. THE REMAINING CAVITY IS ALWAYS 100% FILLED.

TABLE 4-2. TABLES FOR CYLINDRICAL CAVITIES WITH CENTRAL COLUMN (CONT)

$r^2/a^2 = 0.0025$						
τ_0	$n = 1$		$n = 2$		$n = 3$	
	$\frac{c}{a(2j+1)}$	$2R$	$\frac{c}{a(2j+1)}$	$2R$	$\frac{c}{a(2j+1)}$	$2R$
.00	.981	.000	.465	.0000	.299	.0000
.02	1.005	.057	.477	.0063	.307	.0019
.04	1.028	.117	.490	.0130	.316	.0039
.06	1.053	.178	.503	.0202	.324	.0060
.08	1.078	.242	.517	.0279	.333	.0083
.10	1.104	.309	.531	.0361	.343	.0108
.12	1.130	.377	.546	.0449	.352	.0134
.14	1.158	.448	.561	.0541	.363	.0162
.16	1.187	.521	.577	.0640	.373	.0192
.18	1.217	.597	.593	.0746	.384	.0224
.20	1.248	.674	.610	.0857	.396	.0258
.22	1.280	.755	.628	.0976	.408	.0295
.24	1.314	.837	.647	.1102	.420	.0333
.26	1.349	.922	.666	.1236	.433	.0375
.28	1.385	1.009	.687	.1378	.447	.0419
.30	1.424	1.098	.708	.1529	.461	.0467
.32	1.464	1.190	.730	.1689	.477	.0518
.34	1.506	1.284	.754	.1859	.493	.0573
.36	1.550	1.381	.779	.2039	.510	.0631
.38	1.597	1.480	.805	.2231	.528	.0694
.40	1.647	1.582	.833	.2435	.547	.0762
.42	1.699	1.686	.863	.2652	.567	.0835
.44	1.755	1.793	.895	.2882	.588	.0913
.46	1.815	1.903	.928	.3128	.611	.0998
.48	1.878	2.016	.964	.3389	.636	.1089
.50	1.946	2.132	1.003	.3668	.663	.1189
.52	2.020	2.250	1.044	.3966	.691	.1296
.54	2.099	2.373	1.089	.4283	.722	.1413
.56	2.184	2.498	1.137	.4622	.755	.1541
.58	2.278	2.628	1.190	.4985	.792	.1680
.60	2.380	2.762	1.247	.5374	.831	.1832
.62	2.492	2.901	1.310	.5791	.875	.2000
.64	2.616	3.045	1.380	.6239	.924	.2124
.66	2.754	3.195	1.458	.6720	.977	.2387
.68	2.908	3.351	1.544	.7239	1.037	.2612
.70	3.082	3.516	1.641	.7799	1.105	.2861

TABLE 4-2. TABLES FOR CYLINDRICAL CAVITIES WITH CENTRAL COLUMN (CONT)

$r^2/a^2 = 0.02$						
T_0	$n = 1$		$n = 2$		$n = 3$	
	$\frac{c}{a(2j+1)}$	2R	$\frac{c}{a(2j+1)}$	2R	$\frac{c}{a(2j+1)}$	2R
.00	.903	.000	.410	.0000	.262	.0000
.02	.926	.051	.422	.0038	.269	.0016
.04	.949	.105	.434	.0079	.277	.0033
.06	.973	.161	.446	.0124	.285	.0052
.08	.998	.220	.459	.0173	.293	.0071
.10	1.024	.281	.473	.0226	.301	.0092
.12	1.050	.345	.486	.0284	.310	.0115
.14	1.078	.411	.501	.0346	.320	.0139
.16	1.106	.479	.516	.0413	.329	.0165
.18	1.135	.550	.531	.0486	.339	.0192
.20	1.166	.624	.548	.0564	.350	.0222
.22	1.197	.700	.565	.0649	.361	.0254
.24	1.230	.778	.582	.0740	.373	.0288
.26	1.264	.859	.601	.0838	.385	.0324
.28	1.300	.943	.620	.0943	.398	.0363
.30	1.338	1.029	.641	.1056	.411	.0405
.32	1.377	1.118	.662	.1178	.425	.0449
.34	1.418	1.209	.685	.1309	.440	.0497
.36	1.461	1.303	.708	.1450	.456	.0549
.38	1.507	1.400	.733	.1601	.472	.0604
.40	1.555	1.499	.760	.1763	.490	.0664
.42	1.606	1.602	.788	.1937	.509	.0728
.44	1.660	1.707	.818	.2124	.529	.0798
.46	1.718	1.815	.850	.2326	.551	.0873
.48	1.779	1.927	.884	.2542	.574	.0955
.50	1.845	2.041	.921	.2775	.598	.1043
.52	1.916	2.159	.960	.3025	.625	.1139
.54	1.992	2.280	1.002	.3295	.654	.1243
.56	2.075	2.405	1.048	.3586	.685	.1358
.58	2.164	2.534	1.098	.3899	.719	.1483
.60	2.263	2.668	1.153	.4237	.756	.1620
.62	2.371	2.806	1.213	.4602	.797	.1771
.64	2.490	2.950	1.279	.4997	.842	.1938
.66	2.623	3.100	1.352	.5425	.892	.2122
.68	2.771	3.257	1.433	.5888	.948	.2327
.70	2.937	3.421	1.525	.6391	1.011	.2555

TABLE 4-2. TABLES FOR CYLINDRICAL CAVITIES WITH CENTRAL COLUMN (CONT)

$r^2/a^2 = 0.05$						
τ_0	$n = 1$		$n = 2$		$n = 3$	
	$\frac{c}{a(2j+1)}$	2R	$\frac{c}{a(2j+1)}$	2R	$\frac{c}{a(2j+1)}$	2R
.00	.800	.000	.359	.0000	.231	.0000
.02	.822	.043	.370	.0022	.238	.0013
.04	.845	.088	.380	.0045	.245	.0027
.06	.868	.136	.391	.0071	.252	.0042
.08	.892	.186	.403	.0099	.259	.0058
.10	.916	.239	.415	.0130	.266	.0075
.12	.942	.294	.427	.0164	.274	.0094
.14	.968	.352	.440	.0201	.283	.0114
.16	.995	.413	.454	.0242	.291	.0135
.18	1.024	.476	.468	.0286	.300	.0158
.20	1.053	.543	.482	.0334	.309	.0183
.22	1.083	.611	.498	.0387	.319	.0209
.24	1.115	.683	.514	.0444	.329	.0238
.26	1.148	.757	.531	.0507	.340	.0268
.28	1.182	.834	.549	.0575	.352	.0301
.30	1.218	.914	.567	.0649	.364	.0336
.32	1.256	.997	.587	.0730	.376	.0373
.34	1.295	1.083	.607	.0818	.330	.0414
.36	1.336	1.172	.629	.0914	.404	.0458
.38	1.380	1.263	.652	.1019	.419	.0505
.40	1.426	1.358	.677	.1133	.435	.0556
.42	1.475	1.456	.703	.1257	.452	.0611
.44	1.526	1.557	.731	.1392	.470	.0670
.46	1.581	1.661	.760	.1539	.489	.0735
.48	1.640	1.769	.792	.1699	.510	.0805
.50	1.702	1.880	.826	.1874	.532	.0881
.52	1.769	1.995	.862	.2064	.557	.0964
.54	1.841	2.113	.902	.2272	.583	.1055
.56	1.920	2.235	.944	.2498	.611	.1154
.58	2.005	2.362	.990	.2746	.642	.1263
.60	2.097	2.494	1.041	.3016	.676	.1383
.62	2.199	2.630	1.097	.3311	.714	.1516
.64	2.312	2.772	1.150	.3634	.755	.1662
.66	2.437	2.920	1.226	.3987	.801	.1825
.68	2.576	3.074	1.301	.4374	.852	.2007
.70	2.732	3.237	1.386	.4798	.910	.2210

TABLE 4-2. TABLES FOR CYLINDRICAL CAVITIES WITH CENTRAL COLUMN (CONT)

$r^2/a^2 = 0.10$						
τ_0	$n = 1$		$n = 2$		$n = 3$	
	$\frac{c}{a(2j \pm 1)}$	$2R$	$\frac{c}{a(2j \pm 1)}$	$2R$	$\frac{c}{a(2j \pm 1)}$	$2R$
.00	.675	.000	.308	.0000	.201	.0000
.02	.695	.032	.317	.0011	.207	.0010
.04	.715	.066	.326	.0024	.212	.0021
.06	.736	.102	.335	.0037	.218	.0032
.08	.758	.141	.345	.0052	.225	.0044
.10	.780	.182	.355	.0068	.231	.0057
.12	.803	.225	.366	.0086	.238	.0071
.14	.827	.272	.377	.0105	.245	.0087
.16	.852	.320	.388	.0126	.252	.0103
.18	.878	.372	.401	.0149	.260	.0120
.20	.905	.426	.413	.0175	.268	.0139
.22	.933	.483	.426	.0202	.276	.0159
.24	.962	.543	.440	.0233	.285	.0181
.26	.993	.606	.455	.0266	.294	.0205
.28	1.025	.672	.470	.0303	.304	.0230
.30	1.058	.741	.486	.0343	.314	.0257
.32	1.093	.813	.503	.0388	.325	.0286
.34	1.129	.888	.521	.0436	.337	.0318
.36	1.167	.967	.540	.0490	.349	.0352
.38	1.208	1.049	.560	.0550	.362	.0389
.40	1.250	1.134	.582	.0615	.376	.0428
.42	1.295	1.223	.605	.0687	.390	.0472
.44	1.343	1.315	.629	.0767	.406	.0519
.46	1.394	1.411	.655	.0856	.423	.0570
.48	1.448	1.551	.683	.0954	.441	.0626
.50	1.506	1.514	.713	.1063	.460	.0687
.52	1.568	1.722	.746	.1184	.481	.0754
.54	1.634	1.834	.781	.1318	.504	.0828
.56	1.706	1.950	.819	.1467	.529	.0909
.58	1.784	2.071	.860	.1633	.556	.0998
.60	1.870	2.197	.905	.1817	.586	.1097
.62	1.963	2.328	.955	.2023	.619	.1206
.64	2.066	2.464	1.010	.2252	.655	.1328
.66	2.180	2.607	1.071	.2507	.696	.1465
.68	2.307	2.757	1.139	.2792	.741	.1618
.70	2.449	2.915	1.215	.3110	.792	.1790

TABLE 4-2. TABLES FOR CYLINDRICAL CAVITIES WITH CENTRAL COLUMN (CONT)

$r^2/a^2 = 0.15$						
T_0	$n = 1$		$n = 2$		$n = 3$	
	$\frac{c}{a(2j+1)}$	$2R$	$\frac{c}{a(2j+1)}$	$2R$	$\frac{c}{a(2j+1)}$	$2R$
.00	.585	.000	.273	.0000	.179	.0000
.02	.602	.024	.280	.0007	.184	.0008
.04	.620	.050	.288	.0015	.189	.0016
.06	.638	.078	.296	.0023	.194	.0025
.08	.657	.107	.305	.0032	.200	.0035
.10	.677	.139	.314	.0041	.206	.0045
.12	.698	.173	.323	.0052	.212	.0056
.14	.719	.209	.333	.0063	.218	.0068
.16	.741	.248	.343	.0076	.224	.0080
.18	.765	.289	.353	.0090	.231	.0094
.20	.789	.333	.364	.0104	.238	.0109
.22	.814	.373	.376	.0121	.245	.0125
.24	.841	.428	.388	.0135	.253	.0142
.26	.868	.480	.401	.0158	.261	.0160
.28	.897	.534	.414	.0180	.270	.0180
.30	.928	.592	.428	.0204	.279	.0201
.32	.959	.653	.443	.0230	.289	.0224
.34	.993	.718	.459	.0259	.299	.0249
.36	1.028	.785	.476	.0291	.309	.0276
.38	1.065	.856	.493	.0326	.321	.0305
.40	1.104	.931	.512	.0365	.333	.0337
.42	1.146	1.010	.533	.0409	.346	.0371
.44	1.190	1.092	.554	.0458	.360	.0409
.46	1.237	1.178	.577	.0512	.374	.0450
.48	1.236	1.268	.602	.0572	.390	.0494
.50	1.340	1.363	.629	.0640	.408	.0544
.52	1.397	1.462	.657	.0716	.426	.0598
.54	1.458	1.565	.689	.0802	.446	.0657
.56	1.525	1.673	.723	.0899	.468	.0723
.58	1.597	1.787	.760	.1008	.492	.0796
.60	1.675	1.905	.800	.1131	.519	.0877
.62	1.761	2.029	.845	.1271	.548	.0968
.64	1.856	2.159	.894	.1430	.580	.1069
.66	1.961	2.235	.943	.1609	.616	.1184
.68	2.078	2.439	1.011	.1814	.657	.1312
.70	2.208	2.590	1.079	.2047	.702	.1458

TABLE 4-2. TABLES FOR CYLINDRICAL CAVITIES WITH CENTRAL COLUMN (CONT)

$r^2/a^2 = 0.20$						
τ_0	$n = 1$		$n = 2$		$n = 3$	
	$\frac{c}{a(2j+1)}$	$2R$	$\frac{c}{a(2j+1)}$	$2R$	$\frac{c}{a(2j+1)}$	$2R$
.00	.515	.000	.244	.0000	.161	.0000
.02	.530	.018	.251	.0005	.165	.0006
.04	.545	.038	.258	.0009	.170	.0013
.06	.561	.060	.265	.0015	.175	.0020
.08	.578	.083	.273	.0020	.180	.0027
.10	.596	.107	.281	.0027	.185	.0035
.12	.514	.134	.289	.0033	.190	.0044
.14	.633	.162	.297	.0041	.196	.0053
.16	.652	.192	.306	.0049	.201	.0064
.18	.673	.225	.316	.0057	.207	.0074
.20	.695	.259	.325	.0067	.214	.0086
.22	.717	.296	.336	.0077	.220	.0099
.24	.741	.335	.345	.0088	.227	.0112
.26	.765	.377	.358	.0101	.235	.0127
.28	.791	.422	.369	.0114	.242	.0142
.30	.819	.469	.382	.0129	.250	.0159
.32	.847	.519	.335	.0145	.259	.0177
.34	.878	.573	.409	.0163	.268	.0197
.36	.910	.630	.424	.0183	.277	.0218
.38	.943	.690	.440	.0205	.287	.0241
.40	.979	.754	.456	.0229	.298	.0267
.42	1.017	.821	.474	.0256	.310	.0294
.44	1.057	.893	.453	.0286	.322	.0324
.46	1.100	.968	.514	.0320	.335	.0357
.48	1.146	1.048	.536	.0358	.350	.0392
.50	1.195	1.132	.560	.0401	.365	.0432
.52	1.247	1.221	.585	.0449	.381	.0475
.54	1.304	1.314	.613	.0504	.399	.0523
.56	1.365	1.413	.544	.0566	.419	.0576
.58	1.431	1.516	.677	.0637	.440	.0636
.60	1.503	1.626	.713	.0718	.464	.0702
.62	1.583	1.741	.753	.0811	.490	.0776
.64	1.670	1.863	.798	.0918	.519	.0860
.66	1.766	1.991	.847	.1042	.551	.0954
.68	1.874	2.127	.903	.1184	.587	.1062
.70	1.993	2.270	.965	.1349	.628	.1184

TABLE 4-2. TABLES FOR CYLINDRICAL CAVITIES WITH CENTRAL COLUMN (CONT)

$r^2/a^2 = 0.25$						
τ_0	$n = 1$		$n = 2$		$n = 3$	
	$\frac{c}{a(2j+1)}$	$2R$	$\frac{c}{a(2j+1)}$	$2R$	$\frac{c}{a(2j+1)}$	$2R$
.00	.457	.000	.220	.0000	.145	.0000
.02	.471	.014	.226	.0003	.149	.0005
.04	.484	.030	.232	.0006	.153	.0010
.06	.498	.046	.239	.0010	.158	.0016
.08	.513	.064	.245	.0014	.162	.0022
.10	.528	.083	.252	.0018	.167	.0028
.12	.544	.104	.260	.0022	.171	.0035
.14	.561	.126	.267	.0027	.176	.0042
.16	.579	.149	.275	.0032	.182	.0050
.18	.597	.175	.283	.0038	.187	.0059
.20	.616	.202	.292	.0044	.193	.0058
.22	.636	.231	.301	.0051	.199	.0078
.24	.657	.262	.311	.0058	.205	.0089
.26	.679	.295	.321	.0066	.211	.0100
.28	.702	.331	.332	.0075	.218	.0113
.30	.726	.369	.343	.0084	.225	.0126
.32	.752	.410	.354	.0095	.233	.0140
.34	.779	.453	.367	.0106	.241	.0156
.36	.807	.500	.380	.0119	.250	.0173
.38	.838	.550	.394	.0133	.259	.0191
.40	.870	.603	.409	.0148	.269	.0211
.42	.904	.659	.425	.0166	.279	.0233
.44	.941	.719	.442	.0185	.290	.0257
.46	.980	.784	.460	.0206	.302	.0283
.48	1.021	.852	.480	.0230	.314	.0312
.50	1.066	.925	.501	.0258	.328	.0343
.52	1.114	1.003	.524	.0288	.343	.0378
.54	1.165	1.085	.549	.0323	.359	.0416
.56	1.221	1.173	.576	.0363	.377	.0459
.58	1.282	1.266	.606	.0409	.396	.0507
.60	1.348	1.365	.638	.0462	.417	.0560
.62	1.421	1.470	.674	.0523	.440	.0621
.64	1.501	1.581	.714	.0594	.466	.0689
.66	1.589	1.700	.759	.0677	.495	.0766
.68	1.688	1.826	.809	.0774	.528	.0854
.70	1.798	1.961	.865	.0887	.564	.0955

TABLE 4-2. TABLES FOR CYLINDRICAL CAVITIES WITH CENTRAL COLUMN (CONT)

$r^2/a^2 = 0.30$						
τ_0	$n = 1$		$n = 2$		$n = 3$	
	$\frac{c}{a(2j+1)}$	2R	$\frac{c}{a(2j+1)}$	2R	$\frac{c}{a(2j+1)}$	2R
.00	.403	.000	.198	.0000	.131	.0000
.02	.420	.011	.203	.0002	.135	.0004
.04	.432	.023	.209	.0004	.139	.0008
.06	.445	.035	.215	.0007	.142	.0012
.08	.457	.050	.221	.0009	.146	.0017
.10	.471	.064	.227	.0012	.150	.0022
.12	.485	.080	.234	.0015	.155	.0022
.14	.500	.098	.241	.0018	.159	.0034
.16	.515	.116	.246	.0022	.164	.0040
.18	.531	.136	.255	.0025	.169	.0047
.20	.548	.157	.263	.0029	.174	.0054
.22	.566	.180	.271	.0034	.179	.0062
.24	.584	.201	.220	.0039	.185	.0070
.26	.604	.230	.289	.0044	.191	.0079
.28	.624	.258	.298	.0050	.197	.0089
.30	.646	.289	.308	.0056	.203	.0100
.32	.669	.321	.319	.0063	.210	.0111
.34	.693	.356	.330	.0070	.218	.0123
.36	.718	.393	.342	.0079	.225	.0137
.38	.745	.433	.354	.0088	.233	.0151
.40	.774	.477	.368	.0098	.242	.0167
.42	.805	.523	.382	.0109	.251	.0184
.44	.838	.572	.357	.0121	.261	.0203
.46	.873	.626	.413	.0135	.272	.0224
.48	.910	.683	.431	.0151	.283	.0247
.50	.950	.744	.450	.0168	.296	.0272
.52	.994	.810	.470	.0188	.309	.0299
.54	1.040	.881	.433	.0210	.323	.0330
.56	1.091	.957	.517	.0236	.339	.0364
.58	1.147	1.038	.543	.0266	.356	.0402
.60	1.207	1.126	.573	.0300	.375	.0445
.62	1.273	1.219	.605	.0339	.396	.0493
.64	1.346	1.320	.641	.0386	.419	.0548
.66	1.427	1.427	.681	.0440	.445	.0611
.68	1.518	1.542	.725	.0505	.475	.0682
.70	1.618	1.666	.776	.0581	.507	.0764

TABLE 4-2. TABLES FOR CYLINDRICAL CAVITIES WITH CENTRAL COLUMN (CONT)

$$r^2/a^2 = 0.35$$

τ_0	$n = 1$		$n = 2$		$n = 3$	
	$\frac{c}{a(2j+1)}$	2R	$\frac{c}{a(2j+1)}$	2R	$\frac{c}{a(2j+1)}$	2R
.00	.365	.000	.178	.0000	.118	.0000
.02	.375	.009	.183	.0002	.122	.0003
.04	.386	.018	.188	.0003	.125	.0006
.06	.397	.023	.194	.0005	.128	.0010
.08	.409	.038	.199	.0006	.132	.0013
.10	.421	.050	.205	.0008	.136	.0017
.12	.433	.062	.210	.0010	.140	.0022
.14	.446	.075	.217	.0012	.144	.0026
.16	.460	.090	.223	.0015	.148	.0031
.18	.474	.105	.230	.0017	.152	.0037
.20	.489	.121	.237	.0020	.157	.0042
.22	.504	.139	.244	.0023	.162	.0049
.24	.521	.158	.252	.0026	.167	.0055
.26	.538	.179	.260	.0030	.172	.0062
.28	.556	.201	.263	.0033	.177	.0070
.30	.575	.224	.277	.0037	.183	.0078
.32	.595	.250	.286	.0042	.189	.0087
.34	.617	.277	.296	.0047	.196	.0097
.36	.639	.307	.307	.0052	.203	.0107
.38	.663	.338	.318	.0058	.210	.0119
.40	.689	.373	.330	.0065	.218	.0131
.42	.716	.410	.343	.0072	.226	.0145
.44	.746	.450	.357	.0080	.235	.0160
.46	.777	.493	.371	.0089	.245	.0176
.48	.810	.540	.387	.0099	.255	.0194
.50	.846	.530	.404	.0111	.266	.0214
.52	.885	.645	.422	.0123	.278	.0235
.54	.927	.704	.442	.0138	.291	.0260
.56	.973	.768	.464	.0154	.305	.0286
.58	1.023	.837	.487	.0173	.321	.0317
.60	1.078	.912	.513	.0195	.338	.0351
.62	1.138	.993	.542	.0221	.356	.0389
.64	1.204	1.081	.574	.0251	.377	.0433
.66	1.278	1.175	.610	.0286	.401	.0483
.68	1.359	1.278	.650	.0328	.427	.0540
.70	1.451	1.389	.695	.0378	.456	.0606

TABLE 4-2. TABLES FOR CYLINDRICAL CAVITIES WITH CENTRAL COLUMN (CONT)

$r^2/a^2 = 0.40$						
T_0	$n = 1$		$n = 2$		$n = 3$	
	$\frac{c}{a(2j+1)}$	$2R$	$\frac{c}{a(2j+1)}$	$2R$	$\frac{c}{a(2j+1)}$	$2R$
.00	.326	.000	.160	.00000	.106	.0000
.002	.335	.007	.165	.0001	.109	.0002
.04	.345	.014	.169	.0002	.112	.0005
.06	.355	.021	.174	.0003	.115	.0008
.08	.365	.030	.179	.0004	.119	.0010
.10	.375	.038	.184	.0005	.122	.0014
.12	.386	.048	.189	.0007	.125	.0017
.14	.398	.058	.194	.0008	.129	.0020
.16	.410	.069	.200	.0010	.133	.0024
.18	.422	.081	.206	.0011	.137	.0029
.20	.436	.093	.212	.0013	.141	.0033
.22	.449	.107	.219	.0015	.145	.0038
.24	.464	.122	.226	.0017	.150	.0043
.26	.479	.137	.233	.0020	.154	.0048
.28	.495	.154	.241	.0022	.159	.0054
.30	.512	.173	.249	.0025	.165	.0061
.32	.530	.192	.257	.0328	.170	.0068
.34	.549	.213	.266	.0031	.176	.0075
.36	.569	.236	.275	.0035	.182	.0084
.38	.590	.261	.285	.0039	.189	.0093
.40	.613	.288	.296	.0043	.196	.0102
.42	.637	.317	.307	.0048	.203	.0113
.44	.663	.349	.320	.0053	.211	.0124
.46	.690	.383	.333	.0059	.220	.0137
.48	.720	.420	.347	.0065	.229	.0151
.50	.752	.460	.362	.0073	.239	.0166
.52	.737	.504	.378	.0081	.250	.0183
.54	.824	.552	.396	.0090	.261	.0202
.56	.865	.605	.415	.0101	.274	.0223
.58	.910	.662	.436	.0113	.288	.0247
.60	.959	.724	.459	.0127	.303	.0273
.62	1.013	.792	.485	.0143	.320	.0303
.64	1.072	.867	.514	.0162	.338	.0338
.66	1.139	.948	.546	.0185	.359	.0377
.68	1.213	1.037	.581	.0212	.383	.0422
.70	1.295	1.135	.622	.0244	.409	.0474

TABLE 4-2. TABLES FOR CYLINDRICAL CAVITIES WITH CENTRAL COLUMN (CONT)

$$r^2/a^2 = 0.45$$

τ_0	$n = 1$		$n = 2$		$n = 3$	
	$\frac{c}{a(2j+1)}$	2R	$\frac{c}{a(2j+1)}$	2R	$\frac{c}{a(2j+1)}$	2R
.00	.290	.000	.143	.0000	.095	.0000
.02	.298	.005	.147	.0001	.098	.0002
.04	.307	.010	.151	.0001	.101	.0004
.06	.315	.016	.155	.0002	.103	.0006
.08	.324	.022	.160	.0003	.106	.0008
.10	.334	.029	.164	.0004	.109	.0010
.12	.344	.036	.169	.0004	.112	.0013
.14	.354	.044	.174	.0005	.115	.0016
.16	.364	.052	.179	.0006	.119	.0019
.18	.375	.061	.184	.0008	.122	.0022
.20	.387	.071	.190	.0009	.126	.0025
.22	.399	.081	.196	.0010	.130	.0029
.24	.412	.092	.202	.0012	.134	.0033
.26	.425	.104	.208	.0013	.138	.0037
.28	.439	.117	.215	.0015	.143	.0042
.30	.454	.131	.222	.0016	.147	.0047
.32	.470	.146	.230	.0018	.152	.0052
.34	.487	.162	.237	.0021	.158	.0058
.36	.504	.180	.246	.0023	.163	.0064
.38	.523	.199	.255	.0025	.169	.0071
.40	.543	.220	.264	.0028	.175	.0078
.42	.564	.242	.274	.0031	.182	.0087
.44	.587	.266	.285	.0035	.189	.0095
.46	.612	.293	.297	.0038	.197	.0105
.48	.638	.322	.309	.0043	.205	.0116
.50	.666	.353	.323	.0047	.214	.0128
.52	.697	.388	.337	.0053	.223	.0141
.54	.730	.426	.353	.0058	.234	.0155
.56	.766	.467	.370	.0065	.245	.0171
.58	.806	.513	.389	.0073	.257	.0190
.60	.849	.563	.410	.0082	.271	.0210
.62	.897	.619	.432	.0092	.286	.0233
.64	.950	.680	.458	.0104	.302	.0260
.66	1.010	.748	.486	.0118	.321	.0290
.68	1.076	.822	.518	.0135	.342	.0325
.70	1.150	.905	.554	.0155	.365	.0365

TABLE 4-2. TABLES FOR CYLINDRICAL CAVITIES WITH CENTRAL COLUMN (CONT)

$r^2/a^2 = 0.50$						
τ_0	$n = 1$		$n = 2$		$n = 3$	
	$\frac{c}{a(2j+1)}$	2R	$\frac{c}{a(2j+1)}$	2R	$\frac{c}{a(2j+1)}$	2R
.00	.257	.000	.127	.0000	.085	.0000
.02	.264	.004	.131	.0000	.087	.0001
.04	.272	.008	.134	.0001	.089	.0003
.06	.279	.012	.138	.0001	.092	.0004
.08	.287	.017	.142	.0002	.094	.0006
.10	.295	.022	.146	.0002	.097	.0008
.12	.304	.027	.150	.0003	.100	.0010
.14	.313	.033	.154	.0004	.103	.0012
.16	.322	.039	.159	.0004	.106	.0014
.18	.332	.046	.164	.0005	.109	.0017
.20	.342	.053	.169	.0006	.112	.0019
.22	.353	.061	.174	.0007	.116	.0022
.24	.364	.069	.179	.0007	.119	.0025
.26	.376	.078	.185	.0008	.123	.0028
.28	.388	.088	.191	.0010	.127	.0032
.30	.401	.098	.197	.0011	.131	.0035
.32	.415	.109	.204	.0012	.135	.0039
.34	.430	.122	.211	.0013	.140	.0044
.36	.445	.135	.218	.0015	.145	.0048
.38	.462	.149	.226	.0016	.150	.0054
.40	.479	.165	.235	.0018	.156	.0059
.42	.498	.181	.244	.0020	.162	.0065
.44	.518	.200	.253	.0022	.168	.0072
.46	.539	.220	.263	.0025	.175	.0079
.48	.562	.242	.274	.0027	.182	.0087
.50	.587	.266	.286	.0030	.190	.0096
.52	.614	.292	.299	.0034	.198	.0106
.54	.643	.322	.313	.0037	.208	.0117
.56	.675	.354	.328	.0042	.218	.0129
.58	.710	.389	.345	.0046	.228	.0143
.60	.748	.428	.363	.0052	.240	.0159
.62	.790	.472	.383	.0058	.254	.0176
.64	.837	.521	.406	.0066	.268	.0196
.66	.889	.575	.431	.0075	.285	.0219
.68	.948	.636	.459	.0085	.303	.0246
.70	1.014	.704	.490	.0097	.324	.0277

TABLE 4-2. TABLES FOR CYLINDRICAL CAVITIES WITH CENTRAL COLUMN (CONT)

$r^2/a^2 = 0.60$						
τ_0	$n = 1$		$n = 2$		$n = 3$	
	$\frac{c}{a(2j+1)}$	$2R$	$\frac{c}{a(2j+1)}$	$2R$	$\frac{c}{a(2j+1)}$	$2R$
.00	.197	.000	.098	.0000	.065	.0000
.002	.202	.002	.100	.0000	.067	.0001
.004	.208	.004	.103	.0000	.069	.0002
.06	.213	.006	.106	.0001	.071	.0002
.08	.219	.009	.109	.0001	.073	.0003
.10	.226	.011	.112	.0001	.075	.0004
.012	.232	.014	.115	.0001	.077	.0005
.14	.239	.017	.119	.0001	.079	.0006
.16	.246	.021	.122	.0002	.081	.0007
.18	.253	.024	.126	.0002	.084	.0009
.20	.261	.028	.130	.0002	.086	.0010
.22	.269	.032	.133	.0003	.089	.0012
.24	.278	.036	.138	.0003	.092	.0013
.26	.286	.041	.142	.0003	.094	.0015
.28	.296	.046	.146	.0004	.097	.0017
.30	.306	.051	.151	.0004	.101	.0019
.32	.316	.057	.156	.0005	.104	.0021
.34	.327	.064	.162	.0005	.108	.0023
.36	.333	.070	.167	.0006	.111	.0026
.38	.351	.078	.173	.0006	.115	.0028
.40	.364	.086	.180	.0007	.120	.0031
.42	.378	.095	.186	.0008	.124	.0035
.44	.393	.105	.194	.0008	.129	.0038
.46	.409	.115	.202	.0009	.134	.0042
.48	.426	.127	.210	.0010	.140	.0046
.50	.445	.140	.219	.0011	.146	.0051
.52	.465	.154	.229	.0013	.152	.0056
.54	.487	.170	.240	.0014	.159	.0062
.55	.511	.187	.251	.0016	.167	.0068
.58	.537	.206	.264	.0017	.175	.0076
.60	.566	.228	.278	.0019	.185	.0084
.62	.598	.253	.293	.0022	.195	.0093
.64	.633	.280	.310	.0024	.206	.0104
.66	.672	.313	.329	.0027	.219	.0116
.68	.717	.347	.351	.0031	.233	.0130
.70	.766	.387	.375	.0035	.249	.0147

TABLE 4-2. TABLES FOR CYLINDRICAL CAVITIES WITH CENTRAL COLUMN (CONT)

$r^2/a^2 = 0.70$				
τ_0	$n = 1$		$n = 2$	
	$\frac{c}{a(2j+1)}$	$2R$	$\frac{c}{a(2j+1)}$	$2R$
.00	.142	.000	.071	.0000
.02	.146	.001	.073	.0000
.04	.150	.002	.075	.0000
.06	.154	.003	.077	.0000
.08	.158	.004	.079	.0000
.10	.163	.005	.081	.0000
.12	.157	.006	.083	.0000
.14	.172	.008	.086	.0000
.16	.177	.009	.088	.0001
.18	.183	.011	.091	.0001
.20	.188	.013	.094	.0001
.22	.194	.014	.097	.0001
.24	.200	.016	.100	.0001
.26	.206	.018	.103	.0001
.28	.213	.021	.106	.0001
.30	.220	.023	.109	.0001
.32	.227	.026	.113	.0001
.34	.235	.029	.117	.0002
.36	.244	.032	.121	.0002
.38	.252	.035	.125	.0002
.40	.262	.039	.130	.0002
.42	.272	.043	.135	.0002
.44	.282	.047	.140	.0003
.46	.294	.052	.146	.0003
.48	.306	.057	.152	.0003
.50	.319	.063	.159	.0004
.52	.334	.070	.166	.0004
.54	.349	.077	.173	.0004
.56	.366	.085	.182	.0005
.58	.385	.094	.191	.0005
.60	.405	.104	.201	.0006
.62	.428	.115	.212	.0007
.64	.453	.128	.224	.0007
.66	.481	.143	.238	.0008
.68	.512	.160	.253	.0009
.70	.547	.179	.270	.0011

TABLE 4-2. TABLES FOR CYLINDRICAL CAVITIES WITH CENTRAL COLUMN (CONT)

$r^2/a^2 = 0.80$		
$n = 1$		
τ_0	$\frac{c}{a(2j+1)}$	$2R$
.00	.092	.000
.02	.094	.000
.04	.097	.001
.06	.099	.001
.08	.102	.001
.10	.105	.002
.12	.108	.002
.14	.111	.003
.16	.114	.003
.18	.118	.004
.20	.121	.004
.22	.125	.005
.24	.129	.006
.26	.133	.006
.28	.137	.007
.30	.142	.008
.32	.146	.009
.34	.151	.010
.36	.157	.011
.38	.162	.012
.40	.168	.013
.42	.175	.015
.44	.182	.016
.46	.189	.018
.48	.197	.019
.50	.205	.021
.52	.214	.024
.54	.224	.026
.56	.235	.029
.58	.247	.032
.60	.260	.035
.62	.274	.039
.64	.290	.044
.66	.308	.049
.68	.328	.055
.70	.350	.062

CHAPTER 5

EXPERIMENTS

5-0 LIST OF SYMBOLS*

- R' = corner radius of cavity, ft
 Re = Reynolds number
 V_c = volume of original cavity

GREEK LETTERS

- θ = semi-vertex angle of truncated cone
 λ_{\max} = maximum rate of divergence of nutational amplitude, per sec

5-1 INTRODUCTION

In this chapter we shall describe briefly the three sets of experiments, the results of which led to further theoretical developments in the problem of the dynamics of liquid-filled projectiles. The three experiments are: (a) verification of Stewartson's prediction of instability of a projectile containing a cylindrical cavity of a given fineness ratio and with a given percent of fill; (b) instability in noncylindrical cavities; and (c) instabilities occurring during spin-up of the liquid, or in the transient phase. These experiments and the theoretical developments stemming from them have considerably broadened and enhanced the means with which the designer can now handle the problem of instability of liquid-filled projectiles.

While these experiments will be briefly described in this chapter, the corresponding theoretical developments will be considered in Chapters 6, 7, and 8, for the three sets of experiments, respectively.

*For identification of other symbols in this chapter, refer to Chapter 3.

5-2 VERIFICATION OF STEWARTSON'S INSTABILITY CRITERIA

Prior to the experiments conducted in the Ballistic Research Laboratories (BRL), Stewartson's theory had been tested only twice. The first tests were conducted with actual projectiles at the British Proving Ground, Porton, England. Special projectiles with cylindrical cavities were designed and built. The results of the tests were highly successful. For different fineness-ratios of the cavities and different fill-ratios, all projectiles predicted to be unstable gave short ranges, i.e., approximately 50%, and all projectiles predicted to be stable gave full ranges.

Range firings, however — although they provide the final proof of the pudding — are not very informative on details such as levels of yaw along the trajectory, nor yaw history.

The second tests were conducted by G.N. Ward'. He used a gyroscope. With a given fineness-ratio of the cavity, he tested all fill-ratios from zero to 100% in order to detect all resonances which are predicted to occur at various fill-ratios. He observed with certainty only one resonance with fundamental fluid frequency, i.e., the lowest j value, which occurred at the predicted fill-ratio. The maximum rate of divergence of the nutational amplitude, which is predictable by the theory, could not be well determined with his apparatus. The width of the resonance band, however, could be observed. It was found to be about three times as broad as predicted by the theory and curiously asymmetrical, on the fill-ratio scale, relative to the resonant frequency $\tau_0 = \tau_n$. Thus according to Ward's observations, Stewartson's instability criteria should be modified to read:

$$-3.9 < \frac{\tau_0 - \tau_n}{\sqrt{S}} < 2.7$$

instead of as given by Eq. 4-21.

At the time of these experiments the cause of this disagreement with the theory was not known. The gyroscope was suspect, but examination of various possible sources of errors led to inconclusive results.

5-2.1 FREE-FLIGHT FIRINGS

Because of the suspicion that the gyroscope in Ward's experiments might have contributed to the disagreement with the theory, it appeared desirable to test the theory by free flight in the Ballistic Range of BRL under carefully controlled experimental conditions².

The projectiles for these experiments were 20 mm models. These were machined from solid aluminum bar stock to have cylindrical cavities of a prescribed fineness-ratio. The cavities were designed so that the principal fluid frequency $j = 1$ was close to the nutational frequency of this projectile. The aerodynamic characteristics of this configuration, a 5-caliber long Army-Navy spinner rocket, were well-known from previous work³.

To test Stewartson's theory, the fluid must be fully spinning. Consequently, within the inclosed range the fluid must come to the full spin rapidly. Previous tests showed that glycerine—viscosity $\nu = 1000$ centistokes, — reaches full spin at about 40 feet from the muzzle. The BRL inclosed range is 280 feet in length. Therefore, the remaining 240 feet could then be used for relevant observations during which the projectile executes about ten nutational oscillations. Further details of these experiments can be found in Ref. 2.

If one defines the Reynolds number as

$$Re = \frac{\Omega a^2}{\nu}$$

where

Ω = axial spin

a = radius of the cavity

ν = kinematic viscosity of the fluid
the experiments were conducted at
 $Re = 7.2 \times 10^2$.

The results are shown in Fig. 5-1. The ordinates are the yaw undamping rates due to the liquid, i.e., with aerodynamic damping removed. The theoretically predicted resonance band also is shown.

Several discrepancies between theory and observations are at once apparent. These are: (a) the maximum rate of divergence is not as great as predicted; (b) the resonant bandwidth is considerably broader than predicted; and (c) the frequency at which the maximum divergence occurs is displaced relative to the nutational frequency of the projectile. Viscosity of the liquid was at once suspect as a likely cause of the observed differences with the predictions of an inviscid theory. However, to perform tests with liquids of different viscosities or different Reynolds numbers, recourse must be made to the gyroscope.

5-2.2 EXPERIMENTS WITH GYROSCOPE

The BRL gyroscope, as shown in Fig. 5-2, was found to be an excellent experimental tool for studies of its dynamics when liquid-filled. Its design drawings may be requested from the BRL.

The rotor of this gyroscope is a hollow metal cylinder. It may be made either of steel or aluminum, thereby changing the inertial properties of the system. Another hollow Lucite cylinder with end pieces or cups at both ends may be inserted into the metal rotor. The Lucite cavity may be easily made to any desired geometry to simulate the cavity of the projectile. A cavity inner diameter from 2 to 2.5 inches is very convenient for experimental purposes. The moments of inertia of this gyroscope can be changed by an addition of

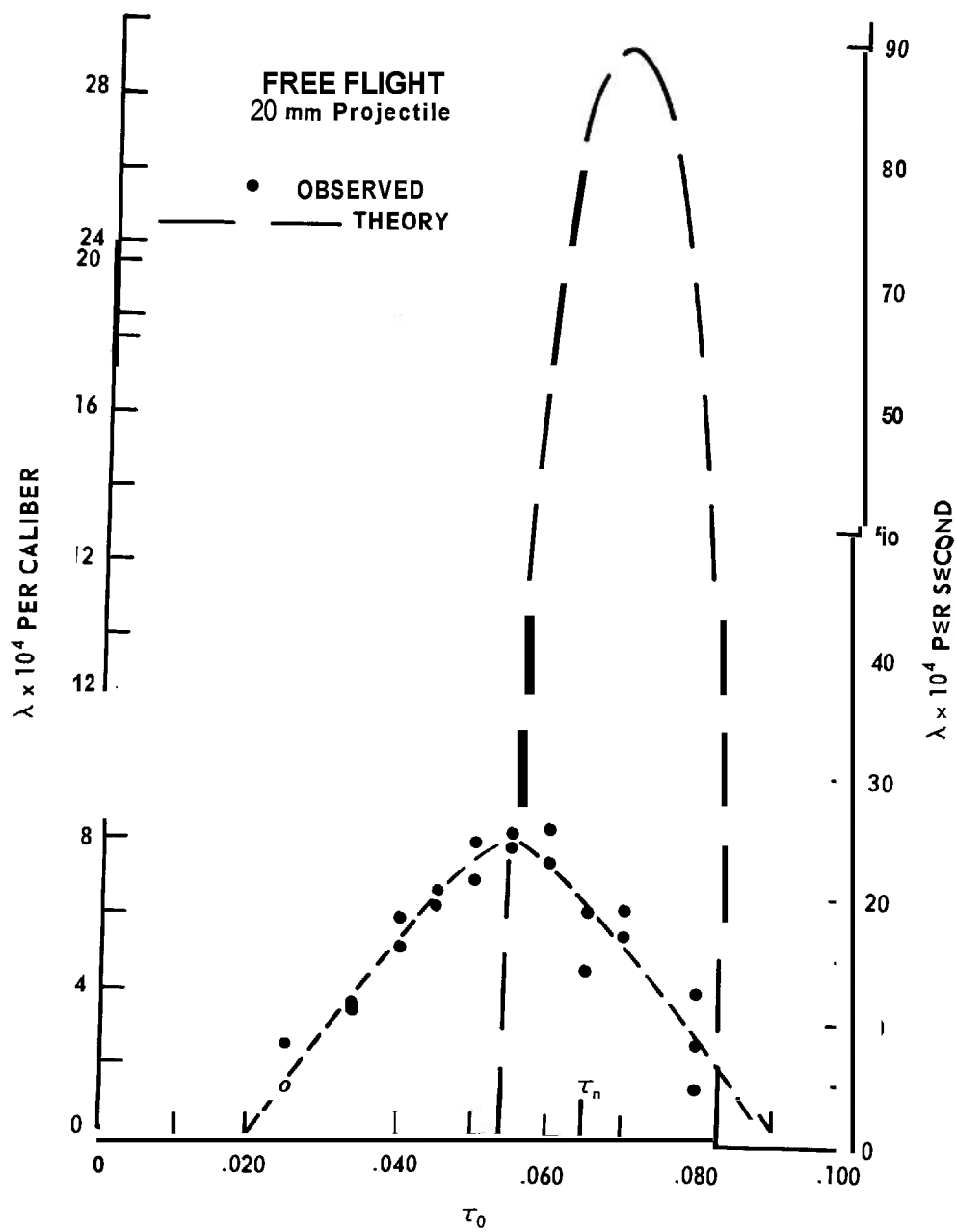
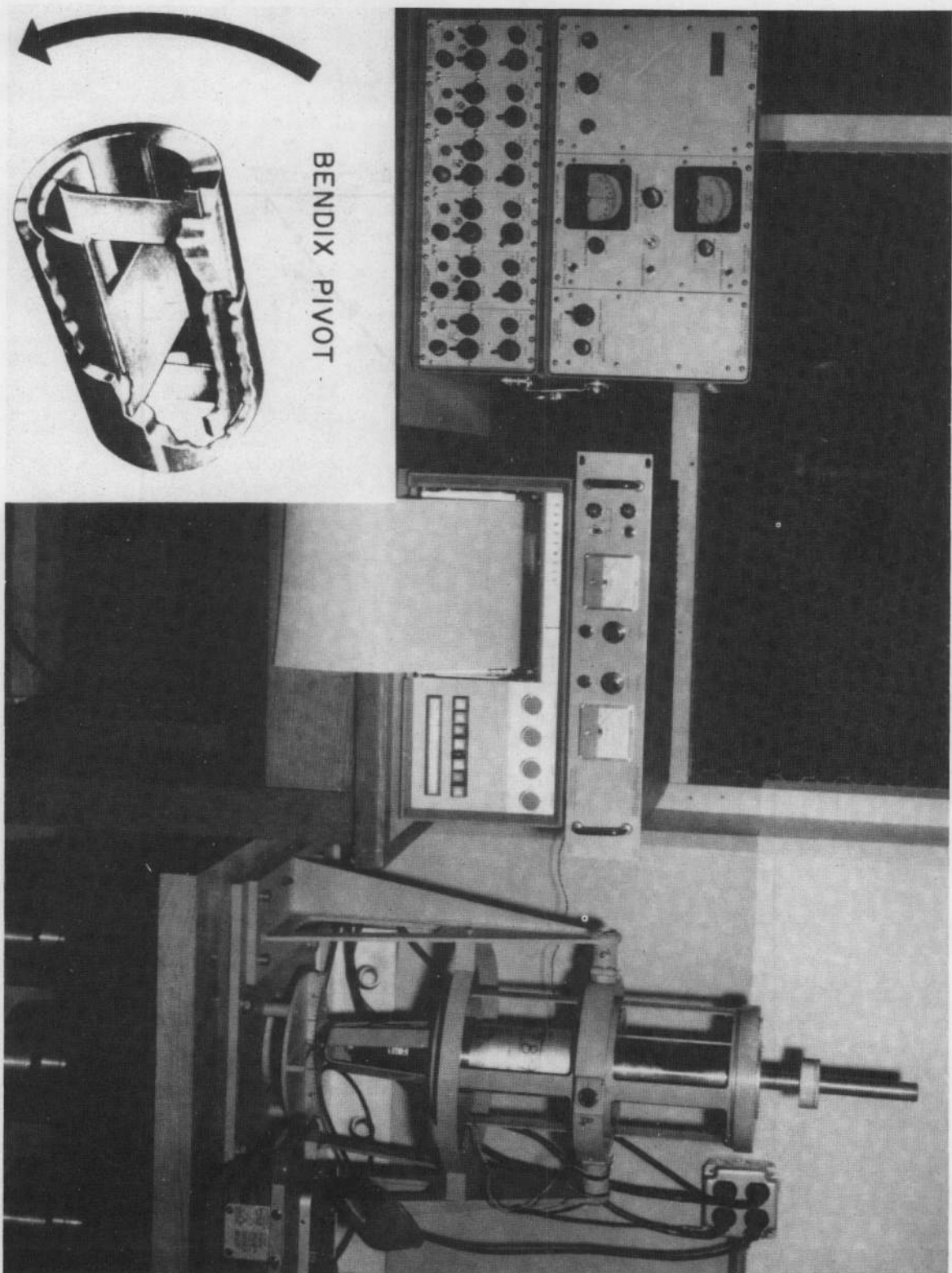


FIGURE 5-7. COMPARISON OF STEWARTSON'S THEORY WITH FREE-FLIGHT TESTS



BENDIX PIVOT

FIGURE 5-2. BRL GYROSCOPE

heavy brass rings to the rotor at its pivot-point. Such rings change largely the axial moment of inertia. Thus the BRL gyroscope has a range of the nutational frequencies from $\tau_n = 0.02$ to $\tau_n = 0.12$ in increments of 0.02. With such an arrangement, the gyroscope can be made to simulate the nutational frequency of the projectile under investigation provided, of course, that the projectile's nutational frequency lies within the range of the gyroscope.

The unique characteristic of the BRL gyroscope is that its inner and outer gimbals are supported by "Bendix Pivots" shown in the insert in Fig. 5—2. These consist of crossed flexible spring leaves so arranged and mounted that one-half of the unit can rotate about the common axis with very little transverse displacement due to an imposed curvature of the springs. The rotation is frictionless; has negligible hysteresis; and is linear (within 2.5%) with applied torque up to deflections of 15 degrees.

To measure angular displacements of the gyroscope, strain gages are attached to one of the pivot spring leaves of the outer gimbal. Since this pivot is stationary, the wires from the strain gages do not interfere with the motion of the gyroscope. The gages form a part of the bridge circuit whose amplified output is continuously monitored on a photographic recorder with calibrated timing lines. The rotor is spun by a 27-volt DC motor which is capable, depending on the load, of spins up to 7000 rpm. The spin is controlled by a variable power supply and is measured by calibrated Strobotac.

For the experiments Silicone oils (Dow Corning Corp.) of various viscosities were used. Table 5—1 summarizes pertinent physical characteristics of these oils together with the Reynolds numbers of corresponding experiments.

In order to observe a complete resonance curve, the cavities for 2- and 2.5-in. diameters were designed to resonate at

an 85% fill-ratio, i.e., $b^2/a^2 = 0.15$. From Stewartson's Tables one finds the required fineness-ratio c/a . For a steel rotor with 2-in. cavity diameter, $\tau_n = 0.060$ (empty), the required fineness-ratios are

$$c/a = 1.0307 (2j \pm 1) \quad j = 0, 1, 2, \dots$$

The chosen cavity was $c/a = 3.092$ ($j = 1$) which had a volume of 328 cc.

For an aluminum rotor with 2.5-in. cavity diameter, $\tau_n = 0.053$ (empty), the required fineness-ratios are

$$c/a = 1.0257 (2j \pm 1) \quad j = 0, 1, 2, \dots$$

The chosen cavity was $c/a = 3.077$ ($j = 1$) with a volume of 605 cc. These were convenient cavity sizes.

For some fluids complete resonance curves were measured by varying the fill-ratio; for others, only the peaks of the resonance curves were established. The results are summarized in Table 5—2.

According to the inviscid theory, the maximum rate of divergence should occur at precisely the nutational frequency $\tau_0 = \tau_n$ and — except for slight variation in the density of tested fluids, which slightly

TABLE 5—1. OILS AND REYNOLDS NUMBERS
SPIN $\Omega = 5000$ RPM

Viscosity v, centistokes	Sp. Gr. at 77°F	Reynolds Numbers	
		2-in. cavity	2.5-in. cavity
1	.818	3.38×10^5	5.19×10^5
3	.900	1.13×10^5	1.73×10^5
5	.920	6.76×10^4	1.04×10^5
13*	.940	2.60×10^4	4.00×10^4
49*	.960	7.53×10^3	1.06×10^4
100	.968	3.38×10^3	5.19×10^3
350	.972	0.97×10^3	1.48×10^3
1000	.972	3.38×10^2	5.19×10^2

*Inadvertently, these two oils were partially mixed resulting in the above viscosities. Original viscosities were 10 and 50 centistokes, respectively.

TABLE 5-2. MAXIMUM RATE OF DIVERGENCE λ_{\max} OF THE NUTATIONAL AMPLITUDE, CORRESPONDING FILL-RATIO, AND ASSOCIATED FLUID FREQUENCY (INVISCID) τ_0 .

Viscosity ν , centistokes	2-in. cavity			2.5-in. cavity		
	λ_{\max} , per sec	Fill, %	τ_0	λ_{\max} , per sec	Fill, %	τ_0
1	0.232	83.9	0.060	0.522	84.5	0.055
3	0.174	83.9	0.060	0.431	83.9	0.056
5	0.138	83.8	0.061	0.355	84.5	0.055
13*	0.091	84.4	0.059	0.295	85.1	0.053
49*	0.046	85.5	0.055	0.160	85.8	0.051
100	0.040	87.2	0.051	0.109	86.8	0.048
350				0.048	88.8	0.043
1000				0.029	90.1	0.039

*Inadvertently, these two oils were partially mixed resulting in the above viscosities. Original viscosities were 10 and 50 centistokes, respectively.

alters Stewartson's parameter — should be independent of viscosity. The maximum rate of divergence of the nutational component at resonance is given by Eq. 4-23

$$\lambda_{\max} = \frac{\Omega}{2} \sqrt{S}, \text{ per sec}$$

Thus, according to the inviscid theory, the λ_{\max} 's in Table 5-2 should be very nearly the same. This is clearly not the case. There is a strong effect of viscosity or, more appropriately, of Reynolds numbers. This implies that the inviscid theory, in order to account for the observed effects, requires a viscous correction. This will be taken up in Chapter 6. When so corrected, the theory and observations are in excellent agreement. This is illustrated in Fig 5-3. Additional illustrations are given in Fig 6-2. Further details of these experiments are to be found in Ref. 4.

53 INSTABILITIES IN NONCYLINDRICAL CAVITIES

In the preceding paragraph and Ch. 6 it is shown that, for a liquid-filled projectile having a cylindrical cavity, Stewartson's theory with viscous correction gives excellent prediction of the fill-ratios, over a wide range of Reynolds numbers, at which resonance with the nutational frequency of the projectile occurs. Unfortunately, however,

most projectile cavities are not cylindrical. The projectiles are usually streamlined and the cavity, in general, follows the outer form. Theoretical prediction of eigenfrequencies in such cavities at present is not feasible. The problem contains fundamental mathematical difficulties, see par. 3-7.1.

In order to shed some light on the behavior of the eigenfrequencies in noncylindrical cavities, the experiments described below were undertaken. The cylindrical cavity was systematically modified in such a manner so as to approximate the geometries of the cavities of streamlined projectiles.

Figs. 5-4(A) and 5-4(B) show the types of cavities which were tested. In the first series of experiments the effect of rounded corners was examined. A previously tested cylindrical cavity, $c/a = 3.077$, designed to resonate at 85% fill-ratio, was progressively modified maintaining, however, the same c/a , by rounding corners as is shown in Fig. 5-4(A). In configuration A **only** one end of the cylinder was so modified; in configuration B both ends were modified. The results are shown in Fig. 5-5. Rounding the corners produces relatively small change in the fill-ratio of the original cylinder; this implies a relatively small shift in the eigenfrequency. It is to be noted that the reference volume V_c is the volume of the original cavity.

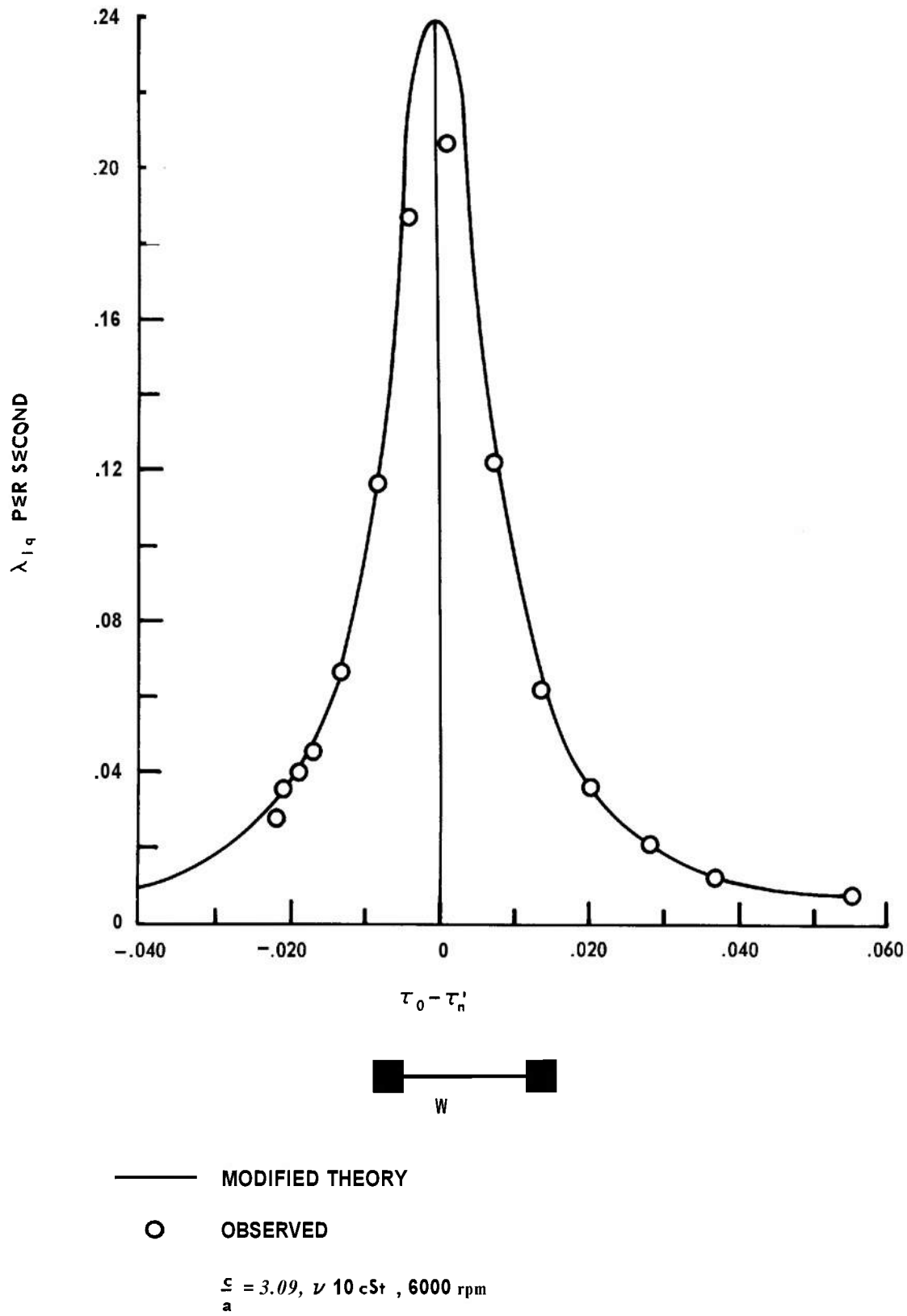


FIGURE 5-3. COMPARISON OF STEWARTSON'S THEORY MODIFIED BY VISCOUS CORRECTIONS WITH THE EXPERIMENTS

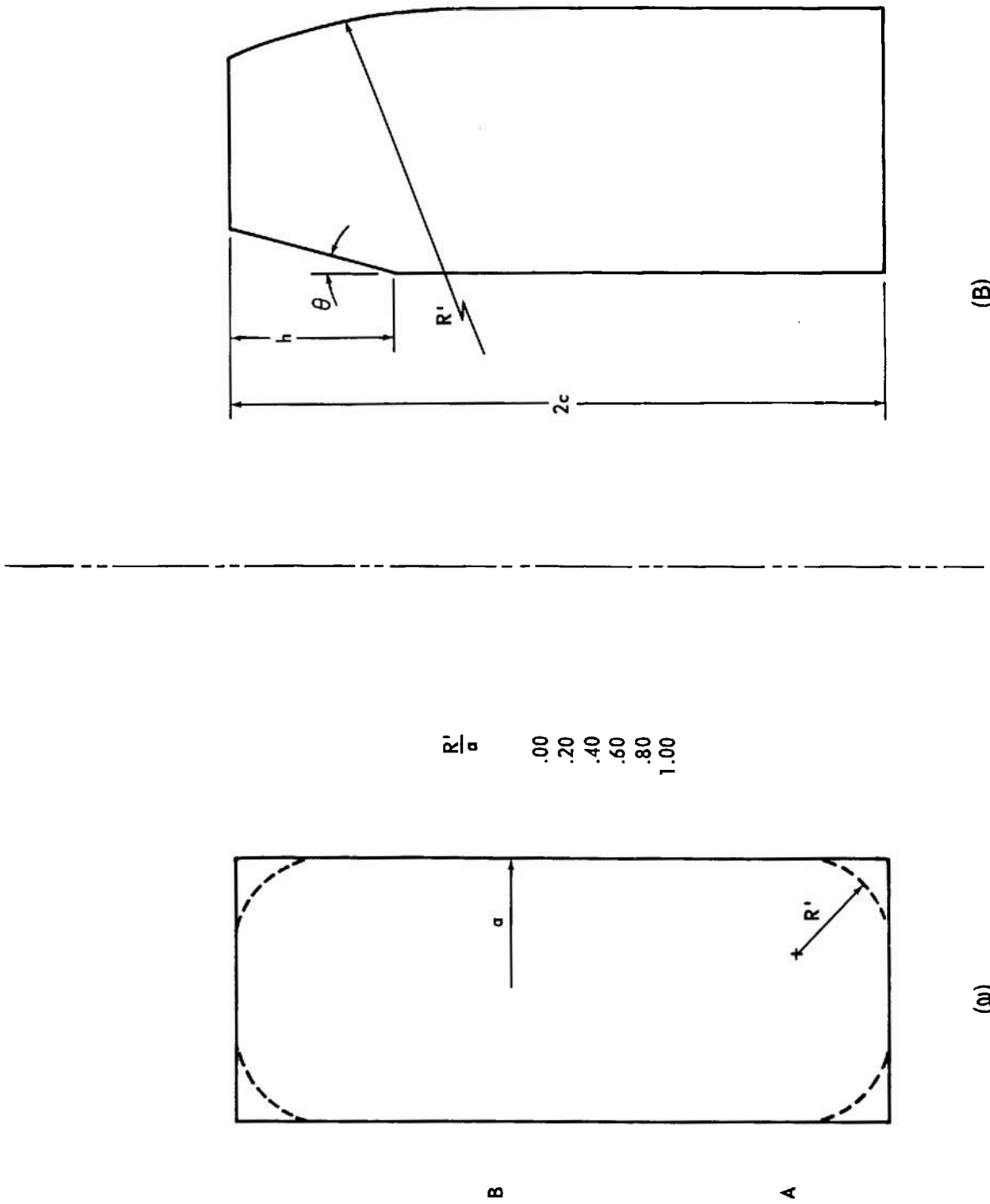


FIGURE 5-4. TYPES OF NONCYLINDRICAL CAVITIES TESTED

EFFECT OF ROUNDING CORNERS RESONANCE AT $\frac{V}{V_c}$

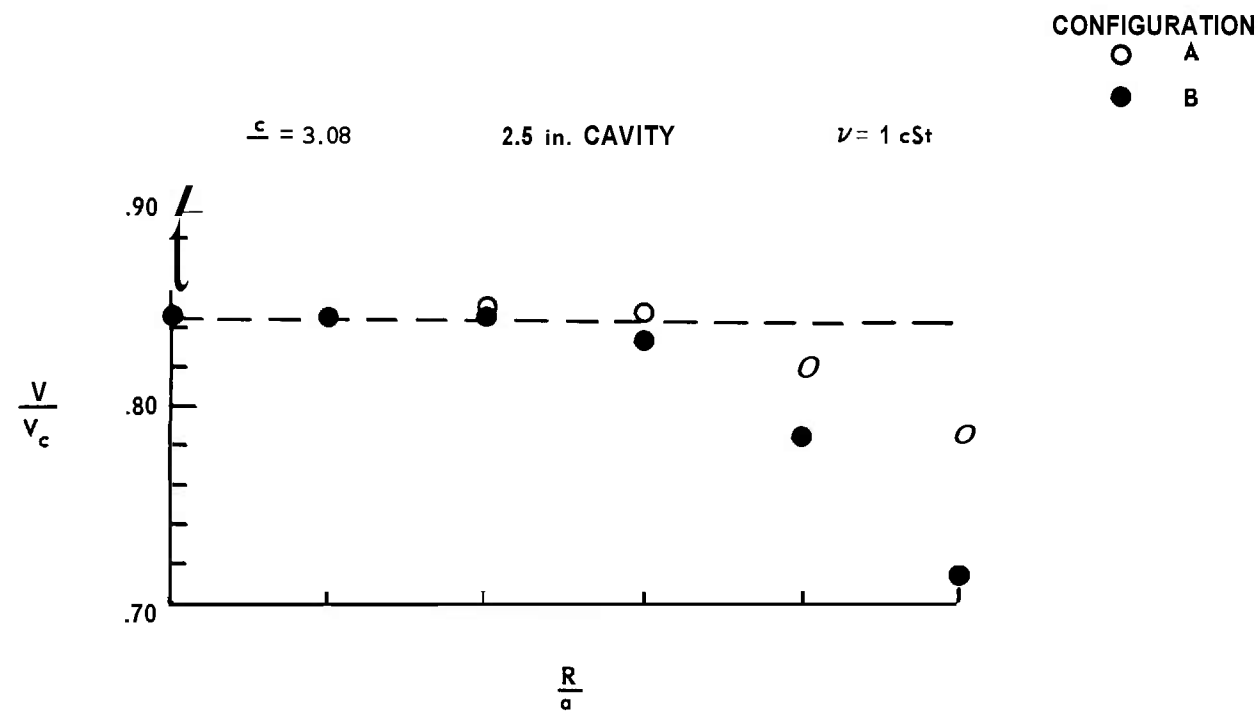


FIGURE 5-5. RESULTS OF TESTS OF CAVITIES IN FIGURE 5-4(A)

Modifications shown in Fig. 5-4(B) are combinations of the cylinder and the truncated cones. The latter are defined by the semi-vertex angle θ , and the nondimensional height $h/2c$. The effect on the fill-ratio for resonance of various modifications was surprisingly large. To accommodate these large changes in the direction of greater fill-ratios for resonance in modified cavities, the original cylindrical cavity, $c/a = 3.077$, had to be redesigned. A new cylindrical cavity was designed to resonate at 60% fill-ratio rather than at 85% of the old cavity. The fineness-ratio of the new cavity was $c/a = 2.687$ with a volume of 534 cc. The results of these tests are shown in Fig. 5-6. The ordinates are the volumes of the fluid at which resonance, $\tau_n = \tau_0 = 0.055$, occurs divided by the total volume of modified cavity, i.e., these are the fill-ratios relative to the volumes of modified cavities all having, however, the same fineness-ratio c/a .

In Chapter 7 a modification of Stewartson's theory will be made which will permit prediction of resonance in noncylindrical cavities provided that the departure of the geometry of the cavity from the cylindrical satisfies certain conditions. It was found that all cavities tested in the above experiments could be treated by the modified theory.

Further details of these experiments are to be found in Ref. 5.

5-4 INSTABILITY DURING SPIN-UP OR TRANSIENT PHASE

Stewartson's theory deals with an inviscid fluid which is spinning as a rigid body with the full spin of the projectile. Real fluids attain such steady state in a relatively short time after the projectile leaves the muzzle. The duration of this spin-up or of the transient phase depends principally on the viscosity of the fluid. Experiments show, however, that significant dynamic instabilities of the projectile may develop during this transient phase. This means that even if the projectile is stable — by Stewartson's criteria in its

steady state, i.e., with liquid fully spinning — severe transient instability may render such a liquid-filled projectile useless in practice. The designer, therefore, has to consider this transient phase.

This phenomenon is exhibited in Fig. 5-7. The projectile was 20 mm with a cylindrical cavity of height $2c = 2.09$ calibers and the cavity diameter of $2a = 0.78$ calibers with the fineness-ratio $c/a = 2.68$. The volume of the cavity was 7.8 cc. These projectiles were fired in the inclosed range of the BRL.

Fig. 5-7 shows the yaw damping rates obtained from the usual analysis of the yawing motion. Hence these are the total rates, due both to the aerodynamic and liquid effects. With water as the filler, the instability manifests itself from about 50% to 95% fill-ratios. With heavier liquids the instability band is broader. Also the severity of the instability is roughly proportional to the specific gravity of the liquid. Within the uncertainty of observations, the precessional yaw damping rates are unaffected by the presence of the liquid.

Further details of these experiments are to be found in Ref. 6.

Stewartson's theory, of course, is inapplicable to these results because the liquid is not yet fully spinning. A few tests with glycerine as a filler, which attains full spin very rapidly, also shown in Fig. 5-7, indicate that this projectile was stable with 70% fill where maximum transient instability appears to occur. The fill-ratios of steady state instabilities, Stewartson's predictions, are also indicated in the figure.

The transient instabilities are manifestations of the same mechanism which is responsible for instabilities in a steady state, i.e., it is a resonance phenomenon with the eigenfrequencies of the liquid. In the transient phase, however, the eigenfrequencies are no longer fixed depending only on the fineness-ratio c/a and the fill-ratio b^2/a^2 , but are variable and time-dependent. They

EFFECT OF CONICAL CUPS RESONANCE AT $\frac{V}{V_{0i}}$

$$\nu = 1 \text{ cSt}$$

$$\underline{R} = 0$$

$$\tau_0 = \tau_n = .055$$

CONFIGURATIONS

- - C X - E₁
 ○ - D

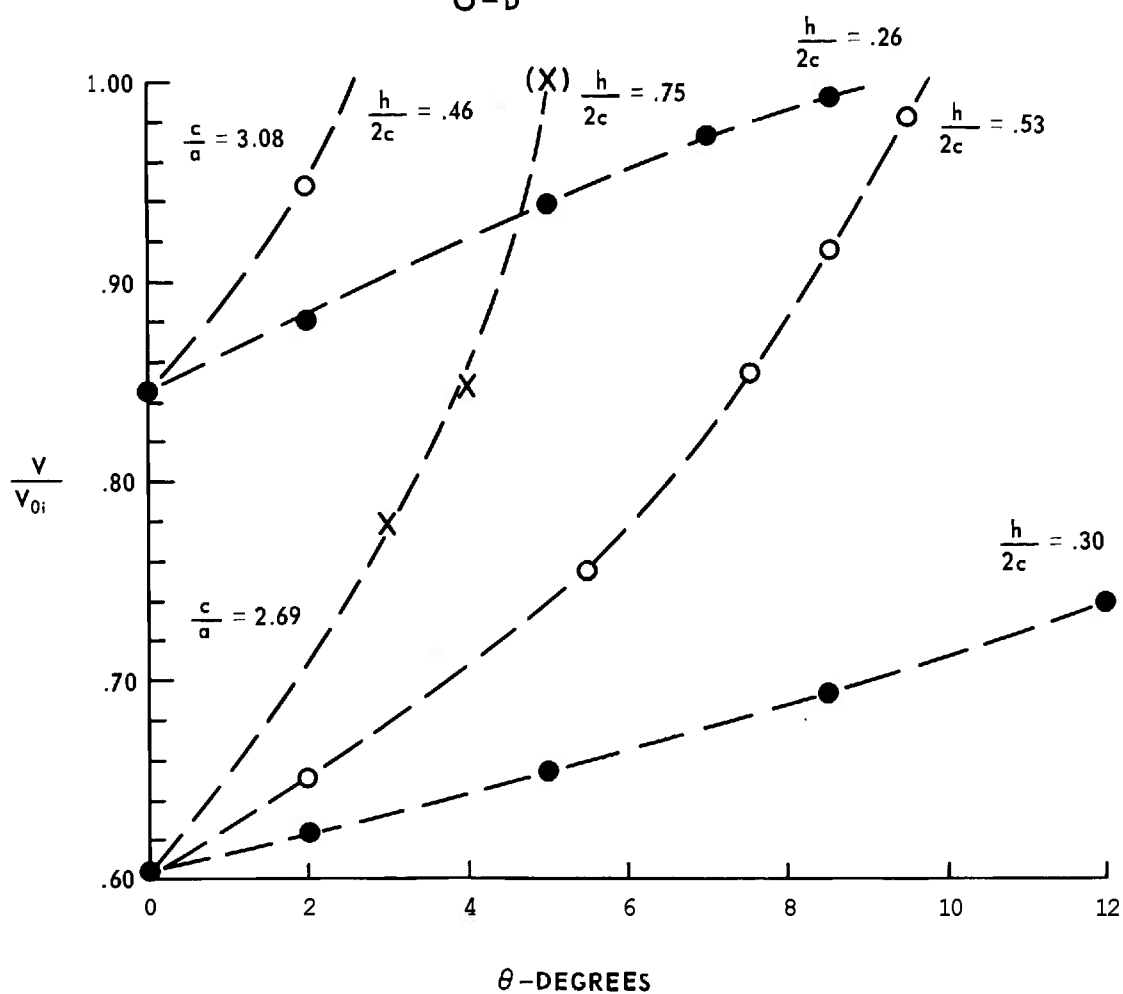


FIGURE 5-6. RESULTS OF TESTS OF CAVITIES IN FIGURE 5-4(B)

LIQUID-FILLED PROJECTILE YAW DAMPING RATES $e\lambda s$

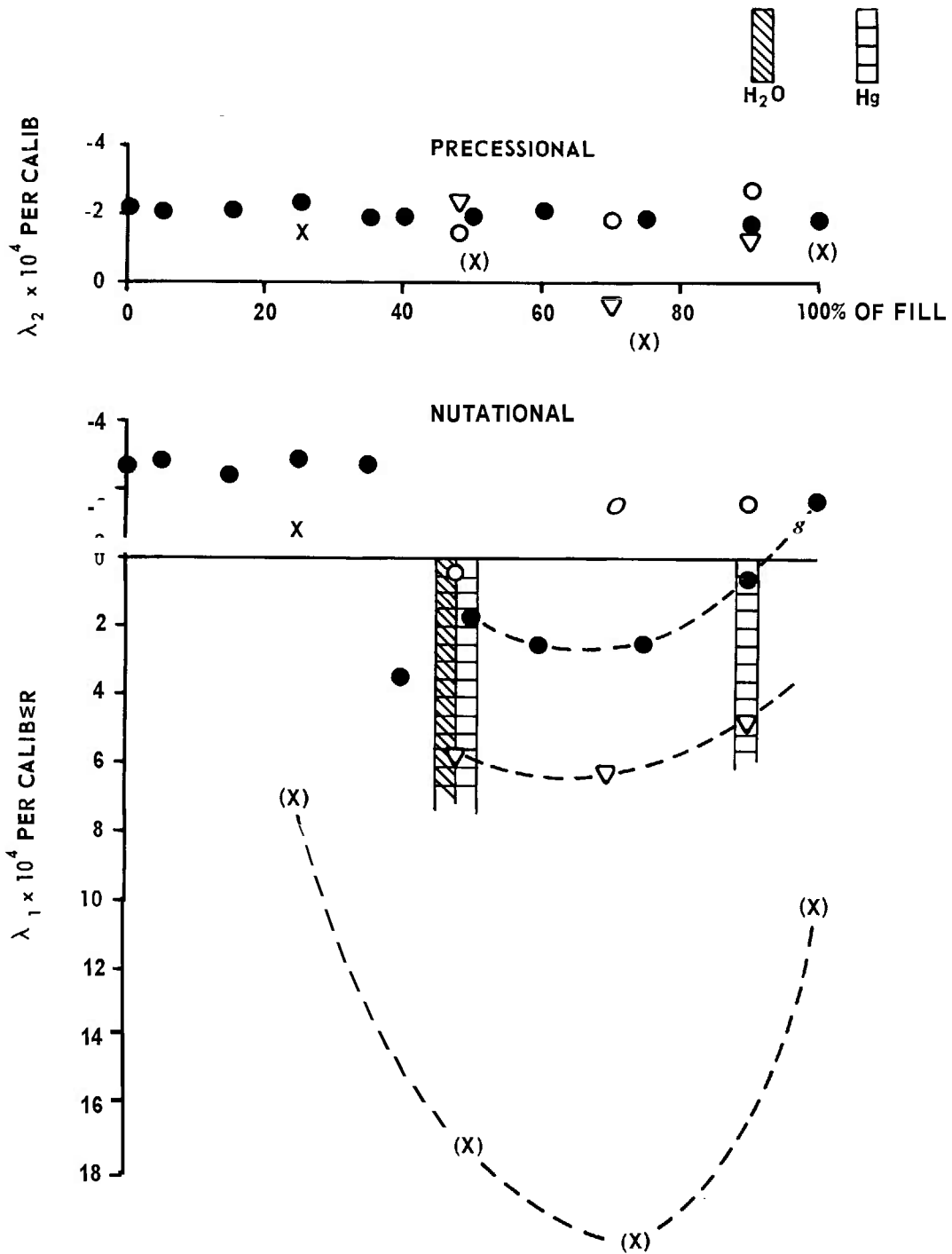


FIGURE 5-7. INSTABILITY DURING SPIN-UP OF THE LIQUID

vary with the radial velocity distribution in the cavity, which continuously changes until a rigid body rotation is reached. Thus during such sweep-up of the eigenfrequencies in a spin-up process, resonance with the nutational frequency of the projectile may occur.

An attempt at the solution of this "unsteady" problem, mathematically much more difficult than the steady state case, will be described in Chapter 8.

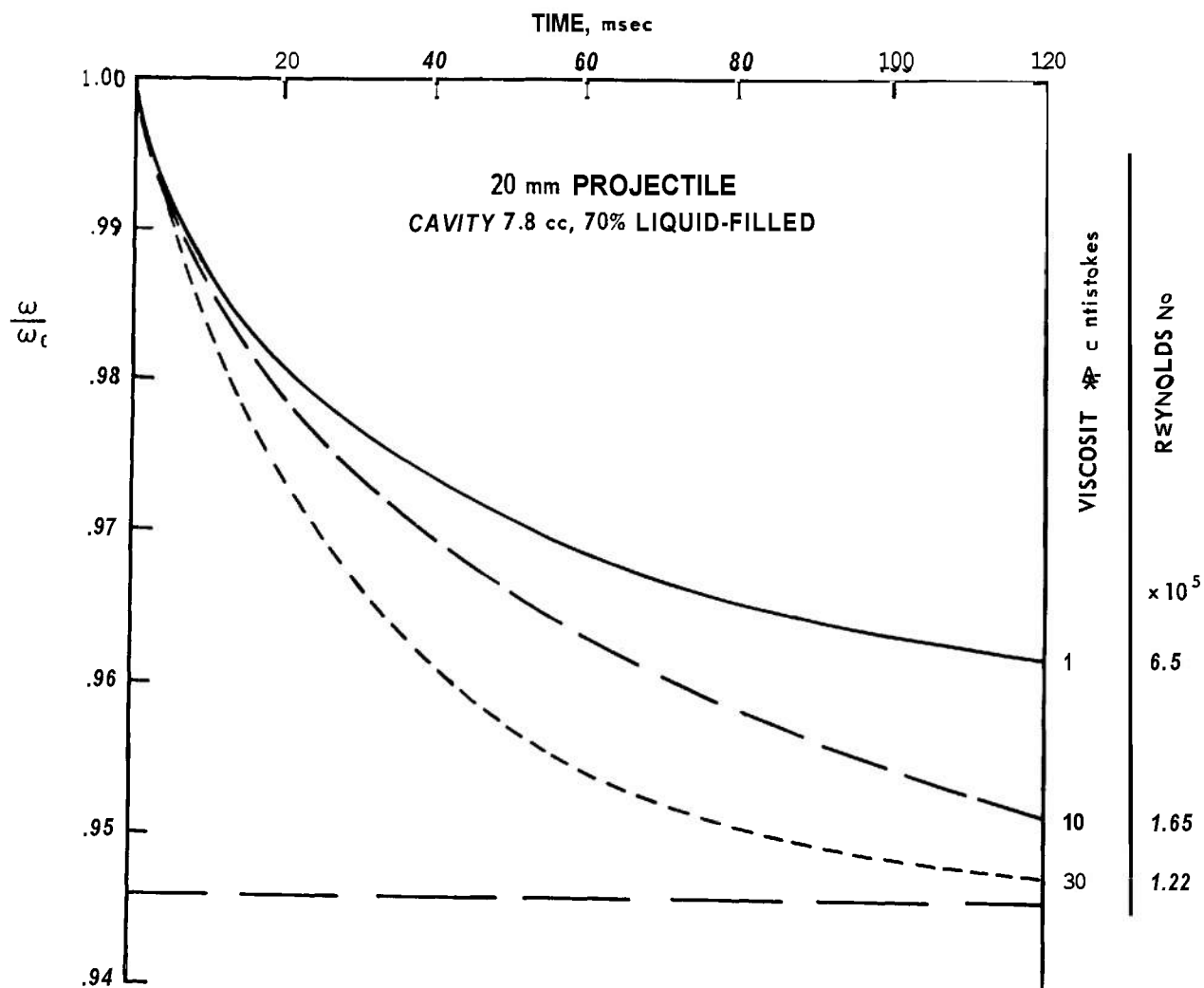
5-5 AXIAL SPIN DECAY

Figs. 5-8 and 5-9 show some typical spin decay curves, in a vacuum, for the same 20 mm projectile, 70% filled. These, of course, are measures of the spin-up process. For these experiments' the liquid was a mixture of glycerine and water. With liquids of higher viscosity, the graphs show that a considerable fraction of the angular momentum of the liquid was acquired while the projectile was still in the gun. Table 5-3 illustrates this.

TABLE 5-3. PERCENTAGE OF THE ANGULAR MOMENTUM AT THE MUZZLE

Viscosity, centistokes	% of angular momentum at the muzzle
1000	40
600	27
100	14
10	10
1	10

Relatively rapid spin decay of the liquid-filled projectile is due to a continuous transfer of the projectile's angular momentum to the liquid. This rate of transfer depends, among other things, on whether the momentum is transferred by the laminar or turbulent shearing stresses at the walls of the cavity. The latter is a many times more efficient process than the former. However, an attempt to represent the observed spin decay by either of these two processes proved unsuccessful^{6,8}. Neither the laminar nor the turbulent shearing stress hypothesis accounted for the observed spin decay. The solution was found in the experimental evidence⁶ that, as a result of end effects, strong secondary flow develops within the cavity. The secondary flow markedly alters the rate of diffusion of vorticity into the liquid thus accelerating the attainment of the full spin. The theoretical analysis of this problem also will be taken up in Chapter 8. There it will be shown that one can predict with reasonable accuracy the angular momentum of the fluid in the cavity, including the effect of the secondary flow, for any instant during the spin-up. This knowledge, in turn, will permit an estimate of the time-dependent eigenfrequencies as the fluid gradually attains its rigid body rotation. At the end of the spin-up the eigenfrequencies become those predicted by Stewartson's theory.

FIGURE 5-8. EXAMPLES OF THE AXIAL SPIN DECAY IN VACUUM, $Re \approx 10^5$

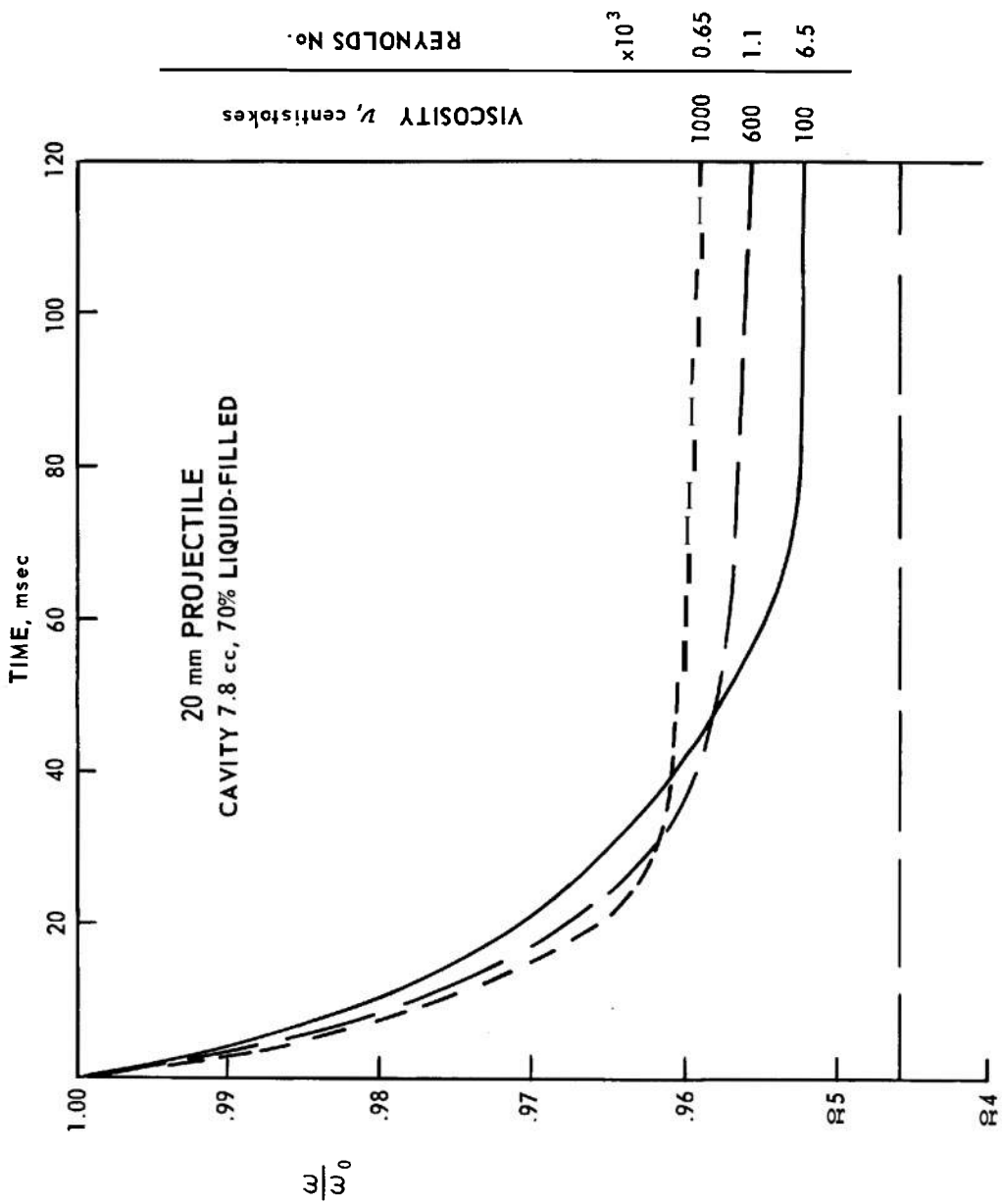


FIGURE 5-9. EXAMPLES OF THE AXIAL SPIN DECAY IN VACUUM, $Re \approx 10^3$

REFERENCES

1. G. N. Ward, Appendix to K. Stewartson, "On the Stability of Spinning Top Containing Liquid," *J. Fluid Mech.* **5**, Part **4** (1959).
2. B. G. Karpov, *Dynamics of Liquid-Filled Shell: Resonance and Effect of Viscosity*, BRL Report **1279**, Aberdeen Proving Ground, Md., May **1965**.
3. C. H. Murphy and L. E. Schmit, *The Effect of Length on the Aerodynamic Characteristics of Bodies of Revolution in Supersonic Flight*, BRL Report **876**, Aberdeen Proving Ground, Md., August **1953**.
4. B. G. Karpov, *Liquid-Filled Gyroscope: The Effect of Reynolds Number on Resonance*, BRL Report **1302**, Aberdeen Proving Ground, Md., October **1965**.
5. B. G. Karpov, *Dynamics of liquid-Filled Shell: Resonance in Modified Cylindrical Cavities*, BRL Report **1332**, Aberdeen Proving Ground, Md., August **1966**.
6. B. G. Karpov, *Experimental Observations of the Dynamic Behavior of Liquid-Filled Shell*, BRL Report **1171**, Aberdeen Proving Ground, Md., August **1962**.
7. B. G. Karpov, *Dynamics of liquid-Filled Shell: Instability During Spin-Up*, RRL Memo Report **1629**, Aberdeen Proving Ground, Md., January **1965**.
8. W. E. Scott, *A Theoretical Analysis of the Axial Spin Decay of a Spin Stabilized Liquid-Filled Shell*, BRL Report **1170**, Aberdeen Proving Ground, Md., August **1962**.

CHAPTER 6

EFFECT OF VISCOSITY

6-0 LIST OF SYMBOLS*

x = scaled frequency interval
 y = scaled rate of undamping

GREEK LETTERS

α = amplitude of yaw
 ϵ = real part associated with a slight change $\Delta\tau_0$ due to viscosity of the filler
 $A = \delta / \left(2 \sqrt{|D| / \sigma L} \right)$, a parameter
 $i\delta$ = imaginary part associated with a slight change $\Delta\tau_0$ due to viscosity of the filler
 = viscous counterpart of τ_0 i.e., $\tau_{0v} = \tau_0 + \Delta\tau_0$
 $\tau_{00} = \tau_0 + \epsilon$
 τ_I = imaginary part of τ
 τ_R = real part of τ
 $\Delta\tau_0 = \epsilon + i\delta$

In a strict sense these assumptions are inconsistent since the liquid cannot achieve any rotation without the action of viscosity.

Clearly, the inconsistency may be removed, assuming that the viscosity is very small so that its effect on the liquid oscillations can be neglected and assuming further that the casing had been spinning sufficiently long to establish a state of uniform rotation of the liquid. The question arises however, whether these assumptions are valid for a liquid-filled projectile leaving the muzzle of a gun. In cases of very high viscosity and small dimensions of the cavity, the rotation of the liquid may be nearly uniform when the projectile leaves the gun but then viscosity has a strong effect on the perturbed motion of the liquid. On the other hand for very low values of viscosity and large cavity dimensions, the effect of viscosity on the perturbed motion may be neglected but the rotation of the liquid is not uniform.

In most practical cases the viscosity has some intermediate value, and both the finite spin-up time and viscous effects on the perturbed fluid motion must be considered.

6-1 INTRODUCTION

The effect of viscosity on the motion of liquid-filled projectiles is twofold: the process of spin-up as well as the perturbed fluid motion are influenced by viscosity. In this chapter we are concerned with the second aspect, namely, the way viscosity influences the perturbed fluid motion.

The theories of Greenhill¹ and Stewartson² are based on the assumption that the liquid within the cavity is in a state of rigid rotation and yet has zero viscosity.

*For identification of other symbols in this chapter, refer to Chapter 3.

6-2 HISTORICAL BACKGROUND AND OUTLINE OF THE PROBLEM

Although Stewartson's theory was very successful to explain the observed instabilities of liquid-filled projectiles, some discrepancies were found when the theory was tested experimentally by Ward³ in 1959. Ward investigated the motion of a liquid-filled gyroscope and observed that the bandwidth of frequencies for which the gyroscope became unstable was considerably broader than predicted and that there was also a shift of the central frequency of the instability band relative to theoretical values.

The findings of Ward were confirmed in 1965 by Karpov^{4,5} who also pointed out that viscous effects are responsible for the discrepancies between predicted and observed ranges of instability. It was shown by Karpov that the bandwidth of instability decreases with decreasing viscosity of the liquid filler so that in the limit of zero viscosity the observed bandwidth approaches asymptotically the value predicted by Stewartson.

A full explanation of the observed facts was obtained by Wedemeyer^{6,7} through a modification of Stewartson's theory, which takes into account viscosity in the form of boundary layer corrections to Stewartson's inviscid solution.

A rough estimate for practical purposes is to consider that the effect of viscosity on the stability of liquid-filled projectile becomes insignificant when

$$1/\sqrt{\text{Re}} \ll \sqrt{|D|/\sigma L} \quad (6-1)$$

6.3 THEORY OF VISCOUS CORRECTIONS

A detailed discussion of the theory of viscous corrections is given in Refs. 6 and 7. The treatment of the problem given in Ref. 7 is preferable and more complete than Ref. 6. The analysis is based on the assumption that the Reynolds number $\text{Re} = \frac{\Omega a^2}{\nu}$ of the flow is sufficiently large, so that the action of viscosity is limited to a narrow boundary layer zone near the walls. The main results of the theory are:

a. The right hand side of the characteristic equation, Eq. 3-87, representing the reaction of the liquid upon the projectile is formally retained except that the eigenfrequencies τ_{nj} are slightly changed. Due to the action of viscosity any of the eigenfrequencies, say τ_0 , is shifted by a small amount $\Delta\tau$, which contains a real part and an imaginary part. The imaginary part of $\Delta\tau$ corresponds to viscous damping of

the free oscillations, while the real part is caused by the displacement effect of the boundary layers. Both the real and imaginary

part of $\Delta\tau_0$ are of the order $1/\sqrt{\text{Re}}$.

b. In contrast to the eigenfrequencies, the residues D of the inviscid theory undergo only negligibly small changes. Thus, the effect of viscosity can be described completely in terms of viscous eigenfrequencies. It is shown in par. 6-3.1 that both the broadening and the shift of the instability bands follow naturally when the viscous eigenfrequencies are substituted in the place of the inviscid values.

c. The broadening of the instability band is caused by the imaginary part of $\Delta\tau$, while the real part of $\Delta\tau$ is responsible for the shift of the central frequency.

6-3.1 THE RATE OF DIVERGENCE

As was mentioned in the previous paragraph, the only significant effect of viscosity is to change the eigenfrequencies by a small amount. We may thus retain the results of the inviscid theory except that the eigenfrequencies τ_0 are replaced everywhere by their viscous counterpart $\tau_{0v} = \tau_0 + \Delta\tau_0$

Eq. 3-81 then reads

$$\tau = \frac{\tau_n + \tau_{0v}}{2} \pm \sqrt{\left(\frac{\tau_n - \tau_{0v}}{2}\right)^2 - \frac{|D|}{\sigma L}} \quad (6-2)$$

It is readily seen that the two solutions for τ are always complex because τ_{0v} is complex

and it will be shown that one of the two solutions, viz. the one corresponding to the negative sign of the square root, has a negative imaginary part and thus gives rise to a divergent yawing motion of the projectile.

Let τ_R and τ_I be the real part and imaginary part of τ , respectively. The complex yaw angle is

$$|1 + im| = \alpha_0 e^{i\Omega(\tau_R + i\tau_I)t} = e^{i\Omega\tau_R t} \cdot \alpha_0 e^{-\Omega\tau_I t} \quad (6-3)$$

The amplitude of yaw diverges for negative τ_I as

$$|1 + im| = \alpha = \alpha_0 e^{-\Omega\tau_I t} \quad (6-4)$$

The relative time rate of divergence is

$$\frac{1}{\alpha} \frac{d\alpha}{dt} = -\Omega\tau_I, \text{ per sec} \quad (6-5)$$

The dimensionless rate $-\tau_I$ is termed simply "rate of divergence" or "rate of undamping".

In order to separate the real and imaginary parts of Eq. 6-2, the following abbreviations are convenient

$$\Delta\tau_0 = \epsilon \tau i \delta$$

$$\tau_0 + \epsilon = \tau_{00}, \quad \text{or} \quad \tau_{0v} = \tau_{00} \tau i \delta$$

$$m = \frac{4|D|}{\sigma L} \tau i \delta - (\tau_{00} - \tau_n)2$$

$$n = 2\delta(\tau_{00} - \tau_n)$$

Eq. 6-2 then reads

$$\tau = \frac{\tau_n + \tau_{00}}{2} + i \frac{\delta}{2} \sqrt{m + in} \quad (6-6)$$

Reducing the square root, one obtains for the real and imaginary parts of τ

$$\tau_R = \pm \frac{1}{2} \sqrt{\frac{\sqrt{m^2 + n^2} - m}{2}} + \frac{\tau_{00} + \tau_n}{2} \quad (6-7)$$

$$\tau_I = \mp \frac{1}{2} \sqrt{\frac{\sqrt{m^2 + n^2} + m}{2}} + \frac{\delta}{2} \quad (6-8)$$

The first solution for τ (corresponding to the upper sign of the square root) has a negative imaginary part and thus yields a positive rate of undamping $-\tau_I$, regard-

less of how large $(\tau_{00} - \tau_n)$ is. When plotted versus $(\tau_{00} - \tau_n)$, the rate of undamping $-\tau_I$ gives a bell-shaped symmetric curve with a maximum at $(\tau_{00} - \tau_n) = 0$. For large values of the argument, the rate of undamping decays like $1/(\tau_{00} - \tau_n)^2$. Actually, the width of the instability band is infinite and one should rather define a characteristic bandwidth of frequencies for which the rate of divergence is larger than a certain small percentage of the maximum rate. For practical purposes it is useful to define a residual bandwidth characterized by a band of frequencies for which the rate of undamping is larger than the aerodynamic damping rate. Eq. 6-8 shows that $-\tau_I$ depends on the two parameters $|D|/\sigma L$ and δ . To eliminate one of the parameters, it is advantageous to define a scaled rate of undamping y , and a scaled frequency interval x by

$$x = \frac{(\tau_{00} - \tau_n)/2}{\sqrt{\frac{|D|}{\sigma L}}}; \quad y = \frac{-\tau_I}{\sqrt{\frac{|D|}{\sigma L}}} \quad (6-9)$$

Then y depends only on x and the *one* parameter

$$A = \frac{\delta/2}{\sqrt{\frac{|D|}{\sigma L}}} \quad (6-10)$$

It is

$$y = \sqrt{\frac{\sqrt{(1 + \Delta^2 - x^2)^2 + 4\Delta^2 x^2} + (1 + \Delta^2 - x^2)}{2}} - \Delta \quad (6-11)$$

The scaled Eq. 6-11 has the advantage that it can be presented conveniently in graphical form or in the form of a table. Fig. 6-1 shows plots of y versus x for

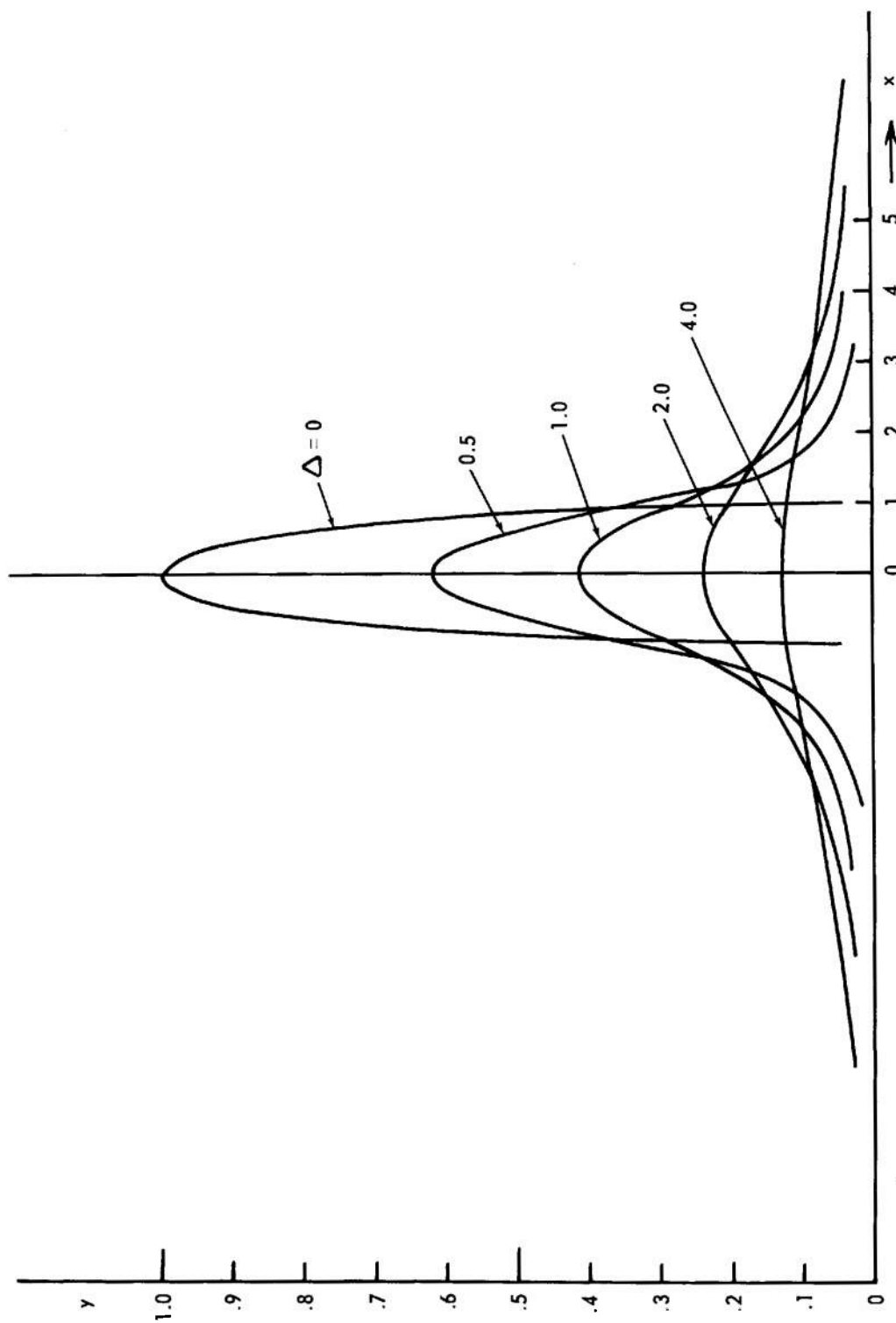


FIGURE 6-1. SCALED REPRESENTATION OF THE RESONANCE BAND FOR VARIOUS VALUES OF SCALED VISCOUS PARAMETER

several values of the parameter A . For $A=0$ the inviscid case is recovered; the undamped curve has an elliptical shape and the bandwidth is finite.

For larger values of A the undamped curve becomes increasingly flat and the bandwidth is at first broadened until finally, for very large A , the curve becomes so flat that an increasing part of it falls below the aerodynamic damping rate and the residual bandwidth of instability shrinks.

The maximum undamping occurs when the nutational frequency τ_n coincides with the central frequency τ_{00} which is shifted away from the inviscid eigenfrequency τ_0 by the amount ε .

To account for viscosity it is necessary to compute both ϵ and δ , i.e., the real and imaginary part of $A\tau$. Once ϵ and δ are known, the rate of divergence may be determined with the aid of Fig. 6-1 or directly from Eq. 6-11. The computation of $\Delta\tau_0$ is discussed in par. 6-3.2.

6-3.2 COMPUTATION OF VISCOUS EIGENFREQUENCIES

In the previous paragraph it was shown that the effect of viscosity on the stability of a liquid-filled projectile can be described completely in terms of complex eigenfrequencies which are substituted for the real eigenfrequencies of the inviscid theory. The subject of this paragraph is the computation of these viscous eigenfrequencies.

To facilitate the understanding of the computational scheme, a few basic notions may be outlined beforehand. It is assumed throughout the following that the Reynolds number of the flow $Re = \frac{\Omega a^2}{\nu}$ is very large, so that boundary layer theory is applicable. An important result of boundary layer theory is that when a flow is in contact with a wall, a thin layer of reduced flow velocity — the so-called boundary layer —

is formed on the walls as a result of friction. The remaining flow outside of the boundary layer — briefly termed “external flow” — is not subjected to friction, i.e., the external flow satisfies the dynamic equations of inviscid flow and the inviscid boundary conditions. However, the boundary conditions for the external flow do not apply at the wall but at the edge of the boundary layer or, precisely, at a surface which is displaced from the wall by the boundary layer displacement thickness. If, for example, the displacement thickness at the curved wall $r=a$ of a cylindrical cavity is δa , the boundary condition requires that the normal component u of the flow velocity be zero at $r=a-\delta a$, i.e., $u(a-\delta a)=0$. Similarly, if at the plane surface $z=\pm c$, the displacement thickness is δc , the boundary condition for the normal component w applies at $z=\pm(c-\delta c)$, i.e., $w(c-\delta c)=w(-c-\delta c)=0$.

Thus, the effect of viscosity is equivalent to a reduction of the cavity dimensions from (a, c) to $(a-\delta a, c-\delta c)$.

The detailed analysis shows that δa and δc are constants, so that the reduced cavity is again cylindrical. Consequently, the viscous eigenfrequency τ_{0v} of a cylindrical cavity with dimensions (a, c) is equal to the inviscid eigenfrequency τ_0 of the reduced cavity $(a-\delta a, c-\delta c)$, or

$$\tau_{0v}(a, c) = \tau_0(a - \delta a, c - \delta c) \quad (6-12)$$

Actually, the physical interpretation of δa and δc as “displacement thickness” is somewhat ambiguous for unsteady flow since δa , δc are not real in this case. The oscillating flow in the cavity of the yawing projectile produces an oscillating boundary layer flow which is not in phase with the inviscid flow outside the boundary layer. Within the mathematical formalism, the displacement flow of the boundary layer is a complex quantity, the real part of which corresponds to the component in phase with the inviscid flow; the imaginary part corresponds to the component 90 degrees out of

phase. The complex displacement flow, in turn, leads to a complex displacement thickness. It appears, that a complex displacement thickness has no physical meaning; however, the essential point is that the use of complex notation leads to complex values for $(\delta a, \delta c)$, so that the boundary conditions for the inviscid flow apply at the complex boundaries $r = (a - \delta a)$ and $z = \pm (c - \delta c)$.

Since the cavity dimensions enter into the theory only via the boundary conditions, it follows that the effect of viscosity is equivalent to replacing (a, c) by $(a - \delta a, c - \delta c)$ in the results; Eq. 6-12 follows regardless whether δa and δc are real or not.

For the cylindrical cavity of radius a and height $2c$, the following expressions are found for the displacement thickness δa at the curved wall and δc at the plane walls

$$\frac{\delta a}{a} = \frac{1}{\sqrt{\text{Re}}} \cdot \frac{1+i}{\sqrt{2}} \cdot \frac{1}{\sqrt{1-\tau}} \quad (6-13)$$

$$\frac{\delta c}{c} = \frac{1}{\sqrt{\text{Re}}} \cdot \frac{a}{c} \cdot \frac{1}{\sqrt{8}} \left[\frac{3-\tau}{\sqrt{1+\tau}} \left(\frac{1-i}{1-\tau} \right) - \frac{1+\tau}{\sqrt{3-\tau}} \left(\frac{1+i}{1-\tau} \right) \right] \quad (6-14)$$

with $\tau = \frac{\omega}{\Omega}$, dimensionless yawing frequency

$$\text{Re} = \frac{\Omega a^2}{\nu}, \text{ Reynolds number}$$

The viscous eigenfrequencies may now be computed from Eq. 6-12 with δa and δc as given by Eqs. 6-13 and 6-14.

Assuming, that $\delta a \ll a$ and $\delta c \ll c$, we may expand the right hand side of Eq. 6-12 and retain **only** terms up to first order in δa and δc . Thus, Eq. 6-12 becomes simply

$$\tau_{0v}(a, c) = \tau_0(a, c) - \frac{\partial \tau_0(a, c)}{\partial a} \delta a - \frac{\partial \tau_0(a, c)}{\partial c} \delta c \quad (6-15)$$

The partial derivatives $\frac{\partial \tau_0}{\partial a}$ and $\frac{\partial \tau_0}{\partial c}$

in Eq. 6-15 may be computed from tables of τ_0 by numerical differentiation.

In Stewartson's Tables, however, τ_0 is tabulated versus $c/[a(2j+1)]$ and b^2/a^2 . It is, therefore, convenient to express the partial derivatives $\partial\tau_0/\partial a$ and $\partial\tau_0/\partial c$ by derivatives with respect to $c/[a(2j+1)]$ and b^2/a^2 . The partial derivatives are

$$\frac{\partial\tau_0}{\partial a} = -\frac{\partial\tau_0}{\partial c/[a(2j+1)]} \cdot \frac{c}{a^2(2j+1)} - \frac{\partial\tau_0}{\partial b^2/a^2} \cdot \frac{2b^2}{a^3}$$

$$\frac{\partial\tau_0}{\partial c} = \frac{\partial\tau_0}{\partial c/[a(2j+1)]} \cdot \frac{1}{a(2j+1)}$$

and Eq. 6—15 becomes:

$$\tau_{0v} = \tau_0 + \frac{\partial\tau_0}{\partial c/[a(2j+1)]} \cdot \frac{c}{a(2j+1)} \left(\frac{\delta a}{a} - \frac{\delta c}{c} \right) + \frac{\partial\tau_0}{\partial b^2/a^2} \cdot \frac{2b^2}{a^2} \cdot \frac{\delta a}{a} \quad (6-16)$$

The evaluation of Eq. 6—16 with the aid of Stewartson's Tables may be illustrated in an example:

Suppose the fineness-ratio is $c/a = 3.60$ and the cavity is 95% filled or $b^2/a^2 = 0.05$.

For the principal mode ($j=1, n=1$) we obtain:

$$\frac{c}{a(2j+1)} = 1.20, \quad \frac{b^2}{a^2} = 0.05$$

and from Stewartson's Tables

$$\tau_0(c/[a(2j+1)], b^2/a^2) = \tau_0(1.20, 0.05) = 0.1600$$

Approximating the partial derivatives by difference quotients we obtain

$$-\frac{\partial\tau_0}{\partial c/[a(2j+1)]} = \frac{\tau_0(1.231, 0.05) - \tau_0(1.20, 0.05)}{0.031} = \frac{0.02}{0.031} = 0.656$$

$$\frac{\partial\tau_0}{\partial b^2/a^2} = \frac{\tau_0(1.20, 0.10) - \tau_0(1.20, 0.05)}{0.05} = \frac{0.0069}{0.05} = 0.138$$

Next, Eqs. 6-13 and 6-14 are evaluated for $c/a = 3.60$ and $\tau = \tau_0 = 0.16$

$$\frac{\delta a}{a} = \frac{1}{\sqrt{\text{Re}}} \cdot \frac{1 + i}{\sqrt{2}} \cdot \frac{1}{\sqrt{0.84}} = \frac{1}{\sqrt{\text{Re}}} (0.77 + 0.77i)$$

$$\frac{\delta c}{c} = \frac{1}{\sqrt{\text{Re}}} \cdot \frac{1}{3.6 \times 0.8} \left[\frac{2.84}{\sqrt{1.16}} \left(\frac{1-i}{0.84} \right) - \frac{1.16}{\sqrt{2.84}} \left(\frac{1+i}{0.84} \right) \right] = \frac{1}{\sqrt{\text{Re}}} [0.22 - 0.38i]$$

Substituting these results into Eq. 6-16 finally yields

$$\tau_{0v} = 1.0 + \frac{1}{\sqrt{\text{Re}}} (0.44 + 0.916i)$$

According to the definition of ϵ and δ

$$\tau_{0v} - \tau_0 = \Delta\tau_0 = \epsilon + i\delta$$

we have

$$\epsilon = \frac{0.44}{\sqrt{\text{Re}}}; \quad \delta = \frac{0.916}{\sqrt{\text{Re}}}$$

Finally the frequency shift and the shape of the instability band follow from ϵ , δ , and Eq. 6-8.

6-4 EXPERIMENTAL VERIFICATION

According to the theory, the broadening and shift of the instability bands is a consequence of the shift of eigenfrequencies by a small amount $\Delta\tau_0 = \epsilon + i\delta$. The theory predicts that both the real and the imaginary part of $\Delta\tau_0$ are proportional to $\text{Re}^{-1/2}$. During the course of experiments on a liquid-filled gyroscope, Karpov⁴ measured the rate of divergence as a function of the fill-ratio for various fluids. Since the functional dependence between fill-ratio and eigenfrequency is known, it was possible to plot the measured rate of divergence versus the (inviscid) eigenfrequency. When the theory is correct, it should be possible to fit a curve of the type shown in Fig. 6-1 to the experimental points, provided the values of ϵ and δ are properly chosen.

The method actually used was to determine ϵ and δ by a curve fitting procedure. The rate of divergence has its maximum when $\tau_0 + \epsilon = 1$.

The frequency τ_0 , at which maximum undamping occurs, and also the nutational frequency τ of the gyroscope can be determined with rather high accuracy. The difference $\tau_n - \tau_0$ then yields the experimental value for ϵ .

The value of b was determined from the observed maximum rate of divergence. Let r be the ratio of the maximum rate of divergence as predicted by inviscid theory divided by the observed maximum rate of divergence, i.e.,

$$r = \frac{\lambda_{\max}(\text{inviscid})}{\lambda_{\max}(\text{viscous or observed})} = \frac{\sqrt{S}}{\sqrt{S + \delta^2} - \delta}$$

Then, according to Eq. 6-11 evaluated for $x = 0$

$$1 = \sqrt{1 + \Delta^2} - \Delta \quad \text{or} \quad \Delta = \frac{1}{2} \left(r - \frac{1}{r} \right)$$

(since $y \approx \lambda_{\max}$, $y_{\max}(\text{inviscid}) = 1$, and

$$y_{\max}(\text{viscous}) = \sqrt{1 + \Delta^2} - \Delta)$$

$$\text{and} \quad \delta = \sqrt{\frac{4|D|}{\sigma L}} \cdot \frac{1}{2} \left(r - \frac{1}{r} \right)$$

With ϵ and δ so determined, the theoretical resonance curves (rate of divergence versus eigenfrequency) were computed and compared to the experimental data. The agreement was very good.

When, however, ϵ and δ were plotted versus the Reynolds number, it appeared that they did not follow the predicted $Re^{-1/2}$ law. The data indicated only to some extent a unique dependence on the Reynolds number and the dependence was more like $Re^{-1/4}$ or $Re^{-1/5}$. The experimental δ 's were larger than expected except for the lowest experimental Reynolds numbers.

The nature of the observed discrepancies suggested the following hypothesis: "For sufficiently large amplitudes of oscillation and high Reynolds number, the boundary layer on the concave wall of the cavity becomes unstable. As a result of this instability a cellular flow and eventually turbulence develops in the boundary layer, yielding a larger skin friction and thus a larger value for δ ." This hypothesis was supported by another observation, namely, the instability of the gyroscope was self-generating only in a close vicinity of resonance, i.e., some of the observed instabilities were absent at small amplitudes.

To resolve this matter, it was necessary to perform the experiments at a smaller amplitude of oscillation. To this end a new gyroscope of greater sensitivity was built, and the previous experiments were repeated at yawing amplitudes of less than one degree⁵. The results of these experiments are in excellent agreement with the theory. In Fig. 6-2 theoretical resonance curves are plotted for different Reynolds numbers together with experimental data. The theoretical and experimental data of Fig. 6-2 are based on the following constants and dimensions of the gyroscope

$$\Omega = 5000 \text{ rpm}; \quad \sqrt{\frac{|D|}{\sigma L}} = 1.6 \times 10^{-3}$$

$$b^2/a^2 = 0.15; \quad \frac{c}{a} = 3.077; \quad j = 1$$

Figs. 6-3 and 6-4 show a comparison of theoretical and experimental values, respectively, of ϵ and δ ; $\epsilon = R(\Delta\tau_0)$ and $\delta = I(\Delta\tau_0)$.

The logarithmic plot $\log \epsilon$ and $\log \delta$ versus $\log Re$ yields straight lines with a slope of $-1/2$. All experimental points fall very close to the theoretical lines.

The data in Figs. 6-3 and 6-4 are based on the following dimensions:

$$\frac{c}{a} = 3.077; \quad j = 1; \quad b^2/a^2 = 0.15$$

Ward's experimental data³, which are obtained for about the same c/a and b^2/a^2 values, also fit the curves very well.

The good agreement with theoretical predictions, which was found for all experimental data taken at small yawing amplitude, can be considered as a full confirmation of the theory. On the other hand, the experiments have disclosed a severe limitation of the theory. The theory of viscous corrections, which is based on the assumption of laminar boundary layer, is not applicable at large yaw amplitudes and Reynolds numbers.

Theoretical considerations suggest that the boundary layer becomes unstable at constant values of $\alpha \sqrt{Re}$, i.e., the higher the Reynolds number, the smaller is the yaw-angle at which transition to a non-laminar boundary takes place. From experimental results⁵ it appears that transition occurs at about $\alpha \sqrt{Re} \approx 3 \times 10^2$ where α is measured in degrees.

In Ref. 5, Karpov investigated thoroughly the effects of large yaw amplitude because of the important practical aspects of the problem. A discussion of these investigations is given in Chapter 10.

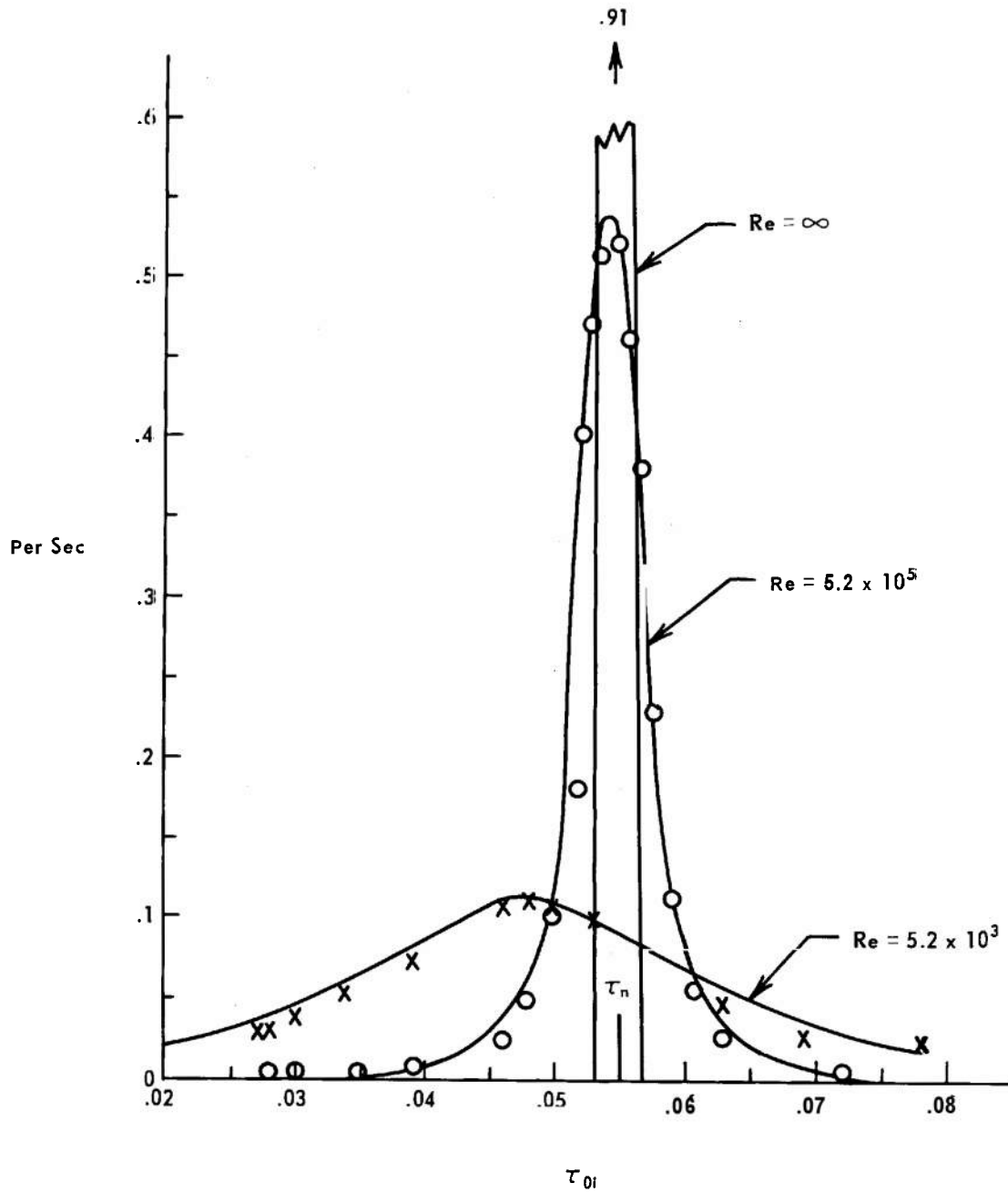


FIGURE 6-2. RATE OF UNDAMPING, $-\Omega\tau_i$ VS INVISCID EIGENFREQUENCY τ_{0i} ($\Omega=5000$ RPM. EXPERIMENTS BY KARPOV)

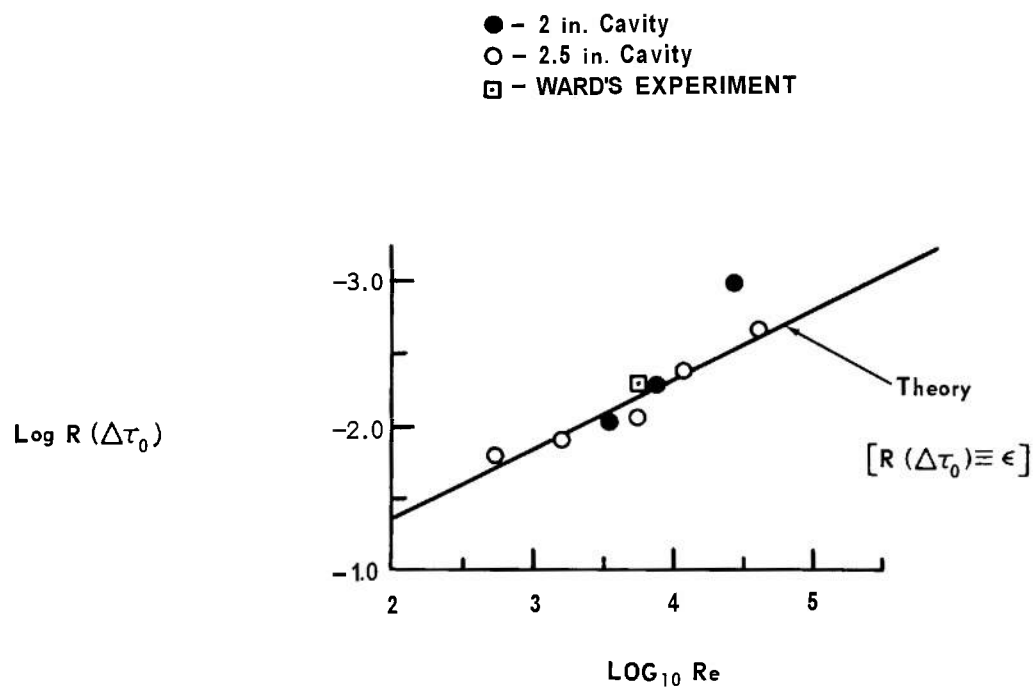


FIGURE 6-3. REAL PART OF THE FREQUENCY SHIFT VS REYNOLDS NUMBER. EXPERIMENTAL POINTS BY KARPOV AND WARD

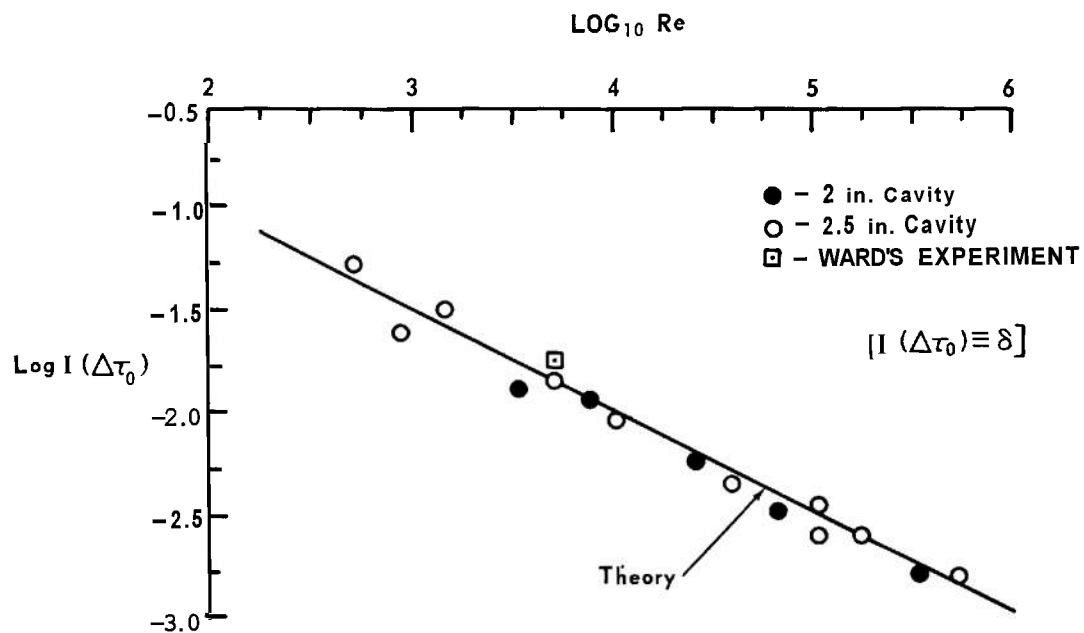


FIGURE 6-4. IMAGINARY PART OF FREQUENCY SHIFT VS REYNOLDS NUMBER. EXPERIMENTAL POINTS BY KARPOV AND WARD

REFERENCES

1. A. G. Greenhill, Proc. Camb. Phil. Soc. **4, 4 (1880)**.
2. K. Stewartson, "On the Stability of a Spinning Top Containing Liquid," J. Fluid Mech. **5**, Part **4 (1959)**.
3. G. N. Ward, Appendix of Ref. **2**.
4. B. G. Karpov, *Dynamics of Liquid-Filled Shell. Resonance and Effect of Viscosity*, BRL Report **1279**, Aberdeen Proving Ground, Md., **1965**.
5. B. G. Karpov, *Liquid-Filled Gyroscope: The Effect of Reynolds Number on Resonance*, BRL Report **1302**, Aberdeen Proving Ground, Md., **1965**.
6. E. H. Wedemeyer, *Dynamics of Liquid-Filled Shell. Theory of Viscous Corrections to Stewartson's Stability Problem*, BRL Report **1287**, Aberdeen Proving Ground, Md., **1965**.
7. E. H. Wedemeyer, *Viscous Corrections to Stewartson's Stability Criterion*. BRL Report **1325**, Aberdeen Proving Ground, Md., **1966**; AGARD Conference Proceedings **10**, **99-116 (1966)**.

CHAPTER 7

NONCYLINDRICAL CAVITIES

7-0 LIST OF SYMBOLS*

A	= a constant
$a(z)$	= radius of cavity at z , i.e., a function of z
a_0	= radius of the cylindrical part of the cavity
b_0	= radius of cavity void at $z = c$
C	= boundary curve in x, y -plane
C_1	= Bessel function
D	= residue at pole, related to non-cylindrical cavity
D_0	= residue at pole, related to cylindrical cavity
D'	= domain, related to boundary curve C
f_j	= modes of oscillations
k	= wave number
K_n	= $\pi/(2\eta_n)$. K_n is tabular value in Stewartson's Tables for a given τ_0 , $c/[a(2j+1)]$, and the n th radial mode
M	= moment on projectile in nonrotating, inertial coordinate system
M'	= moment on projectile in rotating coordinate system
n	= radial mode number; a normal direction to curve C
P_R	= real part of P hydrodynamic pressure
P_I	= imaginary part of P hydrodynamic pressure
P^*	= complex conjugate of P hydrodynamic pressure
p_R	= real part of p perturbation pressure

R'	= radius of rounded corner of cavity
s	= tangential direction to curve C
ΔV	= change in liquid volume
V_c	= volume of original cylinder
x, y, z	= rotating system of coordinates with z along axis of rotation

GREEK LETTERS

β	= $\sqrt{4/(1-\tau)^2 - 1}$
η_n	= parameter depending on τ and b^2/a^2
θ	= cone angle, refer to Fig. 7-1
Λ	= parameter
τ'_0	= nondimensional eigenfrequency in rotating coordinate system
ϕ	= phase of wave in axial direction
ω'_0	= frequency in rotating coordinate system
ω_0	= frequency in nonrotating, inertial coordinate system

7-4 INTRODUCTION

The stability behavior of liquid-filled projectiles can be predicted with high accuracy when the liquid-filled cavity is cylindrical, or when the cavity is spheroidal and completely filled. The cases of spheroidal and cylindrical cavities have been investigated extensively because of their mathematical tractability.

Although most liquid-filled projectiles have cavities of nearly cylindrical shape, there are few cases where the cavity is exactly cylindrical and the question arises whether nearly cylindrical shapes may be approximated by cylinders and how large the encountered error is. In some cases, cavity shapes deviate sufficiently from cylinders so that the applicability of Stewartson's theory is rather questionable.

*For identification of other symbols used in this chapter, refer to Chapter 3.

Solutions for cavity shapes other than spheroidal or cylindrical are not known and it appears that they are very difficult to obtain. Furthermore, special solutions would be of little use for the designer in view of the large variety of practical cavity shapes.

Fortunately, it has become possible to compute the eigenfrequencies for most practical cavities on the basis of an approximate theory¹. Moreover, extensive experimental investigations have been performed*which support and supplement the theory of Ref. 1.

The theory is applicable to cavities of rotational symmetry, provided that the cavity has two plain endwalls and the radius $a(z)$ of the cavity varies only slowly with the distance along the axis, i.e., $\left|\frac{da}{dz}\right| \ll 1$.

Frequently, the corners between endwalls and sidewalls are rounded, and the condition $\left|\frac{da}{dz}\right| \ll 1$ is not fulfilled at the corner. However, the experiments have completely clarified the effect of rounded corners on the eigenfrequencies.

Approximate residues may be computed on an empirical basis. As mentioned in par. 3-7, it is very often sufficient to have just a rough estimate of the bandwidth of instability and thus a rough approximation of the residue. Nevertheless, it appears that residues can be predicted now with reasonable accuracy. The theoretical and experimental results regarding cavities of rotational symmetry are discussed in par. 7-2.

The stability problem becomes extremely difficult when the cavity is not rotationally symmetrical. Fortunately, cavities of nonrotational symmetry are practically unimportant, with the possible exception of cavities formed by partitioning as in Fig. 8-1(A). As yet cavities of other than rotationally symmetrical shapes are not amenable to theoretical treatment. However, some ideas regarding the compu-

tation of eigenfrequencies for such cavities are outlined in par. 7-4.

7-2 CAVITIES OF ROTATIONAL SYMMETRY

The importance of eigenfrequencies and corresponding residues for the stability problem of liquid-filled projectiles was discussed in par. 3-6. Although the stability problem has been solved only for cylindrical and completely filled spheroidal cavities, we may assume with certainty that eigenfrequencies exist also for other cavity shapes and that they are related to instabilities in a manner similar to that for spheroidal and cylindrical cavities.

It is reasonable to assume that small changes of the cavity shape cause small changes of the eigenfrequencies and residues. Thus, as a first approximation, Stewartson's stability criterion may be applied in cases where the cavity is nearly cylindrical, approximating the true cavity shape by a suitable cylinder. On the other hand, Stewartson's solution for the cylindrical cavity has been used in Ref. 1 as a starting point for the construction of higher approximations. In the paragraphs which follow a brief outline of the theory of Ref. 1 is given.

7-2.1 THEORETICAL APPROACH

The equations of perturbed fluid motion for cavities of rotational symmetry were discussed in Chapter 3. It was shown in par. 3-5.1 that, if the cavity has rotational symmetry, the perturbed fluid motion depends on time and azimuthal angle only in the form of a factor $e^{i(\omega t - \theta)}$ which can be separated from the solution. The (r, z) -dependent amplitude function $f(r, z)$ of the pressure perturbation, Eq. 3-56, is described by the partial differential equation, Eq. 3-60, and boundary conditions, Eqs. 3-61 and 3-62.

As shown in par. 3-7.1, the solution becomes particularly simple for cylindrical cavities. In the case of a cylindrical cavity, the solution of the boundary value problem

can be constructed by a series of modes of oscillation f_j where the z -dependence of each mode f_j can be separated in the form of a factor $\cos kz$ so that

$$f_j = \cos kz C_1(\beta kr); \quad (0 < z < 2c); \quad 0 < r < a \quad (7-1)$$

where C_1 is a Bessel function of the argument βkr and

$$\beta = \sqrt{\frac{4}{(1-\tau)^2} - 1}$$

The eigenfrequencies are those frequencies for which one of the modes f_j satisfies the homogeneous boundary conditions, Eqs. 3-61 and 3-62 with $\alpha = 0$. The boundary condition applied at $r=a$ yields the following condition

$$ka = \eta_n(b^2/a^2, \tau), \quad n = 1, 2, 3, \dots \quad (7-2)$$

where a is the cavity radius. The η_n , which are essentially determined by the roots of Bessel functions, depend on τ and b^2/a^2 , where b is the radius of the cylindrical air column. For a completely filled cavity, $b = 0$. The integer number n is related to the number of half-waves in the radial direction.

The boundary condition, Eq. 3-61, applied at $z = \pm c$ leads to

$$k2c = \pi(2j + 1), \quad j = 0, 1, 2, \dots \quad (7-3)$$

where $2c$ is the cavity height, and j is related to the number of axial half-waves (which is $2j + 1$).

A comparison of Eqs. 7-2 and 7-3 gives a condition for the fineness-ratio

$$\frac{c}{a(2j+1)} = \frac{\pi/2}{\eta_n(b^2/a^2, \tau)}; \quad j = 0, 1, 2, \dots \quad (7-4) \\ n = 1, 2, 3, \dots$$

Eq. 7-4 expresses that only certain discrete fineness-ratios $\frac{c}{a}$ exist for given b^2/a^2

and τ or, for given b^2/a^2 and $\frac{c}{a}$ there exists a set of discrete eigenfrequencies $\tau = \tau_n$, according to the choice of j and n in Eq. 7-4. In Stewartson's Tables the various $\frac{c}{a(2j+1)}$ are tabulated as functions of b^2/a^2 and τ . Let us denote these functions with $K_n(b^2/a^2, \tau_0)$, i.e.,

$$\frac{c}{a(2j+1)} = K_n(b^2/a^2, \tau_0) \quad (7-5)$$

where

$$K_n = \frac{\pi/2}{\eta_n} \quad (7-6)$$

(Here, as in previous chapters, the notation τ_0 is used for any eigenfrequency.)

Let us consider now the modification when the cavity is not exactly cylindrical. We will assume, however, that the cavity is "nearly" cylindrical in the sense that it has two plane endwalls at $z = 0$ and $z = 2c$ and that the variation of the radius $a(z)$ is small, i.e.,

$$\left| \frac{da}{dz} \right| \ll 1 \text{ for } 0 < z < 2c \quad (7-7)$$

With this assumption, an obvious approximation of the boundary condition, Eq. 3-61, is to neglect the term containing $\frac{da}{dz}$.

The resulting approximate boundary condition at $r = a$ is formally the same as the condition at a cylindrical surface, the only difference being that the cavity radius is now slowly varying with z . A consequence of the variation of the cavity radius is — roughly speaking — that the radial wavelength and the wavenumber k must vary with z since a fixed number of waves must fit into the variable interval $a(z)$.

Thus instead of Eq. 7-1, one may try, as an approximate solution of the eigenvalue problem,

$$f_j = \cos \phi(z) C_1(\beta kr) \quad (7-8)$$

$$0 < z < 2c, \quad 0 < r < a(z)$$

where k depends now weakly on z . The phase of the wave in the axial direction can no longer be assumed to be equal to kz but rather

$$\phi = \int_0^z k dz \quad (7-9)$$

It can be verified that Eq. 7-8 with Eq. 7-9 satisfies —within our approximation— the perturbation equation, Eq. 3-60.

The homogeneous boundary conditions, Eqs. 3-62 and 3-61 with $\alpha = 0$, applied to the sidewalls yield a condition analogous to Eq. 7-2 except that a is now variable.

Thus

$$k = k(z) = \frac{1}{a} \eta_n(b^2/a^2, \tau_0); \quad n = 1, 2, 3, \dots \quad (7-10)$$

The boundary condition Eq. 3-61 with $\alpha = 0$ applied to the endwalls $z = \pm c$ leads to

$$\phi(2c) = \int_0^{2c} k dz = \pi(2j + 1); \quad j = 0, 1, 2, \dots \quad (7-11)$$

Eq. 7-11 is a generalization of Eq. 7-3 when k is variable. Both, Eq. 7-3 and Eq. 7-11, express the fact that the number of half-waves in an axial direction is an odd integer number. Eq. 7-10 substituted in Eq. 7-11 yields

$$\int_0^{2c} \frac{\eta_n}{a} dz = \pi(2j + 1); \quad j = 0, 1, 2, \dots$$

$$n = 1, 2, 3, \dots \quad (7-12)$$

Finally, expressing η_n by K_n according to Eq. 7-6 and rearranging terms, Eq. 7-12 yields

$$\frac{1}{2c} \int_0^{2c} \frac{c/[a(2j+1)]}{K_n(\tau_0, b^2/a^2)} dz = 1; \quad j = 0, 1, 2, \dots$$

$$n = 1, 2, 3, \dots \quad (7-13)$$

Eq. 7-13 is the generalization of Eq. 7-5 for the case that a is variable. Eq. 7-13 may be used to determine either the eigenfrequency τ_0 when the fill-ratio (i.e., b^2/a^2) is given or vice versa. The K_n are tabulated in Stewartson's Tables as functions of τ_0 and b^2/a^2 . For a cylindrical cavity, the K_n represent the $c/[a(2j+1)]$ value of the cylinder.

The practical computation of eigenfrequencies on the basis of Eq. 7-13 is discussed in par. 7-2.2.

7-2.2 COMPUTATION OF EIGENFREQUENCIES

The evaluation of Eq. 7-13 is difficult when K_n is given numerically (as in Stewartson's Tables) since one has to assume both b and τ_0 in order to perform the integration numerically, and eventually repeat the procedure with changed values of τ_0 (or b) until the correct value of τ (or b) can be obtained by interpolation. For a 100% filled cavity, i.e., $b = 0$, the integration simplifies considerably since K_n becomes independent of z and can be taken out of the integral. One obtains from Eq. 7-13:

$$K_n(0, \tau_0) = \frac{1}{2c} \int_0^{2c} \frac{c}{a(2j+1)} dz \quad (7-14)$$

Since K_n is the $\frac{c}{a(2j+1)}$ value of a cylinder with eigenfrequency τ_0 , Eq. 7-14 can be interpreted in the following way: A completely filled noncylindrical cavity has the same eigenfrequencies as an "equivalent cylindrical cavity"; the latter is defined as a cylindrical cavity having a fineness ratio

c/a equal to the averaged c/a of the non-cylindrical cavity. For a 100% filled cavity, therefore, only one integration must be performed to determine the average c/a .

A way of solving the eigenvalue problem given in Eq. 7-13 is to approximate $1/K_n$ by polynomials in b^2/a^2 . If τ_0 is given and b is to be determined, one could plot $1/K_n$ — for the particular τ_0 given — versus b^2/a^2 and approximate the resulting curve by a polynomial in b^2/a^2 . If neither τ_0 nor b^2/a^2 are too large, the following formula is convenient and quite accurate within specified limits

$$\frac{K_n}{K_{n0}} = \frac{K_{n0}}{K_{n0}} \left[1 + 1.26 \left(\frac{b^2}{a^2} \right)^2 \right] \quad (7-15)$$

K_{n0} is the value $K_n(0, \tau_0)$ as obtained from Stewartson's Tables for $b^2/a^2 = 0$. The approximate Eq. 7-15 is valid within the following limits

$$\begin{aligned} 0 < \tau_0 < 0.12 \\ 0 < b^2/a^2 < 0.15 \end{aligned} \quad (7-16)$$

With Eq. 7-15 substituted into Eq. 7-13 one obtains

$$K_{n0}(\tau_0) = \frac{1}{2c} \int_0^{2c} \frac{c}{a(2j+1)} \left[1 + 1.26 \left(\frac{b^2}{a^2} \right)^2 \right] dz \quad (7-17)$$

Eq. 7-17 has the advantage that the right side is independent of τ_0 and the left side is independent of b . By integration of Eq. 7-17, one finds a relation of the form

$$K_{n0}(\tau_0) = C_1 + C_2 b^4$$

Higher approximations of $1/K_n$, in place of Eq. 7-15, and a practical evaluation of the integral Eq. 7-13 are discussed in par. 9-4.

7-2.3 NONCYLINDRICAL FREE SURFACE

According to the derivation of Eq. 7-13, it can be readily seen that Eq. 7-13 is also valid when b is a slowly varying function of z . The case of variable b is realized when the deceleration — or acceleration — of the projectile is not negligible compared with centrifugal forces. The free surface then forms a paraboloid given by

$$\Omega^2 b^2 = \Omega^2 b_0^2 - 2g(z - c); 0 < z < 2c \quad (7-18)$$

where g is the deceleration and b_0 the radius of the void at $z = c$. For a cylindrical cavity, b_0 is independent of the deceleration g , and the fill-ratio is $1 - b_0^2/a_0^2$.

7-2.4 RANGE OF VALIDITY

Eq. 7-13 was derived on the assumption that $\left| \frac{da}{dz} \right|$ is small against unity.

The approximate solution of the eigenvalue-problem, Eq. 7-8, contains an error which is locally of the order $\left| \frac{da}{dz} \right|$. Nevertheless, the error of the resulting eigenvalue-condition, Eq. 7-13, is far smaller. The mathematical reason for this is that the error of the approximate solution, Eq. 7-8, is orthogonal, or nearly so, to the solution. Experiments have shown that Eq. 7-13 is a valid approximation at least up to $\left| \frac{da}{dz} \right| < 0.2$.

7-2.5 EFFECT OF ROUNDED CORNERS

Sometimes cavities have rounded corners between one or both endwalls and the sidewall. At the rounded corners $\left| \frac{da}{dz} \right|$ attains large values and Eq. 7-13 is not applicable. The effect of rounded corners can, however, be predicted on the basis of the experimental results of Ref. 2 (see also par. 7-3.2.2). The effects of rounded corners are summarized in the paragraphs which follow.

Let R' denote the radius of the rounded corner, then R'/a is a measure of the amount of rounding. $R'/a = 1$ corresponds to hemispherical ends.

Relative to the original cylindrical volume, the fill-ratio at which resonance occurs remains constant up to $R'/a \leq 0.6$, regardless of whether one or both ends are rounded. In other words for $R'/a \leq 0.6$, the liquid volume remains unchanged.

For $R'/a > 0.6$ and the particular experimental conditions, the experimentally observed resonance occurred at progressively smaller fill-ratios. (For hemispherical ends — $R'/a = 1$ — the drop was 7% when one end was rounded and twice as much when both ends were rounded.) The results for $R'/a > 0.6$ must, however, be interpreted with some caution for the conditions of the experiment (see par. 7-3.2.2), resonance occurred at a fill-ratio of about $1 - b^2/a^2 = 0.84$, so that the value of b/a was about 0.4. If now R'/a exceeds the value 0.6, only part of the rounded contour is wetted by the liquid, so that the rounding effectively reduces the length of the cavity and its c/a value. The reduction of the effective c/a value nearly accounts for the observed decrease of the fill-ratio. It is thus very likely that at fill-ratios higher than 84%, the reduction of the liquid volume occurs at correspondingly larger values of R'/a , and earlier at smaller fill-ratios. Experiments with smaller fill-ratios (see par. 7-3.2.2) confirm this conjecture.

At least up to $R'/a = 0.6$ the effect of rounded corners is completely described by the rule that the eigenfrequencies remain constant when the liquid volume is kept constant.

7-2.6 ROUNDED CORNERS IN CONJUNCTION WITH OTHER MODIFICATIONS

Finally, let us consider rounded corners in conjunction with other modifications of the cavity and eventually other fill-ratios. The principle of superposition suggests

that the effects of the different modifications are additive as long as the changes are small. This suggestion was verified also by experiments. Thus, the eigenfrequencies for a given amount of fill may be computed according to the following rule. First, the rounding of the corners is disregarded and the contour of the cavity at the corner is completed by a straight extension of sidewalls and endwalls. The amount of liquid filling the cavity is kept unchanged. (Since the volume of the cavity with straight corners is somewhat larger, while the amount of liquid is unchanged, the radius b of the air-column increases accordingly.) The cavity with straight corners and equal amount of liquid filler has the same eigenfrequencies as the cavity with rounded corners, for which it was substituted. The eigenfrequencies for the substituted cavity then may be computed on the basis of Eq. 7-13.

7-3 NONCYLINDRICAL CAVITIES OF ROTATIONAL SYMMETRY

7-3.1 RESIDUES

An accurate computation of residues for noncylindrical cavities of rotational symmetry requires the solution of the boundary value problem, Eq. 3-60, with inhomogeneous boundary conditions Eqs. 3-61 and 3-62.

By analogy with Stewartson's solution for the cylindrical cavity, Eq. 3-92, it is suggested that the solution of the boundary value problem can be constructed by means of a series

$$f = \sum_{j=0}^{\infty} [X_j J_1(\beta_j r) + Z_j Y_1(\beta_j r)] \cos \phi(z) + \text{regular terms} \quad (7-19)$$

The mathematical problem of determining the coefficients X_j, Z_j and the subsequent computation of the moment on the projectile have not been solved for any modified cavity although an approximate solution

does not appear too difficult. Meanwhile, the residues for modified cylindrical cavities may be estimated on an empirical basis.

For a cylindrical cavity, the residue is

$$\text{(Eq. 3-89)} \quad -D = \frac{\rho a_0^6}{c} R^2 \quad \text{where } a_0 \text{ is}$$

the radius of the cavity and R^2 is a dimensionless factor which depends on the eigenfrequency τ_0 and weakly on the fill-ratio. (It is roughly

$$2R = 2.84 \tau_0 \times (1 + \tau_0) \left[1 - \left(b^4/a_0^4 \right) \right].$$

We may write the residue for modified cavities in a similar way, however, the factors R^2 and $\rho a_0^6/c$ are both to be modified.

Since R^2 depends only on τ_0 and fill-ratio, it is suggested that R^2 changes only via the change of τ_0 and the fill-ratio. In other words, the value of R^2 may be taken from Stewartson's Tables at the appropriate eigenfrequency τ_0 and fill-ratio of the modified cavity.

It is difficult to find a sensible generalization of the factor $\rho a_0^6/c$. Obviously, some mean value of the radius should be substituted in the place of a_0 . However, in averaging the radius over the length of the cavity, different positions must be given a different weight. The parts of the cavity near the ends ($z = 0, z = 2c$) contribute by far the largest portion to the moment on the projectile and, thus, to the residue which is directly proportional to the moment. Very roughly, a_0^6 may be replaced by the mean value of a^6 at both ends. The modified residue then becomes

$$-D = \rho \frac{\bar{a}^6}{c} R^2$$

where

$$\bar{a}^6 = \frac{1}{2} [a(0)^6 + a(2c)^6] \quad (7-20)$$

(the notation means a evaluated at $z = 0$ and $z = 2c$).

Consider, for example, a cavity which is cylindrical at one end and slightly tapered at the other end as shown in Fig. 7-1. The radius of the cavity at $z = 0$ is $a(0) = a_0$, the radius at $z = 2c$ is $a(2c) = a_0 - Aa$ where, in the example of Fig. 7-1, $Aa = h \tan \theta$. If Aa is small as compared to a_0 , Eq. 7-20 becomes

$$\bar{a}^6 = a_0^6 \left[1 - 3 \frac{\Delta a}{a_0} \right] \quad (7-21)$$

With Eq. 7-21 the residue becomes

$$D = D_0 \left[1 - 3 \frac{\Delta a}{a_0} \right] \quad \text{where } -D_0 = \rho \frac{a_0^6}{c} R^2.$$

Thus, the estimated change of the residue, relative to its value for the cylindrical cavity, is $\Delta D/D_0 = -3 \Delta a/a_0$. The experimental data of Ref. 2 suggest that the above crude method slightly overestimates the drop of the residue and that a better approximation is given by

$$\frac{\Delta D}{D_0} \approx -2 \frac{Aa}{a_0} \quad (7-22)$$

$$\text{with} \quad -D_0 = \rho \frac{a_0^6}{c} R^2$$

As mentioned above, R^2 should be taken from Stewartson's Tables not at the proper $c/[a(2) + 1]$ value but at the proper τ_0 and fill-ratio of the modified cavity.

7-3.2 EXPERIMENTS

The effect on resonance of various modifications of cylindrical cavities was investigated experimentally by Karpov².

All experiments of Ref. 2 were carried out with a liquid-filled gyroscope. The nutational frequency of the gyroscope was fixed.

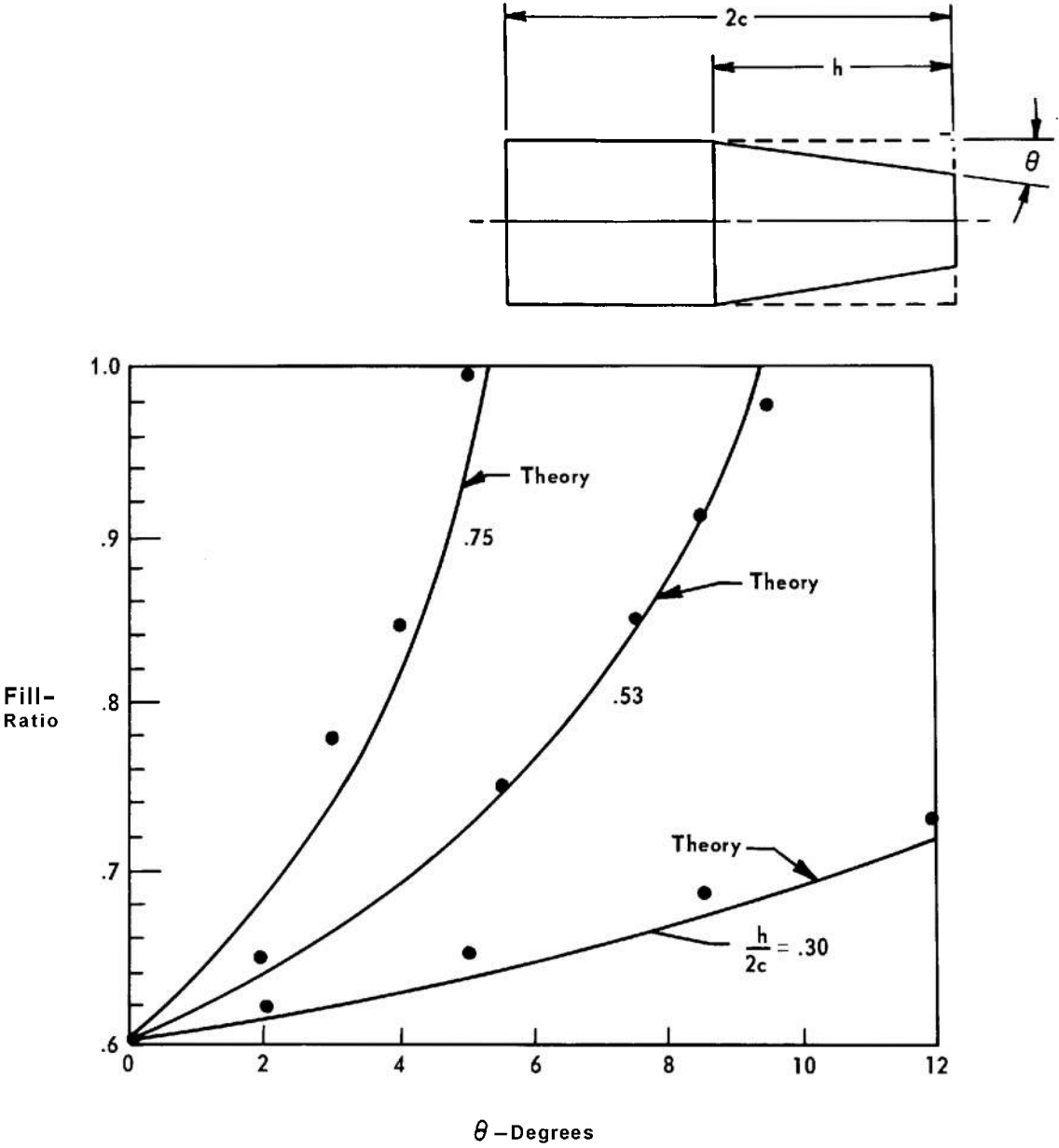


FIGURE 7-1. FILL-RATIO VS CONE ANGLE θ AT FIXED FREQUENCY $T_0=0.055$, $c/a = 2.687$

For a given modified cavity the fill-ratio was determined at which the rate of divergence of the yaw amplitude attained its maximum value. At this fill-ratio, the eigenfrequency equals the nutational frequency of the gyroscope.

Since there are a great many ways in which a cylindrical cavity can be modified, only changes have been investigated which are in the direction of approaching common cavity shapes of actual projectiles.

A number of cavities were combinations of a cylindrical section and a truncated cone section of various heights and cone angles. Other cavities were combinations of two conical sections or of a cylindrical section with rounded corners and a conical section. Also cylindrical cavities with rounded corners at one or both ends were investigated. The radius of curvature of the rounded corners was varied between $R'/a = 0$ and $R'/a = 1.0$.

7-3.2.1 Modified Cylindrical Cavities

The results of the experiments on cavities with one conically tapered end are shown in graphical form in Fig. 7-1. All data refer to the same resonance frequency $\tau = \tau_0 = 0.055$. The fill-ratio at which resonance occurs is plotted for the various configurations versus the cone-angle. For comparison, theoretical curves are plotted in the same graph. The theoretical data were computed on the basis of Eq. 7-13.

Fig. 7-1 shows that the theory gives good predictions even for cone angles θ up to 12° . A cone angle of 12° corresponds

to $\left| \frac{da}{dz} \right| = 0.21$. It is thus shown that Eq. 7-13 may be applied with some confidence at least for $\left| \frac{da}{dz} \right| \leq 0.2$.

For a number of cylinder-cone configurations, Fig. 7-2 shows a plot of residues — as computed from maximum rates of undamping — versus the one variable $\frac{h \tan \theta}{a_0} = \frac{\Delta a}{a_0}$ where $a_0 = \Delta a$ is the radius

of the endwall at the tapered end of the cavity and a_0 the radius at the cylindrical end. Theoretical considerations (par. 7-3.1) suggested that D/D_0 should

approximately depend only on $\frac{h \tan \theta}{a_0}$.

Fig. 7-2 shows that D/D_0 is roughly represented by

$$D/D_0 = 1 - 2 \frac{h \tan \theta}{a_0}$$

7-3.2.2 Rounded Corners

The effect of rounded corners is displayed in Fig. 7-3 where $\frac{\Delta V}{V_c}$ is plotted versus R'/a . ΔV is the change of liquid volume V_c , the volume of the original cylinder. The change in volume is very small for $R'/a < 0.4$.

For $R'/a > 0.4$, the experimental points for $c/a = 3.077$ and $c/a = 2.69$ follow different branches. For $c/a = 3.077$, the fill-ratio is about 84% and $b/a \approx 0.4$. For $c/a = 2.69$, the fill-ratio is about 60% and $b/a \approx 0.63$. Apparently, all experimental data follow the abscissa up to $R'/a \approx 1 - b/a$ and branch off after that point. This behavior can be explained as follows: if $R'/a > 1 - b/a$, only part of the rounded corner is wetted by the liquid so that the effective length of the cavity (the length which is actually felt by the liquid) is reduced. This reduction of the cavity length can account for the observed effect. It is thus suggested that for 100% fill the independence of the liquid volume on R'/a holds even for larger values of R'/a .

The data in Fig. 7-3 show also that the effect of rounded corners is additive, i.e., the change of volume due to rounded corners is independent of other modifications of the cavity. Thus, the effect of rounded corners on fill ratio or eigenfrequency may be added to the effects of other modifications. A scheme of computation was discussed in par. 7-3.1.

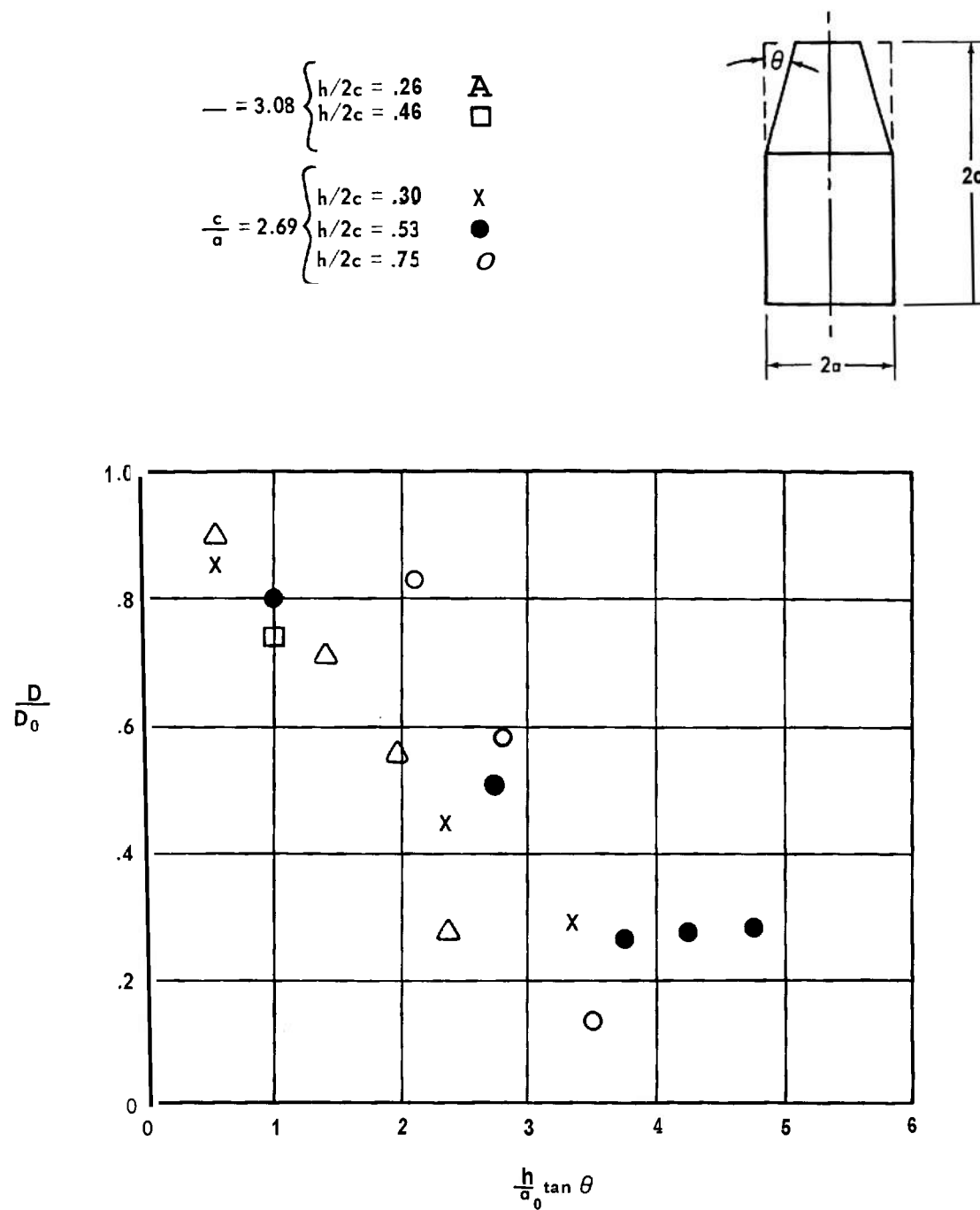


FIGURE 7-2. THE EFFECT OF MODIFICATION OF THE CYLINDRICAL CAVITY ON THE INVISCID RESIDUE

7-40

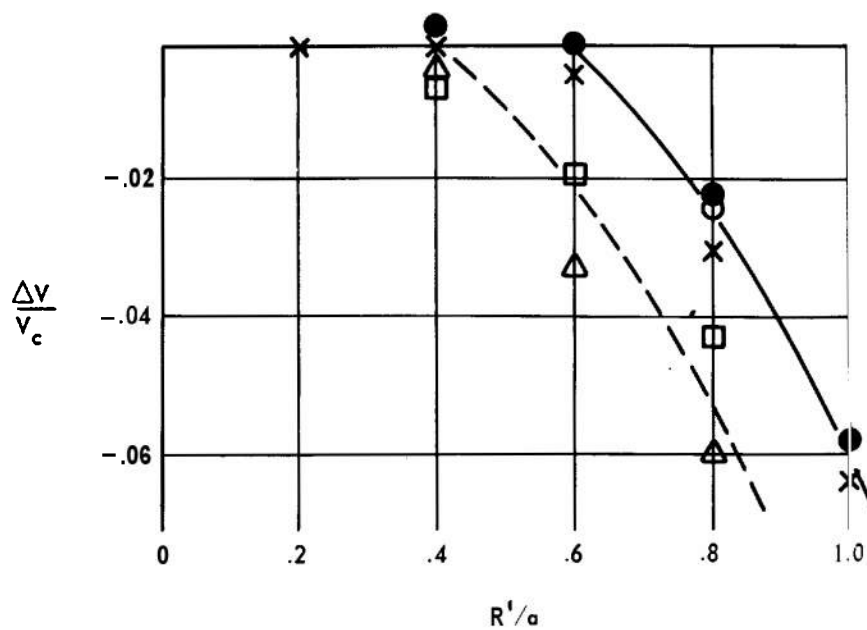
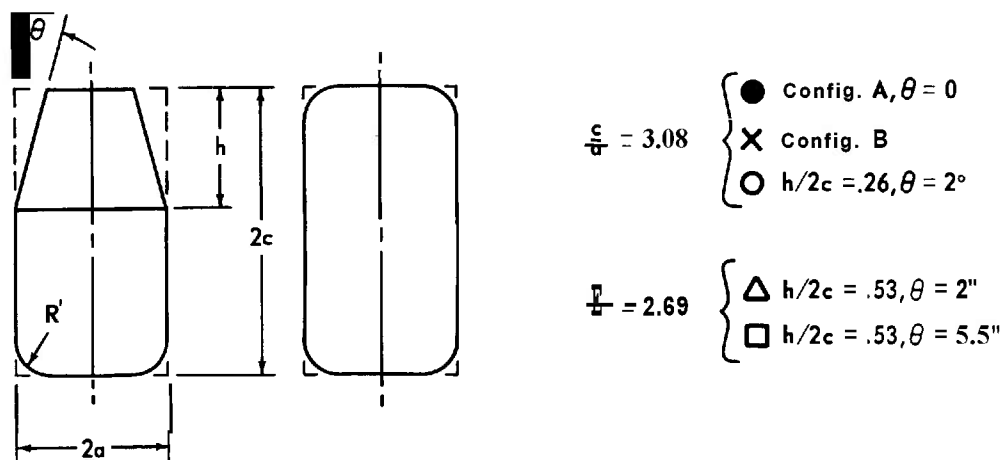


FIGURE 7-3. THE EFFECT OF ROUNDED CORNERS OF THE CYLINDRICAL CAVITY AT FIXED RESONANT FREQUENCY

7-4 ASYMMETRICAL CAVITIES

So far, we have considered only eigenfrequencies corresponding to an odd number $(2j + 1)$ of half-waves. It was shown by Stewartson³ that, for the case of cylindrical cavity, only "odd" eigenfrequencies can produce instability although "even" eigenfrequencies exist as well. Generally, when the cavity is symmetrical about a plane normal to the axis, only odd modes of oscillation interact with the yawing motion and thus only odd eigenfrequencies must be considered. This can no longer be assumed for asymmetrical cavities. Thus, when a cavity is significantly asymmetrical, one should account for the possibility that additional instability bands occur about the even eigenfrequencies (which correspond to half-valued j 's as:

$$j = \frac{1}{2}, \frac{3}{2}, \frac{5}{2}, \dots).$$

For slightly asymmetrical cavities the residues corresponding to even eigenfrequencies are probably very small. At any rate, the residues of Stewartson's Tables are not applicable — not even approximately — for $j = \frac{1}{2}, \frac{3}{2}, \dots$. The eigenfrequencies for half-valued j 's may be computed on the basis of Eq. 7-13.

7-4.1 OTHER CAVITIES AND RITZ METHOD OF APPROXIMATION

Compared with the eigenvalue problem for cavities of rotational symmetry, the corresponding problem for more general cavities is extremely difficult. Mainly responsible for the mathematical simplification achieved in the case of axisymmetrical cavity is the separation of the factor $e^{i(\omega t - \theta)}$ from the solution, which is possible because of the cyclic symmetry of the fluid motion in the axisymmetrical case.

Fortunately, most practical cavities are axisymmetrical, but there is an important exception, namely, cavities which are partitioned by longitudinal baffles as shown in Fig. 8-1(A).

In the absence of a method for obtaining precise analytical solutions of the eigenvalue problem, an approximate method — known as **Ritz Method** — may be employed for cavities which are cylindrical but not axisymmetrical.

The Ritz Method in combination with a method of computation for noncylindrical cavities, which is discussed in par. 7-3, should render possible the computation of eigenfrequencies for a noncylindrical, non-axisymmetrical cavity provided that the cross section changes only slowly with the distance along the axis.

The analysis which follows should be restricted to a completely filled cavity since, in practice, cavities are usually completely or almost completely filled and — inferring from the results for axisymmetrical cavities — the effect of fill-ratio is probably small near 100% fill. On the other hand considerable simplification is gained by the assumption of complete fill.

7-4.2 THE EIGENVALUE PROBLEM

We consider a liquid-filled cylindrical cavity of arbitrary cross section. The liquid is assumed to rotate with the cavity about an axis which is parallel to the sidewalls. It is advantageous to introduce a system of rotating orthogonal triads (x, y, z) so that z lies along the axis of rotation, and x and y rotate with angular velocity Ω about z . Relative to the rotating system, the cavity walls are stationary. We suppose that the endwalls of the cavity are at $z = 0$ and $z = 2c$, and that the constant cross section of the cavity covers a domain D' with boundary curve C in the x, y -plane.

With the above assumptions, the eigenvalue problem for the free oscillations of the liquid reduces to the following set of equations for p

$$p = P(x, y)e^{i\omega t} \cos kz, \quad k = \frac{\pi}{2c}(2j + 1) \quad (7-24)$$

$$\frac{\partial^2 p}{\partial x^2} + \frac{\partial^2 p}{\partial y^2} + \beta^2 k^2 p = 0 \quad (7-25)$$

where

$$\beta^2 = \left(\frac{4}{\tau_0'^2} - 1 \right); \quad \tau_0' = \frac{\omega_0'}{\Omega}$$

τ_0' is the eigenfrequency in the rotating system.

The form of the pressure perturbation, Eq. 7-24, assures that the boundary conditions are satisfied on the endwalls $z = 0, 2c$.

The boundary conditions on the side-walls can be written

$$\frac{\partial P}{\partial n} - \frac{2i}{\tau_0'} \frac{\partial P}{\partial s} = 0 \quad \text{along } C \quad (7-26)$$

where $\frac{\partial P}{\partial n}$ and $\frac{\partial P}{\partial s}$ denote the partial derivatives of P in directions normal (n) and tangential (s) to the boundary curve C .

The coordinate variables (n, s) are defined in the following way: s is the arc length along C , and n is the distance measured from C along the normal to C , so that positive n corresponds to points exterior to C . The arc length is measured in the direction of rotation, starting from any point on the boundary curve C .

Eqs. 7-25 and 7-26 characterize the eigenvalue problem for a cylindrical cavity of arbitrary cross section.

In analogy to the case of axisymmetric cavity, solutions of Eqs. 7-25 and 7-26 exist only for discrete values of τ_0' when k^2 is given. In practice it is simpler to prescribe τ_0' and compute the "eigenvalues" $\beta^2 k^2$. The characteristic cavity length then follows from τ_0' and $\beta^2 k^2$.

It should be mentioned that only the real part of Eq. 7-24 is physically significant. Thus, if $P = P_R + iP_I$ we have

$$P_R = (P_R \cos \omega_0' t - P_I \sin \omega_0' t) \cos kz \quad (7-27)$$

Eq. 7-24 suggests that the moment on the projectile is $M' = Ae^{i\omega_0' t}$ in the rotating

coordinate system where A is a constant. In the inertial system of nonrotating coordinates the moment M is equal to

$$M = M' e^{i\Omega t} \text{ or } M = Ae^{i(\Omega + \omega_0')t} = Ae^{i\omega_0 t} \quad (7-28)$$

Thus, the frequency ω_0 — as measured in the nonrotating system — is related to ω_0' by $\omega_0 = \Omega \pm \omega_0'$.

For the nondimensional eigenfrequency $\tau_0 = \omega_0 / \Omega$, we obtain

$$\tau_0 = \tau_0' + 1 \quad (7-29)$$

We assume that, in analogy to Stewartson's case, the projectile becomes unstable when its nutational frequency τ_n is near τ_0 or, precisely, when

$$|\tau_0 - \tau_n| < \sqrt{S}$$

Lacking the value of S , we cannot predict the width of the instability band, and, hence, may not be able to predict instability even if the eigenvalue problem could be solved. It is believed, however, that the knowledge of the eigenfrequencies is of primary importance for the designer. The width of the instability band may be estimated, assuming a rough value for S .

7-4.3 RITZ METHOD OF APPROXIMATION

For a given cross section and τ_0' , Eqs. 7-25 and 7-26 have a solution only when the quantity $\beta^2 k^2$ assumes certain discrete values, briefly denoted as "eigenvalues". We are interested mainly in the lowest eigenvalue which in Stewartson's case corresponds to the lowest radial mode number. The eigenvalue problem given by Eqs. 7-25 and 7-26 may be stated alternatively in the form of a variational principle (see, e.g., Ref. 4).

It can be shown that the lowest eigenvalue is the minimum of the expression

$$I = \frac{\iint_{D'} \nabla P^* \cdot \nabla P dx dy - \frac{i}{\tau_0} \int_C \left(P^* \frac{\partial P}{\partial s} - P \frac{\partial P^*}{\partial s} \right) ds}{\iint_{D'} P^* P dx dy} \quad (7-30)$$

with respect to all functions $P(x,y)$ which are continuous with their first partial derivatives, everywhere in D' . $P^*(x,y)$ is the complex conjugate of $P(x,y)$.

The Ritz Method of approximation consists of replacing the class of all eligible functions $P(x,y)$ by a suitable subclass and minimizing the expression for I , Eq. 7-30, with respect to this subclass. The minimum of I relative to the subclass of functions is usually a very good approximation for the exact eigenvalue.

The practical computation may proceed in the following manner. A continuous function $P(x,y,\lambda)$ of x,y and a parameter λ is selected, which should satisfy the boundary conditions Eq. 7-26 for all values of λ . If, for example, $P_1(x,y)$ and $P_2(x,y)$ are two linear independent functions which both satisfy the boundary conditions, we may define

$$P(x,y,\lambda) = P_1(x,y) + \lambda P_2(x,y)$$

$P(x,y,\lambda)$ should be smooth, i.e., differentiable, function of (x,y) and should have all the properties which are known about the exact solution. In particular, for the lowest mode of oscillation, P should have the lowest number of nodes, etc. In addition $P(x,y,\lambda)$ should be defined so that the integrals in Eq. 7-30 can easily be evaluated analytically. With $P(x,y,\lambda)$ so defined, Eq. 7-30 is evaluated and I is computed as a function of λ . The approximate eigenvalue then is obtained as the minimum of I with respect to all values of λ .

A better approximation is obtained when P depends on more than one parameter and the minimum value of I with respect to all the parameters is determined. Usually, the one-parameter representation is completely

sufficient; even a representation with no parameters may yield a good approximation as is shown in the example below.

7-4.4 EXAMPLE: CIRCULAR CYLINDER

Although Stewartson's case of a circular cylinder can be treated by exact analytical methods, it is instructive to compare the exact results with those obtained by the Ritz Method.

For the circular cylindrical cavity we know that P and P^* must be of the form

$$P = R(r)e^{-i\theta}; P^* = R(r)e^{i\theta} \quad (7-31)$$

We assume for R the polynomial

$$R = \left(\frac{r}{a}\right) - K \left(\frac{r}{a}\right)^2 \quad (7-32)$$

The constant K is determined by the requirement that P satisfy the boundary condition at $r = a$. We obtain

$$K = \frac{3 - \tau_0}{4 - 2\tau_0} \quad (7-33)$$

With the above function P , Eq. 7-30 yields

$$Ia^2 = \frac{K - \frac{3}{4}K^2}{\frac{1}{4} - \frac{2}{5}K + \frac{1}{6}K^2} \quad (7-34)$$

Since the assumed function for P contains no free parameter, we cannot improve the result by minimizing the value of I . Nevertheless, a very good approximation is already attained by setting

$$Ia^2 = \beta^2 k^2 a^2 \quad (7-35)$$

With $ka = \frac{\pi a(2j+1)}{2c}$ we have

$$\frac{c}{a(2j+1)} = \frac{\pi}{2} \sqrt{\frac{\beta^2}{Ia^2}} \quad (7-36)$$

With $\beta^2 = \frac{4}{(1 - \tau_0)^2} - 1$ and Ia^2 given by Eqs.

7-34 and 7-35, the right hand side of Eq. 7-36 is completely determined as a function of τ_0 .

For several values of τ_0 the approximate $\frac{c}{a(2j+1)}$ value according to Eq. 7-36 is shown in Table 7-1. The agreement with exact values from Stewartson's Tables is excellent.

TABLE 7-1. CIRCULAR CYLINDER:
COMPARISON OF RITZ METHOD AND EXACT
SOLUTION

$c/[a(2j+1)]$		
τ_0	Ritz- Method	Exact
0	0.994	0.995
0.2	1.260	1.262
0.5	1.959	1.963

REFERENCES

1. E. H. Wedemeyer, *Dynamics of Liquid Filled Shell: Non-Cylindrical Cavity*, BRL Report **1326**, Aberdeen Proving Ground, Md., August **1966**.
2. B.G. Karpov, *Dynamics of Liquid-Filled Shell: Resonance in Modified Cylindrical Cavities*, BRL Report **1332**, Aberdeen Proving Ground, Md., August **1966**.
3. K. Stewartson, "On the Stability of a Spinning Top Containing Liquid," *J. Fluid Mech.* **5**, Part **4** (**1959**).
4. R. Weinstock, *Calculus of Variations With Applications to Physics and Engineering*, McGraw-Hill Book Company Inc., N.Y., **1952**.

CHAPTER 8

PARTIALLY SPINNING LIQUID

8-0 LIST OF SYMBOLS*

A	= acceleration of free surface of liquid; axial moment of inertia of empty projectile
A_1	= axial moment of inertia of fully spinning projectile
$2a$	= diameter of free surface of liquid
g	= acceleration due to gravity
I	= angular momentum of liquid at time t
I_∞	= angular momentum of liquid when liquid is rotating as a rigid body, i.e., its maximum steady state value
I/I_∞	= value of angular momentum at time t relative to the rigid or steady state value
k	= function of a/c and Reynolds number (for laminar flow)
k_t	= function of a/c and Reynolds number (for turbulent flow)
k'	= average height of roughness elements
P_1	= pressure perturbation at inward facing side of interface
P_2	= pressure perturbation at outward facing side of interface
P'_1	= derivative of p_1 with respect to r
p'_2	= derivative of p_2 with respect to r
Q_B	= radial flux of boundary layers
Q_C	= radial flux of core-flow
Re	= Reynolds number
r, θ, z	= cylindrical nonrotating coordinate system with z in axial direction of projectile

u, v, w = velocity components along r, θ, z respectively

u_B, v_B, w_B = velocity components of boundary layer flow

= radial component of flow velocity at inward facing side of interface

u_2 = radial component of flow velocity at outward facing side of interface

u^* = nondimensional velocity

GREEK LETTERS

δ = boundary layer thickness

ε = $I_\infty / A \Omega_0$

η = small radial displacement of liquid

λ = rate of undamping, per sec

τ_I = dimensionless rate of undamping

Ω_0 = initial axial spin rate

Ω_∞ = final axial spin rate

ω = frequency of basic mode of oscillation

MATH SYMBOLS

\sim = approximately

\sim = of the order

\propto = proportional

8-1 INTRODUCTION

The stability criteria which have been formulated and discussed in previous chapters are based on the assumption that the liquid within the cavity of the projectile has achieved full spin, i.e., that prior to perturbation the liquid rotates with the casing as if solid. The assumption of solid rotation of the liquid appears to be a valid assumption in most practical cases, except for the earliest part of the projectile's trajectory.

*For identification of other symbols used in this chapter, refer to Chapter 3.

The duration of spin-up of the liquid depends on liquid viscosity, angular velocity, and cavity dimensions. In typical cases a state of nearly solid rotation is attained within a distance of 2000 to 6000 calibers of travel from the muzzle.

During the spin-up period the projectile may become unstable although it is stable at its final state when the liquid has attained solid body rotation. In the course of experimental investigations with a liquid of high specific gravity: severe dynamic instabilities of liquid-filled projectiles have been observed in cases where the projectile should have been stable according to the assumption of rigid rotation of the liquid filler. Theory predicts that the frequencies of free oscillation depend on the state of rotation of the liquid and thus change during spin-up, beginning with high values and approaching asymptotically the final values for solid rotation. Whenever a frequency of free oscillation passes through the resonance band about the nutational frequency, the projectile becomes temporarily unstable. In practice, instabilities during spin-up are not too serious provided that the passage through the main resonance occurs quickly, so that the projectile remains in the unstable regime only for a short duration. During the time of transient instability the yaw angle grows according to $\alpha = \alpha_0 \exp(i\Omega \int \tau_I dt)$ where τ_I is the dimensionless rate of undamping. Although at present the resonance frequencies and bandwidths during spin-up cannot be predicted with high accuracy, it is possible, nevertheless, to give a good estimate of the integrated rate of undamping $\int \tau_I dt$ and thus to estimate the growth of an initial yaw angle during spin-up.

Besides the occurrence of transient instabilities, another practical problem is associated with liquid spin-up, i.e., the projectile loses angular momentum at the rate at which angular momentum is absorbed by the liquid, and the spin rate decreases below its value at the muzzle. The decrease

of spin rate, in turn, has an adverse effect on the stability factor. This latter effect is important when the stability factor is close to one. Eq. 3-88 shows that a decrease of the stability factor s_g — i.e., an increase of $\beta = \frac{1}{s_g}$ — can cause instability via the

broadening of the bandwidth even when $s_g > 1$.

In order to avoid the unwanted effect of slow spin-up, attempts have been made to accelerate the attainment of liquid rotation by use of longitudinal baffles which divide the cavity into a number of compartments as shown in Fig. 8-1(A). Apart from the fact that baffles give rise to serious design problems, the dynamic stability behavior of the projectile with baffles was found to be unreliable. A theoretical prediction of the stability behavior for cavities with longitudinal baffles is, so far, not possible. Thus, longitudinal baffles add an element of uncertainty.

The use of transverse baffles, as shown in Fig. 8-1(B), has the virtue that the stability behavior remains predictable, see par. 9-3.6. However, transverse baffles are not very effective in accelerating the spin-up.

The problem of transient instability during spin-up is not too serious and it can be handled by the designer. It is possible, now, to predict the occurrence of transient instabilities by methods which are discussed in the paragraphs which follow. The computation of transient flow fields during spin-up — a prerequisite for the stability problem — is treated in par. 8-3. Experimental data on the same subject are discussed in par. 8-4 and the prediction of transient instability bands, in par. 8-5.

8-2 ATTAINMENT OF LONGITUDINAL MOTION

When the cavity is only partially filled with liquid, the motion of the liquid just after firing is extremely complex. With the exception of certain particularly simple cases the details of the fluid motion remain

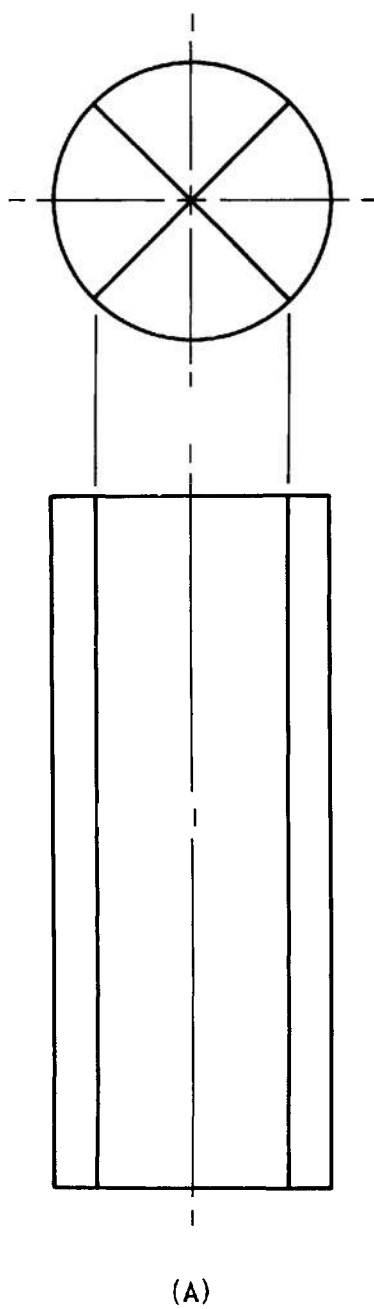


FIGURE 8-1(A). LONGITUDINAL BAFFLES

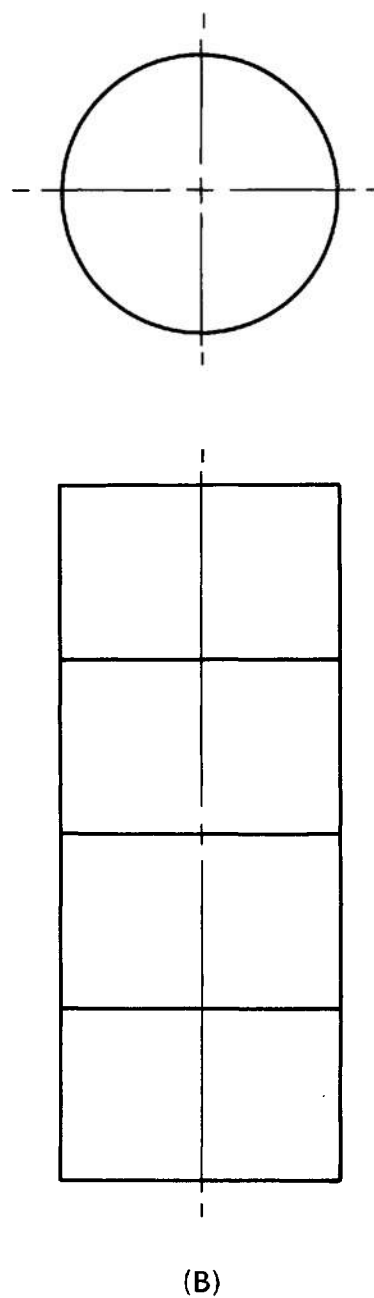


FIGURE 8-1(B). TRANSVERSE BAFFLES

unpredictable. The most prevalent case — a completely or almost completely filled cavity of rotational symmetry — is relatively simple from the analytical point of view.

Roughly, the chain of events taking place in the liquid-filled cavity after firing is as follows, assuming that the cavity is rotationally symmetrical about the spin-axis:

a. Under the action of extremely high accelerating forces the liquid moves into the most backward position forming a free surface perpendicular to the direction of motion. Initial disturbances due to the sudden start of the motion cause rapid oscillations of the free surface. The frequency of the basic mode of oscillation is approximately $\omega = \sqrt{\frac{4A}{a}}$ where $2a$ is the diam-

eter of the free surface and A the acceleration. While the liquid is forced to follow the translational motion of the projectile at once, the spin is only slowly transferred to the liquid when the cavity is rotationally symmetrical. If the cavity is completely filled, the liquid moves, except for the rotational motion, along with the projectile as if solid.

b. The spin of the projectile is transferred to the liquid by viscous friction on the cavity walls. During the short acceleration period only a thin layer of fluid adjacent to the walls attains some rotation.

c. When the projectile leaves the muzzle, the force due to acceleration suddenly changes direction. The following deceleration, due to air-drag, produces a force which tends to move the liquid forward. (For a typical projectile the deceleration — although several orders of magnitude smaller than the initial acceleration — is nevertheless many times greater than g ; thus the effect of gravity can be neglected.) The motion of the liquid subjected to a sudden change of acceleration is very complex whenever a free surface is present. The free surface which was assumed to form during the acceleration period becomes un-

stable when subjected to deceleration. Small deformations of the free surface grow rapidly and eventually form small jets. The development of the free surface may be quite different depending on whether the cavity is almost completely filled or not:

(1) If the cavity is almost completely filled, the gap between the free surface and the forward facing endwall of the cavity is very much smaller than the cavity diameter. Consequently, the surface waves cannot grow very high before the wave crests come into contact with the wall. From then on, the waves spread gently to the sides, and the voids between wave crests become elongated and penetrate the fluid in a backward direction. Finally, a plane and stable free surface forms near the rear endwall. In brief, the fluid moves gently and well-ordered into the most forward position.

(2) Consider now the case where the fill-ratio is not nearly 100%, so that the gap between the free surface and the front wall is large. The deformations of the free surface grow to high amplitudes and form jets which protrude into the air space in front of the liquid. At last the jets impinge with high velocity on the front wall where they cause splashing of the fluid. The free surface breaks up into disconnected parts and the overall flow pattern becomes chaotic. Nevertheless, it appears that this disordered motion prevails only for a very short duration. Probably, the turbulent motion causes rapid mixing of the fluid particles that are close to the wall and the non-rotating inner parts of the fluid. As a result, all parts of the fluid attain a small amount of rotation rapidly. The rotating fluid then is driven by centrifugal forces toward the sidewalls and a new free surface of hollow cylindrical shape is formed. After the formation of the new free surface a state of relatively steady fluid motion is restored. At this time the liquid has achieved only a small amount of rotation. In the final state of rotation the centrifugal forces are approximately $10^5 g$ for typical spin-stabilized projectiles. Thus, the centrifugal forces outweigh the decelerating

forces even when the liquid has attained only a small fraction of its final angular momentum.

Summarizing, we have seen that during the period of launching the liquid within a partially filled cavity undergoes a violent disorderly motion which, however, is attenuated quickly as soon as the fluid has achieved a certain amount of rotation. The fluid, then, forms a hollow body of revolution bounded by a cylindrical free surface on the inside. There is no such period of disorderly motion when the cavity is completely or almost completely filled.

8-3 ATTAINMENT OF ROTATIONAL MOTION

The theory of spin-up to be discussed subsequently was developed in Ref. 2, for a completely filled cylindrical cavity. The theory can easily be extended to partial fill conditions, provided that forces due to gravity or acceleration are small compared to centrifugal forces.

It was shown in par. 8-2 that, except for a very short launching period, the effects of acceleration or deceleration can be neglected. The liquid attains some rotation rapidly and assumes the shape of a hollow body of revolution bounded by a cylindrical free surface.

The analyses of liquid spin-up as given in Ref. 2 are confined to cylindrical cavities although the essential parts of the theory hold as well for any cavity of rotational symmetry.

In par. 8-3.1 a representation of the theory of spin-up is given with emphasis on applications to liquid-filled projectiles. Some parts, especially the one on turbulent boundary layers, of Ref. 2 have been elaborated to the point where the results can be applied immediately to engineering problems.

The practical computation of velocity distributions and total angular momentum is discussed in par. 8-3.2.

8-3.1 THEORY OF SPIN-UP

We consider a cavity of rotational symmetry which is completely or partially filled with liquid. The liquid is assumed to be at rest or to have a small residual amount of rotation relative to a nonrotating frame of reference. For the case of a partially filled cavity, we assume that the liquid is bounded by a cylindrical free surface on the inside. (These assumptions are consistent with the statements of par. 8-2 namely, that gravity and decelerating forces are unimportant relative to centrifugal forces.) We also require that at a time $t=0$ the casing starts to rotate about its axis of symmetry with either constant or time dependent angular velocity.

Due to viscous friction the liquid near the cavity walls is dragged round and acquires rotational motion. It may appear that only rotating flow is generated by the rotation of the cavity walls. However, a closer look on the fluid dynamics shows that in addition to rotating flow, a secondary flow with radial and axial flow components must occur. In fact, the secondary flow proves to be of prime importance for the mechanism of spin-up. Consider, for example, one of the endwalls of a cylindrical cavity. The fluid particles adjacent to the endwall rotate with the wall and are, therefore, subject to centrifugal forces. Because of these centrifugal forces, the fluid particles near the endwalls are driven radially outwards. When the stream of rotating and outward-moving fluid approaches the cylindrical sidewalls, it is deflected into the interior of the cavity while the interior non-rotating fluid moves towards the endwalls to replace the fluid lost by the radial outflow. Thus, a circulating secondary flow is generated.

It is readily seen that the liquid rotation is attained essentially by viscous friction near the endwalls. The secondary flow in turn transports the rotating liquid towards the sidewalls where it builds up a layer of increasing thickness.

A refined analysis shows that the secondary flow is very slow except within a thin boundary layer at the endwalls where the flow is propelled by centrifugal forces.

8-3.1.1 Equations of Motion

Following the usual procedure of boundary layer theory (see e.g., Ref. 3), we divide the flow into two parts: a boundary layer flow which occupies the boundary layer region near the walls and a so-called

core-flow which occupies all of the cavity except the boundary layer region.

Let (r, ℓ, z) be the nonrotating coordinates in radial, circumferential, and axial directions, respectively, with the origin in the center of the cavity and (u, v, w) the respective velocity components in these directions, and p the pressure. With the simplifications resulting from the rotational symmetry of the flow, the equations of fluid dynamics, Eqs. 3-1 and 3-2, in cylindrical coordinates (r, ℓ, z) read

$$\frac{\partial v}{\partial t} + u \left(\frac{\partial v}{\partial r} + \frac{v}{r} \right) + w \frac{\partial v}{\partial z} = \nu \left[\frac{\partial^2 v}{\partial r^2} + \frac{\partial}{\partial r} \left(\frac{v}{r} \right) + \frac{\partial^2 v}{\partial z^2} \right] \quad (8-1)$$

$$\frac{\partial u}{\partial t} + u \frac{\partial u}{\partial r} + w \frac{\partial u}{\partial z} - \frac{v^2}{r} + \frac{1}{\rho} \frac{\partial p}{\partial r} = \nu \left[\frac{\partial^2 u}{\partial r^2} + \frac{\partial}{\partial r} \left(\frac{u}{r} \right) + \frac{\partial^2 u}{\partial z^2} \right] \quad (8-2)$$

$$\frac{\partial w}{\partial t} + u \frac{\partial w}{\partial r} + w \frac{\partial w}{\partial z} + \frac{1}{\rho} \frac{\partial p}{\partial z} = \nu \left(\frac{\partial^2 w}{\partial r^2} + \frac{1}{r} \frac{\partial w}{\partial r} + \frac{\partial^2 w}{\partial z^2} \right) \quad (8-3)$$

$$\frac{\partial(ru)}{\partial r} + \frac{\partial(rw)}{\partial z} = 0 \quad (8-4)$$

The boundary of the cavity may be given by the equation

$$r = f(z) \quad (8-5)$$

Let us assume that the casing starts to spin at $t = 0$ with angular velocity Ω . Then the boundary conditions are

$$\left. \begin{array}{l} u = w = 0 \\ v = r\Omega \end{array} \right\} \quad \text{at } r = f(z), \quad 0 \leq t \quad (8-6)$$

$$u = v = w = 0 \quad \text{for } t < 0 \quad (8-7)$$

As mentioned above, the entire flow can be divided into a boundary layer flow at the walls and a core-flow. The viscous terms on the right hand sides of Eqs. 8-1 to 8-3 are small in the core-flow. In the following, it is also shown that the components of the secondary flow (u, v) are small in the core-flow.

Within the boundary layer the velocity components tangential to the wall are of the order Ωa , where a is the radius of the cavity.

Consider for example the boundary layer on one of the plane endwalls of a cylindrical cavity of diameter $2a$ and height $2c$, and let (u_B, v_B, w_B) be the velocity components of the boundary layer flow. Then u_B and v_B are of the order Ωa . Within the boundary layer, the fluid flows radially outwards with the velocity u_B . If δ is the boundary layer thickness, the radial flux per unit angle is of the order $u_B \delta \approx \Omega a \delta$. Conservation of mass requires that an equal amount of liquid in the core-flow moves radially inwards. Let u be the radial velocity in the core-flow and $2c$ the height of the cylinder. The radial flux in the core-flow then is of the order uc which must be equal to the radial flux in the boundary layer, i.e., $uc = u_B \delta \approx \Omega a \delta$, or:

$$u \approx \left(\Omega a \right) \frac{\delta}{c} \quad (8-8)$$

Eq. 8-4 shows, that w is of the order $u \frac{c}{a}$ or

$$w \approx \left(\Omega a \right) \frac{\delta}{a} \quad (8-9)$$

On the other hand, the rotational component is

$$v \approx \Omega a \quad (8-10)$$

From boundary layer theory it follows that the boundary layer thickness is small of the order

$$\delta/a \approx \text{Re}^{-1/2} \quad \text{for laminar boundary layer} \quad (8-11)$$

$$\delta/a \approx 0.1 \text{Re}^{-1/5} \quad \text{for turbulent boundary layer} \quad (8-12)$$

where the Reynolds number $= \frac{va}{\nu}$ is based on flow velocity v , radius of the cavity a , and kinematic viscosity ν .

In our case, the **flow** velocity is of the order $v = \Omega a$ and the Reynolds number is conveniently defined by

$$\text{Re} = \frac{a^2 \Omega}{\nu} \quad (8-13)$$

In typical cases the Reynolds numbers of liquid-filled spinning projectiles are of the order $\text{Re} \sim 10^6$, i.e., δ/a is very small.

We can now simplify the fluid-dynamic equations, Eqs. 8-1 to 8-3, by retaining only the terms of lowest orders in δ/a .

Eqs. 8-8, 8-9, and 8-10 applied to Eq. 8-2 yield within our approximation

$$\frac{v^2}{r} = \frac{1}{\rho} \frac{\partial p}{\partial r} \quad (8-14)$$

Eq. 8-3 shows that $\frac{1}{\rho} \frac{\partial p}{\partial z}$ is small, of the order $\Omega^2 c (\delta/c)^2$. Thus, within our approximation p is independent of z and, according to Eq. 8-14 v , within the same approximation, is independent of z . Precisely

$$\frac{\partial v}{\partial z} \sim \Omega \frac{c}{a} \left(\frac{\delta}{a} \right)^2 \quad (8-15)$$

Because of Eq. 8-15, the terms with $\frac{\partial v}{\partial z}$ and $\frac{a^2 v}{\partial z^2}$ in Eq. 8-1 may be neglected, and Eq. 8-1 simplifies to

$$\frac{\partial v}{\partial t} + u \left(\frac{\partial v}{\partial r} + \frac{v}{r} \right) = \nu \left[\frac{\partial^2 v}{\partial r^2} + \frac{\partial}{\partial r} \left(\frac{v}{r} \right) \right] \quad (8-16)$$

Eq. 8-16, when supplemented by an additional relation for u , describes the spin-up of the liquid. It is readily seen that

both v and u are independent of z . Thus, Eq. 8-16 constitutes a partial differential equation with the independent variables r and t . The additional relation for u depends on cavity shape and the nature of the boundary layer. The computation of u and the results for the cylindrical cavity are discussed in the paragraph which follows.

8-3.1.2 Computation of the Secondary Flow

Eq. 8-16 contains as an additional unknown the radial component u of the secondary flow. u is a function of the radius r and time t but, as shown above, u is independent of z .

According to Eqs. 8-8, 8-11, and 8-12; the order of magnitude of u is:

$$u \sim \Omega a \left(\frac{a}{c}\right) (Re)^{-1/2}$$

for a laminar boundary layer,

$$u \sim 0.1 \Omega a \left(\frac{a}{c}\right) (Re)^{-1/5}$$

for a turbulent boundary layer.

The transition from laminar to turbulent boundary layer occurs somewhere around $Re = 10^5$. With regard to the transition to turbulent boundary layer, see par. 8-3.1.3.

The computation of u requires an elaborate analysis of the boundary layer flow. For details on the boundary layer calculation see Ref. 2.

Once the boundary layer is known, u is given by the simple condition that, for any radius, the total radial flux within the boundary layers and the core-flow must be zero. As an example, consider a cylinder of height $2c$ and diameter $2a$, and let $u_B(r, z)$ be the radial velocity in the boundary layer and z the axial distance from the endwalls. The radial flux Q_B in each of the boundary layers at the two endwalls is:

$$Q_B = 2\pi r \int_0^6 u_B(r, z) dz \quad (8-17)$$

where 6 is the boundary layer thickness. The radial flux Q_C of the core-flow is

$$Q_C = (2\pi r) 2cu(r) \quad (8-18)$$

Conservation of mass requires

$$2Q_B + Q_C = 0 \quad (8-19)$$

or with Eqs. 8-17 and 8-18

$$u(r) = -\frac{1}{c} \int_0^6 u_B(r, z) dz \quad (8-20)$$

Eq. 8-20 is also valid for noncylindrical cavities when c is interpreted as the variable height $c(r)$ of the cavity.

The calculation of u_B is complicated by the fact that the boundary layer flow depends on the pressure distribution of the core-flow (which is given by Eq. 8-14), so that one has a coupling between the boundary layer equations and the equation for the core-flow. This coupling renders an exact treatment of the problem extremely difficult, and refuge must be taken in approximations.

8-3.7.2.1 Completely Filled Cavity

In Ref. 2, the following approximate expressions for u are derived for a completely filled cylindrical cavity.

(a) For a laminar boundary layer:

$$u = -0.443 \frac{a}{c} (Re)^{-1/2} (r\Omega - v) \quad (8-21)$$

(b) For a turbulent boundary layer:

$$u = -0.035 \frac{a}{c} (Re)^{-1/5} (r\Omega - v)^{8/5} \frac{1}{(a\Omega)^{3/5}} \quad (8-22)$$

Eq. 8-21 and Eq. 8-22 are exact for $v = 0$ and $v = r\Omega$, i.e., at the beginning of spin-up when no rotation is present ($v = 0$) and at the end when a state of solid rotation ($v = r\Omega$) is attained asymptotically.

For special distributions of $v(r)$, exact solutions of the laminar boundary layer equations are known^{4,5,6}, e.g., when v is a solid rotation $v = r\Omega'$ with $\Omega' < \Omega$. It was shown in Ref. 2, that Eq. 8-21 gives good agreement in those cases where solutions have been obtained. Thus, Eqs. 8-21 and 8-22 may be used with some confidence.

8-3.1.2.2 Partially Filled Cavity

Eqs. 8-21 and 8-22 were derived in Ref. 2 for a completely filled cavity, but they may be used — with some reserve — also in the case of a partial fill.

If we assume that the liquid forms a cylindrical free surface at $r=b$ so that the two endwalls are equally wetted, Eq. 8-19 holds as well for the partially filled cylindrical cavity when Q_B is interpreted as radial flux within the wetted part ($r \geq b$) of each of the endwalls.

It can be shown that the radial flux within the boundary layer on the partially wetted surface is nearly equal to the flux on the completely wetted surface, except near $r=b$. The reason for this is that the boundary layer flow is essentially determined by the balance of the centrifugal, Coriolis, and viscous forces while radial acceleration is relatively unimportant. An exception arises where the free surface meets the endwalls. At the free surface u_B is zero and the fluid in the close vicinity is quickly accelerated in a radial direction. Within a short distance the equilibrium between Coriolis forces or centrifugal forces and viscous shear is attained, and the velocity distributions within the boundary layer turn into those of the completely wetted case. Consequently, the radial velocity u in the core-flow assumes a value equal to that of the completely filled cavity (Eqs. 8-21 and 8-22), except within a thin annular layer around the free surface where u sharply drops to zero. Mass conservation requires that within this layer the fluid moves with relatively high axial velocity toward the endwalls.

The preceding considerations show that Eqs. 8-21 and 8-22 may be used for values of r not too close to $r=b$, keeping in mind that u drops to zero near $r=b$.

8-3.1.3 Transition to a Turbulent Boundary layer

In order to compute the attainment of spin, it is necessary to know whether the boundary layer on the cavity wall is laminar or turbulent. Experimental data^{7,8} indicate that transition to turbulent boundary layer occurs between $Re = 0.5 \times 10^5$ and 3×10^5 , i.e., the boundary layer is

$$\text{full turbulent for } 3 \times 10^5 < Re \quad (8-23)$$

$$\text{full laminar for } Re < 0.5 \times 10^5 \quad (8-24)$$

For Reynolds numbers between these limits the character of the boundary layer depends also on the roughness of the walls. As a rule of thumb⁸, the boundary layer is turbulent when

$$\frac{k'}{a} > 20 \times Re^{-3/4} \quad (8-25)$$

where k' is the average height of the roughness elements determined by the usual engineering. Strictly speaking, the boundary layer may be partly laminar (at smaller radii) and partly turbulent (at large radii) and the point of transition may also change during spin-up. Eqs. 8-23, 8-24, and 8-25 refer to the state of the boundary layer at $t=0$ and $r=a$.

For the transitional regime of Reynolds numbers it was found that the computed spin-up times for turbulent and laminar boundary layer do not differ greatly. It is thus not too critical which of the two formulas, Eq. 8-21 or Eq. 8-22, is used if $0.5 \times 10^5 < Re < 3 \times 10^5$.

8-3.1.4 Discussion of the Equation of Spin-up

In Eq. 8-16 the rate of change of v is made up of two parts: the convective term

$u \left(\frac{\partial v}{\partial r} + \frac{v}{r} \right)$, and the viscous term on the right hand side of Eq. 8-16.

The convective term represents that portion of the total rate which is produced in the boundary layers and convected by the secondary flow u into the interior. The viscous term represents the portion produced within the core-flow by viscous forces that drag the fluid around. Depending on Reynolds number and cavity shape, either of the two terms can be dominant so that the other term may be neglected. In both cases considerable mathematical simplification is obtained.

The rate of change of v due to the convective term is of the order

$$\left(\frac{\partial}{\partial t} \right)_{\text{conv}} \approx u \frac{\partial}{\partial r} \sim \frac{u}{a} \quad \text{or with Eq. 8-8}$$

$$\left(\frac{\partial}{\partial t} \right)_{\text{conv}} \approx \Omega \frac{c}{a} \quad (8-26)$$

Considering, for example, the case of laminar boundary layer; Eqs. 8-11 and 8-26 yield

$$\left(\frac{\partial}{\partial t} \right)_{\text{conv}} \approx \Omega \frac{a}{c} (\text{Re})^{-1/2} \quad (8-27)$$

The contribution of the viscous term is of the order

$$\left(\frac{\partial}{\partial t} \right)_{\text{visc}} \approx \frac{v}{a^2} \sim \Omega \text{Re}^{-1} \quad (8-28)$$

Comparison of Eqs. 8-27 and 8-28 shows that the convective term is dominant when

$$1 \ll \frac{a}{c} \text{Re}^{1/2} \quad (8-29)$$

For liquid-filled projectiles, Eq. 8-29 is practically always fulfilled so that — to the first approximation — the viscous terms may be neglected. The resulting reduced equation is

$$\frac{\partial v}{\partial t} + u \left(\frac{\partial v}{\partial r} + \frac{v}{r} \right) = 0; \left(1 < \frac{a}{c} \text{Re}^{1/2} \right) \quad (8-30)$$

For the case of a turbulent boundary layer, the preponderance of the convective term is even larger so that Eq. 8-30 holds for the turbulent case except for very slender cavities.

Eq. 8-30 suggests for the spin-up time $t \approx \frac{a}{v}$ which yields for the case of laminar boundary layer

$$\Omega t \approx \frac{c}{a} \text{Re}^{1/2} \quad (8-31)$$

The general solution of Eq. 8-30 is discussed in par. 8-3.1.5.

For small Reynolds numbers and slender cavities the viscous term of Eq. 8-16 may compete with the convective term and the complete equation should be considered. In the analysis of Ref. 2 approximate solutions of the complete equation are derived in successive steps, starting with the solution of the reduced equation. The results are reported in par. 8-3.2.

The extreme case of an infinitely long cylinder is interesting for comparison. In this case the convective terms are zero since there is no secondary flow. The resulting equation is

$$\frac{\partial v}{\partial t} = v \left[\frac{\partial^2 v}{\partial r^2} + \frac{\partial}{\partial r} \left(\frac{v}{r} \right) \right] \quad (\text{infinite cylinder}) \quad (8-32)$$

Eq. 8-32 is a linear differential equation which can be solved by standard methods.

The spin-up time suggested by Eq. 8-32 is of the order

$$\Omega t \approx \frac{\Omega a^2}{v} = \text{Re} (\text{infinite cylinder})$$

Comparison of Eqs. 8-33 and 8-31 shows that — for larger Reynolds numbers — the secondary flow is very effective to accelerate the spin-up. For a typical liquid-filled projectile $\text{Re} \approx 10^6$ and $c/a = 3$. The spin-up time, according to Eq. 8-31, is approximately 1/300 of the value obtained for the infinite cylinder.

8-3.1.5 General Solution of the Reduced Equation of Spin-up

The reduced equation of spin-up, Eq. 8-30, can be written in the form

$$\frac{\partial(rv)}{\partial t} + u \frac{\partial(rv)}{\partial r} = 0 \quad (8-34)$$

Eq. 8-34 can be integrated at once along certain lines in the (r,t) -plane, the so-called characteristics, which are defined by

$$\frac{dr}{dt} = u \quad (8-35)$$

With Eq. 8-35 we may write the left hand side of Eq. 8-34 as a total differential

$$\frac{\partial(rv)}{\partial t} + \frac{\partial(rv)}{\partial r} \cdot \frac{dr}{dt} = \frac{d(rv)}{dt} = 0 \quad (8-36)$$

Integrating Eq. 8-36 yields

$$rv = \text{constant for } \frac{dr}{dt} = u \quad (8-37)$$

Eq. 8-37 expresses the conservation of angular momentum for any fluid particle. In fact, angular momentum is produced only in the boundary layers, while every fluid element in the core-flow carries its angular momentum rv unchanged along its trajectory which is given in the (r,t) -plane by Eq. 8-35.

It remains to solve the characteristic equation, Eq. 8-35. In the most general case u is a function of r, t and (rv) . Note that (rv) is constant along the path of integration. To avoid confusion, let us denote the angular momentum rv by x , and write

$$\frac{dr}{dt} = u(r, t, x); \quad x = rv \quad (8-38)$$

If u does not depend explicitly on t — which is the usual case — Eq. 8-38 can be simply integrated to give the general solution

$$r(x)$$

The initial conditions are

$$r = r(x) \text{ at } t = 0 \quad (8-40)$$

Usually, the initial conditions are given in a form $x = x(r)$ which is the inverse function of $r = r(x)$.

When solved for x , Eq. 8-39 yields the distribution of angular momentum $rv = x(r, t)$.

Applications of Eq. 8-39 in the case of a cylindrical cavity are given in par. 8-3.2.

8-3.2 VELOCITY DISTRIBUTION DURING SPIN-UP

The velocity distribution and the total angular momentum of the liquid during spin-up can be computed from Eq. 8-39 when $u(r, x)$ is known and the initial conditions are specified. For the cylindrical cavity the method of computation is discussed and results are presented.

8-3.2.1 Method of Computation

The computation of $u(r, x)$ is outlined in par. 8-3.1.2 and in more detail in Ref. 2. For a cylindrical cavity with plane end-walls, u is given approximately by Eqs. 8-21 or 8-22 for laminar or turbulent boundary layers, respectively. Substituting $v = x/r$, Eqs. 8-21 and 8-22 read

$$u = -k(r\Omega - x/r) \quad (\text{laminar}) \quad (8-41)$$

$$u = -k_t(r\Omega - x/r)^{8/5}/(a\Omega)^{3/5} \quad (\text{turbulent}) \quad (8-42)$$

$$\text{with } k = 0.443 \frac{a}{c} (\text{Re})^{-1/2} \quad (8-43)$$

$$k_t = \frac{0.0175}{c} (\text{Re})^{-1/5} \quad (8-44)$$

Ω is the angular velocity of the casing.

8-3.2.7.1 Initial Conditions

The lower limit of the integral $r(x)$ in Eq. 8-39 depends on the initial conditions,

i.e., on the distribution of angular momentum at $t=0$. If this is $x(r)$, then $r(x)$ is the inverse function of $x(r)$.

For the case in which the cavity is started impulsively at $t=0$ to spin with angular velocity Ω , the function $x(r)$ is defined by:

$$\left. \begin{array}{ll} 0 < x(r) < a^2 \Omega & \text{for } r = a \\ x(r) = 0 & \text{for } r < a \end{array} \right\} \quad (8-45)$$

Eq. 8-45 implies that at $t=0$ the liquid is not spinning except within an infinitesimal layer at $r=a$. Within this layer the value of x increases from 0 to $a^2 \Omega$. Note, that this layer must be assumed at $r=a$ in order to have Eqs. 8-21 and 8-22 satisfy the boundary conditions $u=0$ at $r=a$.

The inverse function of Eq. 8-45 is

$$\left. \begin{array}{ll} r(x) = a & \text{for } 0 < x < a^2 \Omega \\ r(x) < a & \text{for } x = 0 \end{array} \right\} \quad (8-46)$$

8-3.2.7.2 Laminar Case

As an example, consider the case of laminar boundary layer. Substituting Eqs. 8-41 and 8-46 into Eqs. 8-39 yields

$$-t = \int_a^r \frac{dr}{k(r\Omega - x/r)} = -2k\Omega \ell_n \frac{r^2 - x/\Omega}{a^2 - x/\Omega} \quad (8-47)$$

for $0 < x < a^2 \Omega$

and

$$-t = \int_{r(0)}^r \frac{dr}{kr\Omega} = \frac{1}{k\Omega} \ell_n \frac{r}{r(0)} \quad (8-48)$$

for $x=0$, $r(0) < a$

8-42

Solving Eq. 8-47 for x and substituting $x = rv$ yields

$$\frac{v}{a\Omega} = \frac{\frac{r}{a} e^{2k\Omega t} - \frac{a}{r}}{e^{2k\Omega t} - 1}$$

$$\text{for } 0 < v \text{ or } r/a > e^{-k\Omega t} \quad (8-49)$$

Eq. 8-49 is supplemented by:

$$v = 0 \text{ for } r/a < e^{-k\Omega t} \quad (8-50)$$

Eq. 8-50 is a consequence of Eq. 8-48.

8-3.2.7.3 Partially Filled Cavity

As shown in par. 8-3.1.2.1, Eqs. 8-21 and 8-22 are valid also for partially filled cylindrical cavity except at points close to the free surface $r=b$, where u drops to zero.

With $u \rightarrow 0$, the integral $\int_a^r \frac{dr}{u}$ of Eq. 8-39

diverges as $r \rightarrow b$, i.e., the time for the liquid to attain rotation increases indefinitely as the distance from the free surface decreases to zero. In practice, the diverging integral has the effect that angular momentum is not convected across the free surface.

The velocity distributions obtained for a partial fill are, for $r > b$, nearly the same as those for completely filled cavity except near the edge $r=b$. For practical purposes the velocity-distributions for a completely filled cavity, cut off at $r=b$, may be used in the case of partial fill.

8-3.2.7.4 Total Angular Momentum

The total angular momentum I of the liquid at any time t is obtained by integration when velocity distribution $v(r,t)$ is known. It is

$$I(t) = \rho \iiint r^2 v(r,t) d\theta dr dz \quad (8-51)$$

where the integral is taken over the liquid-filled part of the cavity volume. Since $v(r, t)$ is independent of θ and z , it is

$$I(t) = 2\pi\rho \int_b^a r^2 v(r, t) 2c(r) dr \quad (8-52)$$

where $2c(r)$ is the height of the cavity at the radius r , $2a$ the maximum diameter of the cavity, and $2b$ the diameter of the cylindrical void. For the cylindrical cavity one obtains simply

$$I(t) = 2\pi\rho 2c \int_b^a r^2 v(r, t) dr \quad (8-53)$$

8-3.2.2 Computation of Angular Momentum

The results given below are for a cylindrical cavity. The velocity distributions are computed — unless otherwise stated — on the bases of Eq. 8-39, i.e., they are valid approximations when $1 \ll \frac{a}{c} Re^{1/2}$.

The equations, Eqs. 8-54 to 8-58, which follow apply when the casing is started impulsively at $t = 0$ to spin with constant angular velocity Ω .

8-3.2.2.1 Laminar Boundary Layer

For the case of laminar boundary layer (see par. 8-3.1.3) the velocity distribution is

$$\left. \begin{aligned} v^* &= \frac{r^* e^{2k\Omega t} - 1/r^*}{e^{2k\Omega t} - 1} ; & r^* &\geq e^{-k\Omega t} \\ v^* &= 0 & ; & r \leq e^{-k\Omega t} \end{aligned} \right\} \quad (8-54)$$

where $v^* = \frac{v}{a\Omega}$, $r^* = \frac{r}{a}$, $k = 0.443 \frac{a}{c} Re^{-1/2}$.

Eq. 8-54 applies also for partially filled cavity when restricted to $r > b/a$.

The total angular momentum for a completely filled cavity is

$$I = I_\infty (1 - e^{-2k\Omega t}) \quad (8-55)$$

with $I_\infty = \rho\pi\Omega ca^4$

The value of the angular momentum of time t relative to a rigid or steady state value for partially filled cavity is

$$I/I_\infty = \frac{1 - e^{-2k\Omega t}}{1 - b^4/a^4} ; \quad b/a < e^{-k\Omega t} \quad (8-56)$$

$$I/I_\infty = \frac{1}{1 - e^{-2k\Omega t}} \left[1 - \frac{2e^{-2k\Omega t}}{1 + b^2/a^2} \right] ;$$

$$b/a > e^{-k\Omega t}$$

with $I_\infty = \rho\pi\Omega ca^4(1 - b^4/a^4)$

As shown by Eqs. 8-54 to 8-56, the velocity distributions and the total angular momentum depend only on the scaled time $k\Omega t$.

For several values of $k\Omega t$ the velocity distributions according to Eq. 8-54 are shown in graphical form in Fig. 8-2.

I/I_∞ versus scaled time $k\Omega t$ is shown in Fig. 8-4 for a 100% filled ($b^2/a^2 = 0.00$) and 70% filled ($b^2/a^2 = 0.30$) cavity.

A somewhat better approximation for the total angular momentum which was derived in Ref. 2 on the basis of the full equation of spin-up, Eq. 8-16, is given implicitly by

$$2k\Omega t = \frac{-1}{1 - 4/(kRe)} \left[\ln(1 - I/I_\infty) + \frac{4}{kRe} \ln \left(1 + \frac{kRe}{4} \frac{I}{I_\infty} \right) \right] \quad (8-57)$$

Eq. 8-57 yields improved values of I/I_∞ especially at short times, when $kRe \left(\frac{I}{I_\infty} \right)$ is not large as compared to unity.

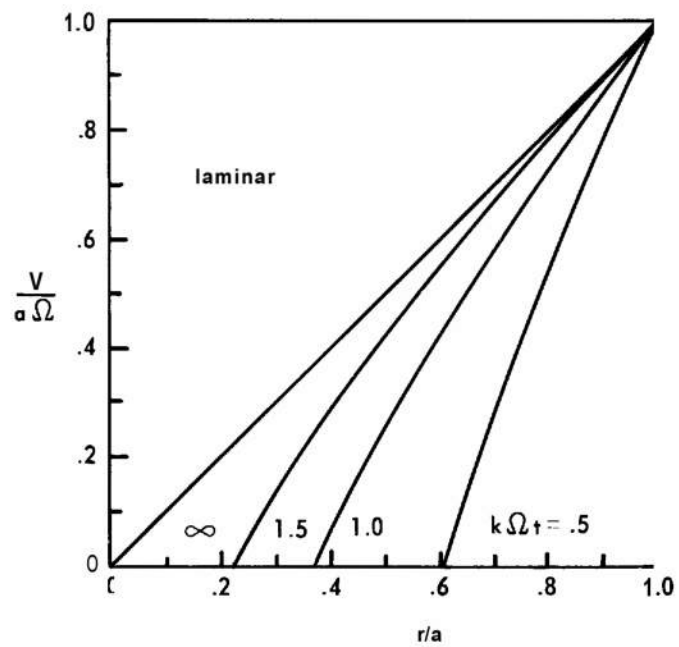


FIGURE 8-2. VELOCITY DISTRIBUTION DURING SPIN-UP FOR LAMINAR BOUNDARY LAYER

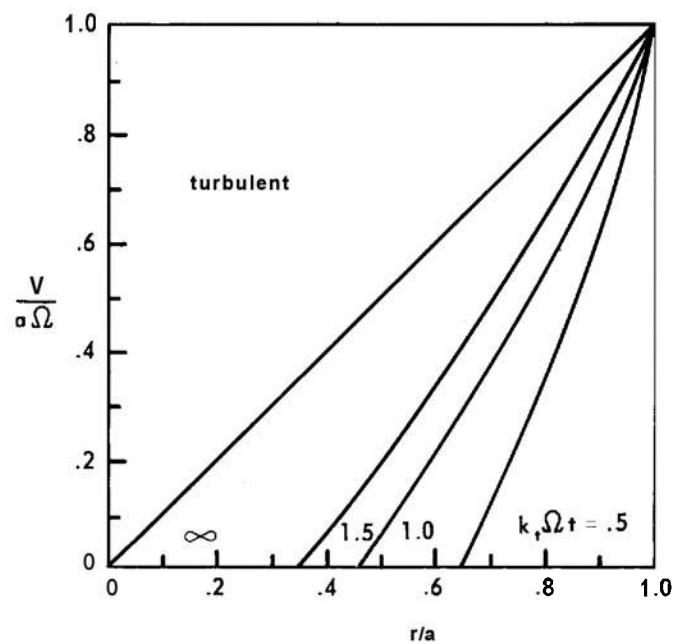


FIGURE 8-3. VELOCITY DISTRIBUTION DURING SPIN-UP FOR TURBULENT BOUNDARY LAYER

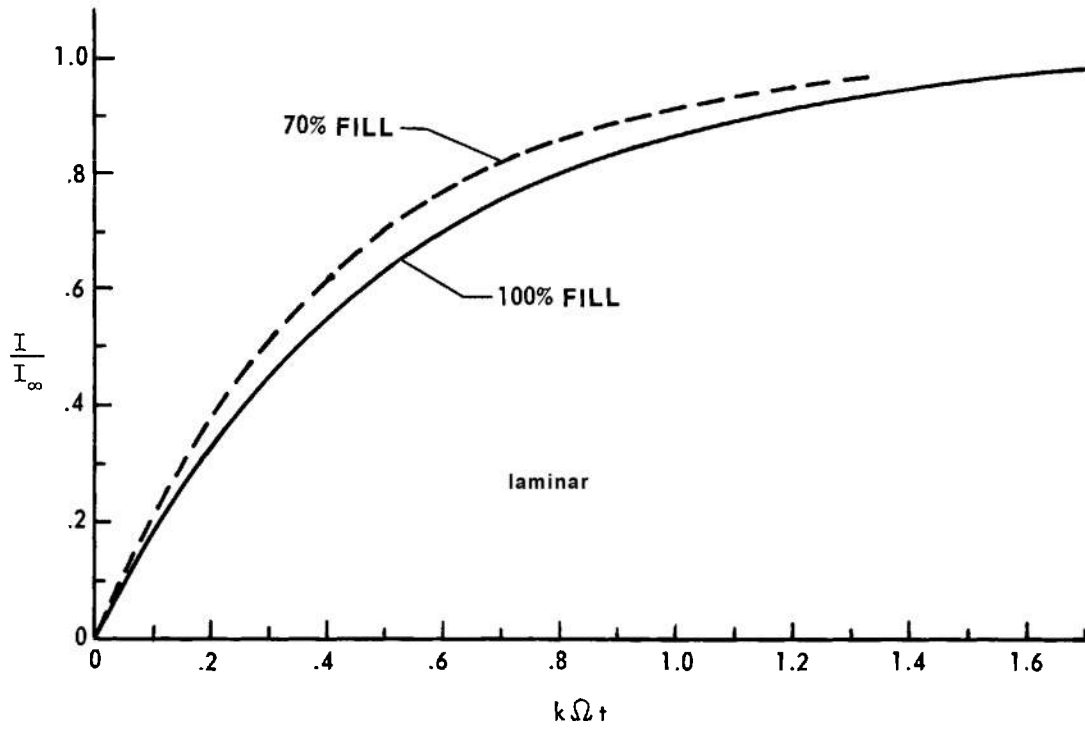


FIGURE 8-4. ATTAINMENT OF THE ANGULAR MOMENTUM (LAMINAR BOUNDARY LAYER)

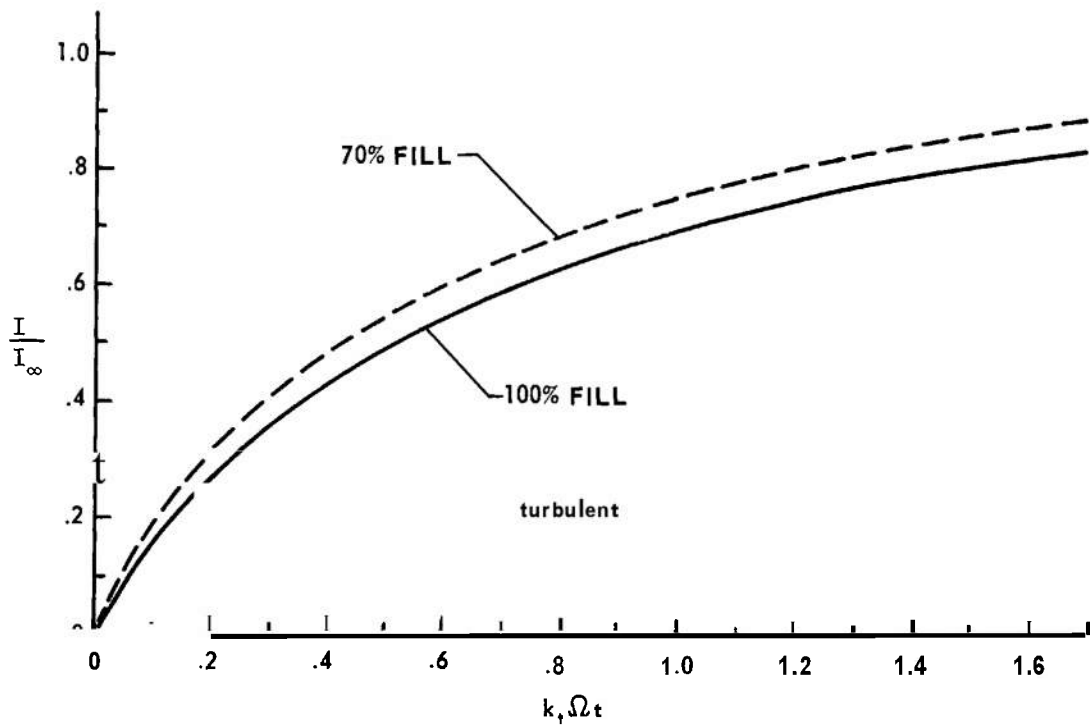


FIGURE 8-5. ATTAINMENT OF THE ANGULAR MOMENTUM (TURBULENT BOUNDARY LAYER)

8-3.2.2.2 *Turbulent Boundary Layer*

The case of a turbulent boundary layer prevails in applications to liquid-filled projectiles (see par. 8-3.1.3). The velocity distribution is obtained via numerical integration of the following equation, Eq. 8-58,

$$k_t \Omega t = \int_{r^*}^1 \frac{dr^*}{(r^* - y/r^*)^{8/5}} \quad (8-58)$$

where $k_t = 0.035 \frac{a}{c} Re^{-1/5}$, $r^* = r/a$,

$$v^* = \frac{v}{a\Omega}, \quad y = r^* v^*$$

(y is kept constant for the integration.) Velocity distributions $v^* = y/r^*$ versus r^* according to Eq. 8-58 are shown in graphical form in Fig. 8-3.

I/I_∞ versus scaled time is shown in Fig. 8-5 for cavities of 100% and 70% fill-ratio.

8-3.2.2.3 *Other Initial Conditions*

The discussions above are the most relevant examples in applications to liquid-filled projectiles.

Spin-up profiles for other initial conditions — e.g., starting from a rigid rotation with $\Omega' \leq \Omega$ at $t = 0$ — can always be computed by evaluating the integral, Eq. 8-39, for the given initial condition $r(x)$. If u depends explicitly on t — e.g., via Ω — Eq. 8-39 does not apply and the original differential equation, Eq. 8-38, must be solved. Generally, if the solution of Eq. 8-38 is given by $F(x, r, t) = 0$, then x is found as function of r and t by solving $F(x, r, t) = 0$ for x .

In the preceding examples it was assumed that the angular velocity Ω remains constant after the casing has been started impulsively. Strictly, Ω is not constant for a liquid-filled projectile leaving the muzzle of a gun. As the liquid absorbs angular momentum from the casing, the angular velocity must decrease until the liquid

reaches full spin. The final angular velocity Ω_∞ is reduced from the initial value Ω_0 according to

$$\frac{\Omega_\infty}{\Omega_0} = \frac{A}{A_1 + A} \quad (8-59)$$

where A is the axial moment of inertia of the empty projectile, and A , the moment of inertia of the fully spinning liquid.

Usually, A , is only a small fraction of A so that the 'change of Ω during spin-up is small and may be neglected for practical purposes.

Taking into account the dependence of Ω on the angular momentum I of the liquid by the relation

$$I + \Omega A = \Omega_0 A, \quad (8-60)$$

the exact solution for I with variable Ω is

$$I/I_\infty = \frac{1 - e^{-2k\Omega_0 t}}{1 - \epsilon e^{-2k\Omega_0 t}}$$

with $\epsilon = \frac{I_\infty}{A\Omega_0}$; $I_\infty = \rho\pi\Omega_\infty c a^4$; $\frac{\Omega_\infty}{\Omega_0} = \frac{A}{A_1 + A}$,

where Ω_0 is the initial axial spin rate and Ω_∞ is the final value. Eq. 8-61 replaces Eq. 8-55 since, in the latter equation, Ω is considered constant.

8-4 EXPERIMENTAL RESULTS ON SPIN-UP

Experiments to determine the attainment of liquid rotation have been performed by Karpov^{1,9} for a completely and partially filled cylindrical cavity.

Most of the data were obtained by observation of the axial spin decay of liquid-filled projectiles in the free flight range. When the projectile has left the gun, its angular momentum decreases continuously. A relatively small fraction of the spin-decay is due to the torque by air friction while most of the spin decay results from absorption of angular momentum in the liquid.

The contribution due to air-friction is determined separately, by observation of the spin-decay of empty projectiles, and then subtracted from the total rate of change of angular velocity. Let Ω be the angular velocity corrected in this manner, A the axial moment of inertia of the empty projectile, and I the angular momentum of the liquid. Then, from the conservation of angular momentum

$$I + \Omega A = \text{const} = \Omega_0 A \quad ; \text{ or } I = (\Omega_0 - \Omega)A \quad (8-62)$$

where Ω_0 is the initial angular velocity when the liquid is at rest.

Thus, observation of angular velocity Ω versus the time of flight is a convenient

way to determine experimentally the attainment of angular momentum via Eq. 8-62.

Experimental data for I , obtained in this manner, have been compared with theoretical predictions and good agreement was found in all cases. Strictly speaking, the variation of angular velocity Ω should be taken into account for the theoretical computation; however, the total change of Ω under the experimental conditions was only a few percent so that within a reasonable approximation the theoretical data, based on constant $\Omega = \Omega_0$, can be used for comparison.

In Figs. 8-6, 8-7 and 8-8 experimental data of I/I_∞ obtained from range firings',⁹

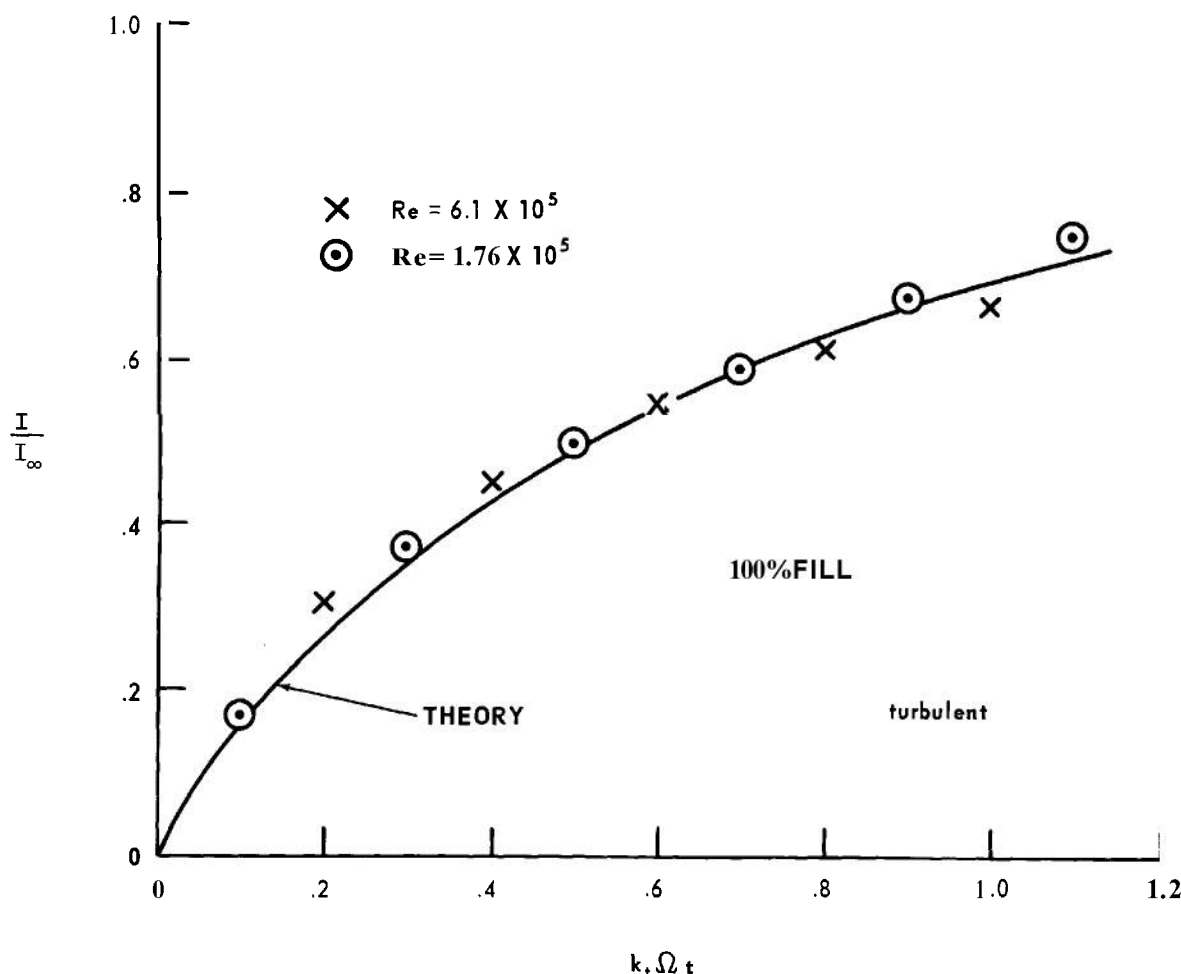


FIGURE 8-6. ATTAINMENT OF THE ANGULAR MOMENTUM (TURBULENT BOUNDARY LAYER, 700% FILL) COMPARISON WITH EXPERIMENTS

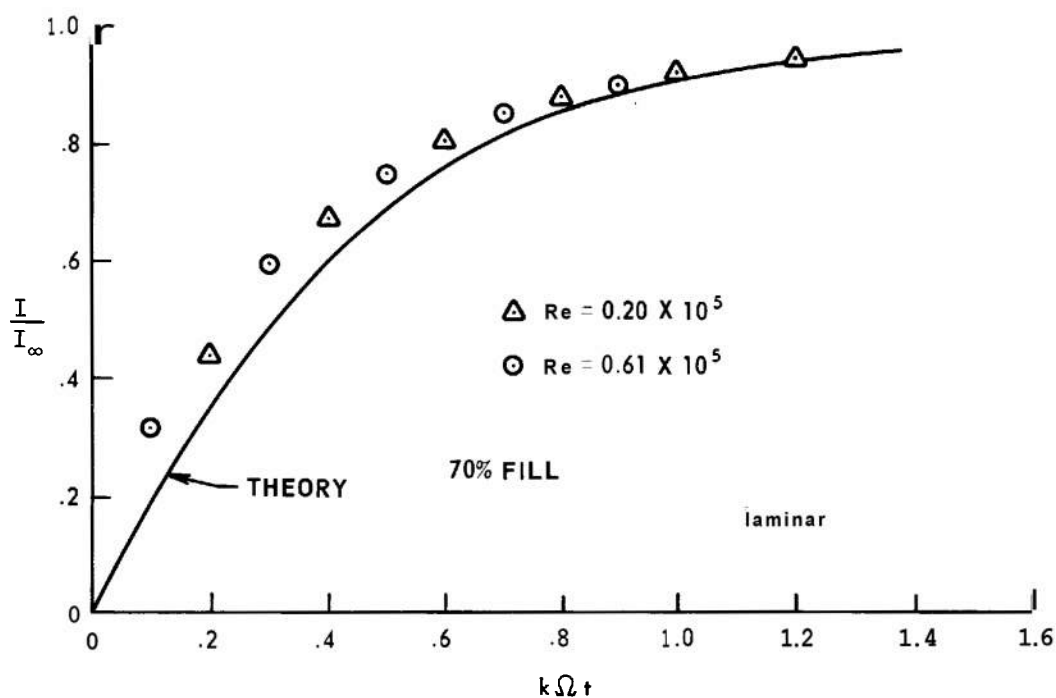


FIGURE 8-7. ATTAINMENT OF THE ANGULAR MOMENTUM (LAMINAR BOUNDARY LAYER, 70% FILL) COMPARISON WITH EXPERIMENTS

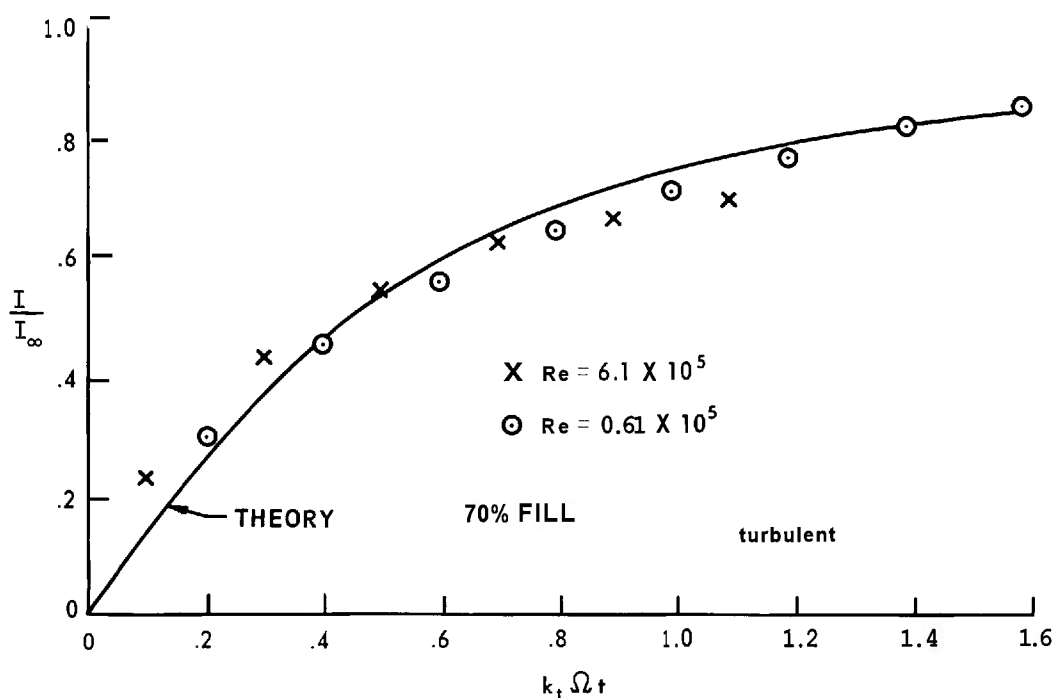


FIGURE 8-8. ATTAINMENT OF THE ANGULAR MOMENTUM (TURBULENT BOUNDARY LAYER, 70% FILL) COMPARISON WITH EXPERIMENTS

are shown for various Reynolds numbers and fill-ratios. The Reynolds numbers were varied by using oils of different viscosities. The projectile used was the 20 mm M56 with a cylindrical cavity of 15.6 mm diameter and 4.18 mm height. The experimental data of I/I_∞ are compared with the theoretical values predicted by Eqs. 8-55 and 8-58. According to the theory, the angular momentum depends only on the scaled time $k\Omega t$ or $k_c\Omega t$ for the laminar or turbulent case, respectively. Thus, when plotted versus $k\Omega t$ (or $k_c\Omega t$, respectively) the experimental data of I/I_∞ for different Reynolds numbers and fineness-ratios should fall on one curve. Figs. 8-6 to 8-8 show that this is indeed the case. The agreement with the theoretical curves is also quite good.

In the laminar case, Fig. 8-7, the experimental increase of I/I_∞ is initially higher than theoretically predicted. The difference can be explained easily by the neglect of the viscous terms (right-hand side of Eq. 8-16) in the theoretical computation. The agreement is improved when the higher order approximation, Eq. 8-57, is used for comparison with the experimental data.

The experimental data for $Re = 0.61 \times 10^5$ (70% filled cavity) were compared with theoretical data both for laminar and turbulent boundary layers. As shown in par. 8-3.1.3, in the range $0.5 \times 10^5 < Re < 3 \times 10^5$ the boundary layer may be laminar or turbulent or mixed. The experimental data for $Re = 0.61 \times 10^5$ fit quite well in both of the theoretical curves so that a decision regarding the type of boundary layer cannot be obtained from this comparison. (It also shows that, for these transitional Reynolds numbers, the theoretical predictions based on laminar and turbulent boundary layer do not differ very much, so that it is not too critical whether the laminar or turbulent formula is used.)

For the data taken at $Re = 1.76 \times 10^5$, however, a comparison with theoretical prediction shows that the assumption of a turbulent boundary layer is certainly favorable.

Few attempts have been made to measure the velocity distribution during spin-up. The experiments reported in Ref. 1 were obtained at relatively low Reynolds numbers. The experimental technique — which is described in Refs. 10 and 11 — utilizes an impulsive spin generator having a transparent liquid-filled cavity ($\frac{c}{a} \approx 3$). A suspension of small particles of exactly the same specific weight as the liquid is used to trace the fluid motion. The particle trajectories are photographed with a high-speed motion camera. By this method it was possible to measure the distribution of rotational velocity and also the secondary flow.

The observed secondary flow is in fairly good agreement with theoretical predictions (see Ref. 2). A very good agreement cannot be expected since the experimental Reynolds number was rather low ($Re = 1.83 \times 10^4$), while the theory is based on the assumption of higher values of $\frac{a}{c} Re^{1/2}$.

Similarly, viscosity has a strong influence on the distribution of angular velocity, which is felt especially at the point $r/a = c^{-2k\Omega t}$ where — according to the "inviscid" formula, Eq. 8-54 — the velocity distribution has a cusp.

Further experiments on the determination of spin-up profiles at higher values of $\frac{a}{c} Re^{1/2}$ are necessary in order to check the theoretical computations. Instead of increasing the Reynolds number — which usually leads to experimental difficulties — the fineness-ratio c/a could be decreased in order to obtain larger values of $\frac{a}{c} Re^{1/2}$. However, the conditions for a turbulent boundary layer can be established only at larger values of Re .

8-5 INSTABILITY DURING SPIN-UP

Transient instabilities of liquid-filled projectiles have been observed during the initial period of flight in cases where the projectile is stable according to Stewartson's theory.

Systematic investigations^{1,9}, have shown overwhelmingly that the occurrence of these instabilities are connected with the spin-up of the liquid. In fact, Stewartson's theory is based on the assumption that the liquid within the cavity is — prior to perturbation — in a state of solid rotation and there is no theoretical reason to expect that the dynamic behavior of a projectile during spin-up should be related in a simple way to its behavior at the final stage of full spin. On the contrary, Stewartson's theory proves that small changes of the geometry or the fill-ratio can have a striking effect on the stability behavior, so that there is every reason to expect that the state of motion of the liquid — which is changing continuously during spin-up — has also a strong effect on the dynamic behavior.

It is suggested by analogy, that the instabilities during spin-up have a similar cause as the instabilities of the Stewartson type; however, it is not possible as yet to give an exact prediction of instability on theoretical grounds.

Lacking an exact theory, fairly successful attempts have been made to derive a crude criterion for the global behavior of the projectile on the basis of empirical facts and a reasonable hypothesis.

In the paragraphs which follow the present criterion and experimental evidence are discussed, and possible refinements of the theory are outlined.

It appears that the present theory describes the essentials of transient instability correctly although it must be conceded that the theory rests on a rather small volume of experimental evidence and much more data must be obtained before final conclusions can be drawn.

8-5.1 THEORETICAL APPROACH

The principal ideas of the theory of transient instabilities are as follows:

(1) As in the case of complete spin, the partially spinning liquid has a number of discrete frequencies of free oscillations (eigenfrequencies) which depend on the cavity shape, fill-ratio, and the velocity distribution.

(2) The projectile becomes unstable when its nutational frequency falls within certain bandwidths about the eigenfrequencies. The bandwidths and the rates of undamping are determined — as in the case of Stewartson's theory — by the residues at the poles which characterize the reaction of the liquid upon the projectile in a given mode of oscillation.

(3) Any of the eigenfrequencies change continuously corresponding to the change of the velocity distribution. However, the change is very slow compared with the frequency of oscillation so that the velocity distribution may be considered as "quasi-steady", which means that the variation of the velocity distribution may be neglected for the purpose of computing the corresponding eigenfrequencies.

8-5.1.1 Mathematical Difficulties of an Exact Computation

Unfortunately, it has not been possible, as yet, to compute the eigenfrequencies or residues for the velocity distributions that are actually encountered (see par. 8-3.2). The mathematical difficulties arise for the following reasons:

(1) The angular velocity — i.e., the frequency at which the fluid particles rotate — varies between zero and its full value at the wall. At some radius the frequency of rotation must coincide with the eigenfrequency. At this radius — briefly called the resonance radius — the equations of perturbed fluid motion have a singularity. At the singularity the amplitude of oscillation becomes infinite and undergoes a phase shift, i.e., the phase of the oscillation is different for radii smaller and radii larger than the resonance radius.

(2) A numerical integration of the equations of perturbed fluid motion, which was attempted in Ref. 12, breaks down at the singularity. It is also likely that — as a result of the phase shift — the eigenfrequencies have a small imaginary component; this, too, would render a numerical treatment very difficult.

(3) If there are complex eigenfrequencies, they must occur always in pairs with conjugate complex values (in contrast to the case of viscous damping where only damped oscillations occur, see Chapter 6). Actually the occurrence of conjugate complex eigenfrequencies means that the fluid motion itself is unstable — a possibility which cannot be excluded for the particular spin-up profiles encountered during spin-up.

8-5.1.2 A Simplified Model

In order to study the essential features of the problem, a simplified model was assumed (see Ref. 9) according to which the liquid rotates with constant angular velocity within an annular layer next to the sidewalls while the rest of the liquid has no rotation. These “rectangular” distributions are not dissimilar to the true distributions (see par. 8-3.2) with which they have in common the two separate regions of spinning and nonspinning liquid, although the true velocity distributions have a non-uniform spin in the annular region at the wall.

To complete the model, it is necessary to give a relation between the true velocity distributions and the rectangular model-distributions, i.e., with constant Ω , so that any one of the latter corresponds to one of the true distributions. For example, the correspondence can be such that the true distribution is represented by either

Case I, the rectangular distribution having the correct angular momentum, or

Case II, the rectangular distribution having the correct volume of rotating liquid.

There are, of course, other possibilities between Case I and Case II and — lacking a theoretical basis — we are free to adapt our model to the experimental facts.

8-5.1.3 Eigenfrequencies for Rectangular Distributions

For the rectangular distribution of angular velocity, the equations of perturbed fluid motion become (compare Chapter 3)

$$p'' + \frac{p'}{r} - \frac{p}{r^2} + k^2 \left[\frac{4\Omega^2}{(\Omega - \omega)^2} - 1 \right] p = 0; \quad \text{for } b < r < a \quad (8-63)$$

$$p'' + \frac{p'}{r} - \frac{p}{r^2} - k^2 p = 0; \quad \text{for } r < b \quad (8-64)$$

where b is the radius of the interface between the nonrotating core $r < b$ and the uniformly rotating annulus $b < r < a$.

The radial velocity u must be zero at $r = a$; this leads to the boundary condition

$$ap' + \frac{2}{1-\tau} p = 0; \quad \text{at } r = a \quad (8-65)$$

On the perturbed interface the pressure must be continuous. This leads to the conditions that if p_2 is the solution of Eq. 8-63 for $b < r$ and p_1 the solution of Eq. 8-64 for $r < b$ then, (see Appendix A for derivation of Eq. 8-66)

$$p_2 - p_1 = \frac{bp'_2 + \frac{2}{1-\tau} p_2}{4 - (1-\tau)^2} \quad \text{at } r = b \quad (8-66)$$

$$p_2 - p_1 = \frac{-bp'_1}{\tau^2}$$

where primes indicate partial derivatives with respect to r . The second of the two Eqs. 8-66 shows that if τ is small, p_1 becomes small like τ^2 compared to p_2 (see

footnote*). Then, neglecting p_1 relative to p_2 , the first of the Eqs. 8-66 simplifies to

$$p_2 = \frac{bp'_2 \tau \frac{2}{1-\tau} p_2}{4 - (1-\tau)^2}, \text{ at } r=b \quad (8-67)$$

Eq. 8-67 agrees with the boundary condition, Eq. 3-62, on the free surface at $r=b$ of a partially filled cavity. (The physical reason for this agreement is that the deformations of the interface produce little reaction in the nonspinning inner core — unless the frequency of oscillation is high — so that the condition on the interface is approximately the same as that on a free surface.) Since we are mainly interested in low values of τ_0 (up to about $\tau_0 = 0.2$ or $\tau_0^2 = 0.04$), Eq. 8-67 is a good approximation and the problem reduces to the case of a partially filled cavity with a free surface at $r=b$. Consequently, Stewartson's Tables for a partially filled cavity may be used.

The exact computation of eigenfrequencies entails no principal difficulties, but the model which we have assumed is so crude that the error encountered by the approximate condition at the interface is probably unimportant against other errors.

We are now able to compute, roughly, the course of eigenfrequencies during spin-up. Fig. 8-9 shows a graph of contour-lines of τ_0 in the plane b^2/a^2 versus $c/[a(2j+1)]$. The graph, which is taken from Ref. 1, is for the lowest radial mode $n=1$.

To determine the course of eigenfrequencies, a line may be drawn at constant $\frac{c/a}{2j+1}$.

*The second of Eq. 8-66 can be written as

$$\frac{p_1}{p_2} = -\frac{\tau^2}{\frac{bp'_1}{p_1} - \tau^2}; \quad \frac{bp'_1}{p_1} \geq 1$$

Therefore, if τ is small, $\frac{p_1}{p_2} \approx \tau^2$

Where the line intersects a contour-line of a given τ_0 , the corresponding value of b^2/a^2 can be read on the ordinate. It is seen readily that τ_0 decreases with decreasing b^2/a^2 . Thus, at the beginning of spin-up, when the "effective" b^2/a^2 is near one, τ_0 is high. As the liquid attains more and more rotation and the effective b^2/a^2 decreases, τ_0 decreases monotonically from its initial value to the final value at full spin. According to our assumption, the projectile becomes temporarily unstable when the principal eigenfrequency passes through resonance. We may certainly neglect the eigenfrequencies of higher modes since these produce rarely more than a mild divergence even in the steady state.

8-5.1.4 Stability Criteria

The above model of transient instability is too crude to give precise values of the eigenfrequency or the rate of undamping at any instant of time. However, from the engineering point of view it is only important to predict the integrated effect on the projectile.

If we trust our model only qualitatively, since it predicts a monotonic decrease of the eigenfrequencies during spin-up, we can draw some important conclusions:

- (1) The projectile remains stable during the spin-up time if the principal eigenfrequency of the steady state lies above the frequency of nutation.
- (2) If the principal eigenfrequency of the steady state lies below the nutational frequency, the projectile becomes temporarily unstable. The instability is less severe when the instantaneous eigenfrequency passes quickly through the resonance band. This is the case, when the steady state eigenfrequency is remote from the nutational frequency. Conversely, when the steady state eigenfrequency is close to (and below) the nutational eigenfrequency, the instability is more severe.

If $\tau_0(t)$ is the variable eigenfrequency, τ_n the nutational frequency, and $|\tau_n - \tau_0| < \sqrt{S}$;

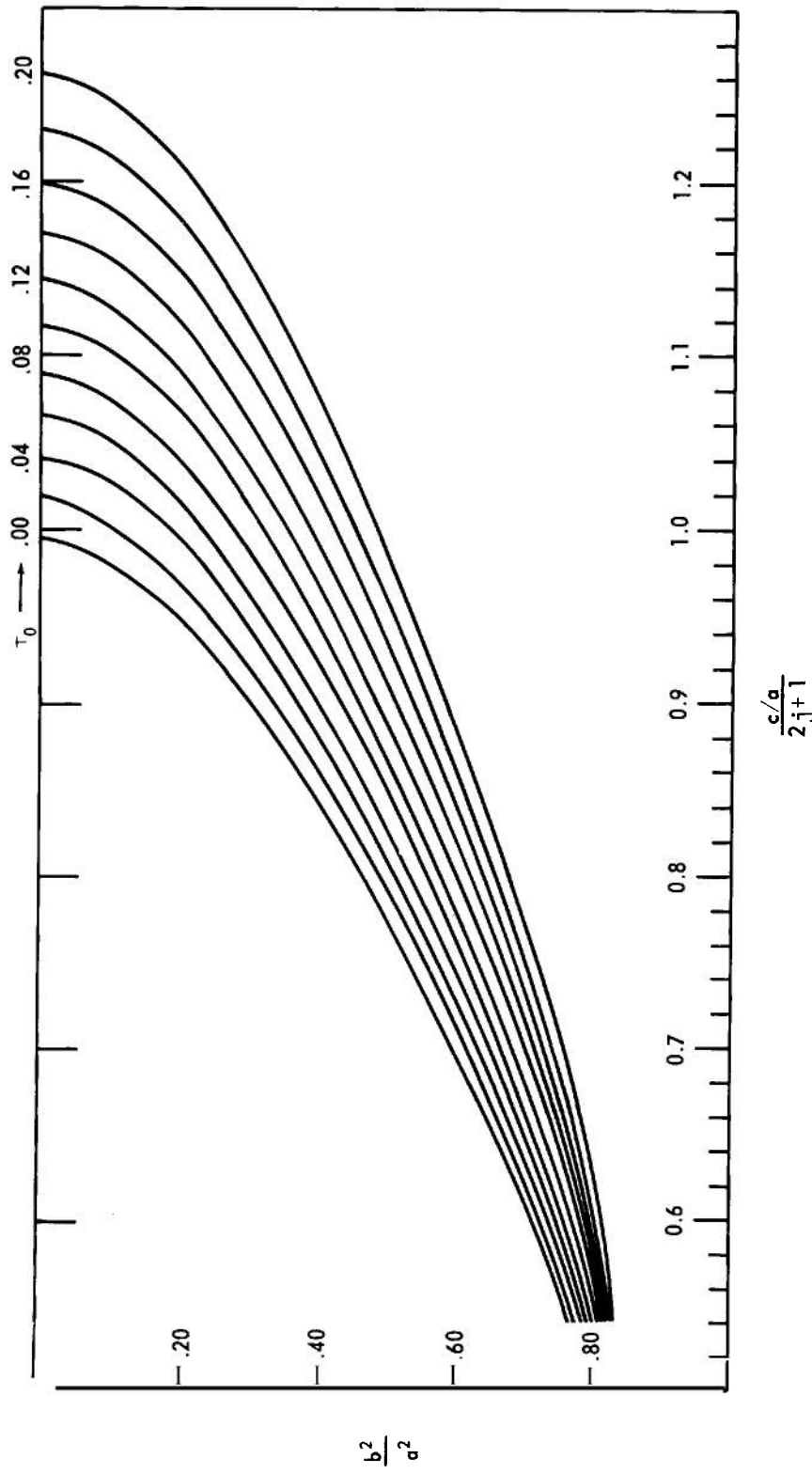


FIGURE 8-9. GRAPH OF AN ELEMENT ($n=1$) FROM SEWATTON'S TABLES

we find for the rate of undamping (Eq. 4-22)

$$\lambda = \Omega \tau_1 = \frac{\Omega}{2} \sqrt{S - (\tau_n - \tau_0)^2}, \text{ per sec} \quad (8-68)$$

The yaw angle increases like

$$\alpha = \alpha_0 e^{\int \lambda dt}$$

If α_1 is the final yaw angle after the passage through the instability band and α_0 the initial yaw angle, we have

$$\ell_n \left(\frac{\alpha_1}{\alpha_0} \right) = \int_{\tau_0}^{\tau_1} \lambda dt \quad (8-69)$$

Substitution of Eq. 8-68 into Eq. 8-69 and change of the variables yields

$$\ell_n \left(\frac{\alpha_1}{\alpha_0} \right) = \frac{\Omega}{2} \int_{\tau_n - \sqrt{S}}^{\tau_n + \sqrt{S}} \sqrt{S - (\tau_n - \tau_0)^2} \left(\frac{d\tau_0}{d\tau_0} \right) d\tau_0 \quad (8-70)$$

$\frac{d\tau_0}{dt}$ is practically constant for the short duration of passage through the instability band. Carrying out the integration, we obtain

$$\ell_n \left(\frac{\alpha_1}{\alpha_0} \right) = -\frac{\pi \Omega}{4} \left(\frac{S}{d\tau_0/dt} \right) \quad (8-71)$$

The value of the Stewartson parameter S may be taken equal to its value for the partially filled cavity.

To compute $\frac{d\tau_0}{dt}$ we must know the spin-up history. The theory of spin-up (par. 8-3) yields the velocity distribution and the "effective" b^2/a^2 as a function of time. Thus, we have

$$\frac{d\tau_0}{dt} = \frac{d\tau_0}{d(b^2/a^2)} \left[\frac{d(b^2/a^2)}{dt} \right] \quad (8-72)$$

$\frac{d\tau_0}{d(b^2/a^2)}$ may be computed by numerical

differentiation of Stewartson's Tables or graphically by means of Fig. 8-9.

Finally, it should be mentioned that Eq. 8-71 remains unchanged by viscous effects. It was shown in Chapter 6 that, as an effect of viscosity, the instability band is broadened while the maximum rate of undamping is decreased. The viscous undamping curve, λ versus τ_0 , is quite different from Eq. 8-68. In spite of this difference, the integral, Eq. 8-69, leads to the same result regardless how much the band is broadened. The flattening of the undamping curves just compensates the broadening, so that the integrated area is independent of the damping factor δ . Thus, Eq. 8-71 may be used irrespective of the effect of viscosity.

8-5.2 EXPERIMENTAL DATA

All pertinent experimental data available on transient instability of liquid-filled projectiles are found in Refs. 1 and 9. The most important of these data are reproduced here and discussed with respect to the theoretical approach of par. 8-5.1.

The experiments have been performed with the 20 mm Projectile, M56 with liquid filler. The projectile had a cylindrical cavity of 15.6-mm radius and 41.8-mm height. According to the physical characteristics of this projectile, a Stewartson-type of instability was expected at fill-ratios between 43% and 48%. The yaw damping rates of the projectile were observed in the free flight range over the initial 4400 calibers of travel and, subsequently, evaluated.

Fig. 8-10 shows the observed nutational yaw damping rates versus fill-ratio for the case where the projectile was filled with water ($Re = 6.1 \times 10^5$).

The damping rate changes in a most striking manner in the vicinity of the steady state instability band at about 45% of fill. The projectile is damped at fill-ratios smaller than 40% and unstable (negative

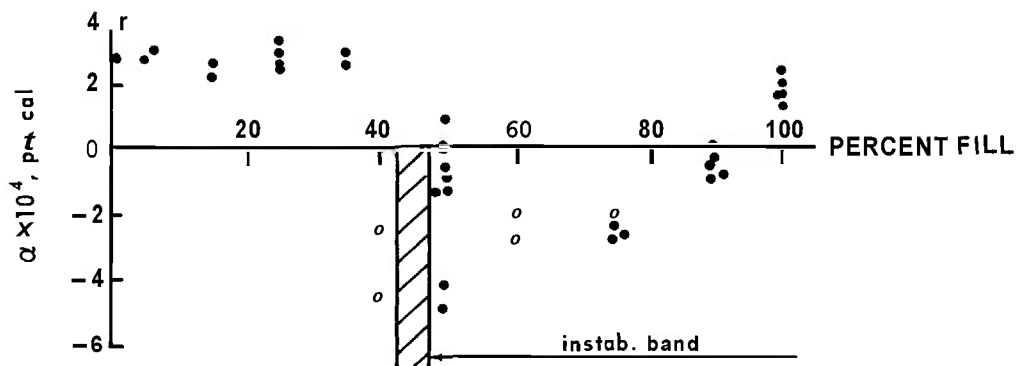


FIGURE 8-10. NUTATIONAL YAW DAMPING RATE OF TEST PROJECTILE

damping rate) at fill-ratios larger than 45%. The largest rate of undamping is attained at fill-ratios just above the instability band. The experimental facts displayed by this diagram are in accord with the stability criterion of par. 8-5. The steady state eigenfrequency at fill-ratio 45% coincides with the nutational frequency — thus there is an instability band at 45% fill. For smaller fill ratios — i.e., larger b^2/a^2 — the steady state eigenfrequency lies above the nutational frequency (see, e.g., Fig. 8-9), thus, according to the statement (1) of par. 8-5.1.4, the projectile is stable. For fill-ratios larger than 45% the steady state eigenfrequency lies below the nutational frequency so that the instantaneous eigenfrequency must at one time during spin-up pass through the resonance band and the projectile becomes temporarily unstable. If the fill-ratio is close to 45% (but above), the eigenfrequency remains for a long time within the instability band, thus the total divergence of the yaw amplitude is largest near 45%.

According to our model, the nutational damping rate should be negative only for a more or less short interval and positive during the remaining time. Such behavior could not be observed with certainty. Possibly, the resolution of the data is insufficient to reproduce the fine details of the yaw history so that the damping rates

shown in Fig. 8-10 must be interpreted as average values! Or we must assume a real band-broadening, like the broadening by viscous effects; however, the cause for such an unusual band-broadening is unknown.

When the cavity of the 20 mm projectile was filled with glycerine instead of water, no divergent yaw was observed except a very mild divergence at 45% fill-ratio. The explanation is simple: the viscosity of glycerine is so high that the liquid has achieved full spin at the muzzle. Thus it becomes unstable only when its steady state eigenfrequency falls near the nutational frequency. And even then the instability is very mild because of the strong viscous flattening of the undamping curve.

Fig. 8-11 shows the ratio of the yaw amplitude to its initial value on a logarithmic scale for 70% filled cavity and three different viscosities of 1, 3 and 30 centistokes. The slope of the curve is directly proportional to the rate of divergence. The figure indicates that:

(1) Initially the yaw is divergent in all three cases as a result of transient instability. At a certain point, the projectile becomes stable and the yaw decreases by aerodynamic damping.

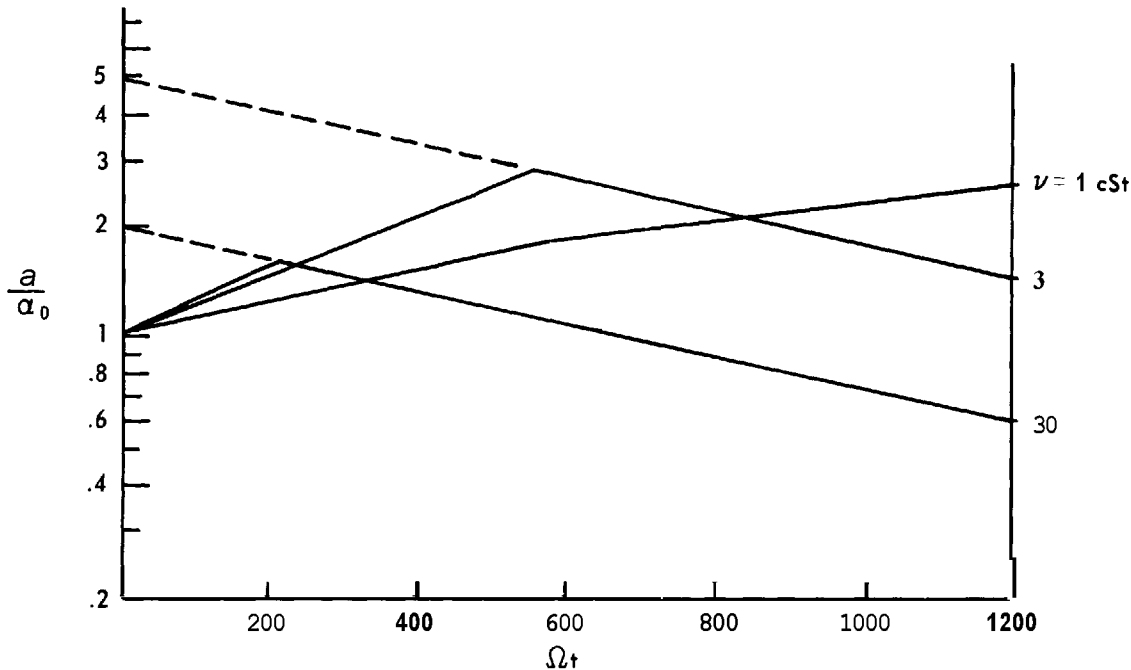


FIGURE 8-77. NUTATIONAL YAW AMPLITUDE VS TIME FOR 70% FILLED CAVITY OF TEST PROJECTILE

(2) The larger the viscosity, the shorter is the period of instability. This is in accord with our expectation since the spin-up time — and thus the unstable period — is shorter for higher viscosity.

In particular, our model predicts that the stability depends on an “effective” value of b^2/a^2 which in turn depends only on the total angular momentum attained by the liquid. Thus, the transition to the stable regime should occur in all three cases at the same angular momentum of the liquid. Fig. 8-12 shows the course of the angular momentum versus time for the three cases $\nu = 1, 3$ and 30 . The point of transition to the stable regime is marked by a dot. (For the case $\nu = 1$ the transition point was not observed; however, from the changing slope of the curve one may conjecture that it lies about at the right edge of the graph.) Fig. 8-12 shows that transition to the stable regime occurs at a value of I/I_∞ of roughly 0.6 in all three cases. The theoretical model, according to which the true distribution of angular velocity is replaced by a rectangular distribution, suggests that transient instability should occur in the

band I or the band II of Fig. 8-12 for the model-distributions I and II, respectively. In Case I the true distribution has been replaced by a rectangular distribution having the correct angular momentum while the model distribution of Case II reproduces the correct volume of spinning liquid. Case II appears to be closer to reality; however, the experimental data are too limited for final conclusions to be drawn. As mentioned above, it is also not clear why the instability band is so much broadened. The broadening may be feigned by the evaluation procedure or we may ascribe it to some unknown mechanism; in either case we may try to estimate the total increase of yaw on the basis of Eq. 8-71. (The validity of Eq. 8-71 is not effected, for example, by viscous broadening, as shown.)

Let us consider the instability band for Case I. We read from the graph, Fig. 8-12, the following time intervals of instability

$$\begin{aligned}\Delta\Omega t &= 88 \quad ; \quad \text{for } \nu = 30 \\ \Delta\Omega t &= 230 \quad ; \quad \text{for } \nu = 3\end{aligned}$$

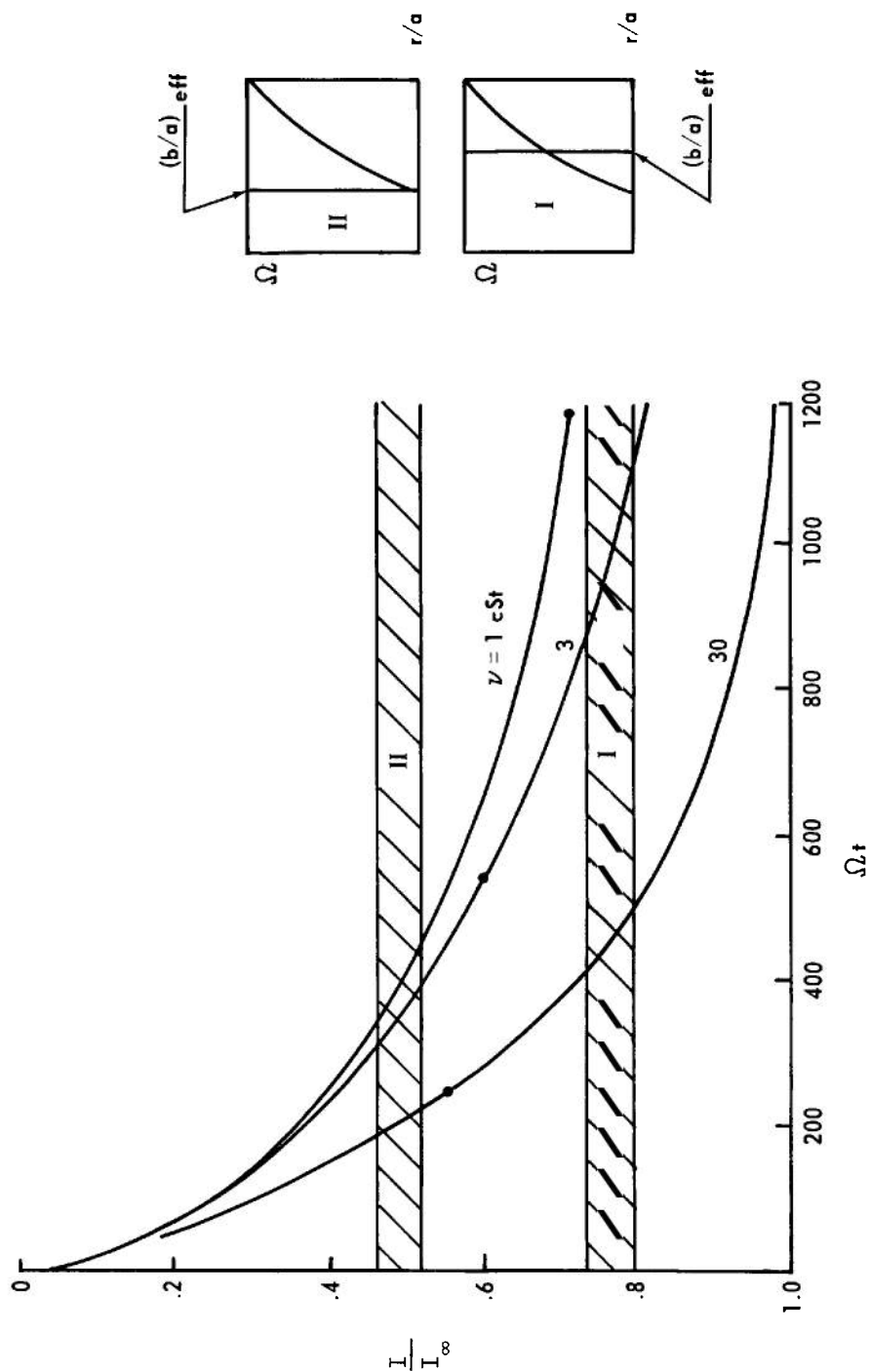


FIGURE 8-12. INCREASE OF ANGULAR MOMENTUM AND PASSAGE THROUGH RESONANCE BAND I OR II

The Stewartson parameter for the two cases was $S = 3.3 \times 10^{-4}$. The width of the unstable interval, in terms of τ_0 is

$$\Delta\tau_0 = 2\sqrt{S} = 3.6 \times 10^{-2}$$

With the above data we obtain, Eq. 8-71,

ν	$\Delta\Omega t$	$\frac{\pi S}{4} \cdot \frac{\Delta\Omega t}{\Delta\tau_0} = \ln\left(\frac{\alpha_1}{\alpha_0}\right)$	$\frac{\alpha_1}{\alpha_0}$
30	88	0.62	1.86
3	230	1.62	5.05

To determine the experimental value of α_1/α_0 , the contribution of aerodynamic damping must be subtracted. This can be done graphically — as indicated in Fig. 8-11 — by extending the damping curves — which are straight lines — backwards to the point where they intersect the ordinate. The point of intersection yields the amplitude ratio for the case in which aerodynamic damping is disregarded. The values of α_1/α_0 obtained in this way are

ν	$\left(\frac{\alpha_1}{\alpha_0}\right)$ experimental
30	2
3	5

The good agreement with the theoretical prediction is fortuitous. The best one can hope for from the present theory is that it gives the correct order of magnitude of the initial growth of yaw.

REFERENCES

1. B.G. Karpov, *Experimental Observations of the Dynamic Behavior of Liquid Filled Shell*, BRL Report 1171, Aberdeen Proving Ground, Md., 1962.
2. E.H. Wedemeyer, "The Unsteady Flow within a Spinning Cylinder," J. Fluid Mech. 20, 383 (1964) and BRL Report 1252, Aberdeen Proving Ground, Md., 1963.
3. H. Schlichting, *Boundary Layer Theory*, McGraw-Hill Book Co., New York, 1960.
4. M.H. Rogers and G.N. Lance, "The Rotationally Symmetric Flow of a Viscous Fluid in the Presence of an Infinite Rotating Disk," J. Fluid Mech. 7, 617-631, (1960).
5. H.P. Greenspan, "On the General Theory of Contained Rotating Fluid Motions," J. Fluid Mech. 22, 449-462, (1965).
6. L. M. Mack, *The Laminar Boundary Layer on a Disk of Finite Radius in a Rotating Flow. Part II: A Simplified Momentum Integral Method*, Jet Prop. Lab. Tech. Report 32-366, 1963.
7. T. Theodorsen and A. Regier, *Experiments on Drag of Revolving Disks, Cylinders and Streamline Rods at High Speeds*, NACA Report 793, 1944.
8. I. Tani, R. Hama, and S. Mituisi, *On the Permissible Roughness in the Laminar Boundary Layer*, Aeron. Res. Inst. Tokyo, Report 199, 1940.
9. B. G. Karpov, *Dynamics of Liquid Filled Shell: Instability During Spin-Up*, BRL Memo Report 1629, Aberdeen Proving Ground, Md., 1965.
10. H.M. Stoller, *Apparatus for Study of Fluid Motion in a Spinning Cylinder*, BRL Tech. Note 1355, Aberdeen Proving Ground, Md., 1960.
11. G. Sokol, *Some Experiments with the Liquid-Filled, Impulsively Started, Spinning Cylinder*, BRL Tech. Note 1473, Aberdeen Proving Ground, Md., 1962.
12. M.M. Reddi, *On the Eigenvalues of Couette Flow in a Fully-Filled Cylindrical Container*, Report F-B2294 Franklin Institute Res. Lab., Philadelphia, Pa., 1967.

APPENDIX A

DERIVATION OF EQ. 8-66, PAR. 8-5.1.3

It is assumed that the basic flow field consists of a nonrotating core ($r < b$) and an annular region ($b < r < a$) of uniform rotation.

After perturbation, the interface at $r = b$ between rotating and nonrotating liquid becomes displaced radially by a small amount $\eta(\theta, z, t)$.

The flow velocity normal to the interface must equal the normal displacement velocity of the interface. This condition, which is analogous to the kinematic condition on a free surface yields, according to Eq. 3-24

$$\frac{\partial \eta}{\partial t} + \frac{V}{r} \frac{\partial \eta}{\partial \theta} = u \quad (A1)$$

V and u are, respectively, the circumferential and radial components of the flow velocity either at the inward facing or at the outward facing side of the interface.

Applying Eq. A1 to the inward facing side, where $V = 0$ and $u = u_1$ yields

$$\frac{\partial \eta}{\partial t} = u_1 \quad (A2)$$

and similarly for the outward facing side, where $V/r = \Omega$ and $u = u_2$.

$$\frac{\partial \eta}{\partial t} + \Omega \frac{\partial \eta}{\partial \theta} = u_2 \quad (A3)$$

u_1 and u_2 are proportional to $e^{i(\omega t - \theta)}$, and the same dependence on the wave factor must be assumed for η .

Thus

$$\eta = \hat{\eta}(z) e^{i(\omega t - \theta)} \quad (A4)$$

Eqs. A2, A3, and A4 yield

$$\frac{-iu_1}{\omega} = \frac{-iu_2}{\omega - \Omega} = \eta \quad (A5)$$

Another condition is that the pressure must be equal at both sides of the interface. Denoting the undisturbed pressure by P_{b1} ,

P_{b2} and the pressure perturbation by p_1 , p_2 at the inward and outward facing sides, respectively, we obtain

$$P_{b1}(b + \eta) + p_1(b + \eta) = P_{b2}(b + \eta) + p_2(b + \eta) \quad (A6)$$

Expanding

$$P_b(b + \eta) = P_b(b) + \left(\frac{\partial P_b}{\partial r} \right)_b \eta + \dots$$

and neglecting higher order terms, yields

$$P_{b1}(b) + \left(\frac{\partial P_{b1}}{\partial r} \right)_b \eta + p_1(b) = P_{b2}(b) + \left(\frac{\partial P_{b2}}{\partial r} \right)_b \eta + p_2(b) \quad (A7)$$

Since the unperturbed pressure must be equal at both sides of the unperturbed interface, we have

$$P_{b1}(b) = P_{b2}(b) \quad (A8)$$

Furthermore, the unperturbed pressure is constant in the nonrotating core, i.e.,

$$\frac{\partial P_{b1}}{\partial r} = 0 \quad (A9)$$

while, in the annular region of rotating flow, we have (see Eq. 3-26)

$$\left(\frac{\partial P_{b2}}{\partial r}\right)_b = \left(\rho \frac{V^2}{r}\right)_b = \rho \Omega^2 b \quad (A10)$$

Substituting Eqs. A8, A9, A10, and A5 into Eq. A7 yields

$$p_2 - p_1 = -\rho \Omega^2 b \eta = \rho \Omega^2 b \frac{u_1}{\omega} = \rho \Omega^2 b \frac{u_2}{\omega - \Omega} \quad (A11)$$

Finally, u_1 , u_2 can be expressed by p_1 , p_2 , respectively. According to Eq. 3-57 we have

$$\frac{u_2}{\omega - \Omega} = \frac{1}{\rho \Omega^2} \left[\frac{\partial p_2}{\partial r} + \frac{2}{1-\tau} \frac{p_2}{r} \right]_b; \quad \tau = \frac{\omega}{\Omega} \quad (A12)$$

Similarly, when Eq. 3-57 is specialized for $\Omega = 0$

$$\frac{u_1}{\omega} = -\frac{1}{\rho \omega^2} \left[\frac{\partial p_1}{\partial r} \right]_b \quad (A13)$$

Substituting Eqs. A12 and A13 into Eq. A11 finally yields:

$$p_2 - p_1 = \left[\frac{b \frac{\partial p_2}{\partial r} + \frac{2}{1-\tau} p_2}{4 - (1-\tau)^2} \right]_b = -\frac{b_2}{\Omega^2} \left[\frac{\partial p_1}{\partial r} \right]_b \quad (A14)$$

CHAPTER 9

DESIGN OF A LIQUID-FILLED PROJECTILE

9-0 LIST OF SYMBOLS

2a	= diameter of cylindrical cavity	I_y	= "effective" transverse moment of inertia of liquid, slug-ft ² , defined in par. 2-5. <i>Note:</i> all transverse moments are referred to the same center of mass.
2a ₀	= diameter of the cylindrical part of a noncylindrical cavity	I_y	= $I_{y0} \pm i_{y0}$ or $I_y = I_{y0} \pm i_{y0}$, the latter to be used whenever it makes a significant difference with a liquid filler, slug-ft ²
2b	= diameter of the cylindrical air volume, ft	I	= angular momentum of fluid at any time t
2c	= height of cavity, ft	I_∞	= total angular momentum of fluid, i.e., maximum steady state value when fluid is spinning as a rigid body
CG	= center of gravity	I/I_∞	= fractional value of the angular momentum at time t relative to the rigid or steady state value
C _D	= drag coefficient	J	= axial mode
C _{Mα}	= static moment coefficient/rad	k	= $0.443(a/c)Re^{-1/2}$ (laminar flow)
C _{Nα}	= normal force coefficient	k_t	= $0.035(a/c)Re^{-1/5}$ (turbulent flow)
CP	= center of pressure	K_n	= tabular value in Stewartson's Tables for a given τ_0 , $c/[a(2j \pm 1)]$, b^2/a^2 , and n th radial mode
c ₁	= as defined by Eq. 9-9	k_y^{-2}	= md^2/I_y transverse radius of gyration, cal
c ₂	= as defined by Eq. 9-10	L	= overall length of fuzed projectile, cal
c/a	= fineness-ratio of the cavity	ℓ_n	= natural logarithm
d	= maximum projectile diameter, ft	M	= $(\rho_a S' d / 2m) k_y^{-2} C_{M\alpha}$ nondimensional moment factor; Mach number
\tilde{g}	= projectile's deceleration as defined by Eq. 9-36, ft/sec ²	M_f	= mass of WP filler, or of any other liquid, slug
g ₀	= acceleration due to gravity, ft/sec ²	m	= mass of loaded projectile, slug
H	= head length, cal	m'	= $(2c/a_0) \tan \epsilon$
h/2c	= nondimensional height of noncylindrical part of cavity	\bar{m}'	= average m'
I_{x0}	= axial moment of inertia of empty casing, slug-ft ²		
I_{x0}	= axial moment of inertia of frozen liquid, slug-ft ²		
I_x	= $I_{x0} \pm i_{x0}$, axial moment of inertia of loaded projectile, slug-ft ²		
I_{y0}	= transverse moment of inertia of empty casing, slug-ft ²		
I_{y0}	= transverse moment of inertia of frozen liquid, slug-ft ²		

n	= radial mode; twist of rifling, cal/turn	x	= $b^2/a^2 = (1 - \beta)$ fractional air volume in cavity
P	= $(2\pi/n)(I_x/I_y)$ nondimensional axial spin	T	= $k_t \Omega t$ scaled time
$2R$	= residue at the pole, obtained from Stewartson's Tables	GREEK LETTERS	
Re	= $\Omega a^2/\nu$ Reynolds number	α_0	= initial yaw upon entering resonance band
$2r$	= diameter of burster, ft	α	= final yaw upon leaving resonance band
r^*	= radius of nonspinning core, i.e., where $v^* = 0$	β	= fractional fill of cavity volume
R'	= corner radius of cavity, ft	δ	= c_2/\sqrt{Re} viscous correction to the inviscid damping
R'/a	= fractional radius of corner of cavity	ϵ	= c_1/\sqrt{Re} viscous correction to the inviscid frequency
r/a	= fractional radius of burster	θ	= semi-vertex angle of truncated cone at height $h/2c$, rad
S	= $\frac{\rho(2R)^2 a^5}{I_x \sigma(c/a)}$ Stewartson's parameter	θ_m	= mid-point of cylindrical arc
S_c	= Stewartson's parameter of original cylindrical cavity	λ	= rate of divergence of nutational amplitude, per sec or per ft
S'	= $\pi d^2/4$ cross-sectional area of projectile, ft ²	μ	= viscosity of working fluid, poise
S_m	= Stewartson's parameter in non-cylindrical cavity	μ_0	= viscosity of water, poise
s	= Ω_c/Ω ratio of critical to actual spin, dimensionless	ν	= kinematic viscosity of liquid, stoke
s_g	= $P^2/4M$ gyroscopic stability factor	ν_{WP}	= kinematic viscosity of white phosphorous, stoke
$(s_g)_L$	= gyroscopic stability factor with liquid filler	P	= liquid density, slug/ft ³
$(s_g)_R$	= gyroscopic stability factor with rigid filler	ρ_a	= air density, slug/ft ³
t	= time, sec	ρ_{WP}	= density of white phosphorus, slug/ft ³
V	= velocity of projectile, ft/sec; volume of fluid required for each modified cavity to bring it into resonance, ft ³	σ	= $\sqrt{1 - 1/s_g}$
V_c	= volume of cylindrical cavity, ft ³	σ'	= specific gravity of working liquid
V_0	= volume of noncylindrical cavity, ft ³	τ_n	= ω_n/Ω nondimensional nutational frequency of projectile
v^*	= circumferential nondimensional velocity of fluid particles at radius r^*	$\tau_0(nj)$	= (or simply τ_0) = ω_{nj}/Ω nondimensional fluid frequency (eigen-frequency)
v_a	= volume of air in cavity, ft ³	Ω	= $(2\pi/nd)V$ axial spin, rad/sec
v_r	= volume of burster, ft ³	Ω_c	= critical spin as defined by Eq. 9-35, rad/sec
w	= axial velocity of fluid, ft/sec	ω_n	= $(I_x \Omega / 2I_y)(1 \pm \sigma)$ nutational frequency, rad/sec

9-4 INTRODUCTION

To design a well behaved, i.e., dynamically stable, liquid-filled projectile sometimes is very difficult. This is largely because of the constraints imposed upon the design such as the size of the projectile, its weight, and the amount of chemical filler the projectile is to carry for its maximum effectiveness. The parameters at the disposal of the designer within the above limitations are the geometry of the cavity, its fineness-ratio, and the fill-ratio. Occasionally, as is the case with the XM410 Projectile, the resonance band is so broad and the instability is so severe that relatively small modifications, which might be permissible within the above constraints, are quite ineffective. In such cases resort must be made either to a drastic redesign of the cavity, at some sacrifice of the optimum design of the system, or to some other

means whose effectiveness, however, rests as yet on a rather slender experimental basis.

Especially difficult problems are encountered with thin-walled projectiles. For such projectiles the value of Stewartson's parameter

$$S = \frac{\rho(2R)^2 a^5}{I_x \sigma(c/a)}$$

is usually large because of the relatively large diameter of the cavity $2a$, small c/a , and small I_x . The width of the theoretical inviscid resonance band is $2\sqrt{S}$ and the maximum divergence rate of the nutational amplitude is proportional to \sqrt{S} . Thus a large S makes the design of stable projectiles much more difficult.

SECTION I

STEADY STATE

We shall consider first the steady state condition, i.e., when the liquid is fully spinning. If the projectile is incurably dynamically unstable in this state, there is no point in worrying about its behavior during spin-up. However, if the projectile is designed to be stable with the full spin, then it behooves the designer to examine its stability in the transient phase. We shall consider this phase in Section 11.

9-2 PRELIMINARY CALCULATIONS: GYROSCOPIC STABILITY AND NUTATIONAL FREQUENCY

To design a well behaved rigid "conventional" projectile is usually not difficult. A variety of methods are available for estimating its inertial and other physical properties. To estimate its aerodynamic characteristics is usually more difficult. In

this connection the recent publication **AMCP 706-242, *Design for Control of Projectile Flight Characteristics***, should be very useful. For estimating moments of inertia, for example, Hitchcock's¹ formula may be used. These pertain to HE-loaded projectiles and are usually good to about 10%; I_x is usually better determined than I_y .

$$\left. \begin{aligned} I_x &= 0.14md^2 \\ I_y &= (0.5 \pm 0.42L^2)I_x \end{aligned} \right\} \quad (9-1)$$

where

m = mass of loaded projectile, slug

d = maximum diameter of projectile, ft

L = overall length of fuzeed projectile, cal

For thin-walled projectiles perhaps a better approximation for I_y is

$$I_y = (0.5 \pm 0.36L^2)I_x$$

Gyroscopic stability factor can be written as (see Ch. 2)

$$s_g = \frac{P^2}{4M} \quad (9-2)$$

$$\text{where } P = \left(\frac{2\pi}{n} \right) \frac{I_x}{I_y} \quad (9-2a)$$

n = twist of rifling, cal/turn

$$M = \frac{\rho_a}{2m} k_y^{-2} C_{M\alpha} \quad (9-2b)$$

ρ_a = air density, slug/ft³

m = mass of loaded projectile, slug

d = diameter of projectile, ft

k_y^{-2} = radius of gyration = $\frac{md^2}{I_y}$, cal

$C_{M\alpha}$ static moment coefficient, per rad

Sometimes it is more convenient to replace $C_{M\alpha}$ by $C_{M\alpha} = C_{N\alpha}(CP - CG)$ where $C_{N\alpha}$ is normal force coefficient, because $C_{N\alpha}$ and CP (center of pressure) depend only on the external shape and are invariant with internal modifications such as changes in the geometry of the cavity. Of course, the CG will probably change as the cavity changes but such changes can be estimated and allowed for. In a preliminary design, for many conventionally shaped projectiles, $C_{N\alpha}$ is about 3, and CP can be taken as $3/4 H$ for square-based and $2/3 H$ for boat-tailed projectile, measured from the fuze nose, where H is the head length in calibers. These rough values are reasonably adequate and are applicable in the range of low supersonic velocities, $1 \leq M \leq 2$, where M is the Mach number.

It should be remembered, see par. 2-5, that with a liquid filler, the gyroscopic stability factor at the muzzle is less than with a rigid filler. If $(s_g)_R$ is the gyroscopic stability factor of the projectile with rigid filler, i.e., with liquid frozen, then the gyroscopic stability factor at the muzzle when the filler is liquid is

$$(s_g)_L = (s_g)_R \left(\frac{I_{x0}}{I_{x0} + i_{x0}} \right)^2 \quad (9-2c)$$

where I_{x0} is the axial moment of inertia of the empty casing and i_{x0} is that of the liquid regarded as rigid. Experience has shown that the safe lower limit for the gyroscopic stability factor is about 1.3. If $(s_g)_L$ is too low, the twist of rifling of the gun may have to be changed.

Once the gyroscopic stability factor is known, compute

$$\sigma = \sqrt{1 - \frac{1}{s_g}} \quad (9-3)$$

and then the nutational frequency

$$\tau_n = \frac{I_x}{2I_y} (1 + \sigma) \quad (9-4)$$

Here the question may well arise as to the proper inertial properties to be used in defining the nutational frequency: those of loaded projectile, of the empty casing, or something in between? Experiments suggest the following:

(1) For I_x use the loaded rigid projectile value,

(2) For I_y the "effective" transverse moment of inertia of the fluid is to be used whenever it makes a significant difference in τ_n , i.e.,

$$I_y = I_{y0} \pm i_y \pm M_f x^2 \text{ (see par. 2-5)}$$

However, in a preliminary design this refinement is unnecessary because of fairly rough estimates of the moments of inertia.

Thus with l_x , σ , and τ_n known, one may proceed to consider whether the designed cavity contains fluid frequencies in close proximity to the nutational frequency of the projectile. We shall consider first the simplest case of the cylindrical cavity.

9-3 CYLINDRICAL CAVITY

9-3.1 VISCOUS CORRECTIONS

It was shown in Ch. 6 and elsewhere that agreement of the inviscid theory with the results of the experiments is markedly improved if viscous corrections are applied to Stewartson's theory. These corrections affect the inviscid fluid frequency and the inviscid damping. The frequency correction is shown to be of the form

$$\epsilon = \frac{1}{\sqrt{\text{Re}}} \quad (9-5)$$

which should be added to the tabulated inviscid frequencies in Stewartson's Tables. Thus the exact resonance with the nutational frequency occurs not when $\tau_0 = \tau_n$ but when $\tau_0 + \epsilon = \tau_n$. The maximum divergence of the nutational amplitude, due to resonance, becomes

$$\lambda = \frac{\Omega}{2} (\sqrt{S + \delta^2} - \delta), \text{ per sec} \quad (9-6)$$

instead of the inviscid maximum divergence

$$\lambda = \frac{\Omega}{2} \sqrt{S} \text{ per sec} \quad (9-6a)$$

where the damping correction has the form

$$\delta = \frac{c_2}{\sqrt{\text{Re}}} \quad (9-7)$$

Stewartson's *instability* criteria is modified to

$$-\left(1 + \frac{\delta}{\sqrt{S}}\right) < \frac{\tau_0 + \epsilon - \tau_n}{\sqrt{S}} < \left(1 + \frac{\delta}{\sqrt{S}}\right) \quad (9-8)$$

The formulas for computation of c_1 and c_2 are given in Ch. 6. The functions c_1 and c_2 depend on τ_0 , c/a , and the inviscid partial derivatives $\frac{\partial \tau_0}{\partial (b^2/a^2)}$ and $\frac{\partial \tau_0}{\partial \{c/[a(2j+1)]\}}$.

The derivatives, as shown in Ch. 6, can be adequately approximated by the quotients of the differences obtained from Stewartson's Tables. The following, however, may assist the designer in computation of c_1 and c_2 . Let

$$\begin{aligned} t_1 &= \frac{1}{\sqrt{2}} \frac{1}{\sqrt{1 - \tau_0}} \\ t_2 &= \frac{1}{2\sqrt{2}} \frac{1}{\sqrt{1 + \tau_0}} \frac{3 - \tau_0}{1 - \tau_0} \\ t_3 &= \frac{1}{2\sqrt{2}} \frac{1}{\sqrt{3 - \tau_0}} \frac{1 + \tau_0}{1 - \tau_0} \end{aligned}$$

Also, for simplicity of writing, let

$$\begin{aligned} x &= b^2/a^2 \\ y &= \frac{c}{a(2j+1)} \end{aligned}$$

Then, in the ranges of τ_0 and x

$$\begin{aligned} 0 &\leq \tau_0 \leq 0.25 \\ 0 &\leq x \leq 0.10 \end{aligned}$$

the following formulas for the derivatives (for $n = 1$ mode) are accurate

$$\begin{aligned} D_x &\equiv \frac{\partial \tau_0}{\partial x} = 0.077 + 1.32x \\ D_y &\equiv \frac{\partial \tau_0}{\partial y} = 0.09 + 32.5x + (0.54 - 28.4x)y \end{aligned}$$

The formulas for c_1 and c_2 can now be expressed as

$$c_1 = 2xD_x t_1 + yD_y [t_1 - (t_2 - t_3) (c/a)^{-1}] \quad (9-9)$$

$$c_2 = 2xD_x t_1 + yD_y [t_1 + (t_2 + t_3) (c/a)^{-1}] \quad (9-10)$$

The following table provides the values of t_1 , $t_2 - t_3$, and $t_2 + t_3$

TABLE 9-1 VALUES OF t_1 , $t_2 - t_3$, AND $t_2 + t_3$ FOR VARIOUS τ_0 's

τ_0	t_1	$t_2 - t_3$	$t_2 + t_3$
0.00	0.707	0.857	1.265
0.04	0.722	0.846	1.292
0.08	0.737	0.836	1.324
0.12	0.754	0.829	1.359
0.16	0.772	0.820	1.400
0.20	0.791	0.812	1.446
0.24	0.811	0.807	1.501
0.28	0.833	0.800	1.562

As an example, take the case considered in Ch. 6: $x = 0.05$, $y = 1.20$, $\tau_0 = 0.16$, $c/a = 3.60$. We compute

$$D_x = 0.143$$

$$D_y = 0.659$$

then

$$c_1 = 2(0.05)(0.143)(0.772) + 1.20(0.659) \left(0.772 - \frac{0.820}{3.60} \right) = 0.44$$

$$c_2 = 2(0.05)(0.143)(0.772) + 1.20(0.659) \left(0.772 + \frac{1.400}{3.60} \right) = 0.929$$

as compared with Ch. 6 values of **0.44** and **0.916**, respectively. The agreement is good.

As was pointed out in Ch. 6 the viscous resonance band is bell-shaped, see Fig. 6-1, hence its width cannot be specified. It was suggested, therefore, that the pertinent width is to be determined relative to the aerodynamic damping — i.e., where, in the wings of the bell-shaped curve, the divergence due to the liquid is just balanced by the aerodynamic damping. Nevertheless, a convenient measure of the viscous resonance bandwidth is

$$\text{Width} = 2(\sqrt{S} \pm 6) \quad (9-11)$$

as compared with the inviscid width $= 2\sqrt{S}$.

9-3.2 REYNOLDS NUMBER

The Reynolds number of the rotating fluid is conveniently defined as

$$Re = \frac{\Omega a^2}{\nu} \quad (9-12)$$

where

$$\Omega = \left(\frac{2\pi}{nd} V \right) \text{ axial spin, rad/sec}$$

a = radius of the cavity of the projectile

d = diameter of projectile

ν = kinematic viscosity

V = velocity of projectile

If ν is expressed in stokes, then a must be expressed in centimeters.

Sometimes the designer is more familiar with the ratio of the viscosity of his working fluid to that of water, i.e., μ/μ_0 where μ is viscosity of his fluid and μ_0 is that of water. If, in addition, he knows the specific gravity σ' of his fluid, then remembering that the kinematic viscosity of water is 0.01 stoke, the kinematic viscosity of his fluid is simply

$$\nu = 0.01(\mu/\mu_0) 1/\sigma' \text{ stoke} \quad (9-13)$$

An example: what is Re of WP in the XM410 Projectile fired at $M = 1.5$?

$$n = 40 \text{ cal/turn}$$

$$d = 0.5 \text{ ft}$$

$$V = 1.5(1120) = 1680 \text{ ft/sec}$$

$$\therefore \Omega = 1056 \text{ rad/sec}$$

$$a = 2.68(2.54) = 6.8 \text{ cm}$$

Assume that the ratio of viscosities $\mu/\mu_0 = 2$, sp.gr. $\sigma' = 1.8$, then $\nu_{WP} = 1.1 \times 10^{-2}$ stoke and $Re = 4.1 \times 10^6$, by Eq. 9—12.

Viscous corrections are inversely proportional to the square root of the Reynolds number. Whether the viscous correction is significant or not depends on how accurately one knows the nutational and fluid frequencies; if these are known to three significant figures, a correction in the fourth place is insignificant. In other words, the usual engineering judgment must be exercised in considering significance of the corrections in view of other uncertainties. Correction to viscous damping δ , for example, must be judged relative to the size of \sqrt{S} . One can rapidly estimate the order of magnitude of these corrections by taking as representative values of $c_1 = 0.4$ and $c_2 = 1$.

9-3.3 DESIGN OF CYLINDRICAL CAVITIES

With the above preliminaries out of the way, one may consider now the design of a cylindrical cavity which will contain no fluid frequencies in a dangerous proximity to the nutational frequency of the projectile.

With the nutational frequency τ_n known from Eq. 9—4, the resonating fluid frequency is $\tau_0 = \tau_n - \epsilon$. Suppose the cavity is to be filled to a certain fraction of its volume, i.e., $1 - b^2/a^2$, say 0.95 or 95%. Therefore, $b^2/a^2 = 0.05$. In Stewartson's Tables, on the page marked $b^2/a^2 = 0.05$, find $\tau_0 = \tau_n - \epsilon$. In the first column, headed by

$c/[a(2j+1)]$ (first radial mode $n=1$), find the corresponding number, say, K_1 . Then all cylindrical cavities whose fineness-ratios satisfy the condition

$$(c/a)_1 = K_1(2j+1) \quad j = 0, 1, 2, \dots$$

will contain this resonating fluid frequency τ_0 . Similarly for the second radial mode, $n=2$

$$(c/a)_2 = K_2(2j+1) \quad j = 0, 1, 2, \dots$$

One can always neglect the third radial mode and in many instances even the second mode because of rapidly decreasing residues (2R) in higher radial modes. The hydrodynamic moment is proportional to 2R.

As stated above, the width of the viscous resonance band should be determined relative to the level of aerodynamic damping. However, for illustrative purposes, we can accept that the width is given by $2(\sqrt{S} \pm \delta)$. Therefore, all cavities with frequencies in the range of

$$\tau_n \pm (\sqrt{S} + \delta)$$

should be avoided. This range of frequencies can be readily converted into the range of fineness-ratios. Let

$$\tau_{01} = \tau_n + (\sqrt{S} + \delta)$$

$$\tau_{02} = \tau_n - (\sqrt{S} + \delta)$$

The width of the resonance band on the frequency scale is from τ_{01} to τ_{02} . From the same Stewartson's Table, on the line τ_{01} find the corresponding K_{11} . Then

$$(c/a)_{11} = K_{11}(2j+1) \quad j = 0, 1, 2, \dots$$

gives one bound for c/a ; similarly for $(c/a)_{12}$. The range of fineness-ratios to be avoided is from $(c/a)_{11}$ to $(c/a)_{12}$ about the central ratio $(c/a)_1$ of the exact resonance. Since δ depends slightly on $c/[a(2j+1)]$ through D_y , Eq. 9—10, it might be necessary to recompute its value for the edges of the band.

In principle, therefore, to design a cylindrical cavity which will contain no fluid frequencies in close proximity to the nutational frequency of the projectile is a simple and straightforward process. In practice the difficulty is usually encountered when S is large. With larger S the frequency band is broader and the range of the fineness-ratios to be avoided is correspondingly wider. It might become impossible to avoid this range because of other constraints imposed upon overall design of the projectile. We shall encounter this condition with the XM4 10 Projectile.

Perhaps a more common practical problem is when the projectile has been designed and produced for other purposes and is being adapted to carry liquid. The designer should investigate whether there is a danger that the cavity contains resonating fluid frequencies. We have dealt briefly with this problem in Ch. 4 in connection with Stewartson's Tables. The examples which follow illustrate in greater detail the proper procedure to be applied.

9-3.4 EXAMPLES

9-3.4.1 105 mm Chemical Projectile

We either estimated or previously measured the following characteristics:

$$\begin{aligned} I_x &= 0.0174 \text{ slug-ft}^2 \\ I_y &= 0.1727 \text{ slug-ft}^2 \\ m &= 1.06 \text{ slug} \\ n &= 27 \text{ cal/turn} \\ \rho_a &= 0.002378 \text{ slug/ft}^3 \\ d &= 0.34 \text{ ft} \\ a &= 0.13 \text{ ft} \\ c/a &= 2.65 \\ C_{M\alpha} &= 4.5 \\ M_f &= 0.087 \text{ slug} \end{aligned}$$

Compute:

$$P = \frac{I_x}{I_y} \left(\frac{2\pi}{n} \right) = 2.37 \times 10^{-2} \quad (\text{see Eq. 2-3})$$

$$4M = 4 \left(\frac{\rho_a S d}{2m} \right) k_y^{-2} C_{M\alpha} = 4.6 \times 10^{-2} \quad (\text{see Eq. 2-3})$$

$$s_g = \frac{P^2}{4M} = 1.2 \quad (\text{see Eq. 2-7})$$

$$\sigma = \sqrt{1 - \frac{1}{s_g}} = 0.41 \quad (\text{see Eq. 9-3})$$

$$\tau_n = \frac{I_x}{2I_y} (1 \pm \sigma) = 0.07 \quad (\text{see Eq. 9-4})$$

The gyroscopic stability factor appears to be too low, i.e., less than **1.3**. If WP becomes liquid, then at the muzzle the **gyroscopic** stability factor becomes (see par. 2-5)

$$(s_g)_L = (s_g)_R \left(\frac{I_{x0}}{I_{x0} + i_{x0}} \right)^2 \quad (\text{see Eq. 9-2c})$$

$$i_{x0} = 0.0007 \text{ slug-ft}^2$$

$$I_{x0} = I_x - i_{x0} = 0.0167 \text{ slug-ft}^2$$

$$\therefore (s_g)_L = 1.2 \left(\frac{0.0167}{0.0174} \right)^2 = 1.1$$

which is undesirably low. Therefore, modification of the twist **of rifling** is desirable. Let $n = 20$. With this twist

$$(s_g)_L = 2.23, \quad \sigma = 0.74, \quad \tau_n = 0.088$$

Next check whether viscous effects are important. Suppose this projectile is to be fired at $V = 1680 \text{ ft/sec}$. What is the Reynolds number of the spinning liquid?

$$\Omega = \frac{2\pi}{nd} V = 1534 \text{ rad/sec}$$

$$a = 0.13 \text{ (12) } (2.54) = 4.0 \text{ cm}$$

$$\nu = 1.1 \times 10^{-2} \text{ stoke}$$

By Eq. 9—12, $Re = 2 \times 10^6$. Let us estimate the viscous corrections using rough values of c_1 and c_2 , i.e., 0.4 and 1, respectively. Then correction to the frequency, Eq. 9—5, is $\epsilon = 0.0003$ and can be neglected. The correction to the damping, Eq. 9—7, is $\delta = 0.0007$. As we shall see in a moment, $\sqrt{S} = 2.1 \times 10^{-3}$. Thus the viscous correction to the damping is on the border line of acceptability. For the present, let us neglect it also.

Suppose now that the cavity is to be fitted to 97% or $b^2/a^2 = 0.03$. Since the fineness-ratio of the cavity is fixed, $c/a = 2.65$, in order to find whether it contains resonating fluid frequencies, construct the following table:

j	$\frac{2.65}{(2j+1)}$	$\tau_0(nj)$	$2R$
	$\frac{2.65}{(2j+1)}$		
0	2.65	—	—
1	0.883	0.25(2, 1)	0.670
2	0.530	0.089(2, 2)	0.0334
3	0.379	0.17(3, 3)	0.0208

τ_0 and $2R$ are found from the table for $b^2/a^2 = 0.03$ by simple interpolation corresponding to various values of $c/[a(2j+1)]$. Clearly, there is a possibility of resonance with $\tau_0 = 0.089(2, 2)$ since $\tau_n = 0.088$. Compute Stewartson's parameter.

$$S = \frac{\rho_a a^5}{I_x \sigma c/a} (2R)^2$$

$$\rho_{WP} = 3.49 \text{ slug/ft}^3$$

$$a^5 = 0.37 \times 10^{-4} \text{ ft}^5$$

$$I_x = 0.0174 \text{ slug-ft}^2$$

$$\sigma = 0.74 \text{ (from previous calculation)}$$

$$c/a = 2.65$$

$$\therefore S = 0.38 \times 10^{-2} (2R)^2$$

For $j = 2$, $n = 2$, $S = 4.2 \times 10^{-6}$ and $\sqrt{S} = 2.1 \times 10^{-3}$. Thus by Stewartson's criteria for instability, Eq. 9—8, since we have found that ϵ and δ may be neglected

$$-1 < \frac{\tau_0 - \tau_n}{\sqrt{S}} < 1$$

$$\frac{0.089 - 0.088}{2.1 \times 10^{-3}} = 0.50 \text{ unstable}$$

The width of the frequency band present in this cavity is from $\tau_{01} = 0.089 \pm 0.002 = 0.091$ to $\tau_{02} = 0.089 - 0.002 = 0.087$. However, the resonance band, i.e., the range of frequencies to which the projectile responds, is from $\tau_{01} = \tau_n \pm \sqrt{S} = 0.088 \pm 0.002 = 0.090$ on the high side, but only $\tau_{02} = 0.087$ on the low side because frequency 0.086 is not present. In the present case these finer points are fairly meaningless because of small differences involved and the uncertainty of the numbers. However, it is important to realize that in a given cavity, i.e., $c/[a(2j+1)]$, a band of frequencies

$\tau_0 \pm \sqrt{S}$ may be present — this is the property of the fluid; but the resonance band, i.e., the frequencies to which the projectile responds, is $\tau_n \pm \sqrt{S}$. The two are co-extensive only in the case of exact resonance, i.e., if $\tau_0 = \tau_n$. Otherwise the resonance band will be asymmetric — terminating, on one side or the other, with the available frequencies. We shall see more of this in a better example later.

The fineness-ratios corresponding to the limits of the resonance band are $c/a = 2.65$ and 2.64, respectively. The band is very narrow and the cavity is just on the edge of its resonance band.

Now, having established that resonance occurs at $j = 2$ and with $x = b^2/a^2 = 0.03$, one can recompute viscous corrections more accurately by Eqs. 9-5 and 9-7 in order to be sure that our neglect of these corrections was justifiable. If so done, one finds $\epsilon = 0.0001$ and $\delta = 0.0004$ instead of our rough values of 0.0003 and 0.0007, respectively. Hence, their neglect was justifiable.

The maximum rate of divergence of the nutational amplitude due to this instability is

$$\lambda = \frac{\pi}{nd} \sqrt{S - (\tau_0 - \tau_n)^2} \quad \text{per ft}$$

$$\lambda = \frac{3.14}{(20)(0.344)} \sqrt{4.2 \times 10^{-6} - (0.089 - 0.088)^2}$$

$$\lambda = 0.82 \times 10^{-3} \quad \text{per ft}$$

This is to be added to the aerodynamic damping of the nutational component λ_1 . The algebraic sum of the two rates will control the nutational amplitude.

Since the resonance band is so narrow; theoretically, a minor modification of the fineness-ratio of the cavity will remove it from resonance. Thus $c/a = 2.60$ or $c/a = 2.70$ will suffice. However, in practice, one should consider possible evaporation of the liquid with a consequent increase in b^2/a^2 . Suppose, therefore, that some liquid evaporates and the fill-ratio becomes $b^2/a^2 = 0.10$. How are the fluid frequencies affected? In the present case, if the cavity were modified to $c/a = 2.60$, the fluid frequency (2, 2) becomes $\tau_0 = 0.125$; if the choice were $c/a = 2.70$, τ_0 becomes 0.15. In the present case, therefore, evaporation of the liquid makes the projectile even safer. This, of course, need not always be the case. If the design of the cavity places τ_0 below τ_n on the frequency scale, then the shift of τ_0 toward higher frequencies due to evaporation may result in resonance.

Another source of possible difficulty is the lack of precision in the knowledge of

the fineness-ratio of the actual cavity. The designer may well impose a specification on the bounds of c/a . He can then perform the analysis for the minimum and the maximum values of c/a . In other words, care should be exercised in foreseeing various eventualities.

9-3.4.2 75 mm Chemical Projectile

The projectile has the following characteristics:

$$I_x = 0.386 \times 10^{-2} \quad \text{slug-ft}^2$$

$$I_y = 4.39 \times 10^{-2} \quad \text{slug-ft}^2$$

$$m = 0.460 \quad \text{slug}$$

$$M_f = 0.0125 \quad \text{slug}$$

$$n = 25 \quad \text{cal/turn}$$

$$C_{M_\alpha} = 4.91$$

$$a = 0.085 \quad \text{ft}$$

$$c/a = 3.25$$

Therefore

$$P = 2.21 \times 10^{-2}$$

$$4M = 3.68 \times 10^{-4}$$

$$s_g = 1.33, \sigma = 0.67, \tau = 0.073$$

Check whether s_g is large enough if WP becomes liquid

$$i_{x0} = 0.00005 \quad \text{slug-ft}^2$$

$$I_{x0} = 0.00381 \quad \text{slug-ft}^2$$

$$\therefore (s_g)_L = 1.30$$

which is acceptable.

Next compute the Reynolds number of the spinning fluid. Suppose $V = 2000 \text{ ft/sec}$.

$$\Omega = 2043 \quad \text{rad/sec}$$

$$a = (0.085)(12)(2.54) = 2.6 \quad \text{cm}$$

$$\nu = 1.1 \times 10^{-2} \quad \text{stoke}$$

$$\therefore \text{Re} = 1.1 \times 10^6$$

By the previous example, since $\text{Re} \sim 10^6$, viscous effects can be neglected.

Suppose the cavity is to be filled to 97%, i.e., $b^2/a^2 = 0.03$. Construct the following table

<u>j</u>	<u>$\frac{3.25}{2j+1}$</u>	<u>$\tau_0(nj)$</u>	<u>2R</u>	<u>S</u>	<u>\sqrt{S}</u>	<u>$\frac{\tau_0 - \tau_n}{\sqrt{S}}$</u>
0	3.25	—	—			
1	1.083	0.074(1, 1)	0.225	0.93×10^{-4}	0.96×10^{-2}	0.10
2	0.464	—	—			

Compute Stewartson's parameter S. Its value is inserted in the above table together with the test for instability.

The band of frequencies present in this cavity is $\tau_0 \pm \sqrt{S} = 0.074 \pm 0.010$. Since $\tau_n = 0.073$, the resonance band is from $\tau_{01} = 0.073 \pm 0.010 = 0.083$ on the high side, and to the limit of frequency band $\tau_{02} = 0.064$. These frequency limits of the resonance band correspond to the fineness-ratios from $c/a = 3.29$ to 3.21, respectively.

The maximum rate of divergence is

$$\lambda = 4.9 \times 10^{-3}, \text{ per ft}$$

Again, this instability can be easily removed by modifying c/a of the cavity either to 3.2 or lower, or to 3.3 or higher. Remarks at the end of the first example should be kept in mind. Check again for possible instability in the new cavity.

9-3.4.3 XM410 Projectile

As before, see par. 4-3, we shall consider this projectile as containing a cylindrical cavity $c/a = 1\%$. In par. 4-3 it was found that the fundamental fluid frequency present in this cavity is $\tau_0 = 0.34$. With $\sqrt{S} = 0.25$, the frequency band covers the range $\tau_0 \pm \sqrt{S} = 0.34 \pm 0.25$ or from 0.59 to 0.09. The nutational frequency, however, is $\tau_n = 0.25$. Since the projectile is unstable only when (Eq. 9-8 neglecting ϵ and δ)

$$S - (\tau_0 - \tau_n)^2 > 0$$

the resonance band is $\tau_{01} = \tau_n + \sqrt{S} = 0.25 + 0.25 = 0.50$ on the high side, but on the lower side it does not go to $\tau_{02} = \tau_n - \sqrt{S} = 0.25 - 0.25 = 0.00$ but only to the lowest frequency which is present in the cavity, i.e., 0.09. Therefore, the resonance band is asymmetric. The corresponding fineness-ratios are $c/a = 2.2$ and 1.1, respectively.

As we have seen, this projectile is violently unstable and unless one is willing to reduce the c/a of the cavity below 1.1, or to increase it above 2.2, no minor modifications will remove it from resonance instability. With any major modification it is essential to recompute τ_n and to perform analysis anew.

To change the fineness-ratio, one can either lengthen the cavity or reduce its diameter. Let us try the latter alternative. Suppose we reduce the diameter of the cavity to, say, 90%, or $a/a_0 = 0.90$ where a_0 is the original radius. If we make the walls of the cavity thicker, the added mass of steel will significantly alter the projectile's inertial properties thus changing τ_n . Simple computations show the following effects of the modification:

	<u>Original</u>	<u>Modified</u>
c/a	1.56	1.73
τ_n	0.25	0.31
τ_0	0.34	0.40
\sqrt{S}	0.25	0.18
$\frac{\tau_0 - \tau_n}{\sqrt{S}}$	0.37	0.52 (unstable)

There is only a very slight improvement. The improvement could be enhanced if one were to insert a sleeve of density equal to that of WP, thus retaining the inertial properties of the original projectile. Similar computations, as above, show that with such an arrangement it is still necessary to reduce the diameter of the cavity to 80% in order to remove this projectile from instability. The volume of the reduced cavity will only be 64% of the original.

9-3.5 CYLINDRICAL CAVITY WITH CENTRAL BURSTER

Thus far we have considered only unencumbered cylindrical cavities. However, many chemical projectiles use bursters in a form of a centrally located cylindrical column. The analysis of such configurations is only slightly different from that of a plain cylindrical cavity.*

Consider, therefore, that a cylindrical cavity contains a central cylindrical burster of external diameter $2r$ with volume v_r . The volume of the cylinder without the burster is V_c . Suppose the available volume $V_c - v_r$ is to be filled to a certain fraction, say, β , i.e.,

$$\beta(V_c - v_r) = \beta V_c(1 - r^2/a^2)$$

Relative to the cylindrical volume V_c , this amount of liquid will occupy a fraction of V_c volume, i.e., $V_c(1 - b^2/a^2)$. Therefore,

$$V_c(1 - b^2/a^2) = \beta V_c(1 - r^2/a^2)$$

or

$$b^2/a^2 = 1 - \beta(1 - r^2/a^2) \quad (9-14)$$

For a cylindrical cavity with a central burster, if the available cavity is filled to β fraction, we should enter Stewartson's Tables with the above b^2/a^2 and not with $1 - \beta$.

*For a treatment of cavities with partial bursters see Appendix B.

For example: the cavity of the XM410 Projectile has a central burster for which $r/a = 0.29$. Suppose the available cavity is to be filled to 93%, i.e., $\beta = 0.93$, then

$$b^2/a^2 = 1 - 0.93[1 - (0.29)^2] = 0.15$$

For the XM410 Projectile with a cylindrical burster cavity one finds from Stewartson's Tables with $b^2/a^2 = 0.15$

$$\tau_0 = 0.346 \text{ and } \sqrt{S} = 0.26$$

or essentially the same situation as without the burster. Changing the fill-ratio does not improve the situation either, as the following table illustrates:

P	0.93	0.82	0.71
b^2/a^2	0.15	0.25	0.35
τ_0	0.35	0.36	0.39
\sqrt{S}	0.26	0.28	0.30
$\frac{\tau_0 - \tau_n}{@-}$	0.37	0.41	0.47

By Stewartson's instability criteria, all configurations are unstable.

9-3.6 100% FILLED CAVITY WITH CENTRAL BURSTER

If one were to consider a cavity with such a burster, and 100% fill; then Stewartson's Tables become inapplicable and one should use the special Central Column Tables given in Ch. 4. For the XM410 Projectile with

$$r/a = 0.29, \quad r^2/a^2 = 0.084, \quad c/a = 1.56$$

one finds from these tables

$$\begin{aligned} \tau_0 &= 0.50 \\ \sqrt{S} &= 0.33 \\ \frac{\tau_0 - \tau_n}{\sqrt{S}} &= 0.76 \text{ (unstable)} \end{aligned}$$

The frequency band is even broader than for a partially filled cavity and covers the range of frequencies from $\tau_{01} = 0.83$ to $\tau_{02} = 0.17$. It is to be noted, however, that as the principal fluid frequency recedes from the nutational frequency, the latter comes closer and closer to the edge of the frequency band. The tables show that for a given $c/[a(2j+1)]$, τ_0 increases as r/a increases. Thus it is conceivable that for this projectile by changing the diameter of the burster an eventual stability may be achieved. This is illustrated in the following table:

r^2/a^2	0.05	0.084	0.15
τ_0	0.45	0.50	0.57
\sqrt{S}	0.32	0.33	0.34
$\frac{\tau_0 - \tau_n}{\sqrt{S}}$	0.63	0.76	0.95

Thus it is possible to achieve stability, at least in principle, by this means if one is willing to pay the price of, say, a 20% reduction in the volume of the cavity. The problem also arises whether a $r^2/a^2 = 0.20$ or $r/a = 0.45$ burster could be inserted through the fuzing hole. It is to be noted, however, that in this exercise τ_n was kept constant. In practice, changing the size of the burster will alter the inertial properties of the projectile thereby changing τ_n . This, of course, should be taken into account in the analysis. However, to fill the cavity 100% is difficult and undesirable because some unoccupied volume must always be provided for possible expansion of the liquid. Accordingly, the cavity is likely to be always only partially filled.

Experiments with the gyroscope showed that if the air gap between the burster and the free liquid surface is reduced below a certain critical value, a very marked reduction in instability occurs? This is due to interference by the central cylindrical column with the oscillations of the free

liquid surface. For the gyroscope, with $c/a = 3.08$, $a = 2.5$ -in. cavity, and $b^2/a^2 = 0.15$, the critical gap was found to be

$$b/a - r/a = 0.05$$

If these experiments have general validity, they suggest that it is possible, in a given burstered cavity, to find a critical fill-ratio which will markedly reduce the instability.

As an example, for the XM410 Projectile with a burster $r/a = 0.29$, if completely filled, $\tau_0 = 0.50$ and the projectile is unstable. If the above rule is to be applied, the critical fill-ratio should be

$$b/a < 0.29 + 0.05 = 0.34$$

or less than $b^2/a^2 = 0.12$ which, corresponds to 96% fill of the burstered cavity. The experiments suggest, therefore, that if one fills more than 96%, there might be interference with a consequent marked reduction of instability.

However, this method of stabilization, even if it works, is of very precarious nature because the liquid may evaporate with a consequent increase in the air gap and a return to a severe instability.

The above technique might also fail if the nutational frequency of the projectile lies between τ_0 as given by Stewartson's Tables for a prescribed b^2/a^2 and τ_0 as obtained from the Central Column Tables for $r^2/a^2 \approx b^2/a^2$. The latter τ_0 is always higher. In the example above for the XM410 Projectile with burster for $b^2/a^2 = 0.15$ (93% full), $\tau_0 = 0.35$; if this cavity is completely filled, $\tau_0 = 0.50$. Thus there is a sharp transition of the frequencies from $\tau_0 = 0.35$ for 93% full to $\tau_0 = 0.50$ for 100% full. If the nutation frequency of the projectile lies in such a gap of frequencies as, say, $\tau_0 = 0.40$, transitional instability might occur as the cavity is filled through the critical range of fill-ratios, i.e., from 93% to 100%. Further discussion of this problem may be found in Ref. 4.

9-3.7 PARTITIONING OF THE CAVITY

Partitioning of the cylindrical cavity by longitudinal baffles sometimes is used by designers as a solution for instability of liquid-filled projectiles. At the present time, however, no theory is available for considering such a design on a rational basis. The problem presents very formidable mathematical difficulties (see Ch. 7). Thus far, several attempts at an approximate theoretical solutions have proved unsuccessful.

However, partitioning of the cylindrical cavity by a transverse baffle or plate, thus dividing the cavity into two cylindrical cavities, presents no difficulty. Each cavity, in turn, can be treated by Stewartson's theory.

9-3.7.1 Full Transverse Baffles

Let us apply this to the XM410 Projectile — a difficult case. As we have seen, the resonance band of this projectile — containing a cylindrical cavity and a burster, with 93% fill — is very broad. It covers a frequency range from $\tau_{01} = 0.50$ to $\tau_{02} = 0.09$, corresponding to the fineness-ratios c/a from 2.2 to 1.1, respectively. Suppose, therefore, we try placing a diaphragm or a baffle at $c/a < 1.1$, say, at $c/a = 1.00$. With such an arrangement, one cavity will have a fineness-ratio $c_1/a = 1.00$; while the other, $c_2/a = 1.56 - 1.00 = 0.56$. We neglect the thickness of the partition, which can be easily taken into account. Performing the analysis of these two cavities in the usual manner, we find the following

$$b_2/a_2 = 0.15, \tau_n = 0.25$$

	c_1/a	c_2/a
$\tau_0(nj)$	0.03(1, 0)	0.22(2, 0)
\sqrt{S}	0.02	0.03
$\frac{\tau_0 - \tau_n}{\sqrt{S}}$	-10.5 (stable)	-1.18 (stable)

Therefore, with such a partition the XM410 Projectile becomes stable. Since the air gap between the free surface of the liquid and the burster — when the liquid is fully spinning — is $b - r = 0.27$ in., the partition need not completely separate the two chambers. The gap between the partition and the burster must, however, be less than $(b - r)$ so that at full spin there will be no communication of the liquid between the two chambers.

A minor problem arises. Suppose that the diameter of the central hole in the partition, for loading purposes and for admitting the burster, is $2r_1$. Clearly, $r_1 > r$ where $2r$ is the diameter of the burster. The loading or the fill of the cavity must be such that $b > r$, where $2b$ is the diameter of the air column. If these conditions are satisfied then, at full spin, there will be no communication of the liquid between the two chambers. However, in the nature of things, there is no assurance that b will be the same in both chambers. It might well happen that there will be slightly more liquid in one chamber than in the other. Thus the diameters of the air columns, or the "effective" fills, in the two chambers will be different. The minimum b in either chamber will be $b = r_1$. Therefore, one should examine this contingency.

Let b_1^2/a^2 be the fill-ratio of the chamber whose fineness-ratio is c_1/a ; and $b_2^2/a^2, c_2/a$ for another chamber. Then, if the overall fill-ratio is b^2/a^2 and the fineness-ratio of the whole cavity is c/a :

$$b^2/a^2(c/a) = b_1^2/a^2(c_1/a) + b_2^2/a^2(c_2/a) \quad (9-15)$$

The two extreme configurations are when either $b_1 = r_1$ or $b_2 = r_1$, provided, of course, that $b > r_1$. From the above relation, the fill-ratios in the two chambers can be determined and the analysis of stability performed in the usual manner.

As an example, consider the XM410 Projectile with a partitioned cavity as above, i.e.,

$$b^2/a^2 = 0.15, c/a = 1.56, c_1/a = 1.00,$$

$$c_2/a = 0.56, a = 2.68 \text{ in.}$$

Suppose $r_1 - r = 0.125 \text{ in.}$

(1) Case 1: $b_1 = r_1$. What is b_2 and what are the consequences of such distribution?

$$r_1/a = r/a + 0.125/a = 0.29 + 0.0337 = 0.324$$

$$r_1^2/a^2 = b_1^2/a^2 = 0.10$$

$$\therefore b_2^2/a^2 = 0.24$$

Such distribution of the liquid in the two chambers leads to $\tau_0 = 0.017$ in the c_1/a chamber (instead of $\tau_0 = 0.03$ for $b^2/a^2 = 0.15$), and $\tau_0 = 0.305$ (instead of $\tau_0 = 0.22$) in the c_2/a chamber. Thus it is a beneficial shift of the frequencies, i.e., away from $\tau_n = 0.25$.

(2) Case 2: $b_2 = r_1$

$$b_2^2/a^2 = 0.10$$

$$\therefore b_1^2/a^2 = 0.18$$

The new frequencies are: $\tau_0 = 0.048$ and 0.175 in chambers 1 and 2, respectively. Such an analysis is worth performing for safety.

Examination of Stewartson's Tables will show that if the thickness of the partition is taken at the expense of the smaller chamber, i.e., $c/a = 0.56$, the fluid frequency in this chamber will shift to the lower frequency and, hence, away from resonance. Similarly, if the overall fill-ratio is increased from 93% to, say, 95% or 96%, the frequencies in both chambers will shift to lower values. From Stewartson's Tables one can find other positions of the transverse baffle which will give a stable projectile.

9-3.7.2 Partial Transverse Baffles

To incorporate a transverse baffle into the projectile's cavity is difficult. If the

transverse baffle offers the only solution to the projectile's instability, then — if the projectile is already built — it has to be cut, the baffle welded into place, and the pieces put together again — a costly process. If the baffle could be introduced into the cavity during the manufacture of the projectile, i.e., before the nose is formed, this would simplify the problem considerably. At any rate, if the transverse baffle is the only solution, incorporating it into the cavity must be left to the ingenuity of the designer.

It would be much simpler if a partial plate, i.e., one not extending through the diameter of the cavity, could do the job. Such a plate could, perhaps, be attached to the burster and be inserted into the cavity through the fuze hole. The effectiveness of partial plates was examined by the previously unreported experiments described below.

The cavity in the gyroscope, described in Ch. 5, has a fineness-ratio $c/a = 3.077$ which was designed to resonate at 85% fill-ratio, i.e., $b^2/a^2 = 0.15$. The fractional radius of the air column, therefore, at full spin, was $b/a = 0.39$. A rod of 3/8-in. diameter was placed along the center line of the cavity. On this rod discs of various diameters could be placed at various positions thus dividing the original cavity c/a into two cavities c_1/a and c_2/a , respectively. The response of the system to various configurations was determined by measuring the maximum divergence rate of the nutational amplitude.

In the original cavity the resonance occurred when $\tau_n = \tau_0(1,1) = 0.055$. It is to be recalled that (1,1) mode corresponds to radial mode $n = 1$, and the axial mode $j = 1$. $j = 1$ signifies that there are 3/2 waves of axial pressure fluctuations in the cavity (varying as the cosine of the distance), or 3/2 waves of axial velocity fluctuations (varying as the sine of the distance) with a node, i.e., axial velocity $w = 0$ at each end. Thus the cavity can be divided into six quarter-wavelength steps. A schematic of various velocity waves in each cavity, c_1/a and c_2/a , respectively, is shown in Fig. 9-1.

$$c/a = 3.077, \tau_n = .055 = \tau_0(1,1)$$

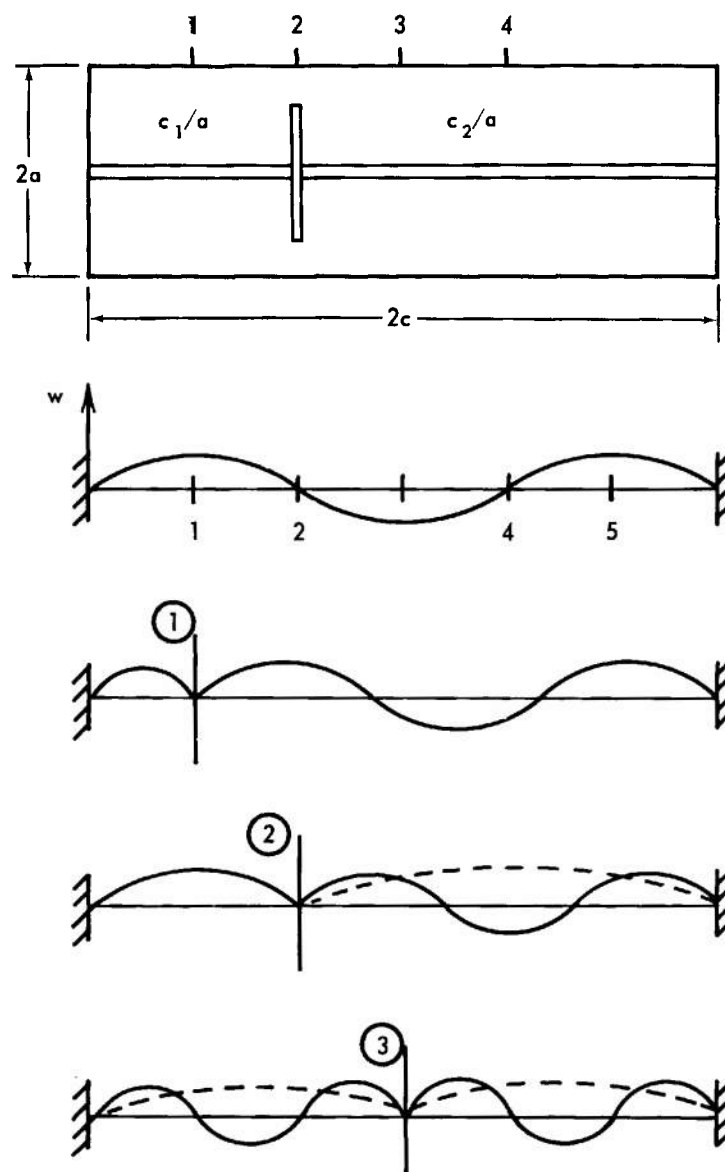


FIGURE 9-1. A SCHEMATIC OF THE AXIAL VELOCITY DISTRIBUTIONS FOR VARIOUS POSITIONS OF THE TRANSVERSE BAFFLE

Let $2r_1$ be the diameter of the disc and its position from, say, the bottom of the cavity, be designated as **1,2,3,..** etc., corresponding to **1/4, 2/4, 3/4,** etc., of the wavelength. Let λ_0 be the maximum rate of divergence for the original cavity. Then we can express the effectiveness of the partial baffle as the ratio of its λ to λ_0 for various discs and positions. The results are summarized in Table 9-2.

TABLE 9-2 EFFECTIVENESS OF PARTIAL BAFFLES

r_1/a	0.91	0.86	0.81	0.76	0.71	0.50
Position	λ/λ_0					
1	0.00	0.00	0.00	0.00	0.20	0.26
2	0.91	0.79	0.87	0.85	0.80	0.77
3	0.00	0.00	0.01	0.21	0.53	0.75
4	0.68	0.95	0.90	0.90	0.87	0.65

Because of symmetry, see Fig. 9-1, Position 4 is the same as Position 2, and Position 5 is the same as 1. Position 5 was not measured.

If one regards each cavity as completely inclosed, then the analysis for fluid frequencies in each cavity can be performed in the usual manner. The results are given in Table 9-3.

TABLE 9-3 FLUID FREQUENCY ANALYSIS

Baffle Position	c_1/a	$\tau_i(nj)$	c_2/a	$\tau_0(nj)$
	$2i \pm 1$		$2i \pm 1$	
1	0.495	0.13 (2,0)	2.546	0.45 (2,1)
2	1.008	0.055(1,0)	2.033	0.46 (1,0) 0.33 (2,1)
3	1.521	0.33 (1,0) 0.15 (2,1)	1.521	0.33 (1,0) 0.15 (2,1)
4	2.033	0.46 (1,0) 0.33 (2,1)	1.008	0.055(1,0)

Thickness of the disc was taken into account in its positioning. The position was measured to half-thickness $\frac{1}{2}t/a = 0.018$.

Resonant frequency, $\tau_n = 0.055$, is present in the c_1/a cavity at Position 2, and at Position 4 in the c_2/a cavity. For other positions of the disc there are no resonances. The appearance of instabilities with smaller discs, for Positions 1 and 3, Table 9-2, is a reflection of their ineffectiveness in suppressing the original resonance in the unencumbered cavity.

Two features are to be noted in Table 9-2: (1) a partial plate, extending to not less than **3/4** of the diameter of the cavity, for $b^2/a^2 = 0.15$, effectively suppresses the original resonance. The most effective position for such a baffle appears to be at a quarter of the wavelength from either end, and (2) even a relatively small disc $r_1/a = 0.50$, at Position 1, has reduced the instability to one quarter of its original value. Sometimes such a reduction might bring the instability within control of the aerodynamic damping and, hence, be beneficial.

The theoretical ratio of λ/λ_0 for resonating cavities — considering cavity 2 or 4 as completely separated, and taking into account different effects of viscosity in the smaller and the original cavities — is **1.65**. The observed ratios for different discs are only about half as great. This suggests that a partial baffle interferes with the flow sufficiently so as to reduce the instability to about one-half of its theoretically predicted value.

9-3.7.3 Cylindrical Partition

Another type of partitioning of the cylindrical cavity was suggested by Frasier (BRL). Following the idea discussed in par. 9-3.6 of changing the diameter of the burster as a means of shifting the fluid frequencies in a **100%**filled cavity, Frasier suggested inserting a cylindrical partition in a place of a large burster. Thus the cavity will be divided into two parts: (1) an annular outer cavity of diameter $2a$ and an inner diameter $2r_c$, i.e., that of the cylindrical partition, and (2) an inner cavity of outer diameter $2r_c$, if the thickness of the partition be neglected, and of inner diameter $2r_b$ — the diameter of the actual

burster. The outer cavity is to be filled **100%** the inner cavity can be only partially filled. In other words, in the exercise of par. 9—3.6 the “larger burster” is to be replaced by a thin-walled “can” while retaining the actual smaller burster in the inner cavity. The “can” may be partially perforated for ease of loading the liquid and for assurance that the liquid will be properly distributed in the two cavities at full spin. It is undesirable to make this “can” into a sieve but only to provide enough perforations for loading purposes.

Let us apply this idea to the **XM410** Projectile. In par. 9—3.6 it was stated that if the diameter of the burster is $r_c^2/a^2 = 0.20$ and the cavity is **100%** filled, the projectile will be stable. Let us confirm this assertion with greater care. From the Central Column Tables, Table 4—2 for $r_c^2/a^2 = 0.20$, $c/[a(2j + 1)] = 1.56$ for $j = 0$, we find $\tau_0 = 0.615$, $2R = 1.712$. From par. 4—3, $S = 3.81 \times 10^{-2}(2R)^2$. Therefore, $\sqrt{S} = 0.332$. With $\tau_n = 0.25$, applying Stewartson's instability criteria, Eq. 9—8 with viscous effects neglected,

$$\frac{\tau_0 - \tau_n}{\sqrt{S}} = \frac{0.615 - 0.25}{0.332} = 1.09 \text{ stable}$$

Therefore, in the **100%** filled outer cavity the fundamental fluid frequency is sufficiently far removed from the nutational frequency of the projectile to cause no trouble.

Consider now the inner cavity. If we neglect, in this exercise, the thickness of the wall of the cylindrical partition, the outer diameter of the inner cavity is $2r_c$ whereas the inner diameter is that of the burster $2r_b$. Therefore, we have $r_c/a = \sqrt{0.20} = 0.45$ and $r_b/a = 0.29$ (par. 9—3.6). The fineness-ratio of the inner cavity is

$$c/r_c = (c/a)(a/r_c) = 1.56/0.45 = 3.47$$

If the whole volume of the burstered cavity, disregarding the volume of the partition, is filled to β fraction, then, by Eq. 9—14

$$b^2/a^2 = 1 - \beta(1 - r_b^2/a^2)$$

Relative to the inner cavity, however, whose outer diameter is $2r_c$, the fractional air volume is

$$b^2/r_c^2 = (b^2/a^2)(a^2/r_c^2)$$

Using the same values as in par. 9—3.5, we have $\beta = 0.93$ and $b^2/a^2 = 0.15$. Therefore, relative to the inner cavity the fractional air volume is

$$b^2/r_c^2 = 0.15/0.20 = 0.75$$

Thus an inner cavity has a fineness-ratio $c/r_c = 3.47$ and a fill-ratio $1 - b^2/r_c^2 = 0.25$. To find the fluid frequencies in this cavity we go to Stewartson's Tables, Table 4—1, with $b^2/r_c^2 = 0.75$ (interpolating) and form the following table:

	$\frac{3.47}{2j + 1}$	$\tau_0(nj)$	$2R$
0	3.47	—	—
1	1.157	0.49(1,1)	1.164
2	0.694	0.20(1,2)	0.270

Stewartson's parameter S has to be computed for the diameter of the inner cavity.

$$S = \frac{\rho r_c^5}{I_x \sigma c / r_c} (2R)^2 = \left(\frac{\rho a^5}{I_x \sigma c / a} \right) (r_c/a)^6 (2R)^2$$

In par. 4—3 the value of the first factor was found to be 3.81×10^{-2} . Therefore

$$S = 3.81 \times 10^{-2} (r_c/a)^6 (2R)^2$$

or

$$\sqrt{S} = 0.195 (r_c/a)^3 (2R)$$

with $r_c/a = 0.45$, $(r_c/a)^3 = 0.091$, Stewartson's test for instability is

i	\sqrt{S}	$\tau_0 - \tau_n$	$\frac{\tau_0 - \tau_n}{\sqrt{S}}$	
1	0.0206	0.24	11.7	stable
2	0.0048	-0.05	-10.4	stable

Therefore, with such cylindrical partitioning of the cylindrical cavity, neither the outer nor the inner cavities will contain fluid frequencies in close proximity to the nutational frequency of this projectile. This, therefore, is another way of stabilizing the XM410 Projectile and, from the design point of view, this method may be much simpler than the insertion of a transverse baffle.

9-4 NONCYLINDRICAL CAVITIES

Thus far we have considered only cylindrical cavities, the geometry for which Stewartson's theory applies. However, in practice most of the cavities are not cylindrical; the projectiles are usually streamlined and the cavity, in general, follows the outer form. For such cavities no general theory is available and the discussion in par. 3-7.1 outlines the reasons. Nevertheless, Wedemeyer² has succeeded in extending Stewartson's theory to noncylindrical cavities provided, as is pointed out in Ch. 7, that variation of the radius of the cavity with the axial distance is small, i.e., $\left| \frac{da(z)}{dz} \right| \ll 1$. Fortunately, however, the

experiments conducted with the gyroscope with noncylindrical cavities showed that Wedemeyer's theory has much broader validity than the above inequality would suggest. It can, therefore, be applied with some confidence to the cavities of many projectiles. The reasons for its broader validity are suggested in par. 7-2.5.

Wedemeyer has shown that in a noncylindrical cavity either the fill-ratio b^2/a^2 can be obtained for a given eigenfrequency τ_0 ,

or the eigenfrequency for a given fill-ratio, from the following condition

$$1 = \frac{1}{2c} \int_0^{2c} \frac{1}{K_n} \frac{c}{a(2j+1)} dz \quad (9-16)$$

where K_n is a tabulated function in Stewartson's Tables, and is a function of b^2/a^2 and τ_0 . The above integral represents an average value of $c/[a(2j+1)]$ in a noncylindrical cavity weighted according to $1/K_n$ values. Since K_n is a function of b^2/a^2 and, hence, of $a(z)$, it will vary throughout the noncylindrical part of the cavity.

The evaluation of Eq. 9-16 is inconvenient since K_n is given only in a tabular form as a function of τ_0 and b^2/a^2 . However, $1/K_n$ can be represented analytically by fitting polynomials to the tabulated values. To facilitate the solution of both problems, i.e., finding b^2/a^2 for a given τ_0 , or finding τ_0 for a given b^2/a^2 , we shall represent $1/K_n$ as a function of both of these variables. Fortunately, this is found to be relatively simple.

$$\text{Let} \quad x = b^2/a^2$$

then within the following limits of τ_0 and x

$$\begin{aligned} 0 &\leq \tau_0 \leq 0.36 \\ 0 &\leq x \leq 0.40 \end{aligned}$$

the following polynomial representation of $1/K_1$ for radial mode $n=1$, and $1/K_2$ for radial mode $n=2$, is accurate:

$$\begin{aligned} \frac{1}{K_1} &= 0.996 + 0.115x + 0.926x^2 \\ &\quad - (1.007 + 0.942x - 0.590x^2) \tau_0 \end{aligned} \quad (9-17)$$

$$\begin{aligned} \frac{1}{K_2} &= 2.056 + 1.390x + 5.545x^2 \\ &\quad - (2.296 + 2.696x + 3.029x^2) \tau_0 \end{aligned} \quad (9-18)$$

These functions represent Stewartson's Table of τ_0 and the column $c/[a(2j+1)]$ for the first two radial modes. It is not necessary to consider the third radial mode.

The accuracy of these formulas can be checked. Consider:

(1) 105 mm chemical projectile previously analyzed in par. 9-3.4.1. We had

$\tau_0(2,2) = 0.089$, $x = b^2/a^2 = 0.03$, and $K_2 = 0.530$ (see par. 9-3.3). If we substitute the above values of τ_0 and x in Eq. 9-18, we should recover K_2 . Eq. 9-18 gives $K_2 = 0.529$ instead of the tabulated value $K_2 = 0.530$. The agreement is good.

(2) 75mm chemical projectile previously considered in par 9-3.4.2. We had $\tau_0(1,1) = 0.074$, $x = 0.03$, $K_1 = 1.083$. Application of Eq. 9-17 with above values of τ_0 and x gives $K_1 = 1.083$ in exact agreement with the tabular value.

As previously indicated, in practice the designer will usually be concerned with radial mode $n = 1$. However, if need arises to consider mode 2, Eq. 9-18 is available. In the analyses which follow we shall be dealing only with Eq. 9-17; the treatment with the other equation is identical.

9-4.1 EVALUATION OF THE INTEGRAL, EQ. 9-16

By substituting Eq. 9-17 into Eq. 9-16, the latter becomes

$$1 = \frac{1}{2c} \int_0^{2c} \frac{c}{a(2j+1)} \left[0.996 + 0.115x + 0.926x^2 - (1.007 + 0.942x - 0.590x^2)\tau_0 \right] dz \quad (9-19)$$

Since all x 's contain $a(z)$, all have to be integrated along the cavity. The cavity has a constant height $2c$ and usually a cylindrical section of radius a_0 . If there is no cylindrical section, then a_0 should be taken as a maximum diameter of the cavity.

Eq. 9-19 can be put into more convenient nondimensional form. Let

$$z' = \frac{z}{2c}, a' = \frac{a(z)}{a_0}, x_0 = \frac{b^2}{a_0^2}, \text{ a constant. Since}$$

$c/[a_0(2j+1)]$ is also a constant, it can be taken from under the integral sign. In normalized form, Eq. 9-19 becomes:

$$\frac{c}{a_0(2j+1)} \int_0^1 \left[0.996(1/a') + 0.115x_0(1/a')^3 + 0.926x_0^2(1/a')^5 - [1.007(1/a') + 0.942x_0(1/a')^3 - 0.590x_0^2(1/a')^5] \tau_0 \right] dz' \quad (9-20)$$

Eq. 9-20 shows that there are three types of integrals which have to be evaluated either numerically or analytically, depending on the shape of the cavity:

$$\begin{aligned} \text{I} &= \int_0^1 (1/a') dz' \\ \text{II} &= \int_0^1 (1/a')^3 dz' \\ \text{III} &= \int_0^1 (1/a')^5 dz' \end{aligned} \quad (9-21)$$

With this symbolic designation of the integrals as I, II, and III, Eq. 9-20 can be written as:

$$1 = \frac{c}{a_0(2j+1)} \left[0.996\text{I} + 0.115x_0\text{II} + 0.926x_0^2\text{III} - (1.007 + 0.942x_0\text{II} - 0.590x_0^2\text{III})\tau_0 \right] \quad (9-22)$$

Before considering a specific cavity shape, let us examine the significance of x_0 . Consider two cases:

(1) Noncylindrical cavity without a burster. Let V_0 be its volume of height $2c$ and of maximum diameter $2a_0$. Let V_c be the volume of the cylinder of the same height and diameter, i.e.,

$$V = \pi a_0^2 2c$$

Suppose that V_0 is to be filled to a certain fraction of its volume β , i.e.,

$$\beta V_0 = V_0 - v_a$$

where v_a is the air volume:

$$v_a = \pi a_0^2 2c (b^2/a_0^2) = V_c (b^2/a_0^2)$$

$$\therefore x_0 = b^2/a_0^2 = (1 - \beta) \frac{V_0}{V_c} \quad (9-23)$$

To recapitulate: if a noncylindrical cavity without a burster is to be filled to β fraction of its volume, then x_0 , to be used in Eq. 9-22, is as defined by Eq. 9-23.

(2) Noncylindrical cavity with a burster. Let the volume of the burster be $v_r = V_c (r^2/a_0^2)$. If this noncylindrical cavity is to be filled to β fraction of its available volume, i.e., $\beta(V_0 - v_r)$, then

$$\beta(V_0 - v_r) = V_0 - v_r - v_a$$

where v_a is air volume

$$v_a = V_c (b^2/a_0^2 - r^2/a_0^2)$$

From this it follows that

$$x_0 = b^2/a_0^2 = (1 - \beta) \frac{V_0}{V_c} + \beta (r^2/a_0^2) \quad (9-24)$$

To recapitulate: if a noncylindrical cavity containing a burster is to be filled to β fraction of its available volume then x_0 , to be used in Eq. 9-22, is as defined by Eq. 9-24. Now we can return to the evaluation of the integrals.

Let us consider a noncylindrical cavity as is shown in Fig. 5-4(B). The cavity consists of a cylindrical section, and a truncated cone of height $h/2c$ and of semi-vertex angle θ . In normalized dimensions, the total height of the cavity is 1, the height of the cylindrical part is $1 - h/2c$, and the height of conical part is $h/2c$. Here some care is necessary in defining the variation of $a(z)$ with z the axial distance. If we choose the origin of the z coordinate at the base of the cavity, then $a' = a(z)/a_0$ has the following values

$$a' = 1 \text{ for } 0 \leq z' \leq z'_1 \text{ where } z'_1 = 1 - h/2c$$

$$a' = 1 - (z' - z'_1) \frac{2c}{a_0} \tan \theta \text{ for } z'_1 \leq z' \leq 1$$

$$\text{Let } m' = 2c \tan \theta, \text{ then } a' = 1 - (z' - z'_1) m'$$

Each integral can be broken into two parts:

$$\int_0^1 = \int_0^{z'_1} \text{cyl} + \int_{z'_1}^1 \text{noncyl}$$

On the other hand, if one were to locate the origin of the z -coordinate at the junction of the cylindrical and noncylindrical parts, then

$$a' = 1 \text{ for } -z'_1 \leq z' \leq 0$$

$$a' = 1 - z' m' \text{ for } 0 \leq z' \leq h/2c$$

and the integral is divided as

$$\int_{-z'_1}^{h/2c} = \int_{-z'_1}^0 \text{cyl} + \int_0^{h/2c} \text{noncyl}$$

The designer may adopt whichever system is more convenient. If the cavity consists of several noncylindrical sections, careful control of the z -coordinate and the limits of integration must be maintained.

We shall use the first system. The first integral becomes

$$I = \int_0^1 (1/a') dz' = \int_0^{z_1'} dz' + \int_{z_1'}^1 \frac{dz'}{1 - (z' - z_1')m'} \\ I = 1 - h/2c - \frac{1}{m'} \ell_n \left(1 - \frac{h}{2c} m' \right) \quad (9-25)$$

where ℓ_n is the logarithm to the base e .

Similarly, performing the integration with integrals II and III, we obtain

$$II = 1 - h/2c + \frac{1}{2m'} \left[\frac{1}{\left(1 - \frac{hm'}{2c} \right)^2} - 1 \right] \quad (9-26)$$

$$III = 1 - h/2c + \frac{1}{4m'} \left[\frac{1}{\left(1 - \frac{hm'}{2c} \right)^4} - 1 \right] \quad (9-27)$$

For this type of noncylindrical cavity, all the integrals can be easily evaluated. When their values are substituted in Eq. 9-22, either the fill-ratio β , i.e., x_0 , for a given τ_0 , or the τ_0 for a prescribed fill-ratio can be readily found.

For the cylinder-truncated-cone configuration the ratio of volumes is

$$\frac{V_0}{V_c} = 1 - h/2c + \frac{1}{\frac{3}{2}m'} \left[1 - \left(1 - \frac{hm'}{2c} \right)^3 \right] \quad (9-28)$$

As stated in Ch. 7, this theory should be applied only if the loading of the liquid is such that the radius of the cavity at its narrowest point is larger than the radius of the air column. For the cylinder-truncated-cone cavity, this condition requires that

$$a' = 1 - m'h/2c > b/a_0$$

In other words, the air column must be cylindrical.

9-4.2 TEST OF THE THEORY

No experiments were performed to test the predictions of the present theory of determining the eigenfrequencies for a prescribed fill-ratio in noncylindrical cavities. Such tests are difficult because they require a continuous variation of the nutational frequency of the apparatus in order to locate the resonating τ_0 . The inverse problem of establishing the fill-ratio for resonance to occur for a given frequency $\tau_n = \tau_0$ is much simpler. It requires only a systematic change in the fill-ratio until resonance is achieved.

We shall describe one comparison of the experiment with predictions of the theory in some detail; other comparisons are shown graphically in Fig. 7-1.

A gyroscope was used as an experimental tool. The original cylindrical cavity had the following characteristics: $c/a = 2.687$; $V_c = 534$ cc; and it resonated at $j = 1$ with $\tau_n = \tau_0(1,1) = 0.050$ at 61% fill-ratio, or $\beta = 0.61$. The maximum rate of divergence was measured to be $\lambda_0 = 0.364$ per sec.

This cavity was modified at one end by a truncated cone, see Fig. 7-1, with $h_1/2c = 0.33$, $\theta = 5^\circ$; and at the other end also by a truncated cone with $h_3/2c = 0.54$, $\theta = 7\frac{1}{2}^\circ$. The resulting volume of the modified cavity V_0 was 413 cc. The same frequency $\tau_n = \tau_0 = 0.050$, i.e., resonance was found in a modified cavity at a fill volume of 390 cc, or at 94% fill-ratio. The maximum divergence was measured to be $\lambda = 0.065$ per sec or considerably less than in the original cylindrical cavity.

The last point — i.e., decrease in instability in a modified cavity as compared with that for the cylindrical cavity, or the effect of modification on the residue or on Stewartson's parameter S — is clearly indicated by the experimental data. In Ch. 7

a rough estimate has been made of this effect in a form

$$\frac{\sqrt{S_m}}{\sqrt{S_c}} \approx 1 - 1.5(m'h/2c)$$

where S_m is Stewartson's parameter of the modified cavity and S_c is that of the original cylindrical cavity. The experimental data lead to the following

$$\frac{A}{\sqrt{S_c}} = 1 - 1.13(m'h/2c) \quad (9-29)$$

with a standard deviation of 0.04. The result, Eq. 9-29, is in good agreement with a very rough estimate given in Ch. 7.

Now we can proceed to test the predictions of the theory of the above experimental results.

Computation of the integrals by Eqs. 9-25, 9-26, and 9-27 is readily accomplished. If we designate, for example, I_1 , I_2 , and I_3 as the first integral for the truncated cone $\theta = 5^\circ$, for the cylindrical part, and for the second truncated cone $\theta = 7\frac{1}{2}^\circ$, respectively, we find the following values for I, II, and III:

$$\begin{aligned} \text{I} &= I_1 + I_2 + I_3 = 0.359 + 0.13 + 0.682 = 1.171 \\ \text{II} &= 0.426 + 0.13 + 1.144 = 1.700 \\ \text{III} &= 0.512 + 0.13 + 2.071 = 2.713 \end{aligned}$$

Substitution of these integrals into Eq. 9-22 and with $\tau_0 = 0.050$, and $j = 1$, the solution of the resulting quadratic in x_0 gives $x_0 = 0.0436$. Therefore,

$$\beta = 1 - x_0 \frac{V}{V_0} = 0.944$$

which is in excellent agreement with the observed value.

This experiment was performed with oil of viscosity 3 centistokes, the Reynolds number $Re = 1.73 \times 10^5$, and

$\sqrt{S_c} = 3.58 \times 10^{-3}$. With the aid of Stewartson's Tables we compute D_x and D_y , see Ch. 6, and then, by Eq. 9-10, we compute c_2 . The viscous damping correction is found to be $\delta = \frac{c_2}{\sqrt{Re}} = 3.45 \times 10^{-3}$. It is to be

noted that to obtain D_x and D_y one can differentiate Eq. 9-17 (radial mode $n = 1$) directly. Since, by definition

$$\frac{1}{K_1} \frac{c}{a(2j+1)} = 1$$

we have

$$\begin{aligned} 1 = c/[a(2j+1)] & \left[0.996 + 0.115x + 0.926x^2 \right. \\ & - (1.007 + 0.942x \\ & \left. - 0.590x^2) \tau_0 \right] \end{aligned} \quad (9-30)$$

For the two truncated cones we have

$$8 = 5^\circ: \quad (m'h/2c)_1 = 0.155$$

$$8 = 7\frac{1}{2}^\circ: \quad (m'h/2c)_3 = 0.382$$

Therefore, by Eq. 9-29

$$\sqrt{S_m} = \sqrt{S_c} \left\{ 1 - 1.13[(m'h/2c)_1 + (m'h/2c)_3] \right\}$$

$$\sqrt{S_m} = 3.58 \times 10^{-3}(0.393) = 1.41 \times 10^{-3}$$

The gyroscope was run at $\Omega = 5000$ rpm, or $\Omega/2 = 0.262 \times 10^3$ rad/sec. Therefore,

$$\lambda = \frac{\Omega}{2} \left[\left(\sqrt{S_m + \delta^2} \right) - \delta \right] = 0.072 \text{ per sec}$$

which is in a good agreement with the measured $\lambda = 0.065$ per sec.

It is to be noted that an inviscid Λ in a modified cavity would be expected to be (Eq. 9-6a)

$$\Lambda = \frac{\Omega}{2} \sqrt{S_m} = (0.262 \times 10^3) (1.41 \times 10^{-3}) \\ = 0.37 \text{ per sec}$$

instead of the observed $\lambda = 0.065$. In this case, therefore, viscosity has very significant effect on instability.

A good agreement of the predictions of the theory with the experimental data should give some confidence to the designer in dealing with noncylindrical cavities. As was pointed out in Ch. 7, in the case of a truncated-cone type of modification, the theory appears to hold up to $\left| \frac{da}{dz} \right| = \tan \epsilon = 0.2$ which was the limit of experimental data.

In a modified cavity the width of the resonance band is given, as before, by $\tau_n \pm \sqrt{S_m}$ if viscous effects are negligible, otherwise by $\tau_n \pm (\sqrt{S_m} \pm 6)$.

9-4.3 THE XM410 PROJECTILE

We return to this projectile as another example. Now, however, we shall consider the real cavity as given by the drawing. The noncylindrical part of the cavity, see Fig. 2-2, cannot be represented by the truncated cone. Hence, to evaluate the integrals I, II, and III in Eq. 9-22, numerical integration is necessary. One can measure the radii directly from the drawing thus computing a' vs z' at enough positions to obtain reasonably accurate values of the integrals. Or, one can fit a circular arc to the curved noncylindrical part and compute a' . The latter procedure was followed here.

A brief note on the numerical integration might be useful. Suppose we have to evaluate the integral

$$\int_0^{h/2c} y dz'$$

where y is either $(1/a')$, $(1/a')^3$, or $(1/a')^5$. It is convenient to divide the interval 0 to $h/2c$ into an *even* number of subintervals — *six* is a convenient number, i.e.,

$$\Delta = \frac{1}{6}(h/2c)$$

Then by Simpson's rule

$$\int_0^{h/2c} y dz' = \frac{\Delta}{3} (y_0 + 4y_1 + 2y_2 + 4y_3 + 2y_4 + 4y_5 + y_6)$$

where y_i are the values of y computed at $z' = n\Delta$, $n = 0, 1, \dots, 6$.

For the ~~XM410~~ Projectile

$$h/2c = 0.325, \quad z'_1 = 1 - h/2c = 0.675,$$

$$c/[a_0(2j+1)] = 1.56, \quad j = 0.$$

The integrals, with the origin of coordinates at z'_1 , have the following values

$$I = \int_{-z'_1}^0 + \int_0^{h/2c} = 0.675 \pm 0.381 = 1.056$$

$$\text{II} \quad \quad \quad = 0.675 \pm 0.544 = 1.219$$

$$\text{III} \quad \quad \quad = 0.675 \pm 0.816 = 1.491$$

Substituting these values into Eq. 9-22, we obtain:

$$1 = 1.56 \left[1.052 \pm 0.140x_0 \pm 1.381x_0^2 \right. \\ \left. - (1.063 \pm 1.148x_0 - 0.880x_0^2) \tau_0 \right]$$

This equation permits, therefore, finding τ_0 for specified β , or finding β for a given τ_0 . The designer is likely to be interested in the former, i.e., of finding whether there is a resonant frequency present in his noncylindrical cavity with a prescribed percent of fill. Therefore, let us find τ_0 for a given β . Previously we used $\beta = 0.93$. By Eq. 9-24

$$x_0 = b^2/a_0^2 = (1 - \beta) \frac{V_0}{V_c} \pm \beta r^2/a_0^2$$

We have

$$V_0/V_c = 0.90, \quad r/a_0 = 0.29, \quad \beta = 0.93$$

$$\therefore x_0 = 0.14$$

With this x_0 the solution for τ_0 becomes from Eq. 9-22

$$1 = 1.56 \left\{ 0.996(1.056) \pm 0.115(0.14)(1.219) \right. \\ \left. \pm 0.926(0.14)^2(1.491) - [1.007(1.056) \right. \\ \left. \pm 0.942(0.14)(1.219) \right. \\ \left. - 0.590(0.14)^2(1.491) \right] \tau_0 \left. \right\}$$

$$0.641 = 1.099 - 1.206\tau_0$$

$$\therefore \tau_0 = 0.38$$

Previously we have found that for this projectile, with a cylindrical cavity with a burster, τ_0 was 0.35. Thus, there is a slight shift toward higher frequencies in a noncylindrical cavity.

The effect of a noncylindrical cavity on the width of the resonance band $\sqrt{S_m}$ can be readily estimated. In general, one computes an average \bar{m}'

$$\bar{m}' = \frac{\int m' dz}{\int dz}$$

In cases when the noncylindrical part can be represented by a circular arc, compute θ_m at mid-point. Then $\bar{m}' = \frac{2c}{a_0} \tan \theta_m$.

For the XM410 Projectile whose noncylindrical section is representable by a circular arc, $\theta_m = 17^\circ 12'$. Therefore, $\bar{m}' = 0.97$ and with $h/2c = 0.325$, $\bar{m}'h/2c = 0.315$. Therefore, the modified Stewartson's parameter is (see Eq. 9-29)

$$\frac{\sqrt{S_m}}{\sqrt{S_c}} = 1 - 1.13(0.315) = 0.64$$

or $\sqrt{S_m} = 0.25(0.64) = 0.16$. Therefore, the frequencies present in this noncylindrical cavity are 0.38 ± 0.16 or from 0.54 to 0.22. The resonance band, therefore, is $0.25 \pm 0.16 = 0.41$ on the high side to 0.22 on the low side. The band, therefore, is more asymmetrical than in a cylindrical cavity. The situation, therefore, has improved somewhat relative to the condition with the cylindrical cavity. But the projectile is still unstable.

The two solutions for instability of this projectile thus far found, therefore, are: (1) the partitioning of the cavity by a transverse baffle as discussed in par. 9-3.7.1, and (2) partitioning of the cavity by a cylindrical baffle, par. 9-3.7.3. In the former case, application of the present theory to the noncylindrical part of the partitioned cavity shows that it contains no resonating frequencies.

9-4.4 ROUNDED CORNERS

Experimentally determined effects of rounding the corners of the cylindrical cavity are shown in Fig. 5-5. Additional data are given in Fig. 7-3. For the experiments depicted in Fig. 5-5, all cavities had the same fineness-ratio $c/a = 3.077$ and the original cylindrical cavity contained a resonant frequency $\tau_n = \tau_0(1,1) = 0.055$ when this cavity was filled to $1 - b^2/a^2$ of its volume. The experiments established the volume of fluid V required for each modified cavity to bring it into resonance, i.e., to contain $\tau_0 = 0.055$.

The designer, however, is interested in an inverse problem—how to find τ_0 in modified cavity. Wedemeyer's theory is inapplicable to rounded corners because of the violation of the restriction of the theory that $|da/dz| \ll 1$. However, experiments indicate that for a practical range of fill-ratios, i.e., from 90% to 98%, and if the radius of the corner R is not large, the procedure for finding τ_0 in a modified cavity is simple.

Let V_0 be the volume of the modified cavity, R'/a is fractional radius of the corner, i.e., for $R'/a = 1$ the end of the cavity is hemispherical; c/a the fineness-ratio; and V_c is volume of the cylindrical cavity ($R'/a = 0$). The experiments show that if τ_0 is present in the cylindrical cavity at a fill-ratio $1 - b^2/a^2$, the same τ_0 will be present in a modified cavity at its fill-ratio $\beta = V/V_0$ provided that

$$b/a \leq (1 - R'/a) \quad (9-31)$$

Fig. 5-5 shows that if Eq. 9-31 is satisfied, then V/V_c — which is plotted in Fig. 5-5 — is a constant. Therefore

$$V/V_c = 1 - b^2/a^2 = \frac{V}{V_0} \frac{V_0}{V_c} = \beta \frac{V_0}{V_c}$$

or

$$b^2/a^2 = 1 - \beta \frac{V_0}{V_c} \quad (9-32)$$

If the cavity contains a burster of radius r then Eq. 9-32 is modified to

$$b^2/a^2 = 1 - \beta \left(\frac{V_0}{V_c} - \frac{r^2}{a^2} \right) \quad (9-32a)$$

Therefore, to find τ_0 in a modified cavity, provided Eq. 9-31 is satisfied, enter Stewartson's Tables with b^2/a^2 as given by Eq. 9-32 or Eq. 9-32a whichever is applicable, and $c/[a(2j + 1)]$ of the cavity.

For cases when Eq. 9-31 is not satisfied, i.e.,

$$b/a > (1 - R'/a) \quad (9-33)$$

the procedure for finding τ_0 at present is unknown. However, for such relatively slight modification of the cylindrical cavity the eigenfrequencies in the modified cavity are probably controlled principally by b^2/a^2 , i.e., if a particular τ_0 is present in the cylindrical cavity at certain b^2/a^2 , then the same τ_0 will be present in a modified cavity if its fill-ratio is such as to give the same b^2/a^2 .

If V_0 is the volume of modified cavity which is filled to β fraction of its volume, then the fractional air volume, regarded as cylindrical, is

$$b^2/a^2 = (1 - \beta)(V_0/V_c) \quad (9-33a)$$

For practical fill-ratios, shortening of the length of the air column — because of the curvature of the ends — is negligible. Then with this b^2/a^2 and the c/a of the cavity, one can find τ_0 from Stewartson's Tables.

One can check this assumption by experiments, the results of which are shown in Fig. 5-5. Only here we shall do the reverse: we assume that β is given by the experiments and then apply Eq. 9-33a to compute b^2/a^2 with known c/a to find τ_0 . If our assumption of the importance of b^2/a^2 in the modified cavity is correct, we should reproduce $\tau_0 = 0.055$.

Eq. 9-33a can be written

$$b^2/a^2 = (V_0/V_c) - (V/V_c)$$

The values of V/V_c are given in Fig. 5-5 and V_0/V_c can be readily computed or measured. The details are given in Ref. 3. The results are shown below for Configurations A and B with one and both ends modified, respectively.

R'/a	Config. A	Config. B
0.80	0.050	0.050
1.0	0.055	0.055

The correct value is $\tau_0 = 0.055$. Thus for $R'/a = 0.80$, the error is about 10% which is acceptable.

Therefore, for the design purposes, if the modified volume V_0 is filled to β fraction in the amount so that

$$b/a > (1 - R'/a)$$

is satisfied, find b^2/a^2 from Eq. 9-33a. Find τ_0 from Stewartson's Tables with this b^2/a^2 and $c/[a(2j+1)]$ of the cavity as if the cavity was cylindrical. The expected error in τ_0 , so found, is not likely to exceed 10%.

Experimental data³ although somewhat limited, nevertheless clearly indicate that S is significantly affected by rounding the corners. For the cylindrical cavity with rounded corners the effect is

$$\text{one end modified: } \frac{\sqrt{S_m}}{\sqrt{S_c}} = 1 - 0.2(R'/a - 0.3)$$

$$\text{both ends modified: } \frac{\sqrt{S_m}}{\sqrt{S_c}} = 1 - 0.4(R'/a - 0.3)$$

i.e., the effect is negligible for R'/a less than 0.3. However, if rounded corners are combined with other modifications as defined by $m'h/2c$, previously considered, then the total effect of these modifications is

$$\frac{\sqrt{S_m}}{\sqrt{S_c}} = 1 - 1.13(m'h/2c) - 0.3(R'/a) \quad (9-34)$$

9-4.5 SLOW SPIN

Another minor problem can profitably be taken up at this time. Occasionally one encounters liquid-filled projectiles with axial spin sufficiently low for the free liquid surface to assume a distinctly parabolic form. The question arises as to what effect such departure of the free surface from the cylindrical will have on the eigenfrequencies. The effect is easily computable if one treats the parabolic surface by Wedemeyer's theory.

Consider, therefore, a cylindrical cavity which is filled to a β fraction of its volume which is spinning sufficiently slowly to form a parabolic free surface. Define a critical spin Ω_c for which the vertex of the parabola lies at the bottom of the cavity. For a flying projectile this, of course, will be at the for-

ward end of the cavity. It can be readily shown that the critical spin is given by

$$\Omega_c^2 = 2(c/a) \frac{\tilde{g}}{a(1-\beta)} (\text{rad/sec})^2 \quad (9-35)$$

c/a = fineness-ratio of the cavity

$1-\beta$ = fractional air volume

\tilde{g} = deceleration of the projectile, ft/sec²

$$\tilde{g} = \left(\frac{\rho_a S' d}{2m} \right) \left(\frac{V^2}{d} C_D \right) \quad (9-36)$$

where

$\frac{\rho_a S' d}{2m}$ = "density factor" (see Ch. 2)

V = velocity, ft/sec

d = diameter, ft

C_D = drag coefficient

Let

$$s = \frac{\Omega_c}{\Omega}$$

where Ω is the actual spin, i.e.,

$$\Omega = \frac{2\pi}{nd} V \text{ rad/sec}$$

Then it can be readily shown that in the range of

$$0 \leq s \leq 1$$

the integrals I, II, and III, see par. 9-4.1, take the following simple values

$$\begin{aligned} \text{I} &= 1 \\ \text{II} &= 1 \\ \text{III} &= 1 + \frac{s^4}{3} \end{aligned} \quad (9-37)$$

If these integrals are substituted in Eq. 9-22, the value of τ_0 can be readily found using $x_0 = (1-\beta)$.

As an example, consider the XM410 Projectile:

$$\frac{\rho_a S' d}{2m} = 0.87 \times 10^{-4} \text{ (see par. 2-4)}$$

$$d = 0.5 \text{ ft}$$

$$\text{at } M = 1.5 \quad V = 1680 \text{ ft/sec}$$

$$C_D = 0.5$$

$$\therefore \tilde{g} = 246 \text{ ft/sec}^2$$

$$\tilde{g}/g_0 = 7.6$$

where $g_0 = 32.2 \text{ ft/sec}^2$. If $\beta = 0.93$

$$\Omega_c = 221 \text{ rad/sec}$$

However, at $M = 1.5, \Omega = 1056 \text{ rad/sec}$ (see par. 9-3.2). Therefore,

$$s = \frac{\Omega_c}{\Omega} = 0.2$$

It can be readily shown from Eq. 9-22 that the shift in the eigenfrequency due to parabolicity of the free surface is approximately

$$\Delta\tau_0 \approx x_0^2 \frac{s^4}{3}$$

Therefore, the effect on τ_0 in the XM410 Projectile, fired at $M = 1.5$, is negligible.

If the spin is so low that the vertex of the parabolic free surface enters the cavity, i.e., $s > 1$, Stewartson's theory is no longer applicable. In this case, see Ref. 5.

SECTION II

TRANSIENT STATE

95 INTRODUCTION

In the preceding section the designers were given a set of simple rules for the analysis of the cavity of liquid-filled projectiles in order to be sure that it contains no fluid frequencies in close proximity of the nutational frequency of the projectile, i.e., how to avoid resonance. Experiments^{6,7} show, however, that the projectile may also become unstable during spin-up of the liquid. This transient instability may be so severe as to render the projectile useless in practice even if it is designed to be stable in its steady state, i.e., with the liquid fully spinning. The designer, therefore, should consider the transient phase as a part of overall design problem of liquid-filled projectiles.

Transient instability has the same underlying cause — resonance. Mathematically, however, the problem of unsteady flow is much more difficult than the steady one

and has not, as yet, been solved. An outline of the difficulties is given in Ch. 8. However, in order to assist the designer in estimating the level of yaw which may occur during temporary instability during spin-up, Wedemeyer suggested treating the problem as quasi-steady, i.e., replacing the actual, time dependent flow by a sequence of steady state solutions. To achieve this, it was necessary to solve a rather sophisticated problem of circulation of fluid in the cavity during spin-up. Once this is done, then it is possible to compute the time history of the angular momentum of the fluid. With this, the matching of unsteady flow with an "equivalent" steady state solutions becomes feasible.

Consider, for simplicity, a 100% full cavity. At a certain time t during spin-up, a fraction of the fluid mass, near the wall, is spinning with a certain velocity distribution as is shown in Figs. 8-2 and 8-3; the inner cylindrical core is not yet spinning.

This fluid possesses a certain angular momentum. Wedemeyer suggests matching this momentum with that of a partially filled cylindrical cavity b^2/a^2 with the fluid spinning as a rigid body, i.e., with a constant angular velocity. The eigenfrequencies of the hollow rigidly spinning cylinder are known from Stewartson's theory. The important assumption is then made that the eigenfrequencies in the actual partially spinning fluid are the same as in an "equivalent" cylinder having the same angular momentum. The influence of different boundary conditions in the actual fluid — with its spinning part and nonspinning core, and in an "equivalent" cylinder with its free surface — is discussed in par. [REDACTED]. Thus by replacing a time sequence of the angular momenta of the actual fluid with those of an equivalent series of partially filled cavities with the fluid spinning as a rigid body, a time history of eigenfrequencies can be found. Once $\tau_0(t)$ is known, it is a simple matter to find the time required for $\tau_0(t)$ to cross the resonance band $\tau_n \pm \sqrt{S}$. And knowing the rate of divergence, the amplification of yaw during transient instability can be readily found by integration. The matching of the angular momenta, as above, Wedemeyer designates as Case I; matching the volumes of rotating fluids he designates as Case II. Comparison of the predictions by these two methods with the experiments should decide which one, if either, is the better method.

The time history of the angular momentum of the fluid depends significantly on the nature of the boundary layer on the walls of the cavity, either laminar or turbulent. The condition for existence of either one or the other is given in Ch. 8 as

$$\text{laminar for: } Re < 0.5 \times 10^5$$

$$\text{turbulent for: } Re > 3 \times 10^5$$

For intermediate Reynolds numbers, the nature of the boundary layer depends on the roughness of the walls of the cavity. This problem is discussed in par. 8-3.1.3. In practice, however, it is adequate to assume a turbulent boundary layer for Re in excess of the laminar limit.

The time history of the angular momentum also depends somewhat on the fill-ratio, see Figs. 8-4 and 8-5. In practice, however, the fill-ratios are usually between 90% and 98%. Therefore, for the purposes at hand and in view of the approximate nature of the theory, it is adequate to treat all practical cases as if the cavity were 100% full.

9-5.1 LAMINAR BOUNDARY LAYER

It was shown by Eq. 8-55 that the value of the angular momentum at time t relative to its rigid or steady state value of a fluid in a completely filled cavity, if the casing is spinning at a constant Ω , is

$$\frac{I}{I_\infty} = 1 - e^{2k\Omega t}$$

where

$$I_\infty = i_{x0}\Omega \text{ total angular momentum for a rigid fluid}$$

$$i_{x0} = \text{moment of inertia of a rigid fluid}$$

$$\Omega = \frac{2\pi}{nd} \text{ V rad/sec}$$

$$k = 0.443(a/c)Re^{-1/2}$$

$$c/a = \text{fineness-ratio of the cavity}$$

$$t = \text{time, sec}$$

If Ω is not constant, see Eq. 8-61. However, the change in Ω during spin-up is usually relatively small and, for our purposes, can be disregarded.

The angular momentum of a hollow cylinder of fluid spinning with constant Ω is

$$\frac{I}{I_\infty} = 1 - (b^2/a^2)^2$$

Case I: We are to equate the angular momentum of the actual fluid, Eq. 8-55, with that of an "equivalent" cylinder above, Eq. 9-38,

$$1 - e^{-2k\Omega t} = 1 - (b^2/a^2)^2$$

Therefore,

$$(b^2/a^2)_e = x_e = e^{-k\Omega t} \quad (9-39)$$

where x_e is an "effective" b^2/a^2 , i.e., time dependent by Eq. 9-39. It is to be noted that during spin-up the "effective" fill-ratios $1-x_e$ cover the whole range of values from zero, at the very beginning, to the actual fill-ratio for the steady state condition.

Thus one finds the time history of an "effective" x_e or, simply $x(t)$. As stated above, the eigenfrequency $\tau_0(t)$ in the actual cavity is assumed to be the same as in a steady state condition for a partially filled cavity as defined by x . With known value of $c/[a(2j+1)]$, $\tau_0(t)$ can be readily found from Stewartson's Tables as a function of $x(t)$.

The computation of $\tau_0(t)$ can be considerably simplified by the use of Eq. 9-30 (for radial mode $n = 1$).

$$1 = \frac{c}{a(2j+1)} [0.996x + 0.115x^2 + 0.926x^3 - (1.007x + 0.942x^2 - 0.590x^3)\tau_0]$$

where x is to be regarded as an "effective" $x(t)$ computed by Eq. 9-39. Since $x(t)$ is time dependent, τ_0 will also be time dependent, i.e., $\tau_0(t)$. Thus one can trace the time history of $\tau_0(t)$ during spin-up. The resonance band covers a frequency range from $\tau_n + \sqrt{S}$ to $\tau_n - \sqrt{S}$. Therefore, if $\tau_0(t)$ attains any of these values during spin-up, resonance instability will occur.

The use of Eq. 9-30 avoids graphical and interpolative processes required with Stewartson's Tables or with Fig. 8-9. Tests show that Eq. 9-30 give reasonably good values of τ_0 even for $x = 0.8$, i.e., with an error of roughly 5% which, for practical purposes, is entirely adequate at such high values of x which occur very early in the flight of the projectile. Below $x = 0.6$, Eq. 9-30 is quite accurate.

Case 11: One finds the volume of the rotating fluid with actual velocity distribution by setting $v^* = 0$ in Eq. 8-54. The radius of nonspinning core r^* is

$$r^* = r/a = b/a = e^{-k\Omega t} \quad (9-40)$$

The fractional volume of the spinning fluid in an "equivalent" cylinder corresponding to b/a is $1 - b^2/a^2$. It follows that

$$(b^2/a^2)_e = x_e = e^{-2k\Omega t} \quad (9-41)$$

Notice the factor 2 in the exponent in Case II as compared to 1 in the angular momentum Case I, Eq. 9-38.

Thus by treating the problem either by the Case I model or by the Case II model the time history of x_e and, by Eq. 9-30, of $\tau_0(t)$ is obtained during spin-up. At the beginning of spin-up τ_0 starts high, then decreases as spin-up progresses and eventually reaches its steady state value as given by Stewartson's Tables for a fully spinning liquid. Of course, if steady state τ_0 lies above $\tau_n + \sqrt{S}$, no resonance would occur during spin-up.

Since the laminar case is probably not of practical usefulness to the designers of projectiles, we shall not pursue it further. Additional details of computation of yaw during transient instability will be taken up in connection with the turbulent case.

9-5.2 TURBULENT BOUNDARY LAYER

As previously stated, the turbulent case is to be used whenever $Re > 3 \times 10^5$. In practice, it may be used to the Reynolds number limit for the laminar case, i.e., to $Re > 0.3 \times 10^5$.

The time history of the angular momentum for the turbulent case is not given by a simple formula as by Eq. 8-55 but graphically as in Fig. 8-5. Nevertheless, to simplify the handling of this case in practice, Fig. 8-5 can be easily represented algebraically in a form similar to the laminar case.

Let $T = k_t \Omega t$ be the "scaled time"; i.e., in terms of T , the graphs in Fig. 8-5 are universal or applicable to all cases satisfying the conditions of the theory. For the turbulent case, as is shown in Ch. 8,

$$k_t = 0.035(a/c)Re^{-1/5} \quad (9-42)$$

Then the formulas below accurately represent the graph of Fig. 8-5 for a 100% full cavity.

Cavity 100%full

For $0 \leq T \leq 0.6$

$$\ell_n \left(1 - \frac{1}{I_\infty}\right) = -1.716T + 0.627T^2 \quad (9-43)$$

For $T \geq 0.6$

$$\ell_n \left(1 - \frac{1}{I_\infty}\right) = -0.226 - 0.964T$$

or

$$\frac{1}{I_\infty} = 1 - 0.80e^{-0.964T} \quad (9-44)$$

As was the case with the laminar boundary layer, the history of angular momentum with the turbulent boundary layer is not particularly sensitive to the fill-ratio. So within the practical range of the fill-ratios, i.e., between 90% and 98%, the use of 100%fill formulas is adequate.

Case I: As before, equating the angular momentum of the fluids with actual velocity distribution with that of an "equivalent" cylinder with rigid body rotation, we have for $T \geq 0.6$, for example, (from Eqs. 9-38, and 9-44)

$$(b^2/a^2)^2 = 0.80e^{-0.964T}$$

or

$$(b^2/a^2)_e = x_e = 0.89e^{-0.482T} \quad (9-45)$$

Thus, again $\tau_0(T)$ can be readily determined from Eq. 9-30. It is more convenient to use as a variable, either Ωt or T , instead

of t . In terms of T , a single graph delineating the time history of $1/I_\infty$ or $\tau_0(T)$, for a given projectile, will be applicable to all conditions of fire, i.e., to different muzzle velocities. The latter will change the scale of T through changes both in k_t (through Re) and Ω .

Case II: If we consider the volume of the rotating fluids, the formula for the turbulent case is different from that of the laminar. To find the radius of the nonspinning core r^* , i.e., where the circumferential velocity v^* of fluid particles is zero, we set $y = r^*v^* = 0$ in the integral equation, Eq. 8-58. The resulting integral becomes

$$T = k_t \Omega t = \int_{r^*}^1 \frac{dr^*}{(r^*)^{8/5}} \quad (9-46)$$

and is readily evaluated. Since $r^* = r/a = b/a$, it follows that

$$b/a = \frac{1}{\left(1 + \frac{3}{5}T\right)^{5/3}}$$

or

$$(b^2/a^2)_e = x_e = \frac{1}{\left(1 + \frac{3}{5}T\right)^{10/3}} \quad (9-47)$$

or

$$\Omega t = \frac{5}{3k_t} (1/x^{3/10} - 1)$$

Again, with an "effective" $x_e(T)$, $\tau_0(T)$ can be readily found by Eq. 9-30.

9-5.3 AMPLIFICATION OF YAW

Amplification of yaw during transient instability can be computed by Eq. 8-71. This equation can be slightly simplified. It was derived on the assumption that the resonance band is sufficiently narrow for $d\tau_0/dt$ to be regarded as constant during the passage of $\tau_0(t)$ through the band. If Ω is constant, then $\Omega dt/d\tau_0 \approx \Delta(\Omega t)/\Delta\tau_0$. But $\Delta\tau_0 = 2\sqrt{S}$ is the width of the band.

On substitution into Eq. 8-71, the amplification of yaw can be written as

$$\ell_n \alpha_0 = \frac{\pi}{2} \sqrt{S} \Delta(\Omega t) \quad (9-48)$$

where α_0 and α_f are the initial and final yaws upon entering and leaving the resonance band, respectively. $\Delta(\Omega t) = (\text{fit})_2 - (\text{fit})_1$ is the nondimensional time interval required for the $\tau_0(\Omega t)$ to traverse the resonance band. $(\Omega t)_1$ corresponds to the higher frequency limit of the resonance band, i.e., $\tau_n t \sqrt{S}$ with associated fill-ratio $(b^2/a^2)_1 = x_1$; $(\Omega t)_2$ corresponds to the lower frequency limit of the band, i.e., $\tau_n - \sqrt{S}$ with associated x_2 . This interval can be readily determined. If, for example, we consider Case I, 100% full cavity, and $T \geq 0.6$,

$$x = 0.89e^{-0.482k_t \Omega t}$$

the width of the resonance band is from x_2 to x_1 . Therefore,

$$\Delta(\Omega t) = \frac{1}{0.482k_t} \ell_n \frac{x_1}{x_2} \quad (9-49)$$

Thus amplification of yaw, for a given S , depends on the value of $\Delta(\Omega t)$. With the Case II model, the transit of $\tau_0(t)$ curve through the resonance band occurs earlier, i.e., at smaller values of $1/I_\infty$ where the $\tau_0(t)$ curve is steeper or its rate of change is greater. Therefore, at earlier times $\tau_0(t)$ will traverse the resonance band in a shorter time resulting in a smaller value of $\Delta(\Omega t)$. At later times the $\tau_0(t)$ curve flattens out in its asymptotic approach to the steady state value of τ_0 . If $\tau_0(t)$ curve crosses the resonance band at later time, as in Case I, $\tau_0(t)$ stays within the resonance band longer resulting in larger value of $\Delta(\Omega t)$. This is clearly shown in Fig. 8-12.

The earlier time of passage of $\tau_0(t)$ through the resonance band on the Case II model can be shown by the following example. Consider, for simplicity, the laminar case. The resonance occurs when $\tau_0(t) = \tau_n$ and, for a given $c/[a(2j+1)]$, at a specific value of $b^2/a^2 = x_0$ as given by Stewartson's Tables. Then by Eq. 9-41, Case II

$$x_0 = e^{-2k\Omega t}$$

Assume that the resonance occurs at $x_0 = 1/e$. Then if $1/e = e^{-2k\Omega t}$, $k\Omega t = 1/2$. At this value of $k\Omega t$ the fractional value of the angular momentum, Eq. 8-55, is

$$\frac{I}{I_\infty} = 1 - e^{-2k\Omega t} = 1 - e^{-1} = 0.63$$

For Case II, therefore, the resonance occurs when the fluid has acquired 63% of its angular momentum. On the other hand, for Case I, by Eq. 9-39

$$x_0 = 1/e = e^{-k\Omega t}$$

Therefore, $k\Omega t = 1$, and the angular momentum is

$$\frac{I}{I_\infty} = 1 - e^{-2k\Omega t} = 1 - e^{-2} = 0.86$$

or the resonance occurs when the fluid has acquired 86% of its angular momentum.

9-5.4 EXPERIMENTAL EVIDENCE

As stated in Ch. 8, the proposed methods of computation of the eigenfrequencies during spin-up and the consequent evaluation of the amplification of yaw during transient instability are relatively crude and no decision, on theoretical grounds, could be made at this time for preferring either Case I or Case II treatments. An appeal, therefore, must be made to the available experimental data. Some of these are depicted in Fig. 8-11 and are discussed in Ch. 8; others are to be found in Ref. 6.

All of the experimental data were obtained with a modified 20 mm M56 Projectile fired in the closed aerodynamic range of the BRL with a few firings outside at a "time of flight" screen. As Fig. 8-11 shows, instability commences very early: for a $\nu = 30$ cSt fluid, for example, instability ceases at about $\Omega t = 200$ or at 50 feet from the muzzle; for a $\nu = 3$ cSt fluid the instability ceases at $\Omega t = 600$ or 160 feet from the muzzle (for these firings $\Omega = 10^4$ rad/sec, $V = 2.7 \times 10^3$ ft/sec). With a mercury filler the projectile developed an excessive yaw

at 150 feet from the muzzle; and with $C(\text{Br})_4$ fluid⁶ (specific gravity = 3, $\nu = 3.4 \text{ cSt}$) early instability also was manifested. As we have seen, early instability favors the Case II model.

However, computations on the basis of models Case I and Case II, and a comparison of the results with the experimental data for the 20 mm M56 Projectile, lead to the following conclusions: (1) Case I gives roughly the correct order of magnitude of yaw amplification but is at variance with the observational data on the time of commencement of instability, and (2) Case II gives more nearly correct time for the onset of instability but underestimates the amplification of yaw.

The designer, however, is usually more interested in the correct estimate of the level of yaw which is likely to occur during transient instability rather than the precise time of its occurrence. Both methods predict reasonably early the onset of instability, i.e., during spin-up. Therefore, it is suggested that the designer confine himself to the Case I model of computation. Mild transient instability, i.e., yaws of 2-4 degrees can usually, be tolerated. The duration of transient instability is usually short, unless the resonance band is very wide, and such mild yaws can usually later be suppressed by the aerodynamic damping. If required, their effect on the trajectory can be computed and allowed for. Occurrence of larger transient yaws present, of course, a more difficult problem. As an illustration we may consider the experiment described in the paragraphs which follow.

20 mm M56 Projectiles were loaded with 90% of $C(\text{Br})_4$ and fired at a "time of flight" screen at 600 yards. None of the projectiles hit the target — all falling short — suggesting the presence of excessive yaws. For this projectile, from Refs. 6 and 7, we have the following information:

$$c/a = 2.68$$

$$\tau_n = 0.156$$

$$\sqrt{S} = 3.1 \times 10^{-3}$$

With $\Omega = 10^4 \text{ rad/sec}$, $a = 0.78 \text{ cm}$, and $\nu = 0.034 \text{ stoke}$ the Reynolds number is 1.8×10^5 .

The width of the resonance band on the frequency scale is

$$\tau_{01} = 0.156 \pm 0.031 = 0.187$$

$$\tau_{02} = 0.156 - 0.031 = 0.125$$

From Stewartson's Tables one finds that the resonance in the above cavity occurs ($n = 1, j = 1$) at $(b^2/a^2)_0 = x_0 = 0.541$ or at 46% fill. The "effective" $(b^2/a^2)_i$ corresponding to the above frequency limits of the resonance band are, by Eq. 9-30, $x_1 = 0.579$ and $x_2 = 0.501$, respectively.

One computes $k_t = 1.16 \times 10^{-3}$. Applying Eq. 9-49, Case I,

$$\Delta(\Omega t) = \frac{10^3}{(0.482)(1.16)} \ln \frac{0.579}{0.501} = 259$$

The amplification of yaw, by Eq. 9-48

$$\ln \frac{\alpha_1}{\alpha_0} = (0.393)(3.1 \times 10^{-3})(259) = 3.155$$

$$\text{or} \quad \frac{\alpha_1}{\alpha_0} = 23$$

Thus the Case I model predicts the occurrence of very large transient yaw which appears to account for the observed behavior of the projectile.

The exact resonance occurs, by Eq. 9-45, at

$$x_0 = 0.541 = 0.89e^{-0.482k_t\Omega t}$$

Therefore, $k_t\Omega t = T = 1.075$ or, with given $\Omega = 10^4 \text{ rad/sec}$ and $V = 2.7 \times 10^3 \text{ ft/sec}$, at

$$X = \frac{TV}{\Omega k_t} = 250 \text{ feet from the muzzle}$$

when, by Eq. 9-44, $1/I_\infty = 0.72$ or the liquid has acquired 72% of its angular momentum.

If, for the same example, we were to use the Case II model computations, then by Eq. 9-47

$$\Delta(\Omega t) = \frac{5}{3k_t} \left(\frac{1}{x_2^{3/10}} - \frac{1}{x_1^{3/10}} \right) \quad (9-50)$$

The amplification of yaw is found to be only $\frac{\alpha_1}{\alpha_0} = 2.6$ which is completely inadequate to account for the observed behavior. The resonance would have occurred at $I/I_\infty = 0.40$ or 75 feet from the muzzle.

9-5.5 TRANSIENT INSTABILITY OF THE XM410 PROJECTILE

We have used the **XM410** Projectile for various illustrative purposes. We will again use this projectile for a final illustration.

As was previously shown, a cylindrical cavity $c/a = 1.56$ of the **XM410** Projectile, for $j = 0$, contains a broad range of fluid frequencies, $\tau_0 \pm \sqrt{S} = 0.34 \pm 0.25$ or from 0.59 to 0.09. The nutational frequency is $\tau = 0.25$. Therefore, the resonance band covers the frequency range from $\tau_{01} = 0.50$ to $\tau_{02} = 0.09$. The principal fluid frequency $\tau_0 = 0.34$ lies above the nutational frequency and, normally, no transient instability would be encountered, (see Ch. 8). However, because of the exceptional width of the resonance band of this projectile, the projectile will be unstable during spin-up.

Its spin-up history is presented graphically in Fig. 9-2. The data were computed by Eq. 9-30 to obtain $\tau_0(\Omega t)$, and by Eqs. 9-43 and 9-44 to find the corresponding $I(\Omega t)/I_\infty$. As the graph shows, the projectile is in serious trouble during its transient phase. The instability commences at about $\Omega t = 300$ or, at $M = 1.5$ with $\Omega \approx 10^3$ rad/sec, at about 0.3 sec from muzzle.

There is no need to integrate Eq. 8-69 in order to find the amplification of yaw

during spin-up. The yaw, on linear theory, will obviously be very large. However, as we shall see in Ch. 10, the maximum amplitude might be limited by nonlinear effects.

In principle, however, Eq. 8-69

$$\ln \frac{\alpha_1}{\alpha_0} = \frac{\Omega}{2} \int_{t_1}^{t_2} \sqrt{S - (\tau_0 - \tau_n)^2} dt$$

can be integrated numerically since $\tau_0(t)$ is a function of time through $x(t)$ by Eq. 9-30 and $x(t)$ is given by, say, Eq. 9-45. The process, however, is cumbersome and usually not worth the effort. It could be used in special cases when it might be desirable to do so.

9-5.6 AMPLIFICATION OF YAW IN NONCYLINDRICAL CAVITIES

Only a rough estimate can be made of the amplification of yaw in noncylindrical cavities because theoretical spin-up history has been developed for the cylindrical cavities. Nevertheless, since the time of occurrence of instability during spin-up is of no particular importance to the designer, one may use the following procedure to arrive at a rough approximation. The width of the resonance band in a noncylindrical cavity is $\tau_n \pm \sqrt{S_m}$, see par. 9-4.2, where S_m is Stewartson's parameter in a noncylindrical cavity and is found by Eq. 9-29. One then computes the corresponding x_1 and x_2 by Eq. 9-30 for the above frequency limits. Then $\Delta(\Omega t)$ is found, as before, by Eq. 9-49. The amplification of yaw would be given by

$$\ln \frac{\alpha_1}{\alpha_0} = \frac{\pi}{8} \sqrt{S_m} \Delta(\Omega t) \quad (9-51)$$

Such a procedure probably can be relied upon to give the correct order of magnitude to the yaw amplification during transient instability with a noncylindrical cavity.

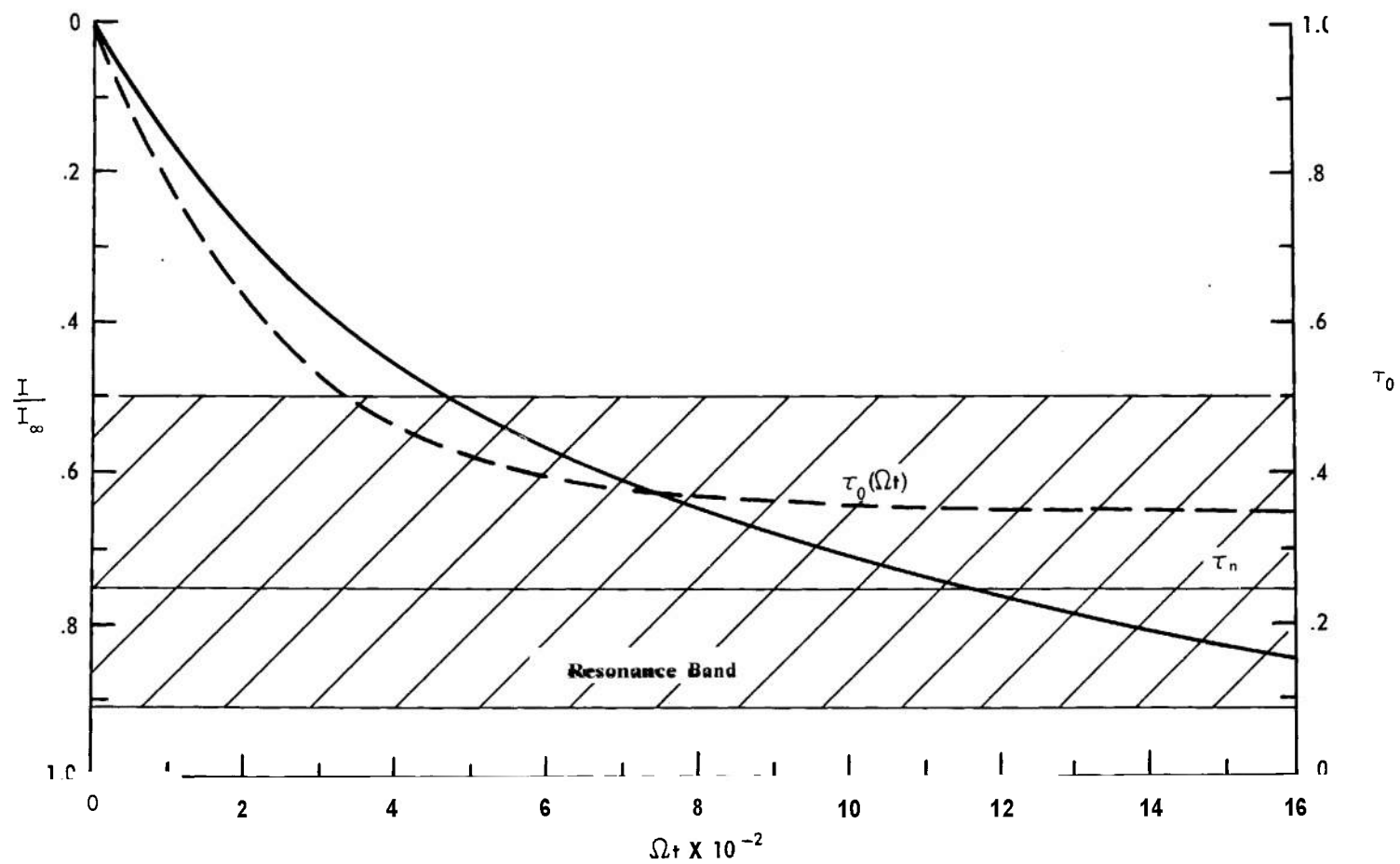


FIGURE 9-2. SPIN-UP HISTORY OF THE 752 MM XM410 PROJECTILE

9-6 BRIEF OUTLINE OF DESIGN STEPS

It may be helpful to the designer to have a brief outline of the main steps to be followed in the design of liquid-filled projectiles.

Given: I , s_g , σ , τ for the rigid projectile, i.e., with liquid frozen.

I. CYLINDRICAL CAVITY

A. NEW DESIGN:

1. Cavity: $2c$ = height, $2a$ = diameter
2. Assign a fill-ratio β
3. Check whether with liquid filler the gyroscopic stability is adequate, Eq. 9-2c
4. Check whether viscous effects are significant, par. 9-3.1
5. From Stewartson's Tables with $b^2/a^2 = 1 - \beta$ find K_1 on the line $\tau_0 = \tau_n$ in the first column headed by $c/[a(2j + 1)]$ for the first radial mode $n = 1$. If viscous effects are significant, use the line $\tau_0 = \tau - \epsilon$.

All cavities with

$$c/a = K_1(2j + 1) \quad j = 0, 1, 2, \dots$$

will have resonating frequency $\tau_0 = \tau$

Repeat for $n=2$. Avoid all such cavities.

6. See par. 9-3.3 on how to deal with the width of the resonance band.

B. CONVERSION OF AN EXISTING PROJECTILE TO ONE CONTAINING A LIQUID

1. Given c/a , β
2. Items IA1, IA2, IA3, and IA4 apply.

3. Construct table $c/[a(2j + 1)]$ vs $j = 0, 1, 2, \dots$
4. From Stewartson's Tables for $b^2/a^2 = 1 - \beta$ find all τ_0 and $2R$ corresponding to each value of $c/[a(2j + 1)]$, $j = 0, 1, 2, \dots$
In practice it is seldom necessary to go beyond $j = 2$.
5. Compute Stewartson's parameter S and test for instability by Eq. 9-8 if viscous effects are significant; otherwise by Eq. 4-24. If unstable, see discussion in pars. 9-3.4 and 9-3.7.

II. NONCYLINDRICAL CAVITY

1. Items IA1, IA2, IA3, and IA4 apply.
2. To find τ_0 either in a newly designed cavity or in an existing cavity- see pars. 9-4, 9-4.1, and 9-4.2.
3. For a cylindrical cavity with rounded corners see par. 9-4.4. Neglect the effect of rounded corners on τ_0 if $R'/a \leq (1 - b/a)$ where R' is the radius of the corner and $b/a = \sqrt{1 - \beta}$.

III. SPIN-UP OR TRANSIENT PHASE

1. If the projectile is designed to be stable in its steady state, i.e., with the liquid fully spinning, examine its stability during spin-up of the liquid.
2. Compute Stewartson's parameter S .
3. The width of the resonance band is $\tau_n \pm \sqrt{S}$. Compute the corresponding x_1 and x_2 by Eq. 9-30.
4. Find $A(\Omega t)$ by Eq. 9-49 and the amplification of yaw during transient instability by Eq. 9-48.

REFERENCES

1. H.P. Hitchcock, *Aerodynamic Data for Spinning Projectiles*, BRL Report **620**, Aberdeen Proving Ground, Md., **1947**.
2. E.H. Wedemeyer, *Dynamics of Liquid-Filled Shell: Non-Cylindrical Cavity*, BRL Report **1326**, Aberdeen Proving Ground, Md., **1966**.
3. B.G. Karpov, *Dynamics of Liquid-Filled Shell: Resonance in Modified Cylindrical Cavities*, BRL Report **1332**, Aberdeen Proving Ground, Md., **1966**.
4. J.T. Frasier and W.E. Scott, *Dynamics of Liquid-Filled Shell: Cylindrical Cavity with a Central Rod*, BRL Report **1391**, Aberdeen Proving Ground, Md., **1967**.
5. J.W. Miles, "Free Surface Oscillations in a Roating Liquid," *The Physics of Fluids*, Vol. **12**, **1959**.
6. B.G. Karpov, *Experimental Observations of the Dynamic Behavior of Liquid-Filled Shell*, BRL Report **1171**, Aberdeen Proving Ground, Md., **1962**.
7. B.G. Karpov, *Dynamics of Liquid-Filled Shell: Instability During Spin-Up*, BRL Memo Report **1629**, Aberdeen Proving Ground, Md., **1965**.

APPENDIX B

TREATMENT OF CAVITIES WITH PARTIAL BURSTERS

The partial burster, i. e., the burster which protrudes only part way into the cavity is considered in this Appendix. It appeared desirable to relegate this matter to the Appendix because, at the present time, it is not known how to compute the eigenfrequencies in such partially burstered cavities. The configurations are shown schematically in Fig. B-1. Theoretical solution appears very difficult because for configurations shown in Fig. B-1, there is a discontinuity in one of the boundary conditions. The best way to deal with this problem, therefore, is by the conduct of experiments. These are planned at the BRL and the results will be published in a BRL Report. Meanwhile, in order not to delay the issuance of this Handbook, a tentative procedure for handling this problem by the designer is outlined below. It is to be understood, of course, that the validity of this procedure might be either confirmed or negated by the forthcoming experiments.

Let V_0 be the volume of the cavity without the burster, and V_c be that of the cylindrical cavity of the same height $2c$ and the same diameter $2a$. Let $2r$ be the diameter of the burster, h its length in the cavity, and v_r its volume. Thus the burster protrudes $h/2c$ fraction into the cavity; a fraction $1 - h/2c$ is without the burster. If the available volume of the cavity $V_0 - v_r$ be filled to β fraction, then we can distinguish three cases for the fill-ratios.

Case 1. If $b^2/a^2 > r^2/a^2$, then the fill-ratio is given by

$$\beta > 1 - \frac{(b^2/a^2) - (r^2/a^2) (h/2c)}{(V_0/V_c) - (r^2/a^2) (h/2c)} \quad (\text{B1})$$

It is to be recalled, par. 9-3.6, that in order for the burster not to interfere with the oscillations of the free surface it is necessary that

$$b^2/a^2 - r^2/a^2 \geq 0.10(r/a) \quad (\text{B2})$$

If this condition is satisfied and β is computed by Eq. B1, then the problem is to be treated as in par. 9-3.5, i. e., the fluid does not feel the presence of the burster and, hence, the length of the burster does not make any difference.

Case 2. This is a special case when $b^2/a^2 = r^2/a^2$. The fill-ratio is given by

$$\beta = \frac{(V_0/V_c) - (r^2/a^2)}{(V_0/V_c) - (r^2/a^2) (h/2c)} \quad (\text{B3})$$

Case 3. If $b^2/a^2 < r^2/a^2$, the fill-ratio is given by

$$\beta < 1 - \frac{(b^2/a^2) (1 - h/2c)}{(V_0/V_c) - (r^2/a^2) (h/2c)} \quad (\text{B4})$$

This case is probably the most commonly encountered in practice. It is to be noted that for the cylindrical cavity $V_r = V_c$.

Thus Case 1 presents no problem. For Case 2, the oscillating free surface will periodically uncover part of the burster and the burster will interfere with these oscillations. Case 3 is more nearly clear cut. But in the absence of any knowledge or evidence to the contrary, we shall assume that Case 2 loading condition and Case 3 are to be treated in a similar manner.

Suppose, therefore, that the cavity has a fineness-ratio c/a ; the diameter of the cylindrical burster is $2r$ and it protrudes $h/2c$ fraction into the cavity. The cavity is filled to β fraction of the available volume $V_0 - v_r$ so that Eq. B4 is satisfied, see Fig. B-1. The fractional air column is given by $b^2/a^2 < r^2/a^2$. The suggested procedure for finding τ_0 in such a cavity is as follows:

A-B-4

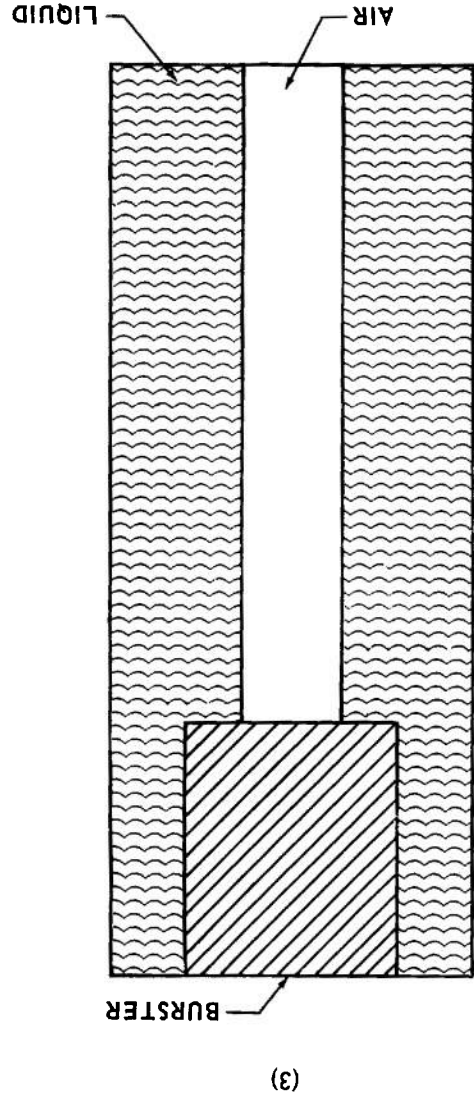
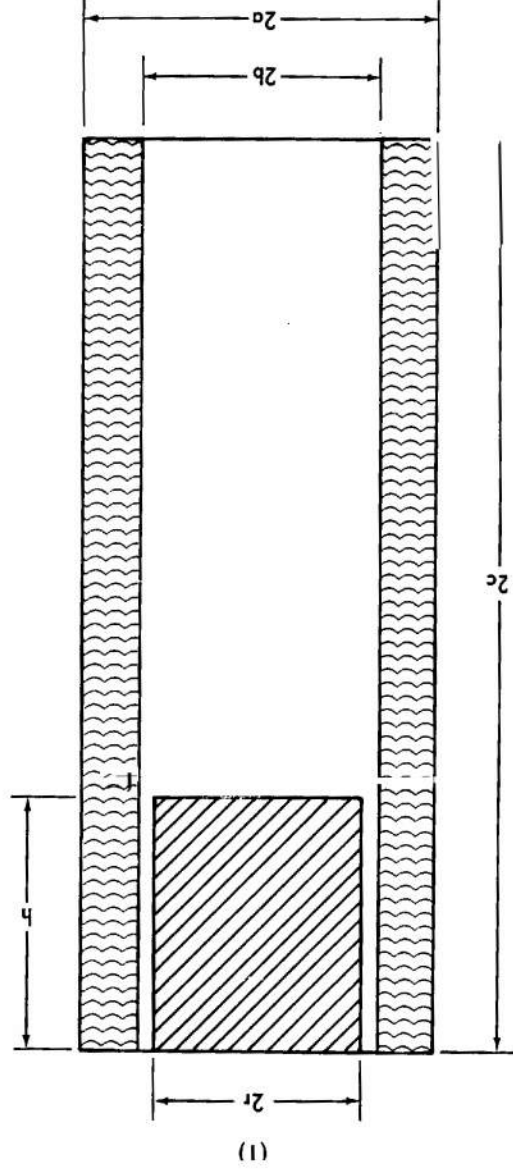
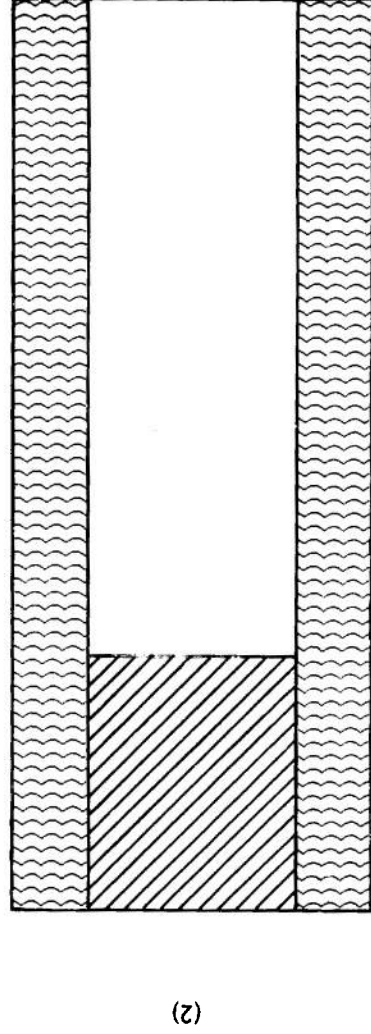


FIGURE B-1. CAVITIES WITH PARTIAL BURSTERS



a. Cylindrical Cavity

Step 1: Disregard the burster. Find τ_0 from Stewartson's Tables, Tables 4-1, with $c/[a(2j+1)]$ and above b^2/a^2 which is either arbitrarily prescribed so as to satisfy the condition that $b^2/a^2 < r^2/a^2$ or computed with prescribed β by Eq. B4. **Call this** τ_{01} .

Step 2: Disregard the air column. Consider the burster as extending through the whole cavity and the cavity is 100% filled. Find τ_0 from Central Column Tables, Tables 4-2, with $c/[a(2j+1)]$ and r^2/a^2 . **Call this** τ_{02} .

Step 3: It is suggested that the effective τ_0 of the actual cavity is the weighted mean of the two τ_0 's found in Steps 1 and 2, i.e.,

$$(\tau_0)_{\text{eff}} = \tau_{01} (1 - h/2c) + \tau_{02} (h/2c) \quad (\text{B5})$$

b. Noncylindrical Cavity

To compute τ_{01} for a noncylindrical cavity we must use Eq. 9-22 with $x_0 = b^2/a_0^2$ as above and evaluate the integrals, Eq. 9-21, for the cavity.

To compute τ_{02} it is necessary to have a function similar to $1/K_1$, Eq. 9-17, but for the Central Column Tables. Call this function $1/K_{c1}$. It is found that for the radial mode $n = 1$, the polynomial, Eq. B6, represents well the tabular values for the following range of τ_0 and r^2/a^2 :

$$0.0 \leq \tau_0 \leq 0.36$$

$$0.05 \leq r^2/a^2 \leq 0.25$$

Let

$$y \equiv r^2/a^2$$

then one can write an equation which is analogous to Eq. 9-22 for a completely burstered 100% filled noncylindrical cavity.

$$1 = c/[a_0(2j+1)] [(1.0121 + 4.6841y_0) - (1.4601 + 6.4941y_0)\tau_0 + (0.8751 + 1.4921y_0)\tau_0^2] \quad (\text{B6})$$

where

$$y_0 = r^2/a_0^2$$

and the integrals I and II are identical to those used in Eq. 9-22 which are given by Eq. 9-21. Because of a somewhat different form of function $1/K_{c1}$ as compared to $1/K_1$ for Stewartson's Tables, the integral III does not appear in $1/K_{c1}$ because there is no y^2 term.

The effective τ_0 for partially burstered noncylindrical cavity is given, as before, by Eq. B5.

Let us consider as an example the XM410 Projectile with a partial burster. Suppose the burster $r/a_0 = 0.29$, $r^2/a_0^2 = 0.084$, par. 9-3.6, protrudes $h/2c = 1/3$ into the cavity. Let the fill-ratio of the available cavity be such that $b^2/a_0^2 = 0.05$ which satisfies the condition for Case 3 that $b^2/a_0^2 < r^2/a_0^2$. The fineness-ratio of the cavity $c/a = 1.56$. What is τ_0 in this cavity?

a. Cylindrical Cavity

If we assume that the cavity is cylindrical then:

Step 1. From Stewartson's Tables for $c/a_0 = 1.56$ for $j = 0$ and $x_0 = 0.05$ we find $\tau_{01} = 0.34$.

Step 2. From Central Column Tables for $c/a = 1.56$ for $j = 0$ and $y_0 = 0.084$ we find $\tau_{02} = 0.50$.

Step 3. The effective τ_0 in such a cavity is, Eq. B5, $(\tau_0)_{\text{eff}} = (0.34)\left(\frac{2}{3}\right) + (0.50)\left(\frac{1}{3}\right) = 0.39$

b. Noncylindrical Cavity

In par. 9—4.3 we found the values of the integrals for the cavity of the **XM410** Projectile:

$$\begin{aligned} \text{I} &= 1.056 \\ \text{II} &= 1.219 \\ \text{III} &= 1.491 \end{aligned}$$

If $x_0 = 0.05$ then applying **Eq. 9—22** to a partially filled cavity without the burster, Step 1, with $j = 0$ and $c/a_0 = 1.56$, we obtain $\tau_{01} = 0.38$.

Using the same values of the integrals I and II and with $y_0 = 0.084$ we obtain from Eq. B6, Step 2, $\tau_{02} = 0.57$.

Therefore, Step 3,

$$(\tau_0)_{\text{eff}} = 0.38\left(\frac{2}{3}\right) + 0.57\left(\frac{1}{3}\right) = 0.44$$

CHAPTER 10

AMPLITUDE DEPENDENT BEHAVIOR

10-0 LIST OF SYMBOLS*

d	= width of gap between rotating cylinders; boundary layer thickness
K	= a constant
M	= Mach number; stability criterion
R	= average radius of inner and outer cylinder
V	= mean value of flow velocity within the gap
ΔV	= change of flow velocity across gap
v	= value which perturbation velocity assumes at edge of boundary layer

10-1 INTRODUCTION

Because of the lack of theoretical development dealing with nonlinear effects in the liquid-filled systems, and extreme scarcity of the experimental data, present comments of necessity will be very brief. The purpose of these comments is to make the designer aware of the existence of the amplitude dependent behavior of the liquid-filled projectile. Such an awareness may prevent injudicial extrapolation from the linear theory and also may, perhaps, save him from unpleasant surprises when sudden instability occurs at larger yaw angles.

In the preceding chapters it has been emphasized that the mathematical descriptions both of the yawing motion of the projectile and the behavior of the liquid in its cavity are predicated on the fundamental assumption that the perturbation of the initially undisturbed motion is small. This assumption permitted linearization of the equations of motion and their solution. But how small is "a small perturbation"? In the case of the motion of the rigid projectile,

practical experience shows that "smallness of the perturbation" cannot be defined in general terms. The extent of the validity of the linearized theory, as applied to the rigid projectile, depends in a large measure on the shape of the projectile. The most important cause of the amplitude dependent behavior in a rigid projectile is the nonlinearity of the aerodynamic coefficients. For some shapes of projectiles these manifest themselves at the origin, i.e., at very small yaws. In other cases the yawing motion of amplitude as large as 6-10 degrees can be adequately described by the linearized theory. As is shown in Ref. 1, certain types of nonlinearities in the aerodynamic coefficients can be handled mathematically thus permitting the description of the yawing motion at larger yaw angles.

For the liquid-filled projectiles the experience of the behavior of such systems at larger yaws is non-existent. Moreover, as was pointed out in Ch. 3, it appears quite hopeless to solve the nonlinear fluid-dynamic problem. *A priori*, therefore, at the present time one cannot hope to theoretically predict the behavior of the liquid-filled projectile at larger yaws.

Fortunately, most projectiles are designed to operate within the regime of small yaws. Thus the linearized dynamics for the rigid projectiles serves an extremely useful purpose. Similarly, the linearized dynamics for the liquid-filled projectiles should be equally valuable to the designer. Nevertheless, it appeared desirable to undertake a few exploratory experiments² with the gyroscope at larger amplitudes. Although some interesting data were obtained, it is clear that these experiments just scratched the surface of a complicated and unexplored field. Most of the experiments were performed with a 2.5-in. cylindrical cavity, with $c/a = 3.08$ at resonant fill-ratio $b^2/a^2 = 0.15$.

*For identification of other symbols in this chapter, refer to Chapter 3.

10-2 GROWTH OF AMPLITUDE AT RESONANCE

Experiments show that Stewartson's theory with viscous corrections accurately predicts the initial rate of growth of the nutational amplitude at resonance. However, the experiments also show that this initial rate of growth persists only up to a certain amplitude where the rate changes abruptly to a new rate. This matter was discussed briefly in Ch. 6 where it was pointed out that this change is probably associated with the development of instability in the laminar boundary layer. Further theoretical consideration of this phenomenon will be considered in par. 10-5. The amplitude at which transition occurs is strongly Reynolds number dependent as is shown in Table 10-1.

TABLE 10-1. REYNOLDS NUMBERS OF TRANSITION FROM THE LAMINAR BOUNDARY LAYER.

v, cSt	$LogRe$	Transition Amplitude, Degrees
1	5.72	0.4
3	5.23	0.6
5	5.00	0.73
13	4.60	1.0
49	4.04	2.6
100	3.72	5.6
350	3.17	<8

For still higher viscosity oils, the transition presumably occurred at amplitudes not reachable by the gyroscope because of its amplitude limitation of about 12°.

As the amplitude continues to grow, the new rate also changes. It may even undergo a series of changes but eventually appears to settle to a more nearly linear rate rather than exponential. Finally, at a certain amplitude, marked by a rather sharp discontinuity, the rate of growth of the amplitude ceases and the gyroscope settles to oscillate at a constant amplitude. This maximum amplitude reached by the gyroscope depends strongly on the Reynolds number. This appears to be a steady state condition because the gyroscope continues to oscillate at this amplitude indefinitely.

The time histories of growth of amplitude, at resonance, at various Reynolds numbers, are shown in Figs. 10-1(A) through 10-1(H). The transition, discussed above, is marked by an arrow on the records. The transition is shown particularly clearly on the larger amplification record, Fig. 10-2(A).

Frasier* (BRL) has observed that such a transition from the laminar boundary layer is progressively delayed, i.e., occurring at larger amplitudes, as one moves away from the exact resonance, i.e., into the wings of the resonance band. This might be expected. The excited liquid frequencies have maximum amplitude at the exact resonance and, hence, have a maximum disturbing influence on the boundary layer. Away from the resonance, these disturbing influences are weaker and should manifest themselves at correspondingly larger amplitudes of the gyroscope.

Thus the first departure from the prediction of the linear theory of the rate of growth of the nutational amplitude is due to the change in the nature of the boundary layer on the walls of the cavity. In this connection, another observation made by Frasier is of interest. He cut slots in the metal rotor shown in Fig. 5-2. With a proper illumination and a stroboscope he could observe the free liquid surface at resonance. Working with silicone oil — $v = 1 cSt$, $c/a = 3.08$ cavity and resonance fill $b_2/a_2 = 0.15$ — he observed, at small amplitudes, a clearly defined 1-1/2 cosine displacement wave ($j = 1$). As the amplitude of the gyroscope increased, the displacement of the free liquid surface became surprisingly large and a number of high frequency wavelets appeared superimposed on the fundamental $j = 1$ wave. In preliminary experiments, no analysis was made of the nature of the frequencies of these wavelets. These might be excited by the transition of the laminar boundary layer to cellular.

*Private communication

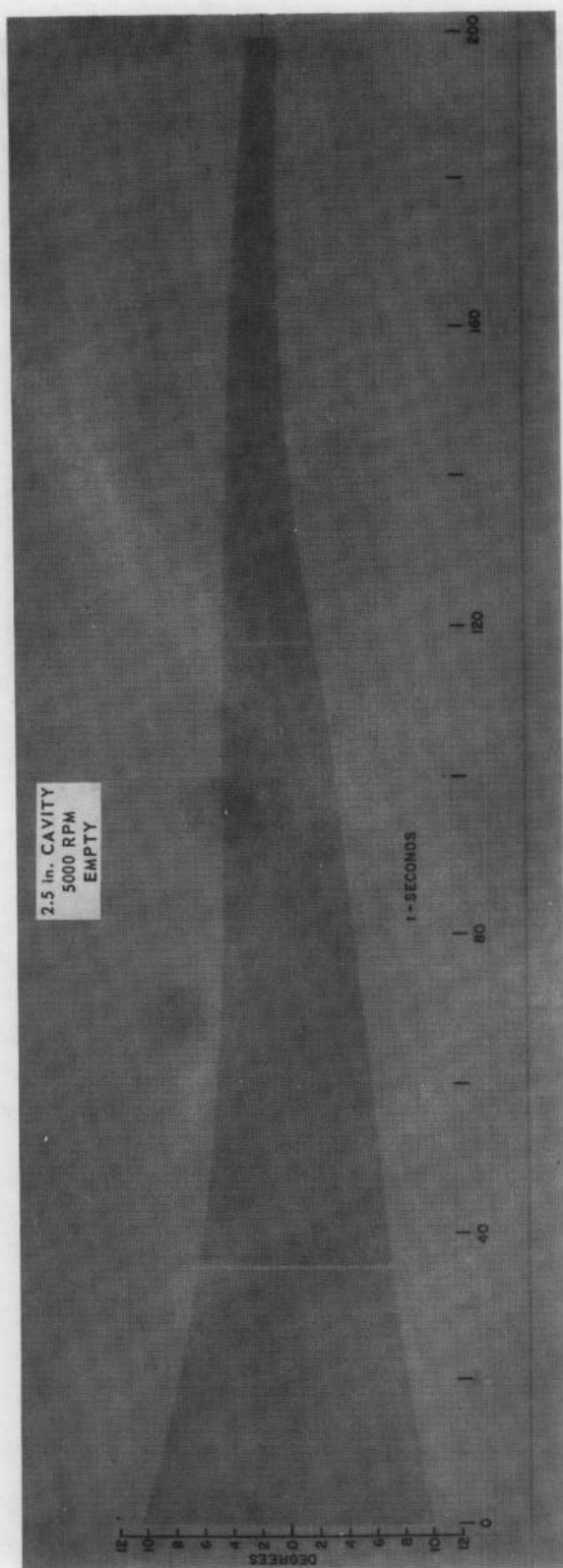
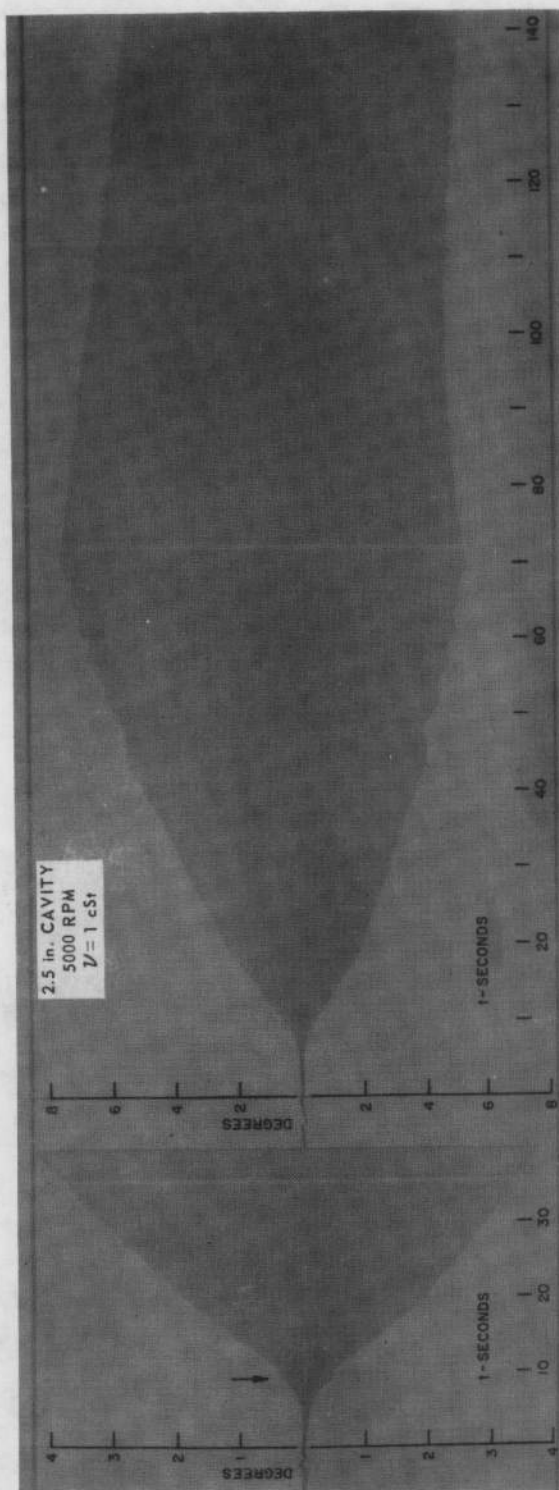


FIGURE 10-1(A). RECORD OF AMPLITUDE HISTORY, EMPTY

FIGURE 10-1(B). RECORD OF AMPLITUDE HISTORY, $\nu = 1 \text{ cSt}$

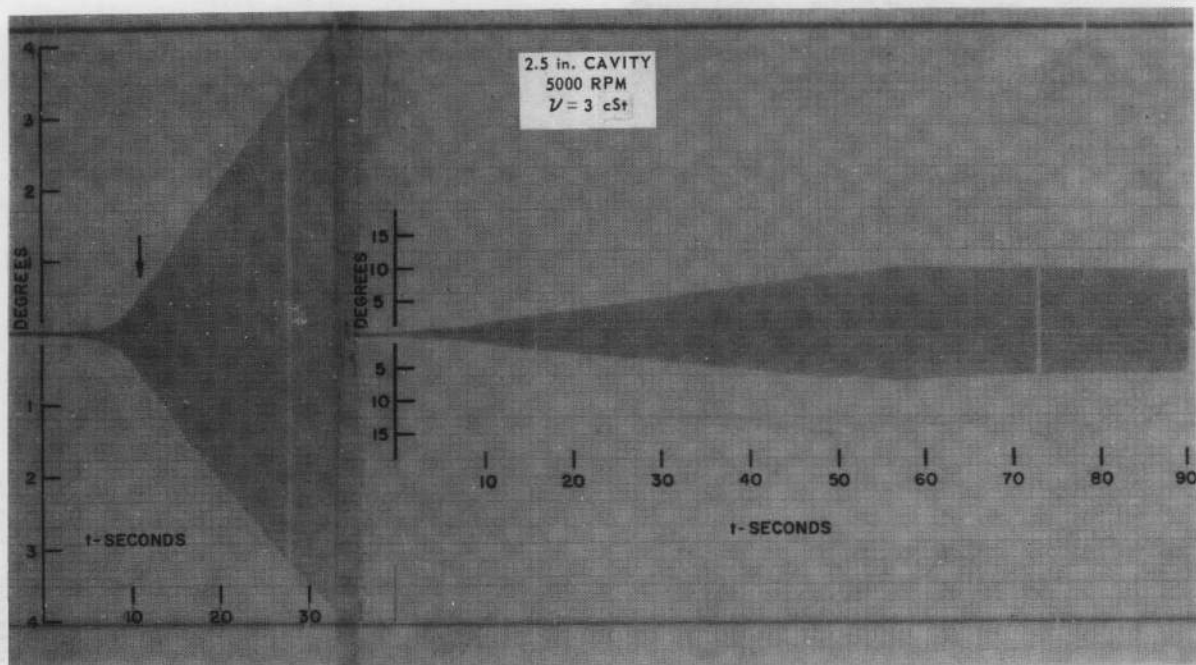


FIGURE 10-1(C). RECORD OF AMPLITUDE HISTORY, $\nu = 3 \text{ cSt}$

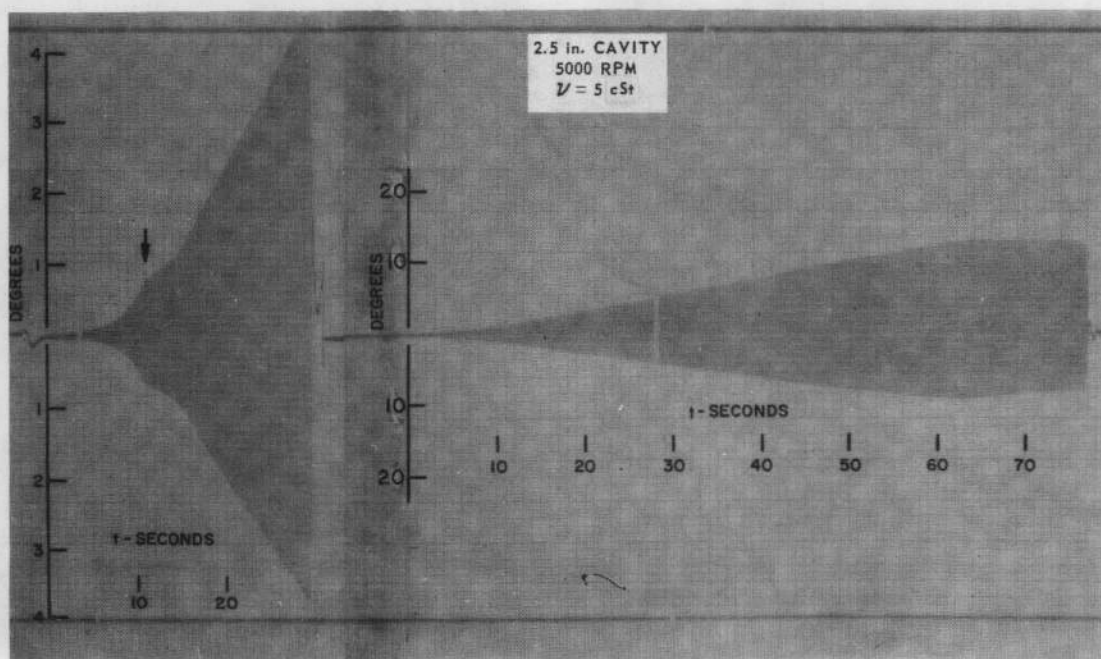
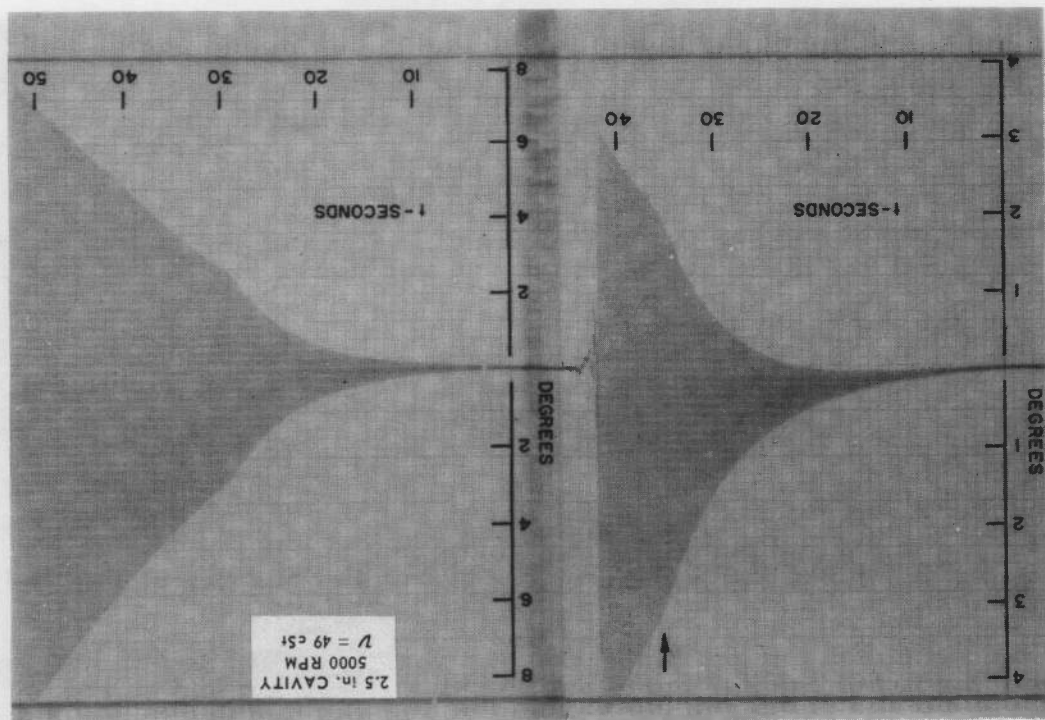
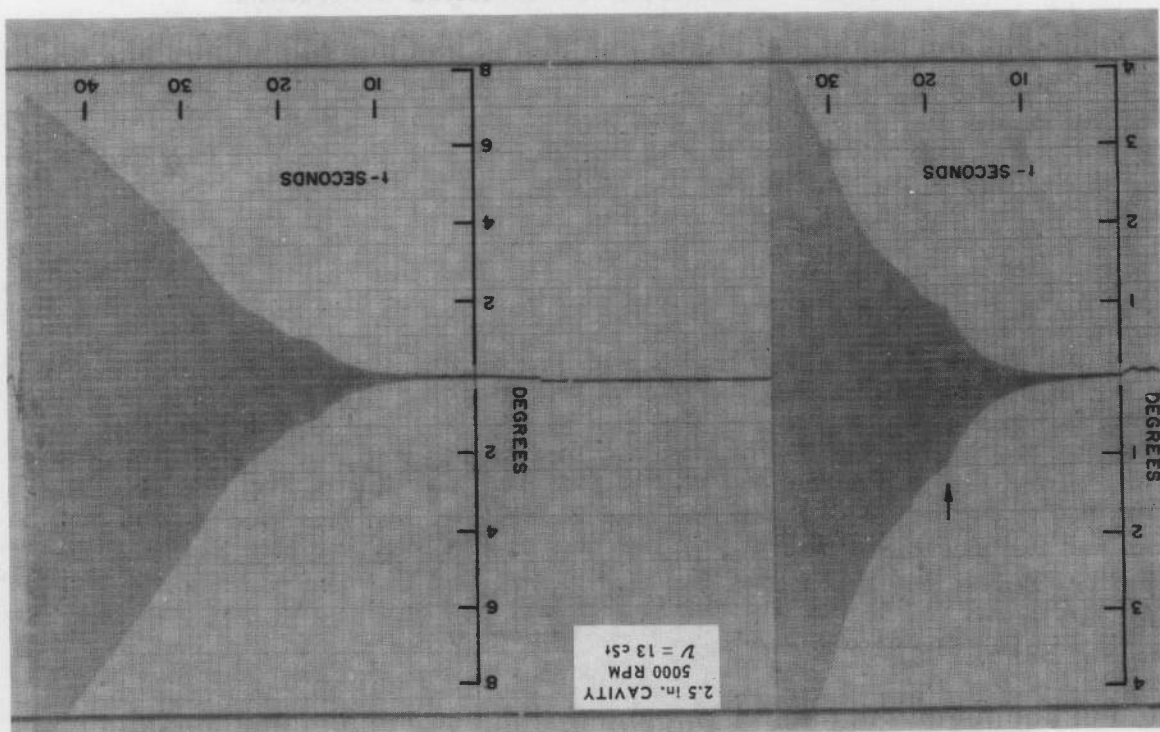


FIGURE 10-1(D). RECORD OF AMPLITUDE HISTORY, $\nu = 5 \text{ cSt}$

FIGURE 10-1(F). RECORD OF AMPLITUDE HISTORY, $V = 49$ c/s.FIGURE 10-1(E). RECORD OF AMPLITUDE HISTORY, $V = 13$ c/s.

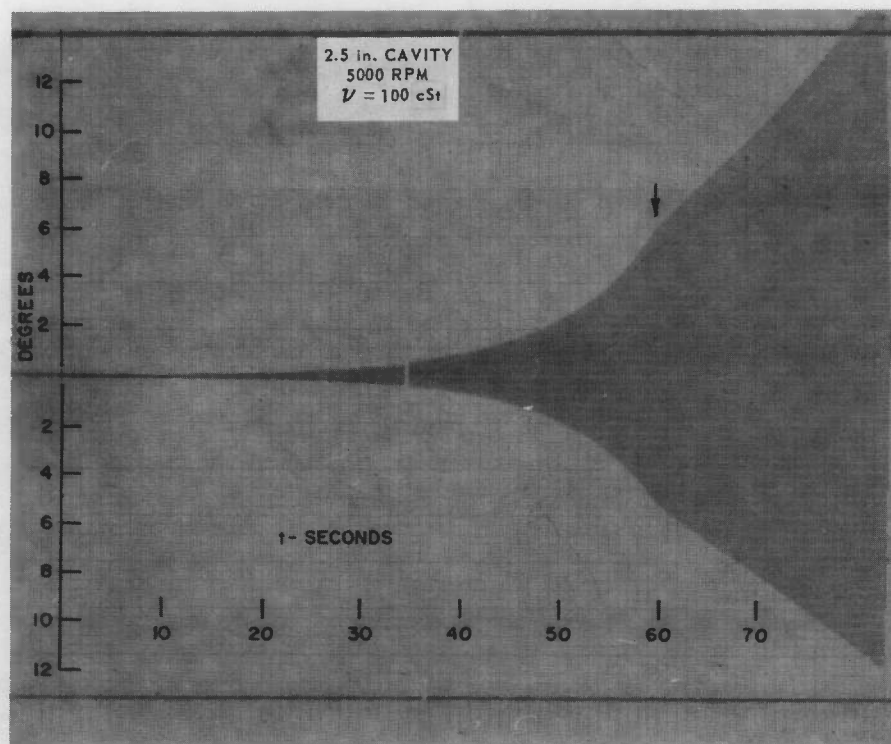


FIGURE 10-1(G). RECORD OF AMPLITUDE HISTORY, $\nu = 100 \text{ cSt}$

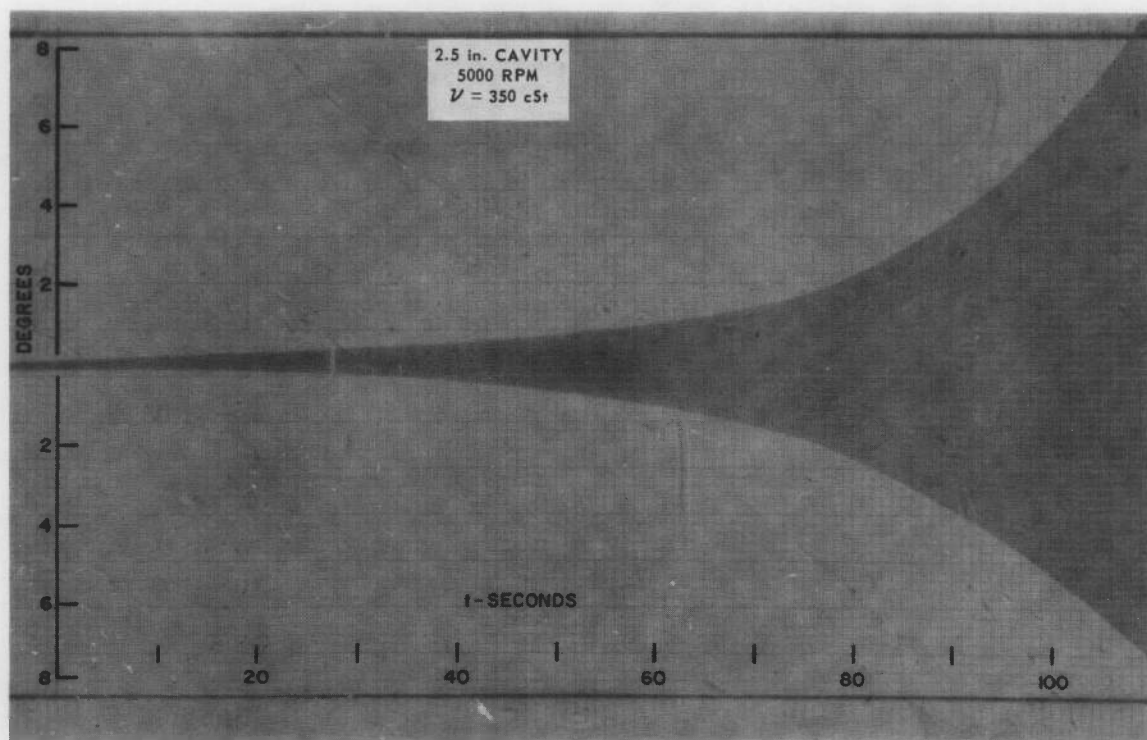


FIGURE 10-1(H). RECORD OF AMPLITUDE HISTORY, $\nu = 350 \text{ cSt}$

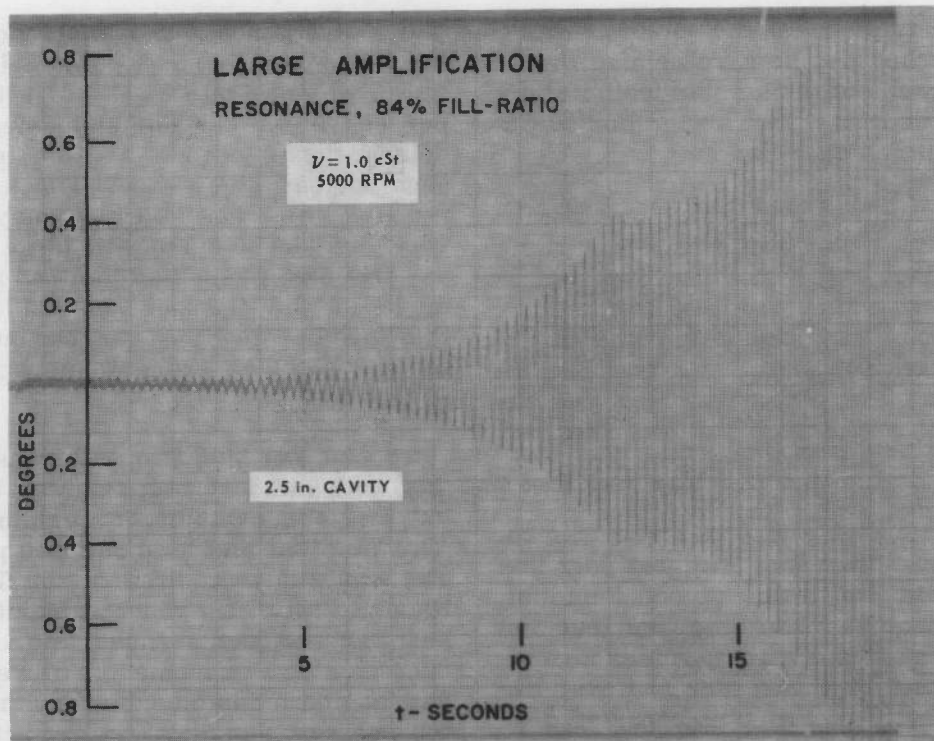


FIGURE 10-2(A). RECORD OF AMPLITUDE HISTORY, LARGE AMPLIFICATION

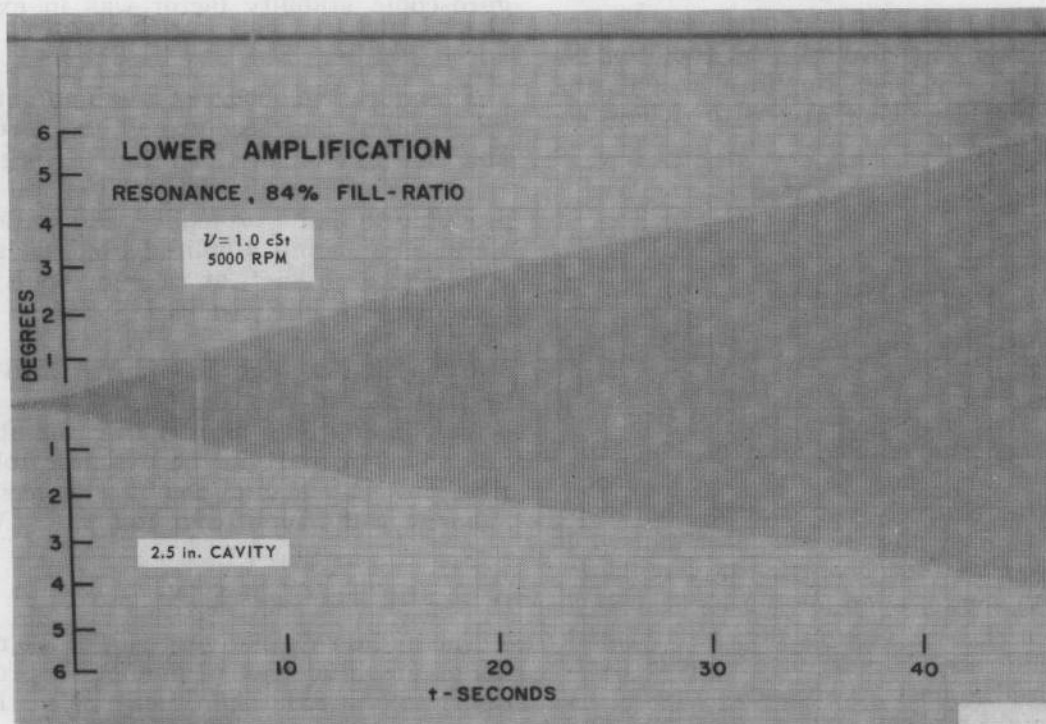


FIGURE 10-2(B). RECORD OF AMPLITUDE HISTORY, LOWER AMPLIFICATION

The observations of the maximum amplitude reached by the gyroscope are very limited because of the amplitude limitation of the gyroscope (12°). The available data are given in Table 10-2.

TABLE 10-2. MAXIMUM STEADY STATE AMPLITUDE AT RESONANCE

$v, \text{ cSt}$	2.5-in. cavity		2-in. cavity	
	LogRe	α_{max} , degrees	LogRe	α_{max} , degrees
1	5.72	5.3		
3	5.23	7.9	5.05	5.2
5	5.00	11.3	4.03	7.9

The above few values suggest only the trend. In addition to the Reynolds number effect, there appears to be an influence of the geometry of the cavity. This is further substantiated by the results of tests in a modified cavity of the type considered in par. 9-4.2. In the modified cavity at $\log Re = 5.23$, the gyroscope had a maximum amplitude of only 3.6° instead of 7.9° , Table 10-2, when the cavity was cylindrical. Also the maximum amplitude appears to be sensitive to the condition of resonance — it is maximum at exact resonance but less elsewhere as the following few values show:

Fill-ratio, %	α_{max} , degrees
82.2 (resonance)	5.2
82.6	4.4
82.9	3.9

It should be noted, however, that the observed amplitude behavior was associated with relatively very slow initial divergence which, for the above experiments, did not exceed $\lambda = 0.5$ per sec. As Fig. 10-1(A) shows, even for the highest Reynolds number tested ($Re = 5 \times 10^5$), at which the rate of divergence is the largest, it required almost 70 seconds to reach its maximum amplitude. The question may well be asked what would happen if the

initial divergence rate is more violent? For the XM410 Projectile, for example, the initial divergence rate at $M = 1.5$ is $\lambda = 62$ per sec. Will the restraining moments which delimit the amplitude be able to contain such violent divergence? The answer is: probably not and the yaw may reach a very high level even with large Re . The experiment described below, although made at the transient instability rather than at the steady state resonance as in the gyroscope experiments, nevertheless is suggestive.

The 20 mm M56 Projectile was filled to 70% with mercury. According to Fig. 5-7, its transient instability is maximum at this percent of fill and is about $\lambda = 8$ per sec. The projectile was fired in the Transonic Range of the BRL, which is about 800 feet long. The projectile rapidly developed an excessive yaw of some 60-70 degrees. It flew at approximately this yaw throughout the observed length of the trajectory with its axis precessing about the mean trajectory at this angle. It did not tumble and, as inferred from its precessional rate, its gyroscopic stability factor was in excess of 2.

Therefore, the observed maximum amplitudes with the gyroscope may not be realizable in practice if the initial divergence rates are sufficiently violent. It is still very probable that the projectile will eventually stabilize at some amplitude but it is impossible to predict at present what this level of yaw is likely to be.

In passing it might be of interest to note that stabilization of the gyroscope at a certain amplitude after initial instability has a counterpart in the dynamics of the rigid projectile acted upon by a cubic static moment of the type (c) in Ref. 1, Ch. VIII.

10-3 THE EFFECT OF SPIN

The initial rate of divergence of the nutational amplitude at resonance is proportional to the axial spin, i.e., $\frac{\Omega}{2}\sqrt{S}$. However, the final constant amplitude reached

by the gyroscope appears to be independent of the spin as Fig. 10-3 shows. The three spins at which the gyroscope was run show different rates of initial divergence but the final amplitude seems to settle to approximately the same value. The data, however, are extremely limited.

10-4 SUDDEN APPEARANCE OF INSTABILITY

As Ward³ pointed out, the liquid-filled gyroscope could be made unstable at almost any fill-ratio by giving it a sufficiently violent initial disturbance. Linearized

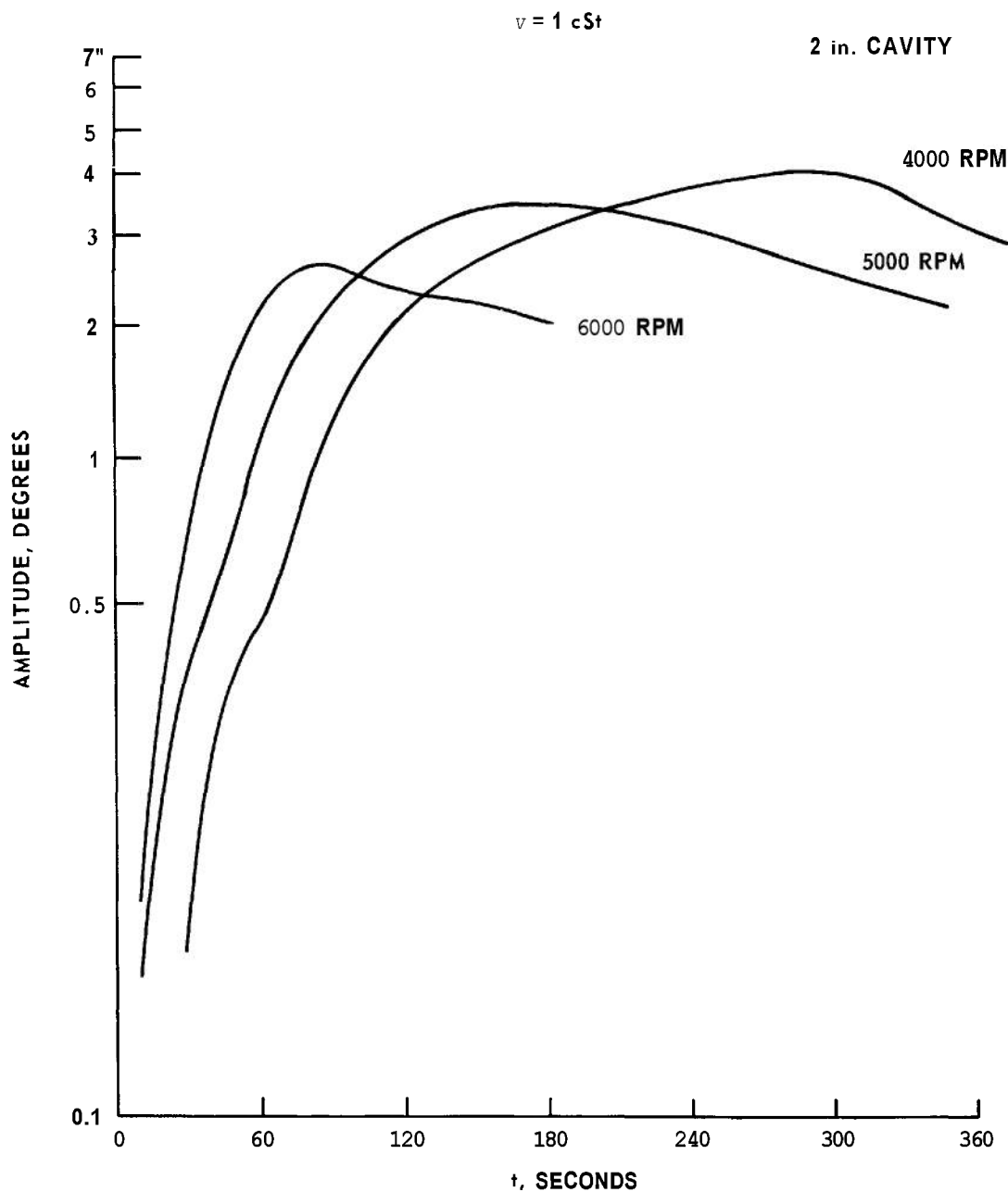


FIGURE 10-3. GROWTH OF AMPLITUDE AT RESONANCE FOR VARIOUS SPIN RATES

theory cannot predict such behavior. In this connection the following experiment is of practical relevance. The $c/a = 3.08$ cavity was completely filled. At this fill-ratio the gyroscope was stable. It was spun at 5000 rpm and gently released at various initial yaw angles. Up to about $\alpha_0 = 6^\circ$ the initial yaw decreased in the usual manner for the stable conditions of the gyroscope, i.e., because of small damping due to the supporting flexures. At an initial angle of slightly above 6° the yaw suddenly diverged, settling eventually at a steady yaw of about 10° . Large yaws might arise in practice in the case of a poorly designed gun-projectile system, in the aircraft gunnery, and at the summit of a high angle trajectory. Such sudden appearance of instability at larger yaws might well be responsible for the occasionally reported correlation of the performance of the liquid-filled projectile with quadrant elevation. At large quadrant elevations the summital yaws are large and, hence, a liquid-filled projectile designed to be stable at small initial yaws may suddenly become unstable at summital yaws. The designer should be aware of such possibilities.

Another type of instability was observed by Frasier working in the wing of the resonance band: $\nu = 1 \text{ cSt}$, $c/a = 3.08$, at $b^2/a^2 = 0.05$. The resonance in this cavity is at $b^2/a^2 = 0.15$ or 85% full. At 95% fill ($b^2/a^2 = 0.05$) one is far out in the wing of the resonance band. At this location the divergence was just barely enough to overcome the natural damping of the system. But the gyroscope was permitted to run with the nutational amplitude increasing very slowly. When it reached about 2° , the amplitude suddenly diverged to about 5° by sharp discontinuity. Further growth continued at a new and higher rate. This phenomenon might also be associated with the instability of the laminar boundary layer.

10-5 SOME THEORETICAL CONSIDERATIONS

There are two possible reasons why the present stability theory should not be appli-

cable at larger yaw amplitudes. First, the nonlinear terms in the dynamic equations, which have been neglected in Stewartson's and extended theories, become appreciable at sufficiently large yaw angles. Second, viscous friction is altered via the transition to cellular or turbulent boundary layer at larger amplitudes of the perturbed flow, an effect which was mentioned in par. 6-4.

The effects due to nonlinear terms in the dynamic equations appear to be insignificant at least to the amplitude of 8 degrees or so. This is shown in Fig. 10-1(H) where for a viscous fluid ($Re = 1.5 \times 10^3$) the boundary layer stays laminar to the observed amplitude of 8 degrees and there-recorded rate of divergence is predictable by the linear theory to this level of yaw.

In contrast, the transition of the boundary layer and a resulting change in the stability behavior can occur — for practical Reynolds numbers — at yaw angles of less than one degree. If transition occurs, it brings about a rather sudden change in viscous damping, resulting in a sudden change of the bandwidth of instability and the rate of divergence.

For the case of laminar boundary layer, the influence of viscosity is inversely proportional to the square root of the Reynolds number (see Ch. 6). In practice, the Reynolds number is usually so large that the effect of viscosity on the bandwidth can be disregarded — provided that the boundary layer is laminar.

On the other hand, transition to a cellular boundary is more likely at high Reynolds numbers and, once transition occurs, viscous effects increase many times and may become important even for large Reynolds numbers.

As yet it is not possible to compute — on theoretical grounds — the increase of viscous damping after transition or even to compute the critical yaw angle at which transition occurs. However, by experimental investigations² the effects of large yaw angle are greatly clarified. It is possible,

now, to estimate the critical yaw angle and the band broadening on semi-empirical grounds.

10-5.1 TRANSITION TO CELLULAR BOUNDARY LAYER

It was shown by Taylor* that the flow in the gap between two rotating cylinders can become unstable when the inner cylinder rotates faster than the outer cylinder, and the mean flow velocity exceeds a critical value. As a result of instability, a cellular vortex pattern develops in the flow which considerably increases the viscous friction at the wall. A similar instability was found by Goertler⁵ for boundary layers on concave walls. The common feature of both these flows is that the flow velocity increases in a direction towards the center of curvature of the streamlines. The stability criterion found by Taylor can be written, for the case of small gap width, as follows: The flow is unstable if

$$\left(\frac{Vd}{\nu}\right)^2 \left(\frac{d}{R}\right) \frac{\Delta V}{V} > M \quad (10-1)$$

where V is the mean value of the flow velocity within the gap, ΔV is the change of the flow velocity across the gap, d the gap-width, and R the average radius of inner and outer cylinder. (For small gap-width, inner and outer cylinder have nearly equal radii.) ν is the kinematic viscosity.

For the case of boundary layers on concave walls, V and ΔV are interpreted, respectively, as mean value and change of the flow velocity in the boundary layer, and d as boundary layer thickness.

The number M is different for the Taylor and Goertler case, and M depends on the shape of the boundary layer.

The boundary layer which is formed at the cylindrical walls of the yawing liquid-filled cavity is of the type investigated by Taylor and Goertler. Therefore, the stability criterion should have the form of Eq. 10-1, where V , ΔV , R and d must be interpreted appropriately, while M may be determined experimentally.

In our case R and V are the cavity radius and the circumferential velocity, respectively, i.e.,

$$\begin{aligned} R &= a \\ V &= a\Omega \end{aligned} \quad (10-2)$$

d is proportional to the boundary layer thickness. According to Eq. 6-13 we may define:

$$d = \frac{a}{\sqrt{Re}} \quad ; \quad Re = \frac{\Omega a^2}{\nu} \quad (10-3)$$

ΔV is proportional to the circumferential component of the perturbation velocity which is proportional to $a\Omega\alpha$, i.e.:

$$\Delta V \propto v \propto a\Omega\alpha \quad (10-4)$$

where α is the yaw angle, and v is the value which the perturbation velocity assumes at the edge of the boundary layer. At the wall, the perturbation velocity is zero, i.e., v is the change of the total velocity across the boundary layer. Actually, v depends on time, azimuthal angle, and axial distance so that the boundary layer becomes at first unstable at a position on the cavity walls, where v attains its maximum value. We may thus interpret v as the maximum value of the perturbation velocity near the wall. The proportionality of v to $a\Omega\alpha$ follows from Eqs. 3-54 for the radial component u , and Eqs. 3-57 and 3-58 which connect u and v . Substituting Eqs. 10-2, 10-3, and 10-4 into Eq. 10-1 yields that the left-hand side of Eq. 10-1 is proportional to $\sqrt{Re}\alpha$.

Thus, the criterion for instability becomes

$$\sqrt{Re}\alpha > K \quad (10-5)$$

where K is some constant. The experiments confirm this relation, see Table 10-1, and suggest for K the value

$$K = 2.5 \times 10^2, \text{ deg} \quad (10-6)$$

when α is measured in degrees.

Although it must be expected that K depends on cavity shape and fill-ratio, the dependence is probably very weak. Hence Eq. 10-6 may be considered a good approximation in all cases where cavity shape and fill-ratio are not too different from those of the experimental configuration. In the experiments of Ref. 2, fineness-ratio and fill-ratio of the cylindrical cavity were kept constant at $c/a = 3.077$, $b^2/a^2 = 0.15$.

Eqs. 10-5 and 10-6 show that transition to cellular boundary layer can occur at relatively small yaw angles. The upper limit of Reynolds numbers of practical projectiles filled with liquid of low viscosity lies around 10^6 . At a Reynolds number of $Re = 10^6$ the critical yaw angle at which transition occurs is only 0.25 degree.

10-5.2 DAMPING FACTORS

The broadening of the bandwidth due to viscous effects was discussed in Chapter 6. It was shown there that the effect of viscosity can be described completely in terms of the viscous eigenfrequencies $\tau_{0v} = \tau_0 + \delta$. In particular it was shown that the broadening and flattening of the bandwidth of instability is caused by the imaginary part δ . The physical significance of δ is that it determines the damping rates of the modes of free oscillations. The amplitudes of the free oscillations decrease like $e^{-\Omega\delta t}$. δ is briefly denoted as damping factor. Once δ is known, the resonance curves (rate of divergence versus eigenfrequency) can be computed. For laminar boundary layer, δ is given by Eq. 6-16. For the case that the yaw angle is larger than the critical yaw angle, the boundary layer is no longer laminar and Eq. 6-16 is not applicable. It can be assumed, however, that the broadening of the resonance curve is related to the damping factor δ in the same way as was the case for the laminar boundary layer.

It was shown experimentally in Ref. 2 that, at large amplitudes, the resonance

curves have indeed the same shape as in the case of laminar boundary layer, but that the corresponding damping factors were much larger. From the shape of the resonance curves, the damping factors were experimentally determined as functions of the Reynolds number for various yaw amplitudes. The results are shown in Fig. 10-4. It is apparent that in the regime of small Reynolds numbers all data follow the original curve for a laminar boundary layer. At higher Reynolds numbers, the experimental curves separate from the theoretical curve and from several branches, a different branch for each yaw amplitude.

The experimental data shown in Fig. 10-4 are taken for a fixed cavity configuration with: $c/a = 3.077$ ($j = 1$) $b^2/a^2 = 0.15$, and $\tau_0 = \tau = 0.055$. It is known that for a laminar boundary layer the damping factor depends on the cavity shape and fill-ratio (Eq. 6-16) and the same must be expected for cellular boundary layer, i.e., the experimental curves shown in Fig. 10-4 are — for the present — valid only for this particular configuration. An investigation of Eq. 6-16 shows that, in the laminar case, the damping factor depends only weakly on cavity shape and fill-ratio as long as the resonance frequency $\tau_0 < 1$. The same weak dependence can be assumed in the case of a cellular boundary layer. Thus, if the fineness-ratio is not too different from $c/a = 3$, the experimental data of Fig. 10-4 may be used to estimate the value of δ at large yaw amplitudes.

It should be mentioned that not only the damping factor but also the frequency shift is subject to change — relative to its laminar value — after transition to a turbulent boundary layer. However, because of its greater practical importance, only the damping factor was determined experimentally. The frequency shift, which is directly related to the displacement thickness of the boundary layer, is not likely to change much as a result of transition to a cellular boundary layer.

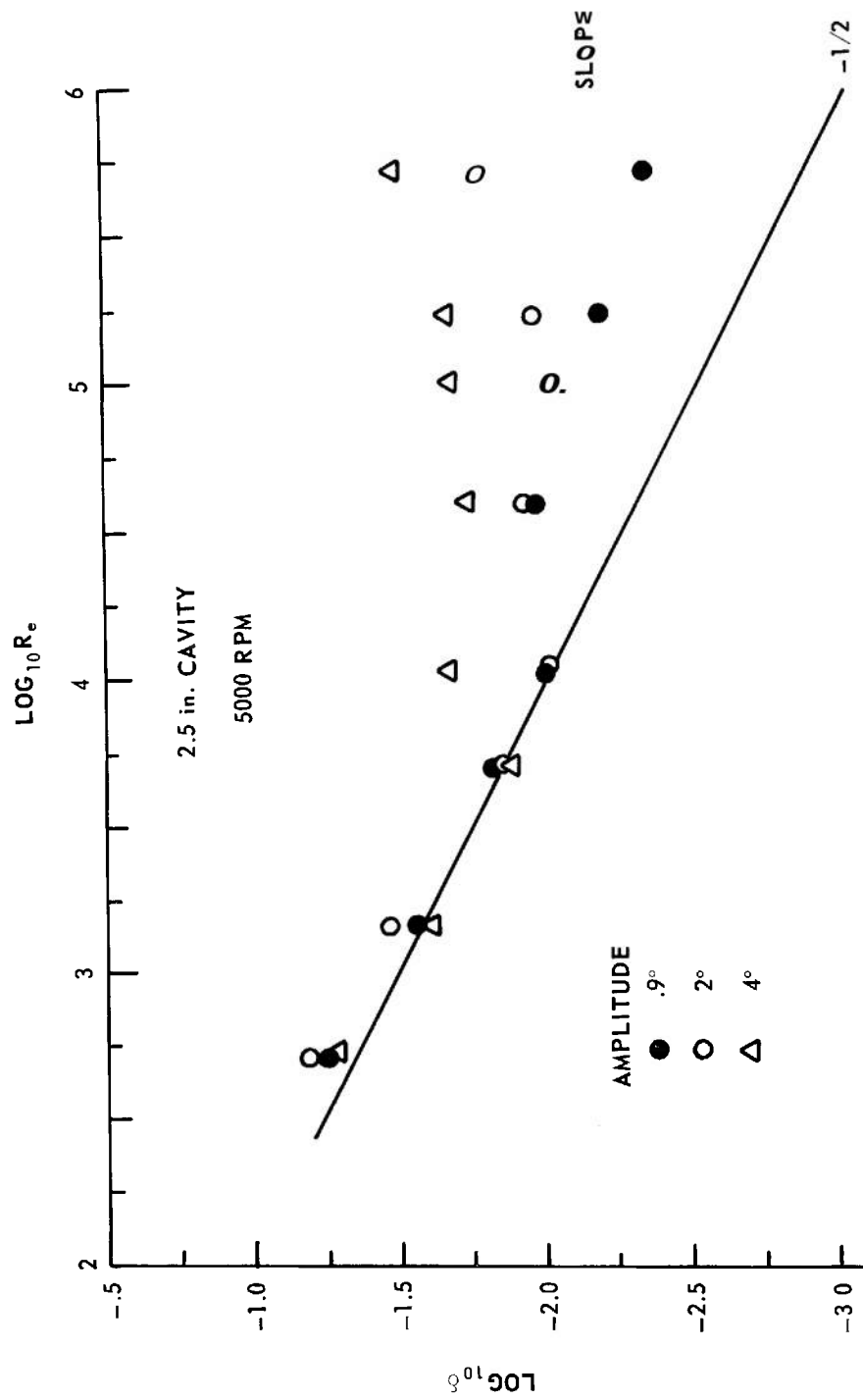


FIGURE 10-4. WISCONSIN DAMPING FACTORS AT VARIOUS YAW LEVELS

REFERENCES

1. C. H. Murphy, *Free Flight Motion of Symmetric Missiles*, BRL Report 1216, Aberdeen Proving Ground, Md., 1963.
2. B. G. Karpov, *Liquid-Filled Gyroscope: The Effect of Reynolds Number on Resonance*, BRL Report 1302, Aberdeen Proving Ground, Md., 1965.
3. G. N. Ward, Appendix to K. Stewartson, "On the Stability of a Spinning Top Containing Liquid," *J. of Fluid Mech.*, **5**, Part 4, 577-592 (1959).
4. G. I. Taylor, "Stability of a Viscous Liquid Contained Between Two Rotating Cylinders," *Phil. Trans. A* **223**, 289 (1923), see also *Proc. Roy. Soc. (A)* **151**, (1935) and **157** (1936).
5. H. Goertler, "Über eine dreidimensionale Instabilität laminarer Grenzschichten an konkaven Wänden," *ZAMM*, **21**, 250 (1941).

APPENDIX C

BIBLIOGRAPHY AND SURVEY OF PAPERS ON THE MOTION OF BODIES
HAVING CAVITIES FILLED WITH LIQUID

The problem of stability of rotating bodies containing liquid-filled cavities has its origin in a number of investigations regarding the shape of the earth^{1,2,3,4}. In 1880, during the course of investigations of the motion of a gravitating liquid ellipsoid, Greenhill⁴ solved the problem of stability of a rotating solid body containing an ellipsoidal cavity completely filled with liquid. The case of a rotating body with a liquid-filled ellipsoidal cavity, which lent itself to theoretical analysis, was further investigated by Hough⁵. Hough was able to show that the general motion of a liquid-filled body can be described exactly by ordinary differential equations if the cavity is ellipsoidal and completely filled with ideal liquid, and the fluid is initially rotating uniformly with the body as if solid.

For the case that the liquid within the ellipsoidal cavity is initially at rest, the solution of the problem was found independently by Beltrami, Bjerknes and Maxwell in 1873[see Lamb⁶].

An ideal inviscid liquid enclosed in a cavity which is initially at rest cannot attain any vorticity by the motion of the cavity walls, so that, for strictly inviscid fluid, the flow is irrotational (potential flow).

Assuming potential flow for the liquid, Joukowski⁸ gave the general solution of the problem of motion of a solid body with cavities filled completely with ideal liquid. In particular, Joukowski has shown that the dynamics of a rigid body with cavities completely filled with an ideal fluid in irrotational motion, can be expressed in terms of an "equivalent rigid body" replacing the liquid. The equivalent rigid body and the liquid have equal mass, and the same

center of gravity; however, the moments of inertia of the equivalent rigid body are only fractions of the moments of inertia of the frozen liquid mass. Thus, the problem of motion is reduced to the computation of "effective" moments of inertia and to solving the equations of motion of a rigid body. The effective moments of inertia, which depend on the cavity shape, are known in many cases. The approach used by Joukowski approximately describes the motion of a liquid-filled projectile if the viscosity of the liquid is small and if the average motion of the projectile is irrotational. If, however, the average motion of the projectile contains a rotation about any axis, the liquid is dragged round to some extent by friction on the cavity walls and the flow ceases to be irrotational. Thus, according to its physical content, Joukowski's theory is not applicable in the case of a spin-stabilized projectile except perhaps at the very beginning of the motion. However, the yawing and pitching motion of a nonspinning liquid-filled projectile or the motion of a liquid-filled pendulum are correctly described by Joukowski's approach.

On the basis of Joukowski's results, Chetaev²¹ solved the precisely stated problem of stability of a solid body containing a cavity completely filled with liquid. The stability criterion given by Chetaev is analogous to the stability criterion for a solid body, except that the moments of inertia of the liquid must be replaced by those of the equivalent rigid body.

Adjoining the work of Greenhill, Hough, and Joukowski, many authors aimed at an extension of the theory. Stretenskii¹⁰, Moiseev^{11,12,13,19}, Okhotsimskii¹⁶, Rabinovich¹⁸, Narimanov^{17,23}, and Rumiantsev¹⁴ have considered the problem of motion of

a solid body with cavities partially filled with liquid. On the assumption that the liquid is ideal and incompressible, the motion of the liquid is irrotational. For the case of small perturbation about a position of equilibrium, the equations of motion for the system of vessel and liquid are derived in Refs. **11**, **16**, **17** and **18**. The displacement of the liquid from its equilibrium position was expanded in a series of functions with time-dependent coefficients and the problem was reduced to an infinite set of ordinary differential equations for the coefficients. A variational method (Ritz Method) to solve the equations was applied by **Bogoriad**⁴⁴.

In Ref. **13** the stability problem is reduced to the problem of showing the positive definiteness of a certain infinite quadratic form. Explicit solutions are obtained only in particular cases¹⁹. The same problem is considered by **Pozharitskii**⁴¹ for the case that only potential forces are acting on the system. By the use of a theorem of Lagrange, it is shown that the system is stable in its equilibrium position when the potential energy of the equilibrium position has a minimum.

The stability of the rotational motion of a body having a cylindrical cavity partially filled with liquid was first investigated by **Narimanov**²³. He derived the equations of small perturbation of the spinning body and liquid. The problem led to an infinite system of ordinary differential equations, reflecting that an infinite number of modes of oscillations is involved in the perturbed motion of the liquid. No numerical results were obtained by **Narimanov**.

An important step was made in 1959 by **Stewartson**²⁶, who solved the stability problem for a spinning top with a cylindrical cavity completely or partially filled with liquid. According to Stewartson's theory, a heavy top with a small mass of liquid becomes unstable when the nutational frequency of the top falls within a narrow bandwidth about any of an infinite number of natural frequencies of the liquid. The stability conditions obtained by Stewartson

were checked experimentally by **Ward**²⁷ who found that in the main form the theory agreed with the experimental findings, but that there is also a certain discrepancy: the bandwidth of instabilities was found to be much broader than predicted. In an attempt to explain this discrepancy, **Kostandian**³⁹ investigated the influence of the deviation of the free surface from an ideal cylindrical shape, but no conclusive results were obtained. A full explanation for the broadening of the bandwidth and a correction of Stewartson's stability criterion was given in Ref. **63**.

Several authors consider the conditional stability relative to certain variables, but not all, that determine the motion of the mechanical system with an infinite number of degrees of freedom. **Rumiantsev**^{29,30,36,37,43,48} gave the general formulation and solutions of the problem of conditional stability of spinning motion of a rigid body with cavities completely or partially filled with liquid. He posed the problem of stability in relation to every variable characterizing the motion of the solid body and to some of the variables characterizing the motion of the liquid. On the basis of methods developed by **Liapunov**^{5,28}, sufficient conditions for the stability of the rotational motion are obtained. Similar methods have been employed by **Sobolov**³³, **Ishlinsky** and **Temchenko**³⁴, **Moiseev**⁴⁰, **Tsel'man**⁴⁵, **Pozharitskii**^{49,54}, et al.

The above investigations have led to general results regarding the stability of certain equilibrium states. However, since only sufficient conditions of stability could be derived, the results have no important applications with regard to the prediction of instabilities of liquid-filled projectiles.

A sufficient condition for stability of rotation about the vertical (z-axis) of a heavy symmetrical top with a cavity completely filled with ideal liquid is:

$$(I_z - I_x) \Omega^2 - M_f g z_0 > 0$$

The above condition is equivalent to the condition: $\tau_n > 1$. If $\tau_n > 1$, instability

could only occur if there exists an eigenfrequency $\tau_0 > 1$ of a mode of liquid oscillation which interacts with the motion of the body. The theories of Greenhill⁴ and Stewartson²⁶ suggest that for all relevant eigenfrequencies $\tau_0 < 1$. Thus, the prediction of Greenhill's and Stewartson's theory is consistent with the above condition $\tau_n > 1$, which was derived by Rumiantsev³⁷ by an entirely different approach.

If dissipative forces are present, it is necessary to distinguish between temporary and secular stability. Joukowski⁸ has shown that, with relative motion between the liquid and the casing, energy is dissipated until a final state of solid rotation about one of the principal axes is attained. The final state is stable in the sense of secular stability. Kolesnikov⁴² derived as a sufficient condition for secular stability: $I_z > I_y \geq I_x$. The motion is stable when the axial moment of inertia is larger than the transverse moments of inertia.

A number of papers is devoted to the effect of viscosity on the motion of the liquid and the stability of a liquid-solid system. Theorems on dissipative mechanical systems with a finite number of degrees of freedom are extended by Pozharitskii⁵⁴ to the liquid-filled projectile system. Making certain assumptions, Pozharitskii shows that the oscillations damp out when the potential energy of the liquid projectile system has an isolated minimum at the equilibrium state.

Rumiantsev⁶⁶ computes the motion of liquid-solid systems in two simple cases where only frictional forces are present: the oscillations of a liquid-filled cylinder about the axis of symmetry and of a liquid-filled sphere about the center. Ievlova⁵⁹ investigates the oscillations about a fixed axis of a pendulum having a spherical cavity filled with viscous liquid.

A solution for the transition to uniform spin of the liquid within a spherical cavity for the case of small perturbation of the angular velocity (linearized problem) was

given by Greenspan^{47,53}. Wedemeyer⁵² solved the problem of spin-up for a cylindrical cavity which, initially at rest, is suddenly started to rotate. Stewartson and Roberts⁴⁶ give a solution for the viscous flow in the spheroidal cavity of a precessing body for the case of small perturbations about a state of steady rotation.

Recently, Chernous'ko^{67-69,72} made important contributions to the theory of motion of a body having cavities filled with a nonrotating liquid. Chernous'ko⁶⁷ derives general equations of motion for the case where the cavity is completely filled with viscous liquid and where the main flow is irrotational. As in the inviscid case considered by Joukowski⁸, the inertia properties of the liquid can be described by effective moments of inertia. The viscosity introduces additional terms into the equations of motion, representing viscous friction. The additional terms can be expressed by a symmetric tensor, similar to the mass tensor, which depends on the cavity shape. Once the moments of inertia and the friction tensor are known, the equations of motion reduce to ordinary differential equations. It is supposed that the averaged motion of the rigid body containing the liquid is irrotational and that the frequencies of oscillation are sufficiently large so that the effects of friction are restricted to a thin boundary layer zone near the cavity walls.

The effect of viscous friction on the motion of a spinning body having a cylindrical liquid-filled cavity was investigated by Wedemeyer⁶³. The solution, which was found in the form of a boundary layer correction to Stewartson's solution, explains the experimentally observed broadening of the bandwidth of instability.

Further investigations on the subject of liquid-filled projectiles, mainly at Ballistic Research Laboratories, have been published⁷⁴⁻⁹⁰. Refs. 76, 77 and 78 are concerned with further analysis of Stewartson's stability criteria. The attainment of

liquid rotation was investigated experimentally and theoretically in Refs. 79-83, the instability during spin-up in Ref. 84, and the effect of liquid viscosity on the instability of liquid-filled projectiles in Refs. 85-

88. Theoretical and experimental investigations regarding eigenfrequencies in non-cylindrical cavities are reported in Refs. 89 and 90.

BOOKS AND ARTICLES

1. B. Riemann, "On the Motion of a Liquid Homogeneous Ellipsoid", *Goettinger Abh.* **9**, 3 (1860).
2. Lord Kelvin, *Nature*, Lond. **15**, 297 (1877).
3. A. G. Greenhill, "On the Rotation of a Liquid Ellipsoid About Its Mean Axis", *Proc. Camb. Phil. Soc.* **3**, 289-293 (1879).
4. A. G. Greenhill, "On the General Motion of a Liquid Ellipsoid Under the Gravitation of Its Own Parts", *Proc. Camb. Phil. Soc.* **4**, 4 (1880).
5. A. M. Liapunov, "On the Stability of the Ellipsoidal Form of Equilibrium of a Rotating Liquid", St. Petersburg (1884).
6. S. S. Hough, "The Oscillations of a Rotating Ellipsoidal Shell Containing Fluid", *Phil. Trans. Roy. Soc. London A* **186**, 469-506 (1895).
7. H. Lamb, *Hydrodynamics*, Cambridge Univ. Press, Sixth Edition, 1932; First American Edition, 1945.
8. N. E. Zhukovskii (Joukowski), "On the Motion of a Solid Which Has Cavities Filled With a Homogeneous Drop-like Liquid", *Collected works*, Vol. 3, *ONTI* (1936); *Sobr. Soch.* Vol. 2, *Gostekhizdat* (1948).
9. S. L. Sobolev, "On the Motion of a Hollow Top Filled With Liquid", *Mat. Inst. Steklova, Akad. Nauk SSSR*, (1945).
10. L. N. Stretenskii, "Oscillations of a Liquid in a Moving Container", *Izv. Akad. Nauk SSSR, OTN* No. 10 (1951).
11. N. N. Moiseev, "The Motion of a Rigid Body Having a Cavity Partially Filled With an Ideal Liquid", *Dokl. Akad. Nauk SSSR*, Vol. 85, No. 4 (1952).
12. N. N. Moiseev, "On the Oscillations of a Weighty Ideal and Incompressible Liquid in a Vessel", *Dokl. Akad. Nauk SSSR*, Vol. 85, No. 5 (1952).
13. N. N. Moiseev, "The Problem of Motion of a Rigid Body Containing a Liquid Mass Having a Free Surface", *Matem. Sb.* No. 1, Vol. 32, 74, (1953).
14. V. V. Rumiantsev, "Equations of Motion of a Rigid Body Having Cavities Not Completely Filled With Liquid", *PMM* Vol. 18, No. 6 (1954).
15. V. V. Rumiantsev, "On the Stability of the Rotation of a Rigid Body Containing an Ellipsoidal Cavity Filled With Liquid", *Trudy of the Mechanics Institute of the Academy of Sciences USSR*, No. 2 (1956).
16. D. E. Okhotsimskii, "On the Theory of the Motion of a Body With Cavities Partially Filled With a Liquid", *PMM* Vol. 20, No. 1 (1956).
17. G. S. Narimanov, "On the Motion of a Rigid Body With a Cavity Partially Filled With Liquid", *PMM* Vol. 20, No. 1, (1956).
18. B. I. Rabinovich, "On the Equations of Disturbed Motion of a Rigid Body With a Cylindrical Cavity Partially Filled With Liquid", *PMM* Vol. 20, No. 1 (1956).
19. N. N. Moiseev, "On Two Pendulums Filled With Liquid", *PMM* Vol. 20, No. 6 (1956).

20. S. G. Krein and N. N. Moiseev, "On the Oscillations of a Solid Body Containing a Liquid Having a Free Surface", *PMM* Vol. 21, No. 2 (1957).
21. N. G. Chetaev, "On the Stability of the Rotational Motion of a Solid Body Whose Interior Cavity Is Filled With an Ideal Liquid", *PMM* Vol. 21, No. 2 (1957).
22. S. V. Zhak, "About the Possibility of Quasi-rigid Motion of a Liquid", *PMM* Vol. 21, No. 4 (1957).
23. G. S. Narimanov, "On the Motion of a Symmetric Gyroscope With a Cavity Partially Filled With Liquid", *PMM* Vol. 21, No. 5 (1957).
24. V. V. Rumiantsev, "The Stability of Rotation of a Solid Body With an Ellipsoidal Cavity Filled With Liquid", *PMM* 21, No. 6 (1957).
25. S. V. Zhak, "On the Stability of Some Particular Cases of Motion of a Symmetrical Gyroscope Containing Liquid Mass", *PMM* 22, 245-249 (1958).
26. K. Stewartson, "On the Stability of a Spinning Top Containing Liquid", *J. Fluid. Mech.* 5, 577-592 (1959).
27. G. N. Ward, Appendix of Ref. 26 (1959).
28. A. M. Liapunov, "Problem of Minimum in a Question on the Stability of Figures of Equilibrium of a Rotating Liquid", *Sobr. Soch. (Collected works)*, Vol. 3, *Akad. Nauk SSSR* (1959).
29. V. V. Rumiantsev, "On the Stability of the Equilibrium of a Solid Body With Cavities Partially Filled With a Liquid", *Dokl. Akad. Nauk, SSSR*, Vol. 124, No. 2 (1959).
30. V. V. Rumiantsev, "On the Stability of Rotational Motions of a Rigid Body With a Liquid Inclusion", *PMM* 23, 1057-1065 (1959).
31. B. Budiansky, "Sloshing of Liquids in Circular Canals and Spherical Tanks," *J. A. S.* Vol. 27, No. 3 (1960).
32. S. V. Malashenko and M. E. Temchenko, "On an Experimental Method of Investigation the Stability of Motion of a Gyroscope Inside Which There Is a Fluid Filled Cavity", *PMTF* No. 3 (1960).
33. S. L. Sobolov, "On the Motion of a Symmetric Top With a Cavity Filled With Liquid", *PMTF* No. 3, 20-55 (1960).
34. A. Iu. Ishlinsky and M. E. Temchenko, "On Small Vibrations of the Vertical Axis of a Top With a Cavity Which Is Completely Filled With Ideal Incompressible Liquid", *PMTF* No. 3 (1960).
35. B. A. Kostandian, "On the Stability of Rotational Motions of a Top With a Cavity Not Completely Filled With Liquid", *PMTF* No. 3 (1960).
36. V. V. Rumiantsev, "A Theorem of Stability", *PMM* 24, 47-54 (1960).
37. V. V. Rumiantsev, "On the Stability of Rotation of a Top With a Cavity Filled With a Viscous Liquid", *PMM* 24, 603-609 (1960).
38. G. N. Mikishev and N. I. Dorozhkin, "Experimental Investigation of Free Oscillations of a Liquid in Containers", *Izv. Akad. Nauk USSR, OTN Mekhanika i Mashinostroyeniye*, No. 4 (1961).
39. B. A. Kostandian, "The Influence of Oscillations of a Free Surface of the Liquid on the Stability of Rotational Motion of a Spinning Top Containing the Liquid", *PMM* 25, No. 4, 646-656 (1961).
40. N. N. Moiseev, "Variational Problems in the Theory of Oscillations of Liquid and Liquid Solid Systems", *VTS Akad. Nauk SSSR*, M. (1962).
41. G. K. Pozharitskii, "The Minimum Problem of the Stability of Equilibrium of a Solid Body Partially Filled With a Liquid", *PMM* 26, 593-605 (1962).
42. N. N. Kolesnikov, "On the Stability of a Free Rigid Body With a Cavity Filled With an Incompressible Viscous Fluid", *PMM* 26, 606-612 (1962).

43. V. V. Rumiantsev, "On the Stability of Stationary Motions of Rigid Bodies With Cavities Containing Fluid", *PMM* 26, 977-991 (1962).
44. J. B. Bogoriad, "On the Solution By a Variational Method of the Problem of the Oscillations of a Liquid Partially Filling a Cavity", *PMM* 26, 1122-1127 (1962).
45. F. Kh. Tsel'man, "On the Stability of Rotation of a Solid With an Ellipsoidal Cavity Filled With Liquid", *PMM* 26, 1128-1130 (1962).
46. K. Stewartson and P. H. Roberts, "On the Motion of a Liquid in the Spheroidal Cavity of a Precessing Rigid Body", *J. Fluid Mech.* 17, 1-20 (1963).
47. H. P. Greenspan, and L. N. Howard, "On a Time Dependent Motion of a Rotating Fluid", *J. Fluid Mech.* 17, 385-404 (1963).
48. V. V. Rumiantsev, "Liapunov Method in the Study of Stability of Motion for Solid Bodies With a Cavity Filled With Liquid", *Izv. Akad. Nauk SSSR, Mekhanika i mashinostroenie*, No. 6 (1963).
49. G.K. Pozharitskii and V.V. Rumiantsev, "Problem of the Minimum in the Question of Stability of Motion of a Solid Body With a Liquid Filled Cavity", *PMM* 27, 16-27 (1963).
50. P. S. Krasnoshchekov, "On Oscillations of a Physical Pendulum Having Cavities Filled With a Viscous Liquid", *PMM* 27, 193-202 (1963).
51. N. N. Moiseyev, "Introduction to the Theory of Oscillations of a Fluid and Body Containing Fluid", *Advances in Applied Mechanics*, Academic Press, New York-London, Vol. 8 (1964).
52. E. H. Wedemeyer, "The Unsteady Flow Within a Spinning Cylinder", *J. Fluid Mech.* 20, 383-399 (1964).
53. H. P. Greenspan, "On the Transient Motion of a Contained Rotating Fluid", *J. Fluid Mech.* 20, 673-696 (1964).
54. G. K. Pozharitskii, "On the Influence of Viscosity on the Stability of Equilibrium and Steady-state Rotation of a Rigid Body With Cavity, Partially Filled With a Viscous Liquid", *PMM* 28, 60-67 (1964).
55. F. L. Chernous'ko, "Motion of a Solid Body With a Cavity Containing an Ideal Fluid and an Air Bubble", *PMM* 28, No. 4, 735-745 (1964).
56. V. V. Rumiantsev, "On the Stability of Motion of a Rigid Body Containing a Fluid Possessing Surface Tension", *PMM* 28, 746-753 (1964).
57. A. A. Petrov, "Variational Statement of the Problem of Liquid Motion in a Container of Finite Dimensions", *PMM* 28, 754-758 (1964).
58. B. N. Rumiantsev, "On the Motion of a Rigid Body Containing Cavities Filled With a Viscous Liquid", *PMM* 28, 1127-1132 (1964).
59. O. B. Ievlova, "Small Oscillations of a Pendulum Having a Spherical Cavity Filled With a Viscous Liquid", *PMM* 28, 1132-1134 (1964).
60. H. P. Greenspan, "On the General Theory of Contained Rotating Fluid Motions", *J. Fluid Mech.* 22, 449-462 (1965).
61. F. L. Chernous'ko, "Motion of a Rigid Body With Cavities Filled With a Viscous Fluid At Small Reynolds Numbers", *Zh. Vychisl. Mat. i mat. Fiz.*, Vol. 5, No. 6 (1965).
62. N. N. Vakhaniia, "On the Stability of Spinning of a Top With a Liquid Filled Cavity", *PMM* 29, 35-45 (1965).
63. E. H. Wedemeyer, "Viscous Corrections to Stewartson's Stability Criterion", *AGARD Conference Proceedings No. 10*, 99-116 (1966).
64. N. N. Moiseev and V. V. Rumiantsev, "Dynamics of a Body With Cavities Containing a Fluid", *Izd. "Nauka"* (1966).

65. A. Iu. Ishlinskii and M. E. Temchenko, "On the Stability of Rotation of a Rigid Body Suspended on a String and Possessing an Ellipsoidal Cavity Completely Filled With an Ideal Incompressible Fluid", *PMM* 30, 30-41 (1966).
66. V. V. Rumiantsev, "On the Theory of Motion of Rigid Bodies With Fluid Filled Cavities", *PMM* 30, 51-66 (1966).
67. F. L. Chernous'ko, "Motion of a Body With a Cavity Filled With a Viscous Liquid at Large Reynolds Numbers", *PMM* 30, 476-494 (1966).
68. F. L. Chernous'ko, "On Free Oscillations of a Viscous Fluid in a Vessel", *PPM* 30, 836-847 (1966).
69. F. L. Chernous'ko, "The Motion of a Body With a Cavity Partly Filled With a Viscous Liquid", *PMM* 30, 977-992 (1966).
70. V. A. Samsonov, "On the Stability of the Equilibrium of a Physical Liquid Filled Pendulum", *PMM* 30, 1112-1114 (1966).
71. Rubanovskii, "On the Stability of Motion of a Body in a Fluid", *PMM* 31, 134-136 (1967).
72. F. L. Chernous'ko, "Rotational Motions of a Solid Body With a Cavity Filled With Fluid", *PMM* 31, 416-432 (1967).
73. V. A. Samsonov, "On the Problem of a Minimum of a Functional In The Investigation of the stability of Motion of a Body Containing Fluid", *PMM* 31 523-526 (1967).
74. E. A. Milne, *Report on the Stability of Liquid Filled Shell*, (U) EBD Report No. 6, 1940 (Confidential).
75. E. Widmayer, Jr. and J. R. Reese, *Moments of Inertia and Damping of Fluid in Tanks Undergoing Pitching Oscillations*, NACA RM L53E01a, 1953.
76. J. E. Ash and R. M. Gundersen, *Investigations in the Exterior Ballistics of Shell with Nonsolid Fillers, Final Report*, Armour Research Foundation (now IIT Research Inst.) Project 4187, 1960.
77. W. E. Scott, *The Free Flight Stability of a Liquid Filled Spinning Shell, Part Ia*, BRL Report 1120, Aberdeen Proving Ground, Md., 1960.
78. W. E. Scott, *The Free Flight Stability of a Liquid Filled Spinning Shell, Part Ib*, BRL Report 1135, Aberdeen Proving Ground, Md., 1961.
79. H. M. Stoller, *Apparatus for Study of Fluid Motion in a Spinning Cylinder*, BRL Tech. Note 1355, Aberdeen Proving Ground, Md., 1960.
80. G. Sokol, *Some Experiments With the Liquid Filled Impulsively Started Spinning Cylinder*, BRL Tech. Note 1473, Aberdeen Proving Ground, Md., 1962.
81. W. E. Scott, *A Theoretical Analysis of the Axial Spin Decay of a Spin Stabilized Liquid Filled Shell*, BRL Report 1170, Aberdeen Proving Ground, Md., 1962.
82. B. G. Karpov, *Experimental Observations of the Dynamic Behavior of Liquid Filled Shell*, BRL Report 1171, Aberdeen Proving Ground, Md., 1962.
83. E. H. Wedemeyer, *The Unsteady Flow Within a Spinning Cylinder*, BRL Report 1225, Aberdeen Proving Ground, Md., 1963.
84. B. G. Karpov, *Dynamics of Liquid Filled Shell: Instability During Spin-up*, BRL Memo. Report 1629, Aberdeen Proving Ground, Md., 1965.
85. B. G. Karpov, *Liquid Filled Shell: Resonance and Effect of Viscosity*, BRL Report 1279, Aberdeen Proving Ground, Md., 1965.
86. E. H. Wedemeyer, *Dynamics of Liquid Filled Shell: Theory of Viscous Corrections to Stewartson's Stability Problem*, BRL Report 1287, Aberdeen Proving Ground, Md., 1965.

REPORTS

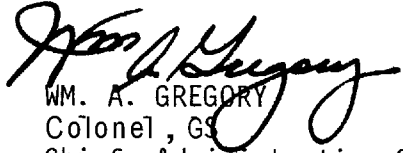
87. B. G. Karpov, *Liquid Filled Gyroscope: The Effect of Reynolds Number on Resonance*, BRL Report 1302, Aberdeen Proving Ground, Md., 1965.
88. E. H. Wedemeyer, *Viscous Corrections to Stewartson's Stability Criterion*, BRL Report 1325, Aberdeen Proving Ground, Md., 1966.
89. E. H. Wedemeyer, *Dynamics of Liquid Filled Shell: Non-cylindrical Cavity*, BRL Report 1326, Aberdeen Proving Ground, Md., 1966.
90. B. G. Karpov, *Dynamics of Liquid Filled Shell: Resonance in Modified Cylindrical Cavities*, BRL Report 1332, Aberdeen Proving Ground, Md., 1966.

(AMCRD-TV)

FOR THE COMMANDER:

OFFICIAL:

CLARENCE J. LANE
Major General, USA
Chief of Staff


WM. A. GREGORY
Colonel, GS
Chief, Administrative Office

DISTRIBUTION:
Special

ENGINEERING DESIGN HANDBOOK

Listed below are the Handbooks which have been published or are currently being printed. Handbooks with publication dates prior to 1 August 1962 were published as 20-series Ordnance Corps pamphlets. AMC Circular 310-38, 19 July 1963, redesignated those publications as 706-series AMC pamphlets (i.e., ORDP 20-138 was redesignated AMCP 706-138). All new, reprinted, or revised Handbooks are being published as 706-series AMC pamphlets.

No.	Title	No.	Title
100	Design Guidance for Producibility	212(S)	Fuzes, Proximity, Electrical, Part Two (U)
104	Value Engineering	213(S)	Fuzes, Proximity, Electrical, Part Three (U)
106	Elements of Armament Engineering, Part One, Sources of Energy	214(S)	Fuzes, Proximity, Electrical, Part Four (U)
107	Elements of Armament Engineering, Part Two, Ballistics	215(C)	Fuzes, Proximity, Electrical, Part Five (U)
108	Elements of Armament Engineering, Part Three, Weapon Systems and Components	235	Hardening Weapon Systems Against RF Energy
110	Experimental Statistics, Section 1, Basic Concepts and Analysis of Measurement Data	238	Recoilless Rifle Weapon Systems
111	Experimental Statistics, Section 2, Analysis of Enumerative and Classificatory Data	239	Small Arms Ammunition
112	Experimental Statistics, Section 3, Planning and Analysis of Comparative Experiments	240(C)	Grenades (U)
113	Experimental Statistics, Section 4, Special Topics	241	Land Mines
114	Experimental Statistics, Section 5, Tables	242	Design for Control of Projectile Flight Characteristics
115	Basic Environmental Concepts	244	Ammunition, Section 1, Artillery Ammunition--General, with Table of Contents, Glossary and Index for Series
121	Packaging and Pack Engineering	245(C)	Ammunition, Section 2, Design for Terminal Effects (U)
123	Hydraulic Fluids	247	Ammunition, Section 4, Design for Projection
125	Electrical Wire and Cable Design	248	Ammunition, Section 5, Inspection Aspects of Artillery Ammunition Design
127	Infrared Military Systems, Part One	249	Ammunition, Section 6, Manufacture of Metallic Components of Artillery Ammunition
130	Design for Air Transport and Airdrop of Materiel	250	Guns--General
134	Maintainability Guide for Design (Revised)	251	Muzzle Devices
135	Inventions, Patents, and Related Matters (Revised)	252	Gun Tubes
136	Servomechanisms, Section 1, Theory	255	Spectral Characteristics of Muzzle Flash
137	Servomechanisms, Section 2, Measurement and Signal Converters	260	Automatic Weapons
138	Servomechanisms, Section 3, Amplification	270	Propellant Actuated Devices
139	Servomechanisms, Section 4, Power Elements and System Design	280	Design of Aerodynamically Stabilized Free Rockets
140	Trajectories, Differential Effects, and Data for Projectiles	281(S-RD)	Weapon System Effectiveness (U)
145	Dynamics of a Tracking Gimbal System	282	Propulsion and Propellants
150	Interior Ballistics of Guns	283	Aerodynamics
160(S)	Elements of Terminal Ballistics, Part One, Kill Mechanisms and Vulnerability (U)	284(C)	Trajectories (U)
161(S)	Elements of Terminal Ballistics, Part Two, Collection and Analysis of Data Concerning Targets (U)	285	Elements of Aircraft and Missile Propulsion
162(S-RD)	Elements of Terminal Ballistics, Part Three, Application to Missile and Space Targets (U)	286	Structures
165	Liquid-Filled Projectile Design	290(C)	Warheads--General (U)
170(C)	Armor and Its Application to Vehicles (U)	291	Surface-to-Air Missiles, Part One, System Integration
175	Solid Propellants, Part One	292	Surface-to-Air Missiles, Part Two, Weapon Control
176(C)	Solid Propellants, Part Two (U)	293	Surface-to-Air Missiles, Part Three, Computers
177	Properties of Explosives of Military Interest	294(S)	Surface-to-Air Missiles, Part Four, Missile Armament (U)
179	Explosive Trains	295(S)	Surface-to-Air Missiles, Part Five, Counter-measures (U)
180	Principles of Explosive Behavior	296	Surface-to-Air Missiles, Part Six, Structures and Power Sources
185	Military Pyrotechnics, Part One, Theory and Application	297(S)	Surface-to-Air Missiles, Part Seven, Sample Problem (U)
186	Military Pyrotechnics, Part Two, Safety, Procedures and Glossary	327	Fire Control Systems--General
187	Military Pyrotechnics, Part Three, Properties of Materials Used in Pyrotechnic Compositions	329	Fire Control Computing Systems
189	Military Pyrotechnics, Part Five, Bibliography	331	Compensating Elements
190	Army Weapon System Analysis	335	Nuclear Effects on Weapon Systems
205	Timing Systems and Components	340	Carriages and Mounts--General
210	Fuzes, General and Mechanical	341	Cradles
211(C)	Fuzes, Proximity, Electrical, Part One (U)	342	Recoil Systems
128	Infrared Military Systems, Part Two	343	Top Carriages
120	Design Criteria for Environmental Control of Mobile Systems	344	Bottom Carriages
195-	Development Guide for Reliability	345	Equilibrators
200	(6 vols)	346	Elevating Mechanisms
		347	Traversing Mechanisms
		355	The Automotive Assembly (Revised)
		356	Automotive Suspensions
		357	Automotive Bodies and Hulls
		350	Wheeled Amphibian Design
		352	Military Bridges and Stream-Crossing Equipage